VOLUME 116 NUMBER 1

THE ASTROPHYSICAL JOURNAL

AN INTERNATIONAL REVIEW OF SPECTROSCOPY AND ASTRONOMICAL PHYSICS

JULY 1952

THE SPECTROGRAPHIC EQUIPMENT OF THE 200-INCH HALE TELESCOPE *Ira S. Bowen* 1
THE VARIABLE MAGNETIC FIELD OF α^2 CANUM VENATICORUM *Horace W. Babcock and Sylvia Burd* 8
THE POSTMINIMUM SPECTRUM OF R HYDRAE . . . . . *Paul W. Merrill* 18
SPECTROSCOPIC OBSERVATIONS OF STARS OF CLASS S . . . *Paul W. Merrill* 21
THE SPECTRUM OF THE ECLIPSING VARIABLE R ARAE . . . . *Jorge Sahade* 27
THE SPECTRUM OF S VELORUM . . . . . *Jorge Sahade* 35
THE SPECTRUM OF U CYGNI (MINIMUM) IN THE VISUAL AND INFRARED REGIONS . . . . . *Yoshio Fujita* 46
RADIAL VELOCITIES AND MASSES OF DOUBLE GALAXIES . . . . *Thornton Page* 63
THE RADIAL VELOCITY OF 16 LACERTAE *O. Struve, D. H. McNamara, R. P. Kraft, S. M. Kung, and A. D. Williams* 81
THE LIGHT-VARIABILITY OF 16 LACERTAE . . . . . *G. R. Miczaika* 99
A PHOTOELECTRIC STUDY OF 16 LACERTAE . . . . . *Merle F. Walker* 106
DWARF M STARS FOUND SPECTROPHOTOMETRICALLY—THIRD LIST *A. N. Vyssotsky and Betty Ann Mateer* 117
THE SPECTRA OF THE BRIGHT STARS OF TYPES F5–K5 . . . . *Nancy G. Roman* 122
A THEORY OF THE SPATIAL DISTRIBUTION OF GALAXIES *J. Neyman and E. L. Scott* 144
THE TIME OF RELAXATION FOR STARS IN A FLUCTUATING DENSITY FIELD *Donald E. Osterbrock* 164
MODEL SOLAR ATMOSPHERES . . . . . *Lawrence H. Aller and A. Keith Pierce* 176
THE EQUATION OF TRANSFER AND THE RESIDUAL INTENSITIES IN SPECTRUM LINES . . . . . *G. R. Burbidge and E. Margaret Burbidge* 185
THE PHYSICAL THEORY OF METEORS. III. CONDITIONS AT THE METEOR SURFACE . . . . . *Richard N. Thomas* 203
THE DETERMINATION OF A LIGHT-TIME ORBIT . . . . . *John B. Irwin* 211
THE DETERMINATION OF A SPECTROSCOPIC BINARY ORBIT . . *John B. Irwin* 218
NOTES
HD 160641, A HYDROGEN-DEFICIENT O-TYPE STAR . . . . . *William P. Bidelman* 227
THE SPECTRUM OF NOVA DQ HERCULIS (1934) IN 1950 . . . *P. Swings and P. D. Jose* 229

THE UNIVERSITY OF CHICAGO PRESS
CHICAGO, ILLINOIS, U.S.A.

July 1952 Vol. 116, No. 1

THE ASTROPHYSICAL JOURNAL

AN INTERNATIONAL REVIEW OF SPECTROSCOPY AND ASTRONOMICAL PHYSICS

Published in Collaboration with the American Astronomical Society

S. CHANDRASEKHAR
Managing Editor

GERARD P. KUIPER
Associate Editor

Yerkes Observatory of the University of Chicago

EDITORIAL BOARD

O. HERZBERG (1952-56)
National Research Council, Ottawa

C. D. SHANE (1952-55)
Lick Observatory, University of California

FRED L. WHIPPLE (1952-54)
Harvard College Observatory

LYMAN SPITZER, JR. (1952-53)
Princeton University Observatory

PAUL W. MERRILL (1952)
Mount Wilson Observatory of the Carnegie Institution of Washington

---

The Astrophysical Journal is published bimonthly by the University of Chicago at the University of Chicago Press, 5750 Ellis Avenue, Chicago 37, Illinois, during July, September, November, January, March, and May. ¶Two volumes are published per year, one beginning with the January issue and the other beginning with the July issue. The subscription price is $6.00 per volume or $12.00 per year; the price of single copies is $3.00. (Orders for service of less than a volume will be charged at the single copy rate.) ¶Postage is prepaid by the publishers on all orders from the United States and its possessions. No extra charge is made for postage to countries in the Pan American Postal Union. ¶Postage is charged extra as follows: for Canada, 20 cents per volume, 40 cents per year (total $6.20 per volume, $12.40 per year); on single copies 5 cents (total $3.05); for all other countries in the Postal Union, 40 cents per volume, 75 cents per year (total $6.40 per volume, $12.75 per year), on single copies 10 cents (total $3.10). ¶Subscriptions are payable in advance. Please make all remittances payable to The University of Chicago Press, in United States currency or its equivalent by postal or express money orders or bank drafts.

The following is an authorized agent:

For the British Empire, except North America and Australasia: The Cambridge University Press, Bentley House, 200 Euston Road, London, N.W. 1, England. Prices of yearly subscriptions and of single copies may be had on application.

Claims for missing numbers should be made within the month following the regular month of publication. The publishers expect to supply missing numbers free only when losses have been sustained in transit, and when the reserve stock will permit.

Business correspondence should be addressed to The University of Chicago Press, Chicago 37, Illinois.

Communications for the editors and manuscripts should be addressed to: S. Chandrasekhar, Editor of THE ASTROPHYSICAL JOURNAL, Yerkes Observatory, Williams Bay, Wisconsin.

Line drawings and photographs should be made by the author, and all marginal notes such as co-ordinates, wave lengths, etc., should be included in the cuts. It will not be possible to set up such material in type.

One copy of the corrected galley proof should be returned as soon as possible to the editor, Yerkes Observatory, Williams Bay, Wisconsin. Authors should take notice that the manuscript will not be sent to them with the proof.

The cable address is "Observatory, Williamsbay, Wisconsin."

The articles in this journal are indexed in the *International Index to Periodicals*, New York, N.Y.

Applications for permission to quote from this journal should be addressed to The University of Chicago Press, and will be freely granted.

Microfilms of complete journal volumes are available to regular subscribers only and may be obtained at the end of the year. Orders and inquiries should be addressed to University Microfilms, 313 North First Street, Ann Arbor, Michigan.

Notice to subscribers: If you change your address, please notify us and your local postmaster immediately.

Entered as second-class matter, July 12, 1940, at the Post-Office at Chicago, Ill., under the Act of March 3, 1879.
Acceptance for mailing at special rate of postage provided for in United States Postal Act of October 3, 1917, Section 1103, amended February 28, 1925.

[PRINTED IN U.S.A.]

THE ASTROPHYSICAL JOURNAL

AN INTERNATIONAL REVIEW OF SPECTROSCOPY AND ASTRONOMICAL PHYSICS

VOLUME 116 JULY 1952 NUMBER 1

THE SPECTROGRAPHIC EQUIPMENT OF THE 200-INCH HALE TELESCOPE

IRA S. BOWEN

MOUNT WILSON AND PALOMAR OBSERVATORIES
CARNEGIE INSTITUTION OF WASHINGTON
CALIFORNIA INSTITUTE OF TECHNOLOGY

Received April 11, 1952

ABSTRACT

The relationships between spectrograph speed and the various parameters entering into spectrograph design are discussed, and a description is given of the optical designs that have been worked out for the spectrographs of the Hale telescope to take advantage of these relationships.

Three new optical features were introduced in the design of the coudé spectrograph: (1) As dispersing element, a composite of four matched gratings is used; (2) cameras are of the Schmidt type, with the corrector plate placed practically in contact with the grating, the light passing through the plate twice, once before and once after reflection at the grating (this eliminates many of the vignetting problems present when the corrector plate is placed in the conventional position); (3) for the shortest focal-length camera an aplanatic sphere is combined with a Schmidt camera, thereby permitting a considerably higher camera speed than that attainable with the Schmidt camera alone.

With the aid of these new features, a spectrograph has been constructed having a 12-inch aperture collimator beam and a series of five cameras with focal lengths ranging from 144 to 8.4 inches and yielding dispersions of 2.3 to 40 A/mm.

For the study of the faintest objects a small spectrograph has been built for use at the prime focus. This has a 3-inch aperture collimator and cameras of focal length 1.4 and 2.8 inches.

The Hale 200-inch telescope possesses the largest light-gathering power of any instrument now built or planned. The combination of the Hale telescope and its spectrographs should therefore set the ultimate limit of object faintness that can be observed in the foreseeable future with a given dispersion and resolving power. It was therefore obviously of the greatest importance that these spectrographs be designed with the highest possible speed and efficiency.

In discussing the various features of this design let us examine, first, the effect on the speed of a spectrograph of the various parameters that enter into its design.

Let

D = Aperture of telescope.
β = Size of seeing image in radians. For purposes of this elementary discussion, it is assumed that the star image is square and is uniformly illuminated. The effect of this assumption will be discussed later.
f = Focal length of spectrograph camera.
d = Aperture of collimator beam in spectrograph.
Δ = Width of slit image permissible at the plate, usually set about equal to limit of resolution of plate.

W = Minimum width of spectrum permissible.
α = Angular dispersion of grating or prism in A/radian.
K = Linear dispersion of spectrograph in A/mm; thus $f = \alpha/K$.
r = Change in angle of camera beam along direction of dispersion produced by unit angular change of collimator beam. With a grating this is equal to ratio of cosines of angle of incidence and of diffraction. With a symmetrical prism system it is usually equal to 1.

If the slit is removed from the spectrograph, a monochromatic star image at the spectrograph plate has a linear size of $S_1 = Df\beta/d = Da\beta/dK$ in the direction perpendicular to the dispersion. In the direction parallel to the dispersion this becomes $S_2 = Df\beta r/d = Da\beta r/dK$. That is, neglecting any deviation of r from unity, the telescope-mirror-spectrograph system is equivalent to a single lens having an aperture D and the same focal ratio as the spectrograph camera lens.

Three cases must be considered depending on the relative size of the star image and the slit-width, i.e., on the relative values of S_2 and Δ, and on whether the normal width of the spectrum S_1 is greater or less than the minimum necessary width W, i.e., on whether or not the spectrum must be widened.

CASE I. $S_2 > \Delta$ AND $S_1 > W$

In this case, in order that the proper resolving power may be attained, it is necessary that the slit be narrowed to the point at which the fraction of the light passing the slit is

$$\frac{\Delta}{S_2} = \frac{\Delta d K}{D r \beta a}.$$

Since the spectrum is already wider than the minimum required, the width may be allowed to remain at S_1. The speed of the spectrograph is therefore proportional to the amount of light passing the slit, namely, $D^2\Delta/S_2$ divided by the area of the plate over which light in a given wave-length range, say 1 angstrom, is spread, i.e., S_1/K.

$$\text{Speed} = \frac{\Delta D^2}{S_2} \Big/ \frac{S_1}{K} = \frac{\Delta d^2 K^3}{r a^2 \beta^2}. \tag{1}$$

Case I obviously also applies to all extended sources.

CASE II. $S_2 > \Delta$, $S_1 < W$

This differs from Case I in that the spectrum is widened to a width of W. A procedure such as Case I gives the speed as

$$\text{Speed} = \frac{\Delta D^2}{S_2} \Big/ \frac{W}{K} = \frac{\Delta d K^2 D}{W r a \beta}. \tag{2}$$

CASE III. $S_2 < \Delta$, $S_1 < W$

All the light passes the slit and the width is again W.

$$\text{Speed} = \frac{D^2}{W/K} = \frac{K D^2}{W}. \tag{3}$$

A fourth case may occur in which the slit is wider than the star image ($S_2 < \Delta$) but the spectrum is not widened. As already indicated, however, Δ is normally set at a value approximately equal to the limit of resolution of the plate. Furthermore, the width of the optical image of the spectrum S_1 is approximately equal to S_2, which is less than Δ.

Since the optical spectrum, therefore, has a width equal to or less than the limit of resolution of the plate, scattering in the emulsion will spread the spectrum to a width equal to this limit of resolution. Formula (3) therefore applies if W is set equal to this limit of resolution.

As already stated, the foregoing simplified theory assumes a square star image of uniform intensity instead of the actual form whose energy distribution is usually given by the formula

$$I = I_0 \exp\left(-\frac{x^2+y^2}{\psi^2}\right).$$

The results for this actual distribution are very similar to those of the simplified theory, except in the region near the boundaries between cases. In these boundary regions there is a gradual transition from the formula for one case to that for the next rather than a sudden discontinuity, as given by the simplified theory.

While the boundaries between these cases are not sharp, it is of interest to have a rough idea of the ranges to which the formulae for the three cases apply for the Mount Wilson and Palomar telescopes. The boundary between Cases I and II occurs when

$$S_1 = \frac{\beta D f}{d} = W \quad \text{or} \quad \frac{f}{d} = \frac{W}{\beta D}; \tag{4}$$

and between Case II and Case III when

$$S_2 = \frac{\beta D f r}{d} = \Delta \quad \text{or} \quad \frac{f}{d} = \frac{\Delta}{\beta D r}. \tag{5}$$

The minimum permissible width of spectrum W and the diameter of the seeing image β may vary through wide ranges. Thus, for precision photometric work, a width W of a substantial fraction of a millimeter is often desirable. On the other hand, when observing faint stars near the limit of a given spectrograph, it is usually necessary to accept a value of W of 0.1 mm or even less. Since it is precisely when dealing with these faint stars that the question of speed is a major consideration, a value of W of 0.1 mm will be assumed for the present discussion. Similarly, β, the size of the seeing image, varies from 25 or 50×10^{-6}, i.e., 5–10 seconds of arc for poor seeing to 2×10^{-6} or less than half a second for extremely fine seeing. For the present calculations β is assumed to be 6×10^{-6} or $1\frac{1}{4}$ seconds of arc, since this corresponds to good average seeing at these observatories and represents the best images that can be counted upon for any extensive program. If we also assume $\Delta = 0.02$ mm and $r = \cos 30°$, we obtain the boundary values given in Table 1.

TABLE 1

VALUE OF f/d AT BOUNDARY BETWEEN CASES

Telescope	Case I – Case II	Case II – Case III
200-inch	3.3	.8
100-inch	6.7	1.5
60-inch	11	2.6

Since all cameras of the 100-inch coudé spectrograph operate at values of f/d ranging from 6 to 30, it is evident that Case I applies and would also apply if similar cameras were installed at the 200-inch telescope. Formula (1) for the speed in Case I leads to the rather disconcerting conclusion that the speed is independent of telescope aperture and there-

fore that, if the present 100-inch coudé spectrograph were duplicated at the 200-inch telescope, no gain in speed would be attained over that already available at the 100-inch telescope. The same conclusion is reached from direct physical reasoning, if one considers that under similar seeing conditions the star image formed by the 200-inch has twice the linear diameter as that formed by the 100-inch but has the same surface brightness. If widening is not used, the spectrum formed with a given spectrograph on the 200-inch is therefore twice as wide as that formed by the same spectrograph on the 100-inch, but it is not brighter.

When faced with the above theoretical results, it was evident that if the hoped-for gains in speed were to be attained with the 200-inch equipment, especially for the higher dispersions, it would not be sufficient to duplicate the 100-inch equipment but that drastic new designs must be attempted. If we examine equation (1) for clues as to the parameters that might be varied to gain the desired increase in speed, it is at once evident that the parameters β, Δ, and K are fixed by seeing and by the resolving power and dispersion necessary for a given type of problem. The parameter r is likewise normally fixed at a value close to unity. The speed of the spectrograph, however, varies directly as the square of d, the diameter of the collimator beam, and inversely as the square of α, the angular dispersion expressed in A/radian.

Of these two possibilities, the second, which required substantially decreasing α, seemed the least certain of achievement. In the first place, it was doubtful whether one could obtain a very efficient blaze in a much higher order or with a much finer grating than those now in use in the 100-inch coudé spectrograph. In the second place, it would require cameras with a much wider angular field than those now available to cover in one exposure the range of 1500 to 2000 A that is usually desirable for most problems.

A major increase in d and therefore in the size of the grating required also presented serious difficulties, since present ruling engines are not capable of making gratings substantially larger than those in use on the present 100-inch coudé; these gratings limit the maximum beam size to 6 inches. Recourse was therefore made to the use of a composite made up of four gratings, each having a ruled surface of $5\frac{1}{2} \times 7$ inches. These matched gratings were ruled on the Mount Wilson ruling engine with 10,000 lines per inch and were blazed in the third-order violet and second-order red, 60–70 per cent of the incident light going into the one blazed order. By this procedure it was possible to use a value of d of 12 inches.

The largest focal length planned for this instrument is 144 inches. The resolving power of each individual grating is therefore considerably greater than that of the photographic plate. Since the composite grating is used solely to increase intensity rather than resolving power, it is not necessary to mount the gratings so that the ruled lines of the four gratings are in phase with one another. The only condition is that the gratings be so placed that the spectra from all gratings coincide within the limit of plate resolution. While this requires a high precision of adjustment, it has not proved impractical of attainment. For these adjustments, rotation about an axis normal to the grating surface and about an axis in the grating surface normal to the ruled lines is made through screws bearing on the back or sides of the gratings.

A somewhat higher order of precision is required for rotation of each grating about an axis parallel to the ruled lines, since any maladjustment broadens the spectrum lines obtained. Rough adjustment for this rotation is made with screws bearing on the back of the mirror. Final fine adjustment about this axis is then attained by deforming the 1- to 2-inch thick steel plate on which the gratings are mounted. This is accomplished by connecting with a screw the outer end of the plate to a steel spring having a force constant about 1/500 as great as the mounting plate. A full turn of this screw results in a deformation of the plate by about 1/10,000 of an inch. Adjustments with the required accuracy of about 1/100,000 of an inch are therefore relatively easy.

Since the coudé optics of the 200-inch telescope operate at f-30, a focal length of

30 feet is required for the off-axis mirror collimator. The camera yielding the highest dispersion, as already mentioned, has a focal length of 144 inches. This makes use of the Schmidt principle by having a mirror placed with its center of curvature at the grating. Since this mirror operates at f- 12, spherical aberration may be neglected, and no corrector plate is therefore required.

Other cameras are provided of focal lengths of 72, 36, 18, and 8.4 inches. The first three of these cameras are of Schmidt type and are mounted to have their axes normal to the grating, while the collimator beam has an angle of incidence on the grating of 30°.

If the conventional Schmidt corrector plate had been used, it would have been necessary to place it about 36 inches away from the grating to avoid interference with the collimator beam. Since the fields of view of these cameras are about 1/5 of their focal lengths, this would have required an increase in the diameter of both mirror and corrector plate by over 7 inches to avoid additional vignetting. This not only would have added substantially to the cost but would have greatly increased the aberrations. Thus it can easily be shown that for a Schmidt camera both the chromatic aberrations and the off-axis aberrations for the size of the field used with these cameras become prohibitive when the focal length is reduced below that given by $f^2 = d^3/8$, in which all lengths are in inches. For the maximum aperture of the beam leaving the grating of $d/\cos 30° = 13.8$ inches, a focal length as short as 18 inches is permissible. On the other hand, a 21-inch corrector plate, which would be necessary with the corrector plate 36 inches from the grating, requires a minimum focal length of 35 inches. This would have necessitated the omission of the shortest of the Schmidt cameras.

An arrangement suggested by Hendrix and Christie[1] was considered in which the corrector plate, tilted to parallelism with the grating, is placed in the collimator beam. Again the corrector plate must be placed at a minimum of 36 inches from the grating. While this arrangement gives satisfactory definition with a very narrow spectrum, the large separation of the corrector plate from the center of curvature of the camera mirror causes the development of serious aberrations when a wide spectrum is photographed, particularly with the shorter-focus cameras.

A design was therefore developed by which a corrector plate of slightly less than half-strength is placed parallel to, and within a very few millimeters of, the grating. The light therefore passes through the plate twice, once before and once after reflection from the grating. In general, this procedure is feasible only if the camera axis remains approximately normal to the grating.

Since it was not feasible to figure the corrector plate on the basis of tests made in the spectrograph, a theory including all terms to the fifth order was developed which permitted tests being made in the laboratory with the corrector plate in contact with the mirror with which it was to be used. This theory gave the zonal differences in focus which should be present in the laboratory tests, in order that satisfactory performance should be achieved in the spectrograph.

In order to reduce aberrations to a minimum all plateholders are mounted on axis. They are therefore designed to take rather narrow plates 1 inch in width.

As indicated earlier, 18 inches is the shortest-focus standard Schmidt camera that can be used with a beam of the aperture here adopted. The use of the somewhat better-corrected solid-block or thick-mirror[2] types of Schmidt camera would reduce the permissible focal length by a factor of n, the index of the glass used, i.e., in this case to about 12 inches. However, the absorption in the light-path in the glass equal to $2n$ times the focal length would more than nullify any gains from the shorter focal ratio. To attain a still shorter focal length and therefore still higher speed, recourse was had to the principle of the aplanatic sphere to shorten the focus of the light coming from the 18-inch Schmidt

[1] *Scientific American*, **161**, 118, 1939.

[2] Hendrix, *Pub. A.S.P.*, **51**, 158, 1939; R. Minkowski, *J. Opt. Soc. America*, **34**, 89, 1944.

camera. The focal length was thereby reduced to $18/n^2 = 8.4$ inches, with a sphere of optical quality fused quartz having a radius of 2.5 inches.

The focal surface of the 18-inch Schmidt camera is a sphere of 18-inch radius convex toward the Schmidt mirror, while, to have satisfied the aplanatic condition at all points of the field, this surface should have had a radius of $n \times 2.5 = 3.67$ inches concave toward the mirror. This introduces a certain amount of spherical aberration at all but the two points in the spectrum where the two surfaces coincide. It was found possible, however, both to reduce substantially the amount of this aberration and to flatten completely the field by grinding a concave surface of 5.13-inch radius on the rear face of the aplanatic sphere against which the photographic plate is placed. To correct for the dispersion of the quartz sphere, this face and the photographic plate are tilted at an angle of just over 1° from the normal to the camera axis. Likewise, the radius of curvature of the rear surface of the quartz sphere was slightly modified to correct for the field curvature caused by the nonlinearity of the variation of the index with wave length. When the sphere is used for a different wave-length range than that for which it is designed, some spherical aberration is introduced. This may be satisfactorily corrected, however, by spacers which

TABLE 2

COUDÉ SPECTROGRAPH CAMERAS

Camera focus (inches)	144	72	36	18	8.4
Focal ratio f/d	12	6	3	1.5	0.7
Mirror diameter (inches)	48	36	30	20	20
Usable plate length (inches)	22	16	12	6	0.68
Dispersion:					
3d-order (violet) A/mm	2.3	4.6	9	18	39
2d order (red) A/mm	3.4	6.8	14	27	59
Limiting magnitude photographic:					
Widened to 0.1 mm	7.5	9.8	11.9	13.4	15.0
Unwidened	7.5	9.8	12.0	14.3	16.6

separate the plate from the rear of the quartz sphere by an appropriate amount, usually a few thousandths of an inch. By these procedures a well-corrected flat field 17 mm in diameter was attained, thereby providing a range for one exposure of 670 A in the third-order blue spectrum or 1000 A in the second-order red spectrum.

The dimensions and other properties of the five cameras of the coudé spectrograph are summarized in Table 2. The last two lines of the table give estimates of the limiting photographic magnitude that can be reached in an exposure lasting one night of 8 or 10 hours. These estimates were made on the basis of fairly good seeing, i.e., $\beta = 6 \times 10^{-6}$ and either on widening to 0.1 mm or on leaving the image unwidened. While the exact values given in the table are calculated, all observations to date confirm the general correctness of these limits.

Figure 1 shows the grating mount, corrector plate, and the mirrors and plateholders of the shorter-focus cameras. The mirror and aplanatic sphere of the 8.4-inch cameras are in operating positions, while the parts of other cameras are moved out of the way. Sample spectra obtained with the 144-inch, 36-inch, and 8.4-inch cameras are shown in Figure 2.

The 8-inch camera provides about the shortest focal length and therefore the highest speed it is feasible to design for the 12-inch beam of the coudé spectrograph. For still lower dispersions and higher speeds it is therefore necessary to use smaller apertures. Furthermore, at these very small focal ratios one is in the region of Case II or even Case

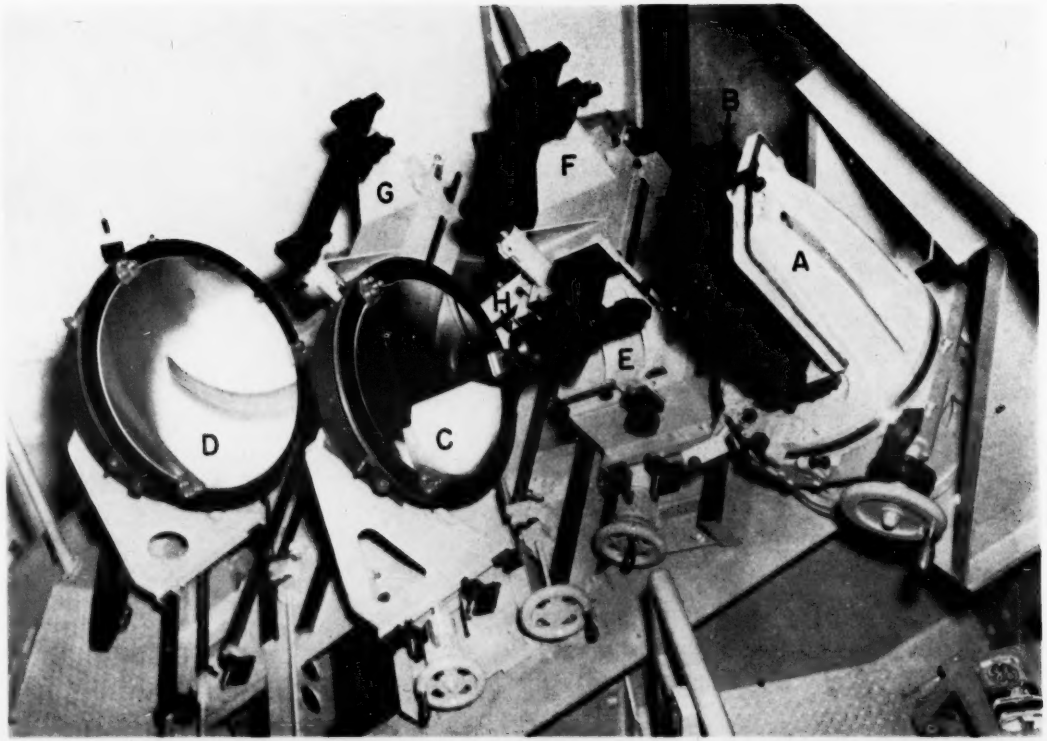

FIG. 1.—Short-focus camera of coudé spectrograph. *A*, grating mount; *B*, corrector plate. Mirrors: *C* 18-inch, *D*, 36-inch. Plateholder mounts: *E*, 18-inch; *F*, 36-inch; *G*, 72-inch; *H*, aplanatic sphere.

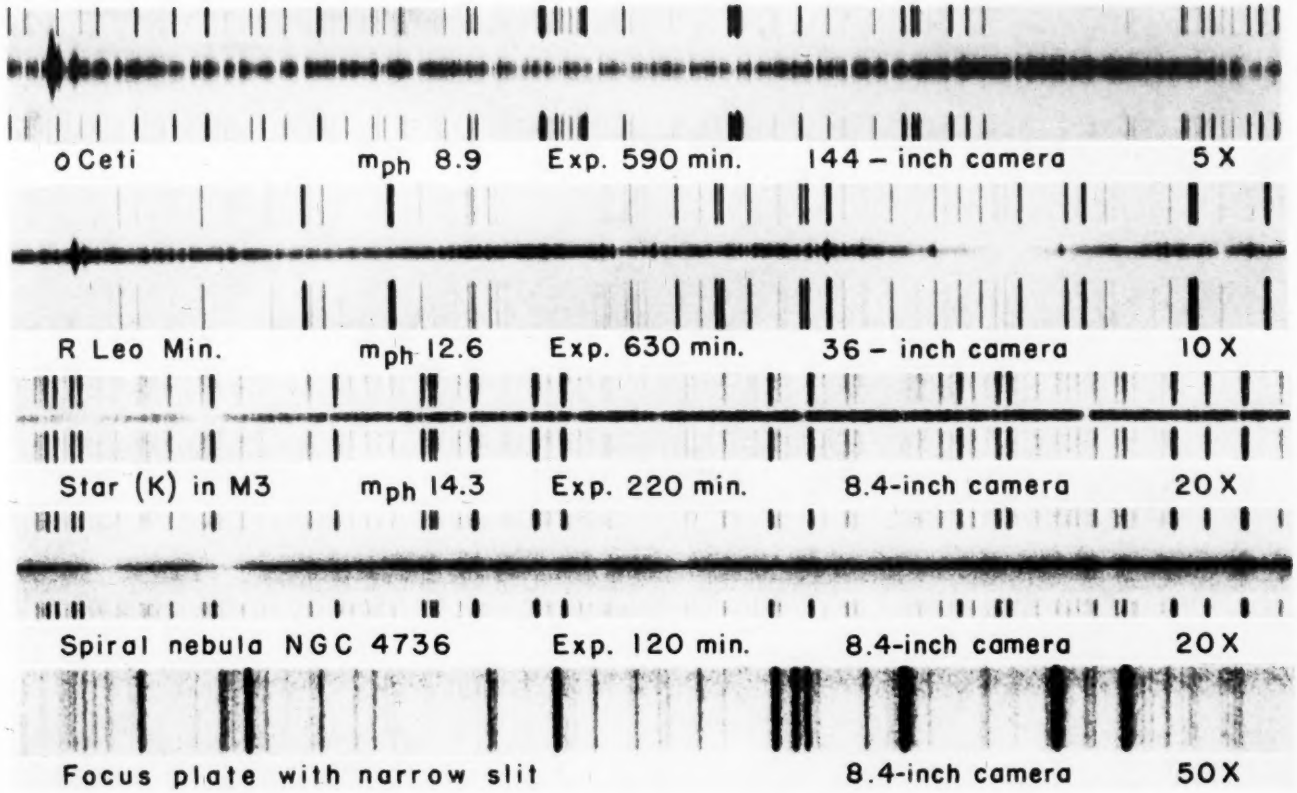

FIG. 2.—Sample spectra taken with coudé spectrograph

III, in which the value of the aperture, d, plays a much smaller role in determining the speed of the spectrograph.

For these lower dispersions a small spectrograph having a beam diameter of 3 inches has been constructed. Because of its small size it is feasible to mount this at the prime focus, where the light losses at the two or four additional mirrors of the coudé system may be avoided. As dispersing systems, gratings of 7500 and 15,000 lines per inch with the blaze in the second-order violet are used. Two cameras of the thick-mirror Schmidt type of 1.4- and 2.8-inch focus are provided which operate at focal ratios of f 0.47 and f 0.95. The 1.4-inch camera has the shortest focal length that is permissible for a thick-mirror Schmidt of 3-inch aperture. Dispersions of 430, 210, and 105 A/mm are obtained with the various combinations of gratings and cameras.

Since many objects to be observed with this instrument are too faint to be seen visually, provision is made for accurately offsetting the slit from a near-by bright star.

As these instruments provide a complete range of dispersions, no additional spectrographs are planned for the Cassegrain focus.

The design and construction of these instruments would have been impossible without the co-operation of many people. Thus the very difficult Schmidt corrector plates and many of the other optical parts were made by Mr. Don Hendrix. All gratings, including the carefully matched gratings of the composite grating of the coudé spectrograph, were ruled under the supervision of Dr. Horace Babcock. The mechanical designs were made in the California Institute shop under the direction of Mr. Bruce Rule, most of the specifications for the prime-focus spectrograph being supplied by Dr. Rudolph Minkowski. Finally, Dr. O. C. Wilson assisted greatly in the adjustment of the various parts of the coudé spectrograph.

THE VARIABLE MAGNETIC FIELD OF α^2 CANUM VENATICORUM

HORACE W. BABCOCK AND SYLVIA BURD
MOUNT WILSON AND PALOMAR OBSERVATORIES
CARNEGIE INSTITUTION OF WASHINGTON
CALIFORNIA INSTITUTE OF TECHNOLOGY
Received February 26, 1952

ABSTRACT

This well-known peculiar star is found to have a strong magnetic field, the polarity of which is reversed in step with the periodic changes in line intensity. The Zeeman effect has been investigated on twenty-one spectrograms made with the double polarizing analyzer. Polar magnetic-field strength and radial velocity for various elements have been tabulated as a function of phase in the period of 5.5 days. The extremes of H_p are approximately -4000 gauss when the *Eu* II lines are at maximum intensity and $+5000$ gauss a half-period later, when *Cr* II is at maximum.

The bright star α^2 Canum Venaticorum is the classical example of the spectrum variables of type A. Beginning with the discovery of variable lines by Ludendorff[1] in 1906, the derivation of a period for the line intensities by A. A. Belopolsky[2] in 1913, and the identification of some of the lines as due to the rare earth element europium by Baxandall[3] in the same year, several investigators have devoted much effort to the description of its spectrum and its attempted interpretation. A comprehensive discussion of this work up to 1942 has been given by O. Struve,[4] and in the same year Struve and Swings[5] published a new list of wave lengths of over thirty-one hundred absorption lines obtained largely from coudé spectrograms.

In 1949, following the observation of strong magnetic fields in several other peculiar stars and spectrum variables of type A, the spectrum of α^2 CVn was examined at Mount Wilson for the Zeeman effect, and it was found at once that this star possesses a strong magnetic field, the polarity of which is reversed in step with the changes in line intensity. In many respects α^2 CVn is quite similar to the magnetically variable star HD 125248. Earlier investigators have shown that the periods of spectrum variation of these stars are 5.5 and 9.3 days, respectively, and that in the spectrum of each, groups of lines typified by *Eu* II and by *Cr* II undergo large variations of intensity in opposite phase. The magnetic phenomena observed in HD 125248 have been discussed in a recent paper.[6] The investigation of α^2 CVn reported here was made subsequently, because accurate measurements of its magnetic field are more difficult, even though it is nearly 3 mag. brighter. The lines in its spectrum are shallower and somewhat broader than those of HD 125248, and the amplitude of its periodic magnetic variation is slightly lower. Also there is a practical complication in observing it for the Zeeman effect because of the star's northerly declination. This complication results from the oblique reflection from the coudé flat mirror in the optical system of the telescope, which introduces a phase shift between the *p* and *s* vibration components that are, respectively, parallel to and perpendicular to the plane of incidence. If this phase shift is not compensated, the elliptical polarization in the line profiles is considerably altered, particularly when the angle of incidence is large, and the derived magnetic field is smaller. For observations of α^2 CVn and other stars north of the equator, an optical compensator has been used; this device will be described elsewhere.

The double circular analyzer used was the same as that employed in the observations

[1] *A.N.*, **173**, 4, 1906.
[2] *A.N.*, **196**, 1, 1913.
[3] *Observatory*, **36**, 440, 1913.
[4] *Proc. Amer. Phil., Soc.*, **85**, 349, 1942.
[5] *Ap. J.*, **98**, 361, 1943.
[6] H. W. Babcock, *Ap. J.*, **114**, 1, 1951.

of HD 125248, and the methods of measuring and reducing the spectrograms were similar. The dispersion was 4.5 A/mm, and for most of the plates an emulsion of rather high contrast (Eastman type III-O) was used. All the lines measured lie in the range λλ 3800–4600. Twenty-one plates were measured for magnetic-field strength and for radial velocity, the average number of lines measured on each plate being forty-four. For each observation the epoch and phase were computed according to the formula established by Miss G. Farnsworth:[7]

$$\text{Maximum intensity of } Eu\text{ II} = \text{JD } 2419869.720 + 5.46939E\text{ ,}$$

which was also used by Struve and Swings.

Results are listed in Table 1, where the observations are arranged according to phase. For each plate the derived values of H_p, the magnetic field at the pole of the star, and of v, the radial velocity, are given separately for the various elements. The probable error of H_p for each element represented by three or more lines is also given. Usually the probable errors in H_p amount to a few hundred gauss. For each plate the mean H_p from all lines weighted equally is listed, but without a probable error, since for physical reasons the various elements yield more or less discordant values of field strength, depending upon phase.

In Figure 1 the mean H_p for all lines is plotted as a function of phase in the 5.5-day period. The abrupt reversal of the field at the cross-over phases (0.32 and 0.71) is particularly striking. The curve seems better defined when the magnetic polarity is negative and the *Eu* II lines are strong than near mid-period, when the polarity is positive. This must be due in part to the fact that the lines are less numerous as well as broader and shallower near mid-period and so are more difficult to measure; it may also be attributable in part to lack of uniformity in the magnetic behavior of the star in the positive portion of various magnetic cycles. The negative part of the magnetic curve centered on zero phase has a well-defined central hump, so that two negative extremes occur near phases 0.73 and 0.25. In this the curve for α^2 CVn differs from the smoother magnetic curve observed for HD 125248. The notch at phase 0.612 results from one observation that appears to be quite reliable; this plate gives a range of values of H_p for various elements that is considerably greater than normal. For example, *Fe* II and *Cr* II give -70 ± 270 gauss and -3150 ± 470 gauss, respectively; each element is represented by seventeen measured lines. The observations are insufficient in number to establish whether the notch is a real feature of the magnetic curve that is repeated in all cycles or whether it is the result of inconsistent or nonuniform magnetic activity.

A sequence of ten spectrograms was taken between May 20 and May 28, 1951. The corresponding values of H_p are plotted for this sequence alone in Figure 2. A much higher time-resolution would have been desirable.

In Figure 3 the magnetic measurements for *Cr* II and for *Eu* II are plotted individually, together with the solid line representing the mean for all elements. No pronounced systematic differences are revealed, although there appears to be a tendency for *Cr* II to lie below the mean curve and for *Eu* II to be slightly above. *Eu* II is not represented in the middle of the cycle because its lines are then practically absent or so weak as to be almost impossible to measure.

On plates taken near the phases when the magnetic curve passes through zero, the cross-over effect on the profiles of certain lines was observed. It is similar to that previously found in the spectrum of HD 125248,[6] although less pronounced. At phase 0.354 of α^2 CVn some lines in the levogyrate spectrum had broader and shallower profiles than in the dextrogyrate spectrum; this was reversed at phase 0.612. Lines most affected were those of *Fe* II and *Cr* II; *Eu* II does not clearly show the effect. According to the interpretation previously suggested, the affected lines arise in two areas on the surface of the star

[7] *Ap. J.*, **75**, 364, 1932.

TABLE 1

MAGNETIC INTENSITY, H_p, AND RADIAL VELOCITY, v, FOR ELEMENTS AT VARIOUS PHASES

Epoch and Phase	Element	H_p (Gauss)	No. of Lines	v (Km/Sec)
2393.**009**	*Fe* II	−6000	2	+ 3.5
Ce 5541	*Ti* II	−1700	1	+ 1.1
1949 Feb. 10.521	*Si* II	−7900	2	+ 1.7
	Ca II	−1300	1	− 5.5
	Mg II	−8400	1	− 0.6
	Ni I	−2100	1	+ 3.2
	Sr II	−3700	1	+ 2.5
	Eu II	−1600 ± 400	4	− 0.6 ± 0.9
	Gd II	−3550 ± 650	5	+ 0.5 ± 0.5
	Mean	−3450	18	.....
2545.**063**	*Fe* I	−1920 ± 290	7	−11.3 ± 0.6
Ce 7039	*Fe* II	−2780 ± 380	16	− 9.1 ± 0.6
1951 May 23.164	*Ti* II	−2890 ± 640	5	− 7.6 ± 1.1
	Si II	−4150	2	+ 1.9
	V II?	− 400	1	+ 1.5
	Ca II	−5500	1	− 2.9
	Mg II	−5200	1	− 0.4
	Cr II	− 850 ± 710	6	−13.0 ± 0.9
	Sr II?	−7400	1	+ 1.3
	Eu II	−4030 ± 320	6	+ 2.6 ± 0.1
	Ce II	−3860 ± 1400	3	− 8.5 ± 1.3
	Gd II?	− 900	1	+ 4.3
	Y II?	−2800	1	+ 1.5
	Mean	−2840	51	.....
2461.**176**	*Fe* I	−3680 ± 730	6	− 4.5 ± 0.6
Ce 6128	*Fe* II	−3580 ± 310	23	− 3.7 ± 0.3
1950 Feb. 18.352	*Ti* II	−5335 ± 440	14	− 0.7 ± 0.2
	Si II	−3950	2	0.0 ± 0.5
	Ca II	−4700	1	− 0.9
	Mg II	−6300	1	− 0.4
	Cr II	−3215 ± 210	18	− 6.3 ± 0.3
	Sr II	−5900	1	+ 4.2
	Eu II	−3900 ± 420	4	+ 8.8 ± 0.2
	Gd II	−2800	1	+ 9.4
	Ce II	−7330 ± 390	4	− 1.5 ± 0.5
	Pr III?	−2200	1	+ 5.9
	Mean	−4000	76	.....
2527.**176**	*Fe* I	−2535 ± 250	10	− 6.3 ± 0.6
Ce 6851 (a)	*Fe* II	−3390 ± 270	22	− 5.1 ± 0.3
1951 Feb. 14.333	*Ti* II	−4390 ± 360	14	− 2.0 ± 0.3
	Si II	−5320	2	− 1.4 ± 0.9
	Ca II	−3000	1	− 3.0
	Cr I	−3710	2	− 3.8
	Cr II	−3830 ± 200	24	− 7.8 ± 0.4
	Sr II	−6200	1	+ 2.4
	Eu II	−3300 ± 210	5	+ 6.7 ± 0.8
	Gd II	−4240 ± 820	3	+ 5.2 ± 1.7
	Mean	−3650	84	.....

TABLE 1—*Continued*

Epoch and Phase	Element	H_p (Gauss)	No. of Lines	v (Km/Sec)
2545.**248**	*Fe* I	−4600±2200	3	− 2.2±1.0
Ce 7044	*Fe* II	−5300± 380	15	+ 0.4±0.3
1951 May 24.174	*Ti* II	−5610± 560	12	+ 5.3±0.2
	Si II	−2100	2	+ 1.4±0.2
	Ca II	−3850	1	− 1.4
	Cr II	−4870± 420	17	− 2.0±0.5
	Eu II	−2500± 470	4	+18.3±2.2
	Ce II	−5830± 470	4	+ 7.4±1.3
	Y II?	−3440± 760	3	+ 7.7±2.9
	Pr II?	−3500	1	+ 2.7
	Mean	−4690	62	.....
2461.**354**	*Fe* I	+3300± 460	5	− 2.0±0.5
Ce 6136	*Fe* II	+2160± 320	17	− 0.5±0.3
1950 Feb. 19.326	*Ti* II	+ 900	1	+ 2.6
	Si II	+3670± 200	5	− 0.3±0.5
	Ca II	+3000	1	− 2.3
	Cr II	+1480± 360	17	+ 1.2±0.4
	Sr II	+4000	1	− 3.9
	Mean	+2200	47	.....
2518.**435**	*Fe* I	+5925± 550	5	− 0.7±0.2
Ce 6763	*Fe* II	+4175± 480	15	− 1.2±0.2
1950 Dec. 28.521	*Ti* II	+4910± 880	6	− 0.5±0.9
	Si II	+3700	2	+ 0.2
	Ca II	+3850	1	− 3.0
	Cr II	+3700± 400	7	+ 4.0±0.7
	Sr II	+8080	2	− 1.0
	Gd II	+4050	1	+ 1.8
	Mean	+4620	39	.....
2458.**451**	*Fe* I	+2260± 330	5	− 1.6±0.6
Ce 6120	*Fe* II	+3330± 400	21	− 0.5±0.3
1950 Feb. 3.445	*Ti* II	+2420± 430	9	− 1.4±0.4
	Si II	+3490	2	+ 1.3±0.6
	Ca II	+1590	2	− 1.7
	Cr II	+1340± 720	10	+ 1.0±0.5
	Mean	+2580	49	.....
2545.**461**	*Fe* I	+3580± 970	3	− 3.3±0.9
Ce 7050	*Fe* II	+3950± 400	23	− 0.8±0.3
1951 May 25.340	*Ti* II	+4360±1120	4	− 0.8±0.5
	Si II	+5750	2	− 0.4±0.2
	Ca II	+4010	2	− 2.5
	Mg II	+6700	1	+ 0.6
	Cr II	+4770±1300	3	+ 4.3±1.3
	Mean	+4170	38	.....
2544.**519**	*Fe* I	+3900± 970	4	− 2.4±0.1
Ce 7028	*Fe* II	+3995± 270	18	− 1.6±0.3
1951 May 20.185	*Ti* II	+3185± 290	4	− 0.2±0.6
	Si II	+4835± 860	5	− 2.7±0.2
	Ca II	+4700	1	− 2.0
	Cr II	+4400±1250	3	− 3.0±0.5
	Eu II	+1500	1	− 1.7
	Mean	+3900	36	.....

TABLE 1—*Continued*

Epoch and Phase	Element	H_p (Gauss)	No. of Lines	v (Km/Sec)
2461.**536**	*Fe* I	+4670± 550	4	− 4.3±0.7
Ce 6143	*Fe* II	+4195± 300	22	− 2.4±0.3
1950 Feb. 20.323	*Ti* II	+4970± 700	6	− 2.4±0.6
	Si II	+3500	2	− 1.9±0.3
	Ca II	+4560	2	− 0.8
	Mg II	+5900	1	− 3.0
	Cr II	+3420± 500	6	− 2.6±1.0
	Sr II	+5200	1	− 5.2
	Mean	+4280	44	.....
2544.**544**	*Fe* I	+5840± 300	4	− 4.2±0.5
Ce 7030	*Fe* II	+5750± 520	25	− 1.2±0.2
1951 May 20.325	*Ti* II	+5660± 560	9	+ 0.5±0.6
	Si II	+2860± 800	5	+ 0.1±0.7
	Ca II	+3400	1	− 2.4
	Mg II	+8250	1	− 0.0
	Cr II	+3280	2	− 4.5
	Mean	+5340	47	.....
2545.**612**	*Fe* I	+1080±1590	3	− 1.3±0.2
Ce 7052	*Fe* II	− 70± 470	17	− 0.9±0.3
1951 May 26.167	*Ti* II	+1700	1	− 1.1
	Si II	−3490	2	+ 0.7±0.5
	Ca II	+3850	1	− 0.9
	Cr II	−3150± 480	17	− 4.9±0.7
	Mean	−1200	41	.....
2398.**644**	*Fe* I	+3470± 730	5	− 3.9±0.2
Ce 5585	*Fe* II	+2115± 590	21	− 1.0±0.3
1949 Mar. 13.339	*Si* II	+2640±1460	5	− 1.7±0.2
	Ca II	+5600	1	− 0.9
	Mg II	+5600	1	− 4.4
	Cr II	+2510± 530	13	− 4.6±0.6
	Mean	+2565	46	.....
2522.**702**	*Fe* I	+1540±1100	3	− 3.3±0.9
Ce 6808	*Fe* II	+2330± 380	16	− 2.9±0.3
1951 Jan. 20.431	*Si* II	− 466	2	− 2.0±0.6
	Ca II	+3000	1	− 5.2
	Cr I	+1600	1	− 0.4
	Cr II	+1330± 330	17	− 6.1±0.5
	Mean	+1720	40	.....
2544.**734**	*Fe* I	−5340± 350	4	− 2.9±0.3
Ce 7034	*Fe* II	−4030± 600	20	− 1.4±0.6
1951 May 21.365	*Ti* II	−2100	1	− 8.3
	Si II	−9470	2	− 0.2
	Ca II	−3850	1	− 2.6
	Mg II	−1170	1	+ 0.7
	Cr II	−4730± 410	19	− 2.7±0.5
	Sr II	−4000	1	− 5.3
	Ce II?	−6600	1	− 1.0
	Gd II?	−3300	1	− 5.6
	Nd II?	−9100	1	− 8.7
	Mean	−4620	52	.....

TABLE 1—*Continued*

Epoch and Phase	Element	H_p (Gauss)	No. of Lines	v (Km/Sec)
2518.796	*Fe* I	−2400	1	+ 1.5
Ce 6776	*Fe* II	−4220 ± 440	20	− 0.2±0.3
1950 Dec. 30.500	*Ti* II	−5280 ± 490	4	− 5.6±0.8
	Si II	−4400	2	+ 0.3±1.3
	Ca II	−5200	1	+ 0.3
	Cr II	−4340 ± 230	22	+ 0.8±0.3
	Sr II	−2000	1	− 2.8
	Eu II	−2900 ± 190	4	−10.2±1.1
	Gd II	−3340 ± 440	4	− 5.9±1.4
	Mean	−4060	59	.....
2545.796	*Fe* I	−3500 ± 940	3	+ 0.2±0.4
Ce 7057	*Fe* II	−4250 ± 540	17	+ 0.7±0.3
1951 May 27.170	*Ti* II	−3700 ± 900	3	− 4.5±1.1
	Si II	−3500	2	− 1.2
	Cr II	−4560 ± 340	18	+ 1.4±0.5
	Sr II	−3400	2	− 0.9
	Eu II	−3060 ± 270	3	− 8.6±0.6
	Gd II	−2740 ± 500	8	− 7.4±0.6
	Ce II	−3340 ± 1120	6	− 2.8±0.9
	Pr II	−3600 ± 420	5	− 4.1±0.4
	Mean	−3810	67	.....
2544.889	*Fe* II	−3150 ± 440	11	+ 3.2±0.5
Ce 7036	*Ti* II	−4800 ± 450	9	− 0.3±0.9
1951 May 22.210	*Si* II	−2800	2	− 2.1
	Ca II	−2550	1	− 4.9
	Cr II	−3430 ± 330	9	+ 5.6±0.7
	Eu II	−3240 ± 670	4	− 6.8±0.9
	Ce II	−4680 ± 810	4	+ 3.5±0.9
	Gd II	−3090 ± 340	4	+ 1.2±1.1
	Zr II?	−4860 ± 580	5	+ 3.4±1.5
	Pr II?	−3940	2	+ 9.1
	Mean	−3710	51	.....
2457.904	*Fe* II	−2750 ± 920	9	+ 7.8±0.6
Ce 6108	*Ti* II	−3880 ± 570	6	+ 5.3±1.3
1950 Jan. 31.458	*Si* II	−7140	2	+ 2.3
	Ni I	−3700	1	− 0.2
	Mn II	−3000	1	+14.6
	Cr II	−4240 ± 820	7	+ 9.3±0.4
	Sr II	−1930	2	+ 7.6
	Eu II	−2610 ± 20	3	− 0.3±0.3
	Gd II	−2880 ± 490	5	+ 1.1±1.3
	Ce II	−8000	1	+ 9.2
	Pr II	−7000	1	+12.7
	Mean	−3510	38	.....
2545.978	*Fe* II	−4100	2	+ 1.7
Ce 7062	*Ti* II	−2750 ± 610	4	+ 1.7±3.2
1951 May 28.167	*Si* II	−2560	2	+ 1.1
	Eu II	−2300 ± 490	4	− 0.9±0.6
	Gd II	−2080 ± 410	9	+ 1.3±0.8
	Y II?	−2600	2	− 0.2
	Zr II?	−5140 ± 1840	3	− 1.0±3.2
	Mean	−2630	26	.....

that are characterized by opposite magnetic polarity and by a small differential radial velocity. The sign of the cross-over effect in α^2 CVn is such that, when the lines of *Cr* II are becoming more intense, that portion of the surface characterized by positive effective magnetic polarity is approaching the observer, or moving outward from the center of the star. Near the other cross-over phase (0.612), when *Cr* II is growing weaker, conditions are reversed.

With regard to the measurement of radial velocities, our material is less extensive than that of Struve and Swings[5] as to the number both of observations and of elements represented. The precision of our measures, however, compares favorably with theirs,

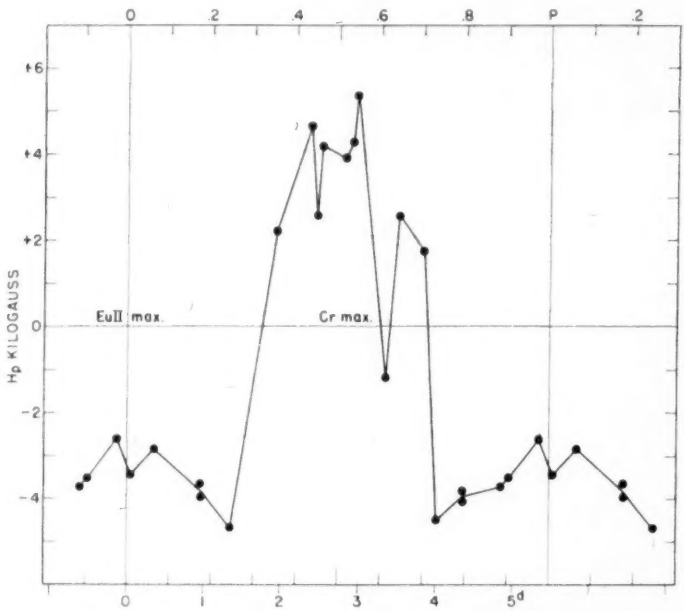

FIG. 1.—The mean magnetic-field intensity at the pole, H_p, in kilogauss, as derived from all lines measured, and plotted in the cycle of 5.46939 days. The lines of *Eu* II are strong when the magnetic polarity is negative; those of *Cr* II are at maximum intensity when the polarity is positive. The plotted points represent observations made over a two-year interval.

although the dispersion of our spectrograms is lower. For this reason we present in Figure 4 plots of radial velocity against phase for several elements; in the main, these confirm the results of Struve and Swings, who distinguished three types of velocity-curve:

a) Lines which show a large range in velocity, with a pronounced maximum at phase 4.5 days (from our data 4.3 days or 0.79 of the period) after the epoch of maximum intensity of *Eu* II. Maximum velocity occurs at phase 1.5 days (0.25*P*). The curve is characterized by a nearly steady rise during the interval when the lines are of strong intensity. *Eu* II with a range of 30 km/sec is the best example. The only other element of this group in our list is *Gd* II, with a range of 15 km/sec. Struve and Swings state that probably all other rare earths, as well as *Al* II, *Ca* I, *Mn* I, and *Ni* I share in this type of variation.

b) Lines which show a remarkable double wave, of which *Cr* II is the best example. Our data agree with those of Struve and Swings as to the phases of primary and secondary

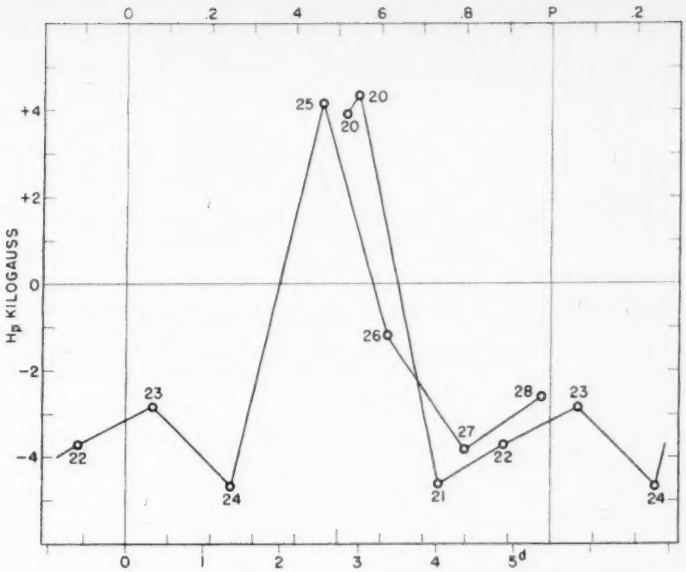

FIG. 2.—Magnetic intensities from a sequence of ten spectrograms. The figures indicate dates of the observations in May, 1951.

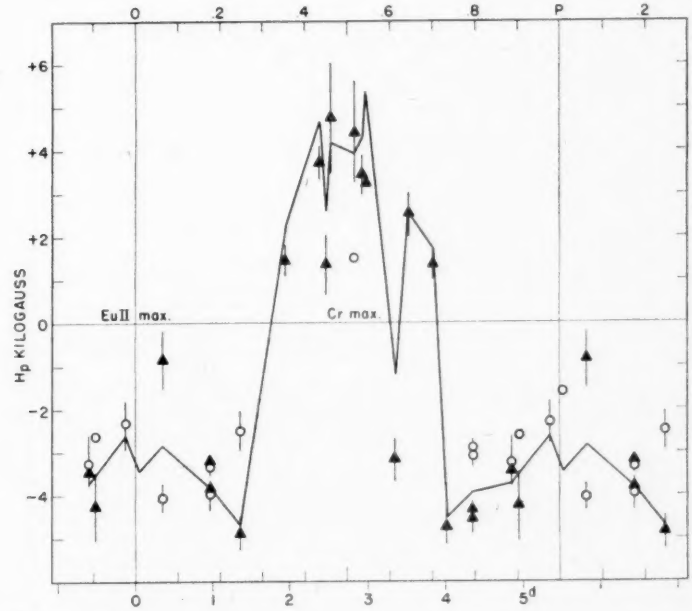

FIG. 3.—Magnetic intensities derived from lines of *Eu* II (*circles*) and of *Cr* II (*triangles*) compared with the mean from all elements (*solid line* from Fig. 1).

minima, except that our secondary maximum occurs slightly later, at 2.5 days (0.45*P*) instead of 2.0 days. Further, we find a total range of 22 km/sec, as compared to their 15 km/sec for *Cr* II. Struve and Swings found the same type of variation for *Fe* I and *Fe* II, whereas for these our data show a slightly greater range, but scarcely any suggestion of secondary maxima or minima. Our curve for *Ti* II is rather similar to that for *Cr* II, but with an earlier maximum near 1.4 days (0.25*P*).

c) Lines which show little or no variation. From our measures we list *Si* II and *Ca* II in this group; for both, there is a suggestion of a velocity fluctuation with an amplitude of

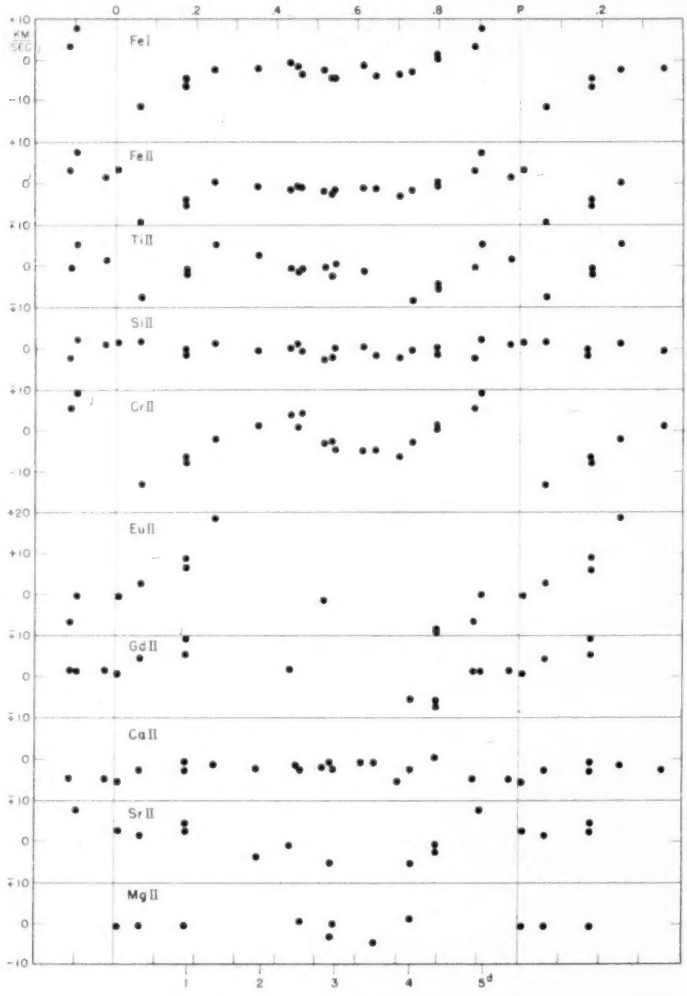

FIG. 4.—Radial velocities of α^2 Canum Venaticorum

about 1 km/sec, but this is too small to be definite. *Mg* II may also be included, although our data are scanty. Struve and Swings listed the elements mentioned, together with *H* and *Sr* II. We find, however, that *Sr* II shows a distinct variation, with a maximum near phase 0.9 and a minimum near 0.65; the amplitude is about 10 km/sec.

The velocity-curves plotted from our data give no clear-cut indication of systematic differences in mean velocity. With the possible exception of *Si* II, all are consistent with a mean velocity of about -2 km/sec. *Si* II, of group *c*, has a mean velocity of 0.1 km/sec. Struve and Swings, on the other hand, found systematic differences, with *Mg* II giving -9 km/sec in the mean and *Sr* II giving $+7$ km/sec.

The diversity of form and amplitude of the velocity-curves of the various elements suggests that their classification into three groups, while useful in a preliminary discussion, may have limited physical significance; this is emphasized by the difficulty of classifying the curves of *Ti* II and *Sr* II. It is no doubt true, however, that the various rare earths have velocity-curves similar in form.

THE POSTMINIMUM SPECTRUM OF R HYDRAE

PAUL W. MERRILL
MOUNT WILSON AND PALOMAR OBSERVATORIES
CARNEGIE INSTITUTION OF WASHINGTON
CALIFORNIA INSTITUTE OF TECHNOLOGY
Received February 12, 1952

ABSTRACT

Five spectrograms, dispersion 10 A/mm, were obtained during the time when the light was increasing after minimum. Near minimum, ground-level lines of *Ca* I, *Al* I, and *K* I became extraordinarily intense. Bright hydrogen lines appeared in low intensity about 50 days after minimum, with displacements algebraically greater than those measured previously at maximum light. The emitting hydrogen atoms appear to have an outward acceleration until they disappear before the next minimum. The dark lines, on the other hand, yield about the same velocity shortly after minimum as they do at maximum.

A previous article[1] on the long-period variable star R Hydrae 132422, period 387 days, class M6e, dealt with the spectrum from a few weeks before maximum light to about four months after maximum. The present article is based on five spectrograms, dispersion 10 A/mm, obtained in the first few months of 1950 and of 1951 during the time when the brightness was increasing after minimum. I am grateful to I. S. Bowen and O. C. Wilson for taking two plates with the coudé spectrograph of the 200-inch telescope, one of which is especially important because it was taken only 18 days after minimum light. Pertinent data are in Table 1 and Figure 1. The light-curve was supplied through the courtesy of

TABLE 1

SPECTROGRAMS OF R HYDRAE

PLATE	DATE	JD 243	MAG.	DAYS AFTER MINIMUM	RADIAL VELOCITIES (KM/SEC)		
					Abs.	No. Abs. Lines	*H* Em.
Ce 6163	1950 Feb. 22	3335	7.7	72	−10.0	39	(−12)
Pc 50	1951 Jan. 21	3668	8.9	18	− 9.0	54	.....
Ce 6884	Feb. 24	3702	7.6	52	− 7.4	59	(−11)
Pc 65	Mar. 19	3725	6.6	75	− 6.9	77	−12
Ce 6961	Mar. 27	3733	6.3	83	− 4.7	24	−12

Mrs. M. W. Mayall, of the Harvard Observatory. The curve differs from the typical curve of a long-period variable in that the rising branch is no steeper than the declining branch.

The spectrum at minimum differs markedly from that at maximum. Emission lines are weak or absent, while *TiO* bands are much stronger. Ground-level atomic lines, especially of metals of low ionization potential, become extraordinarily intense. Notable examples are λ 4227 *Ca* I, I.P. 6.0 volts; λ 3944, λ 3961 *Al* I, I.P. 6.1 volts; and λ 4044, λ 4047 *K* I, I.P. 4.3 volts. In Figures 2 and 3, the *Al* I and *K* I lines on plate Pc 50 taken near minimum are compared with the same lines on a previous plate near maximum.

[1] P. W. Merrill, *Mt. W. Contr.*, No. 717; *Ap. J.*, **103**, 6, 1946.

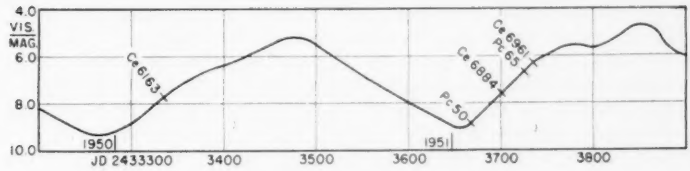

FIG. 1.—Light-curve of R Hydrae, showing dates of spectrograms

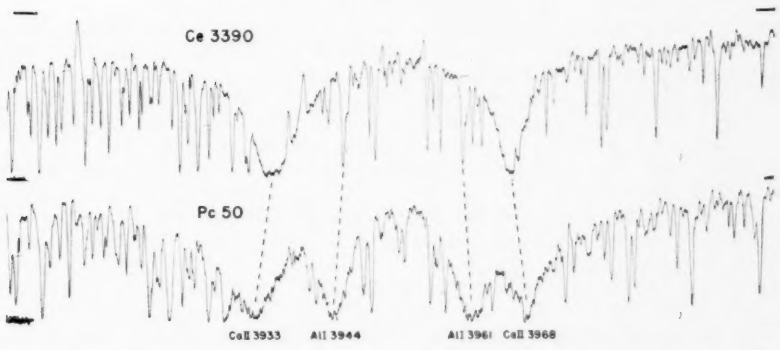

FIG. 2.—Comparison of lines of *Al* I in the spectrum of R Hydrae. *Above*, Ce 3390, taken on February 10, 1944, magnitude 4.7, 19 days before maximum. *Below*, Pc 50, taken on January 21, 1951, magnitude 8.9, 18 days after minimum. The scale of the lower tracing is slightly greater than that of the upper.

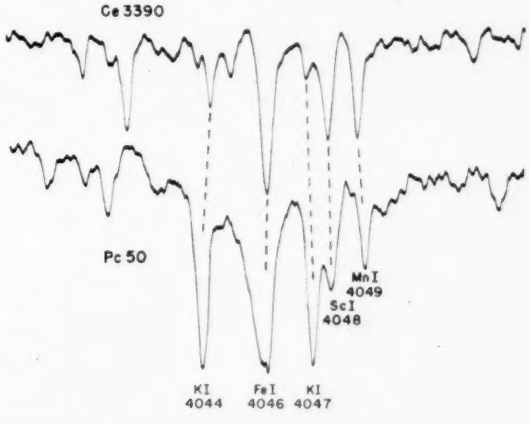

FIG. 3.—Comparison of lines of *K* I in the spectrum of R Hydrae. *Above*, Ce 3390, taken on February 10, 1944, magnitude 4.7, 19 days before maximum. *Below*, Pc 50, taken on January 21, 1951, magnitude 8.9, 18 days after minimum. The scale of the lower tracing is slightly greater than that of the upper.

These lines are sensitive indicators of temperature; they should be subjected to quantitative study at various phases of the light-cycle. For the *Al* I lines the form of the profile as well as the equivalent width may be of interest; on the maximum plate (Fig. 2) the lines are asymmetrical, having wings on the longward edges of strong cores. Micrometer measurements of these cores show them to be displaced −0.07 A with respect to numerous other dark lines. On the minimum plate the *Al* I lines are about as strong as H and K of *Ca* II, an effect seldom seen in stellar spectra. The surprisingly high intensity of the *Ca* II lines near minimum light may be due to the extremely low density of the star's outer atmosphere. The *Fe* I line λ 4045, E.P. 1.5 volts, appears in Figure 2 to be weaker at maximum than at minimum, but this is probably due partially to the filling-in of the shortward side by emission; possibly at minimum the dark line is reinforced on the shortward side by another dark line too close to be seen separately.

One or more bright lines of the Balmer series were measured on all plates except Pc 50, the intensity increasing from month to month after minimum. The first one to appear is *Hδ*, which is notched by a minimum whose wave length is close to that of the *In* I line λ 4101.76. Because the bright lines have a negative shift with respect to the dark lines, the *In* line lies clearly longward from the center of *Hδ*. The apparent maximum of the bright *Hδ* line would yield a fictitiously large negative displacement.

On plate Pc 50, the bright *Fe* I line λ 4308 is clearly seen, a holdover from the preminimum phase; another holdover line, *Mg* I λ 4571, was probably bright at the same time but was not included in the spectral region observed. Both of these bright lines disappeared before the next plate was taken. On the following plates two bright lines of *Si* I and one or two of *Fe* II were present.

Radial velocities derived from bright and dark lines are listed in Table 1. The velocities from the bright hydrogen lines are considerably higher algebraically than those measured previously at maximum light. The new results combined with the earlier observations[1] indicate that, from the first appearance of the bright hydrogen lines during the rising phase of the light-curve to their disappearance before the next minimum, their radial velocity falls continuously through about 13 km/sec. This represents an outward acceleration of the emitting hydrogen atoms as they rise through the star's atmosphere.

The dark lines, on the other hand, yield about the same velocity shortly after minimum light as they do at maximum. There is a drop of some 8 km/sec after maximum.[1]

Generally speaking, the motions of the reversing layers of Me variables are relatively small and appear to differ not only from star to star but from cycle to cycle in the same star. At present, general conclusions concerning pulsations of the reversing layer or other types of systematic motion affecting the dark lines are most uncertain.

SPECTROSCOPIC OBSERVATIONS OF STARS OF CLASS S

PAUL W. MERRILL
MOUNT WILSON AND PALOMAR OBSERVATORIES
CARNEGIE INSTITUTION OF WASHINGTON
CALIFORNIA INSTITUTE OF TECHNOLOGY
Received February 27, 1952

ABSTRACT

This paper presents a brief survey of S-type spectra based largely on spectrograms with dispersion 9 A/mm of eight stars obtained by I. S. Bowen with the 200-inch telescope. The intensities of several groups of absorption lines and bands and of the more important emission lines are compared in various stars. Radial velocities from both bright and dark lines and a supplementary list of absorption lines identified in the green region are included. The remarkable behavior of certain bright lines of *V* I and of *Cr* I in the spectrum of R Cygni is described.

The spectrograms that, many years ago, led to the recognition of a third type of red stars[1] paralleling the M-type and N-type branches were taken with the 60-inch and 100-inch telescopes with a dispersion at $H\gamma$ of about 35 A/mm.[2,3] The spectrum was well shown only between $H\beta$ and $H\gamma$. More recently, special studies of R Andromedae[4,5] and of χ Cygni,[6] a long-period variable apparently intermediate between classes M and S, were made with a scale of 10 A/mm, and the spectral region studied was extended shortward to about λ 3400. With the 100-inch telescope, unduly long exposures would be required to obtain satisfactory spectra of additional stars on the same scale. The Hale telescope, with its greater light-gathering power and its larger coudé spectrograph (allowing the use of a wider slit), has greatly reduced the necessary exposure times and has thus made it feasible to obtain observations of additional S-type stars.

This paper presents a brief survey of S-type spectra based largely on spectrograms of eight of the brighter S-type stars (Table 1) obtained by I. S. Bowen during the course of testing and adjusting the 200-inch telescope and coudé spectrograph. I am greatly indebted to him for these valuable photographs.

The new material provides more detailed information than that previously available concerning the atomic lines in the spectra of six long-period variables near maximum light; one irregular variable of small range, AA Cygni; and one nonvariable star, HD 22649. Three plates of R Cygni at intervals of a month show marked changes, especially in the bright lines.

The intensities of several features of the spectrum are indicated by the estimates in Table 2. Several additional variables are included for comparison. The wave lengths upon which these estimates are chiefly based are listed in Table 3.

Estimates of the intensities of *ZrO* and *TiO* bands are accordant with those previously made[3] on low-dispersion spectrograms. Stars with pure, well-advanced S-type spectra—bands of *ZrO* well marked, those of *TiO* weak or absent—are R Gem, T Sgr, and R Cyg. The star R And is of type S with fairly strong bands of *TiO*. Stars that may be said to be intermediate between types S and M are U Cas, HD 22649, AA Cyg, Z Del, and

[1] *Trans. I.A.U.*, **1**, 98, 1922.
[2] P. W. Merrill, *Mt. W. Contr.*, No. 252; *Ap. J.*, **56**, 457, 1922.
[3] P. W. Merrill, *Mt. W. Contr.*, No. 325; *Ap. J.*, **65**, 23, 1927.
[4] P. W. Merrill, *Mt. W. Contr.*, No. 730; *Ap. J.*, **105**, 360, 1947.
[5] P. W. Merrill, *Mt. W. Contr.*, No. 743; *Ap. J.*, **107**, 303, 1948.
[6] P. W. Merrill, *Mt. W. Contr.*, No. 735; *Ap. J.*, **106**, 274, 1947.

χ Cyg. An example of pure M type is R Leo; o Cet and R Hya are principally M type but with departures in the direction of the S-type characteristics.

Lines of *Ba* II λ 4554 and λ 4934 appear especially strong in S-type stars. In comparing estimates of their intensities in various stars, however, it should be remembered that *TiO* bands, when present, tend to obscure these *Ba* II lines.

The intensities of certain low-temperature (ground-level) lines (Tables 2 and 3) may

TABLE 1

SPECTROGRAMS OF S-TYPE STARS TAKEN WITH THE 200-INCH TELESCOPE
(Dispersion 9 A/mm)

Star	Desig.	Mag. Range	Period (Days)	Plate Pc	Date 1951	Mag.	Phase (Days from Max.)	Exp. Min.
U Cas	004047	7.7– 15.0	281	127	July 25	8.9	+ 5	338
HD 22649	033362	5.3		141	Aug. 19	5.3	.....	30
				192	Oct. 16	5.3	.....	45
R Gem	070122	6.5– 14.3	370	68	Mar. 23	7.9	+39	305
S UMa	123961	7.0– 12.0	229	110	June 21	8.0	+ 9	305
				254	Jan. 14*	(8.5)	(−10)	190
T Sgr	191017	7.2–<13.1	396	124	July 21	8.4	+18	264
				137	Aug. 19	8.6	−39	280
R Cyg	193449	5.6– 14.4	428	154	Sept. 16	7.9	−11	300
				191	Oct. 16	8.0	+19	342
AA Cyg	200036	8.4– 9.2	202	115	June 26	(9)	.....	220
Z Del	202817	8.2– 14.0	304	112	June 22	9.5	+20	460

* 1952.

TABLE 2

INTENSITIES OF LINES AND BANDS

Star	Plate	Absorption					Emission					
		ZrO	*TiO*	*Ba* II	Low-Temp.	*Tc* I	*H*	*Fe* II	*Mg* I	*Si* I	*In* I	*Co* I
R And	Ce 3522	8	3	5	8	4	10	3	2	3	3	2
U Cas	Pc 127	7	7	5	6	3	10	3	1	3	1	2
HD 22649	Pc 192	2	2	5	6	1	0	0	0	0	0	0
R Gem	Pc 68	5	0	10	7	5	10	3	2	2	3	3
S UMa	Pc 110	1	0	7	4	1	10	3	1	2	1	1
T Sgr	Pc 124	7	0	7	5	3	10	3	2	3	4	3
R Cyg	Pc 137	10	0	10	5	3	10	2	2	2	2	3
AA Cyg	Pc 115	8	7	7	8	4	0	0	0	0	0	0
Z Del	Pc 112	2	7	3	3	1	10	3	1	2	0	2
χ Cyg	Ce 3762	5	20	3	10	3	10	3	2	5	4	2
o Cet	Ce 4109	1	15	1	7	2	5	1	0	2	1	0
	Ce 5925	1	10	2	6	1	10	3	1	2	0	1
R Hya	Ce 3390	1	15	3	7	1	7	3	1	3	0	1
R Leo	Pc 40	0	20	1	10	0	10	4	4	6	3	0

be taken to indicate the temperature of the reversing layer, 8 or 10 corresponding to about 2300°, lower intensities to higher temperatures.

Lines of *Tc* I, an element believed to have no completely stable isotope, appear to be stronger in the stars with the more dominant S-type characteristics. This fact, together with others, might suggest that S-type stars represent a comparatively transient phase of stellar existence.

TABLE 3

WAVE LENGTHS OF FEATURES USED FOR ESTIMATES IN TABLE 2

Ident.	Wave Length
ABSORPTION	
ZrO	4471, 4620, 4638
TiO	4584, 4626, 4761, 4955
Ba II	4554, 4934
Low-temp.:	
Al I	3944, 3961
K I	4044, 4047
Ca I	4226
Cr I	4254, 4274, 4289
Sr I	4607
Tc I	4031, 4238, 4262, 4297
EMISSION	
H	*Hβ*–*H*11
Fe II	4233, 4583, 4924, 5018
Mg I	3829, 3832, 3838 5167, 5172, 5183
Si I	3905, 4103
In I	4511
Co I	3894, 3997, 4118, 4121

Identified absorption lines in the green in addition to those recorded in Table 2 of *Mount Wilson Contributions*, No. 743,[5] are listed in Table 4.

The radial velocities of these eight S-type stars measured on the coudé spectrograms are recorded in Table 5. They do not differ greatly from those measured previously[7] with low dispersion. The relative displacement of bright and dark lines tends to increase with the period of light-variation, but for the longer periods the difference is somewhat less than that previously found.[8]

In addition to the bright lines mentioned in *Mt. W. Contr.*, No. 730,[4] Tables 7–12, the green lines of *Mg* I λλ 5167, 5172, 5183 have been observed in emission in several S-type variables. These, like the ultraviolet lines λλ 3829, 3832, 3838, behave so differently from the postmaximum line *Mg* I λ 4571 that they must be produced by a different mechanism. The upper level of λ 4571, 4^3P^o, is fed by the emission of λ 3832 and of λ 5172, but toward minimum light the population of this level must be increased by some other process. A promising investigation would be a comparative study of multiplets 1, 2, and 3 of *Mg* I in the spectrum of an S-type variable at various phases of its light-cycle.

[7] P. W. Merrill, *Mt. W. Contr.*, No. 649; *Ap. J.*, **94**, 171, 1941.

[8] P. W. Merrill, *Mt. W. Contr.*, No. 644; *Ap. J.*, **93**, 380, 1941.

TABLE 4

ADDITIONAL ABSORPTION LINES IN SPECTRA OF CLASS S*

λ	El.	Mult.	λ	El	Mult.
4799.79	*V*	3	5079.74	*Fe*	16
4937.72	*Ti*	39	5081.55	*Sc*	13
4939.69	*Fe*	16	5083.34	*Fe*	16 bl
4947.99	*Ti*	39	5083.71	*Sc*	13 bl
4964.71	*Ti*	173	5085.55	*Sc*	13
4977.73	*Ti*	173	5086.95	*Sc*	13
4978.19	*Ti*	173	5098.70	*Fe*	66
4989.14	*Ti*	173	5099.23	*Sc*	13
5021.90	*Cr*	8	5101.12	*Sc*	13
5025.57	*Ti*	173	5107.45	*Fe*	16
5035.91	*Ti*	110	5110.41	*Fe*	1
5036.47	*Ti*	110	5123.72	*Fe*	16
5038.40	*Ti*	110	5127.36	*Fe*	16
5039.96	*Ti*	5	5133.42	*Zr*	27
5040.64	*Ti*	38	5142.93	*Fe*	16
5041.07	*Fe*	16	5147.48	*Ti*	4
5041.76	*Fe*	36	5152.18	*Ti*	4
5043.58	*Ti*	38	5166.29	*Fe*	1
5045.40	*Ti*	38	5168.90	*Fe*	1
5046.61	*Zr*	62	5171.60	*Fe*	36
5048.75	*Cr*	20	5173.74	*Ti*	4
5049.82	*Fe*	114	5192.77	*Ti*	4
5051.64	*Fe*	16 bl	5206.04	*Cr*	7
5051.90	*Cr*	8 bl	5208.44	*Cr*	7
5053.30	*W*	1 ?	5210.39	*Ti*	4
5065.98	*Ti*	110	5219.68	*Ti*	4
5068.29	*Cr*	20	5225.53	*Fe*	1
5070.25	*Sc*	13	5247.05	*Fe*	1 bl
5071.48	*Ti*	110	5247.56	*Cr*	18 bl
5072.92	*Cr*	8	5254.96	*Fe*	1
5075.81	*Sc*	13	5264.15	*Cr*	18
5078.28	*Zr*	62	5265.72	*Cr*	18
5079.23	*Fe*	66			

*See *Mt. W. Contr.*, No. 743; *Ap. J.*, **107**, 303, 1948.

TABLE 5

RADIAL VELOCITIES OF S-TYPE STARS

STAR	PLATE PC	PHASE (DAYS)	EMISSION (KM/SEC)		ABS. (KM/SEC)	NO. ABS. LINES
			H	Misc.		
U Cas	127	+ 5	−59	−56	−44.8	49
HD 22649	141	.....	.....	.....	−16.4	30
	192	.....	.....	.....	−13.9	31
R Gem	68	+39	−53	−51	−40.5	121
S UMa	110	+ 9	− 5	− 6	+ 5.2	102
	254	(−10)	+ 1	.....	+11.2	24
T Sgr	124	+18	− 8	−10	+ 5.4	64
R Cyg	137	−39	−40	−39	−23.3	90
	154	−11	−45	−42	−28.8	99
	191	+19	−48	−42	−32.1	126
AA Cyg	115	.....	.....	.....	+ 9.0	183
Z Del	112	+20	+24	+23	+36.8	57

In the spectrum of R Gem, Plate Pc 68, numerous bright lines in addition to those of *H* are present. Elements represented are *Mg* I, *Si* I, *Ti* II?, *V* I?, *Cr* I?, *Fe* I, *Fe* II, *Co* I, *Ni* I, *In* I.

An even more remarkable set of bright lines is present on the first plate, Pc 137, of R Cyg. In *Cr* I all the strongest lines of multiplets 23, 24, 25, and 26 are present. Table 6

TABLE 6

EMISSION LINES IN THE SPECTRUM OF R CYGNI
Pc 137

λ	J	Intensity	
		Lab.	Star
	V I (24) $a^6D-y^4F^\circ$		
4209.86	$4\frac{1}{2}$–$4\frac{1}{2}$	20	1
4198.61	$3\frac{1}{2}$–$3\frac{1}{2}$	4	0.7
4218.71	$4\frac{1}{2}$–$3\frac{1}{2}$	4	1
4219.51	$3\frac{1}{2}$–$2\frac{1}{2}$	2	0.3
4189.84	$3\frac{1}{2}$–$4\frac{1}{2}$	12	0.7
4182.59	$2\frac{1}{2}$–$3\frac{1}{2}$	10	1
4191.56	$1\frac{1}{2}$–$2\frac{1}{2}$	10	1.4
	V I (25) $a^6D-z^6G^\circ$		
4179.42	$4\frac{1}{2}$–$4\frac{1}{2}$	15	1.6
4159.69	$3\frac{1}{2}$–$4\frac{1}{2}$	8	1
	Cr I (22) $a^5D-z^5F^\circ$		
4351.77	5–5	100	1
4344.51	3–4	100	Tr
4339.6	2–3	75	2
	0–1	60	
4337.57	1–2	75	Tr
4384.98	4–4	75	1
4371.28	3–3	75	3
4359.63	2–2	75	1
4351.05	1–1	75	3
4412.25	4–3	40	1
4391.75	3–2	40	1.5
4373.25	2–1	35	4

shows the relative intensities in laboratory and star. The spread appears to be considerably less in the star. An equally interesting example is furnished by multiplet 22 of *Cr* I (Table 6). Here the correspondence of intensities is poor, the lines from upper-level $z^5F_1^\circ$ appearing to be unduly intense in the star. The energy of this level corresponds to a line of wave length 3247.18 A. This wave length is 0.36 A shorter than that of a strong line of *Cu* I, but the near-coincidence is probably not significant. The bright lines of Table 6 are much stronger on plate Pc 137 taken 39 days before maximum light than on plates

taken, respectively, 28 and 58 days later. Thus they behave differently from most emission lines in the spectra of long-period variables, in that they are strongest a month or more *before* maximum light. The curious behavior of these emission lines poses several interesting problems: (1) Why are certain multiplets emphasized? (2) Why do the relative intensities of the lines differ from those in the laboratory? (3) Why do the intensities decrease so abruptly as the star approaches maximum light? R Cyg obviously deserves intensive spectroscopic observation at various phases of the light-cycle.

I wish to thank Mrs. Mary Coffeen for valuable assistance in measuring and computing.

THE SPECTRUM OF THE ECLIPSING VARIABLE R ARAE

JORGE SAHADE
Observatorio Astronómico de Córdoba, Argentina
Received February 25, 1952

ABSTRACT

R Arae is probably a system similar to β Lyrae, and the differences in spectroscopic behavior between the two systems may be due principally to differences in the relative dimensions of the objects. The spectrum is B9 and shows changes throughout the cycle of light-variation. The secondary spectrum is not observed even at mid-eclipse. Photoelectric observations of R Arae and an orbital solution from them are highly desirable.

R Arae[1] is another southern eclipsing variable on the writer's observing program, the photometric elements of which suggest that the star is promising for spectrographic observations. The material on which this investigation is based includes 118 measurable plates obtained through the years 1946, 1947, 1948, 1950, and 1951, with a dispersion of about 42 A/mm and a projected slit-width which varied from 0.019 to 0.038 mm. Prior to October, 1946, the exposures were made on Eastman 103-O plates, thereafter on Eastman 103*a*-O emulsion; there are also some exposures taken on Eastman 103-F, 103*a*-F or 103*a*-E emulsions, practically always trailing the star along the slit.

The variability in light of R Arae was discovered by Roberts[2] at Lovedale in 1892. He readily established its Algol type of variation and determined a light-curve, based on 958 visual observations, which "on either side of minimum can be represented under the form Mag. $= m + \alpha t + \beta t^2$, where m is the magnitude at minimum, and t the time to or from minimum. The light changes are completed in 9^h12^m. There is no stationary phase at minimum, and only the slightest evidence of a secondary minimum."[3] According to Roberts, the magnitude is 6.8 at maximum and 7.9 at the middle of primary eclipse.

R Arae has been further studied photometrically by Hertzsprung[4] and by Mrs. C. Payne-Gaposchkin.[5] The former derived, for the epoch of minimum, the expression

$$\text{JD } 2425818.028 + 4.42507E \text{ days} \pm 0.007 \pm 0.00003 \text{ (m.e.)},$$

"which does not indicate any change of period since the observations by Alexander W. Roberts." Hertzsprung's expression has been used for the computation of the phases of our spectrograms; the time of minimum thus computed seems to fit the present spectrographic observations.

Mrs. Gaposchkin's study of 1340 estimations on Harvard plates led to the following elements:

Period	4.42509 days	m_1	6.97 mag.
M_1	6.05 mag.	m_2	6.20 mag.
M_2	6.05 mag.		

[1] $\alpha = 16^h35^m6$; $\delta = -56°54'$ (1950.0). h 4866 A = CD−56°6482 = CPD−56°7804 = GC 22364 = HD 149730 (Sp. B9).

[2] *A.J.*, **14**, 113, 1894.

[3] *A.J.*, **21**, 81, 1901.

[4] *B.A.N.*, **9**, 277, 1942. Some of the magnitude estimations used by Hertzsprung were made by Kruytbosch.

[5] *Harvard Ann.*, **115**, 46, 1945.

("the epoch 2429433.348 being perhaps a good starting point"). "$D \sim 0.12\ P$. The light curve is a β Lyrae type with two well-defined minima. The period of R Arae seems to be constant within the 45 years of our observations."[6] In his recent catalogue, Plaut[7] states that "the [Harvard] magnitudes probably include the light of the visual companion."

R Arae shows only one spectrum, of type around B9, whose spectral features undergo changes throughout the cycle of light-variation (Fig. 1); they may not exactly repeat themselves at different cycles and may even be slightly different on consecutive plates.

The *H* lines, around mid-eclipse, are faint. Immediately after it, the lines begin to deepen and to be better defined, and at phase 0.09 days they are sharp and strong. This is the general appearance of the *H* lines, which sometimes even look like "shell" lines, suggesting that they are produced in a gas of low pressure, of a density somewhat different at different phases and/or cycles. However, on some plates between phases 0.28 and 0.35 days the lines look narrow and flat-bottomed; on those taken at phases 0.64, 1.61, 1.76, 2.23, 2.89, 2.96, 3.08, 3.18, 3.67, 3.76, and 4.24 days the *H* lines are also narrow but are fainter than usual, suggesting a smaller optical depth; or they give the impression of a core superimposed upon a wider and shallower line, as at phase 3.32 days. This underlying and relatively wide line is seen alone at phases 0.5–0.6, 1.4, 2.0, 2.77, and 3.91 days. At phases 0.92, 0.97, 1.26, 1.29, 1.50, 1.64, 2.08, 2.19, 2.27, and 2.34 days the *H* lines are strongly asymmetric, with a sharp violet core, giving the appearance of double lines but with such a profile that there is no doubt that we are dealing with a stellar line upon whose violet edge the quite narrow and strong core is superimposed. After about phase 2.4 days there may still be a slight asymmetry in the *H* lines, which seems to be in the opposite sense at around phase 3 days. The Balmer series is seen up to about *H*17 when the lines are narrow, and up to *H*15 when the lines are relatively wide. In order to find out whether or not the spectrum displays *H* emission at *Hα*, six plates were obtained at phases 1.355, 2.282, 3.078, 3.224, 3.269, and 4.121 days, on F or E emulsions; the observational facts are that *Hα* in absorption is missing as though it were covered by emission; that, at phases 1.355 and 3.078 days, very faint emission borders are suspected at *Hα*, in the first case, and at *Hβ* and *Hα* in the second case; and that, at phase 4.121 days, there seems to be present a strong red emission at *Hα*.

As far as the K line of *Ca* II is concerned, it is extremely faint or absent around mid-eclipse, and, outside of it, it is usually narrow and relatively strong. However, sometimes it is relatively faint and wide, as at phases 0.35, 0.64, 1.64–1.76, 2.21, 2.27, 2.30, 3.16, 3.43, 3.76, and 4.41 days; or it is extremely faint or absent, as at phases 0.50, 1.43, 2.00, 2.10, 2.23, 2.96, 3.08, 3.18, 3.42, 3.45, 3.91, and 4.06 days. At other times it is very sharp and gives the impression of being an interstellar line, as at phases 0.6, 1.26, 1.92, 3.07, 3.34, 3.67, and 4.11–4.35 days.

The *He* I lines are generally very faint, and, at around mid-eclipse, they are extremely faint or absent.

On a very few plates, the K line of *Ca* II and perhaps *He* I 4026 look double, but they are very faint for measurement except on the plate taken at phase 0.972 days.

The *Mg* II 4481 line is very faint (on some plates it is practically absent)—too faint for the spectral type concerned and usually fainter than *He* I 4471. But, in some cases, the situation is reversed, as observed at phases 1.663, 2.048, 2.152, 2.297, 2.959, 3.155, 3.184, and 3.388 days. The behavior of the line of *Mg* II indicates that dilution effect of variable amount is present.

The radial velocities of R Arae were determined by measuring the lines of *H*, *Ca* II, *He* I, and *Mg* II in the wave-length interval λλ 3770–4482. As mentioned in the description of the spectrum, the *He* I lines are very faint, and, therefore, the measurement of this element has been limited to a small number of plates; furthermore, the lines meas-

[6] Private communication of Dr. Sergei Gaposchkin, September 19, 1950.

[7] *Pub. Kapteyn Astr. Lab. Groningen*, No. 54, 1950.

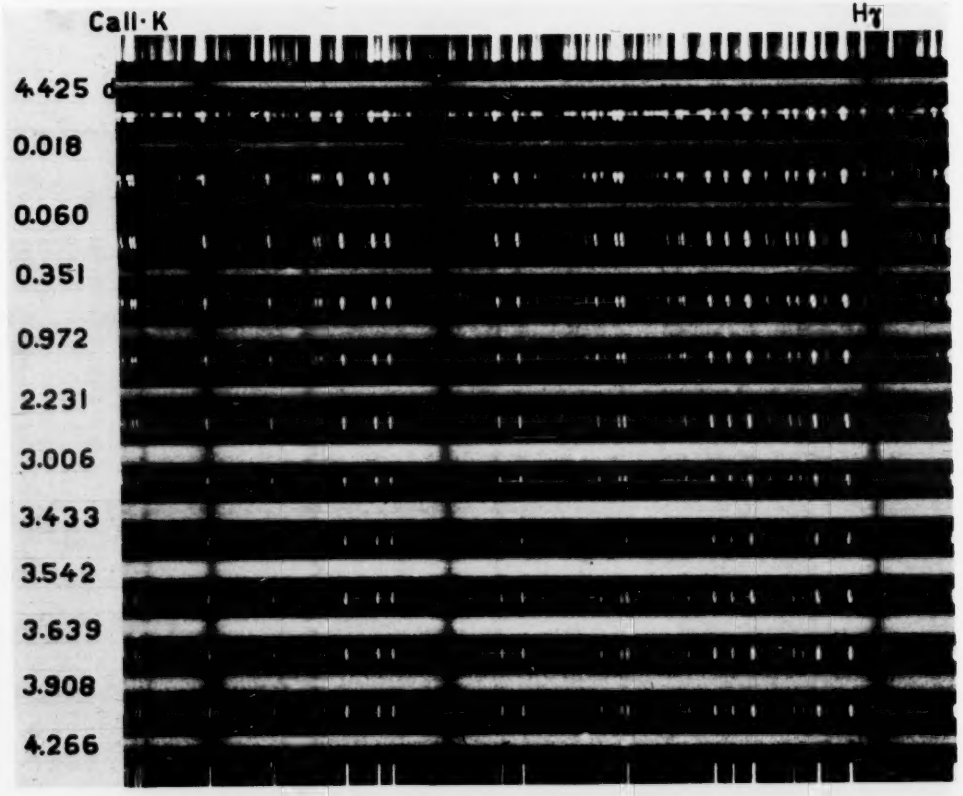

FIG. 1.—Positive enlargements of spectra of R Arae

ured were very few, usually 4026, and/or 3820 and 4471. The measurement of the *Mg* II line has been possible only on six plates. The wave lengths used are those which were employed in previous work. Table 1 gives the radial-velocity values for the individual plates, and Figures 2, 3, and 4 show their plots for the four elements measured. On the *H* plot, "p" indicates a poor plate and the circles represent the results from the measurement of the red wings of the clearly asymmetric lines. The emission borders suspected on the plate taken at phase 3.078 days suggest velocities of ± 300 km/sec and the red emission on the plate obtained at phase 4.121 days ones of $+280$ km/sec.

The double lines of *Ca* II and *He* I, measured at phase 0.972 days, give -120 and $+6$ km/sec for *Ca* II, and -176 and -19 km/sec for *He* I 4026. These values are not shown on the plots.

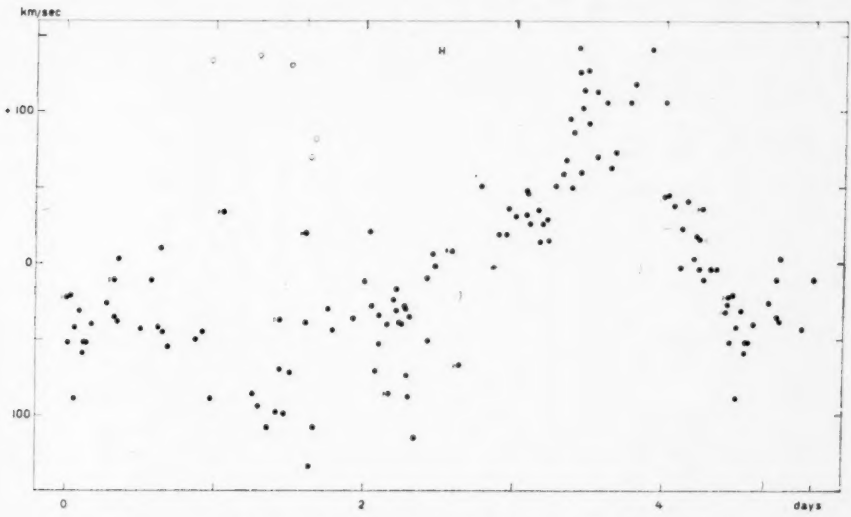

FIG. 2.—Radial velocities of R Arae from *H*

If we combine the radial-velocity results with the spectral characteristics shown by our material, we may make the following statements.

1. Immediately after mid-eclipse, according to Hertzsprung's time of minimum, the velocities are more negative than the velocity of the system as suggested by the plots; therefore, we may conclude that, immediately after mid-eclipse, we face a mass of gas moving toward us. This seems to be true for *H*, *Ca* II, and *He* I.

2. After about phase 0.28 days the measured velocities of *H* are less negative than at the previous phases. The line profiles are sometimes suggestive of turbulent motion.

3. After phase 0.35 days the *H* lines begin to look asymmetric, with a sharp violet core. This appearance is not very clearly defined until about phase 0.97 days, that is, near first quadrature, and we are therefore able to measure the core only after that phase. The asymmetry in the sense mentioned is clearly shown on several plates up to around phase 2.4 days. The core velocities are very negative. The measurement of the red part of the asymmetric lines gives high velocities of recession, which are indicated by circles on the plot shown in Figure 2, but these results are probably spurious because we may be measuring only a wing of the underlying line. Sometimes, during the asymmetric stage, the core is not shown, and the velocities obtained are more positive than

TABLE 1

RADIAL VELOCITIES OF R ARAE

PLATE	DATE	U.T.	PHASE (DAYS)	RADIAL VELOCITIES (KM/SEC)			
				*H**	*Ca* II	*He* I	*Mg* II
S 348	1946 Oct. 16	23:42	0.010	− 22p	.....	.....	.....
I 165	1948 June 23	1:55	0.018	− 52	.....	.....	.....
166	23	2:22	0.036	− 21	.....	.....	.....
S 577	1947 July 27	5:48	0.060	− 89	−152	.....	.....
I 167	1948 June 23	2:58	0.061	− 42	− 67	.....	.....
S 165	1946 June 15	4:00	0.091	− 31	− 34	−101	.....
P	May 6	8:45	0.115	− 59	− 41	.....	.....
S 166	June 15	4:44	0.122	− 52	.....	.....	.....
167	15	5:12	0.141	− 52	− 37	.....	.....
168	15	6:01	0.175	− 40	− 24	.....	.....
I 1415	1950 Aug. 20	0:01	0.276	− 26	− 53	.....	.....
S 483	1947 Mar. 12	7:57	0.326	− 11p	− 40	.....	.....
48	1946 Apr. 23	7:07	0.329	− 35	.....	.....	.....
49	23	7:45	0.348	− 38	.....	.....	.....
484	1947 Mar. 12	8:32	0.351	+ 3	+ 29	.....	.....
I 147	1948 June 19	3:19	0.501	− 43	.....	.....	.....
149	19	5:06	0.575	− 11	.....	.....	.....
S 74	1946 May 11	7:06	0.620	− 42	.....	.....	.....
618	1947 Aug. 10	2:17	0.638	+ 10	− 21	.....	.....
75	1946 May 11	7:50	0.651	− 45	.....	.....	.....
76	11	8:40	0.686	− 55	.....	.....	.....
G	Oct. 9	0:00	0.873	− 50	.....	− 56	.....
S 583	1947 July 28	2:26	0.919	− 45	− 33	− 81	.....
584	28	3:42	0.972	− 89	†	†	.....
596	Aug. 6	2:10	1.058	+ 34p	+ 31	.....	.....
I 98	1948 Apr. 23	8:49	1.256	− 86	+ 8	−111	.....
1664	1951 Aug. 10	0:33	1.293	− 94	.....	.....	.....
1665	10	2:04	1.356	−108	− 31	− 30	.....
1666	10	3:22	1.410	− 98	− 59	− 95	.....
G	1947 Oct. 2	23:47	1.433	− 37p	.....	.....	.....
I 156	1948 June 20	1:46	1.436	− 70	.....	−128	.....
1667	1951 Aug. 10	4:41	1.465	− 99	.....	− 75	.....
158	1948 June 20	3:20	1.502	− 72	.....	− 71	.....
S 91	1946 May 12	6:46	1.607	+ 20p	+ 3	.....	.....
625	1947 Aug. 11	1:34	1.608	− 39	− 13	.....	.....
92	1946 May 12	7:26	1.635	−134	.....	.....	.....
93	12	8:08	1.663	−108	.....	−134	.....
469	1947 Mar. 9	8:04	1.756	− 30	− 17	.....	.....
470	9	8:50	1.788	− 44	.....	.....	.....
593	July 29	2:34	1.925	− 36	− 9	.....	.....
638	Oct. 7	23:36	2.000	− 12	.....	− 91	.....
639	8	0:24	2.034	+ 21	.....	− 27	+ 4
I 1381	1950 Aug. 4	1:45	2.048	− 28	− 50	.....	.....
S 531	1947 July 7	3:12	2.077	− 71	− 26	.....	.....
I 1382	1950 Aug. 4	2:57	2.098	− 34	− 34	− 46	.....
175	1948 June 25	3:52	2.099	− 53	− 42	− 85	−43
1383	1950 Aug. 4	4:14	2.152	− 40	.....	.....	.....
S 185	1946 June 17	5:46	2.165	− 86p	.....	.....	.....
I 105	1948 Apr. 24	7:18	2.193	− 24	.....	.....	.....
106	24	7:47	2.213	− 31	.....	.....	.....
178	June 25	6:37	2.213	− 17	.....	+ 90	−16
107	Apr. 24	8:13	2.231	− 39	.....	.....	.....
108	24	8:40	2.250	− 40	.....	− 20	.....
109	24	9:04	2.266	− 28	.....	− 46	.....
S 491	1947 Mar. 14	6:41	2.274	− 30	+ 4	.....	.....
I 1695	1951 Sept. 2	3:18	2.282	− 74	− 71	.....	.....
S 552	1947 July 25	1:18	2.297	− 88	− 80	.....	.....
492	Mar. 14	7:21	2.301	− 35	− 57	.....	.....

* "p" indicates a poor plate. † See text.

TABLE 1—*Continued*

Plate	Date	U.T.	Phase (Days)	Radial Velocities (Km/Sec)			
				*H**	*Ca* II	*He* I	*Mg* II
S 553	1947 July 25	2:18	2.339	−115	− 63	.....	.....
323	1946 Oct. 14	23:18	2.418	− 10	.....	.....	.....
G.	1947 Oct. 3	23:36	2.425	− 51	.....	.....	.....
S 324	1946 Oct. 15	0:05	2.451	+ 6	+ 14	.....	.....
G.	1947 Oct. 4	0:40	2.470	− 2	+ 2	− 80	.....
S 105	1946 May 13	6:10	2.582	+ 8p	.....	.....	.....
107	13	7:28	2.635	− 67p	.....	.....	.....
I 44	1948 Feb. 27	8:34	2.772	+ 51	.....	+ 54	.....
1426	1950 Aug. 27	0:14	2.860	− 3	.....	.....	.....
1563	1951 Apr. 5	7:08	2.894	+ 19	+ 11	.....	.....
1564	5	8:22	2.945	+ 19	− 24	.....	.....
131	1948 June 17	4:06	2.959	+ 36	.....	.....	.....
1387	1950 Aug. 5	0:44	3.006‡	+ 31	− 3	+ 7	+36
1350	July 5	2:57	3.074	+ 48	.....	.....	.....
1388	Aug. 5	2:28	3.078	+ 32	.....	+ 87	.....
S 197	1946 June 18	3:50	3.084	+ 46	+ 67	.....	.....
543	1947 July 8	3:45	3.100	+ 26	.....	.....	.....
I 1389	1950 Aug. 5	4:18	3.155	+ 35	+ 10	+ 13	−25
1352	July 5	5:14	3.169	+ 14	+ 2	.....	− 9
127	1948 June 4	2:54	3.184	+ 26	.....	.....	.....
1390	1950 Aug. 5	5:44	3.214	+ 29	+ 20	.....	.....
1428	Sept. 14	1:46	3.224	+ 15	+ 42	.....	.....
1699	1951 Sept. 3	2:59	3.269	+ 51	+ 32	.....	.....
S 562	1947 July 26	1:47	3.317	+ 59	.....	+ 52	.....
I 1656	1951 July 12	2:10	3.335	+ 68	+ 49	.....	.....
S 563	1947 July 26	2:49	3.360	+ 95	+ 54	+ 39	.....
I 1675	1951 Aug. 20	23:02	3.379	+ 50	+ 45	.....	.....
1657	July 12	3:26	3.388	+ 86	− 11	.....	.....
S 332	1946 Oct. 15	23:20	3.420	+142	.....	.....	.....
G.	1947 Oct. 4	23:40	3.428	+126	+ 92	+117	.....
I 1676	1951 Aug. 21	0:20	3.433	+ 60	+ 79	.....	.....
1658	July 12	4:46	3.444	+102	+ 49	.....	.....
S 333	1946 Oct. 16	0:09	3.454	+114	.....	.....	.....
G.	1947 Oct. 5	0:55	3.480	+127	+ 65	+ 77	.....
I 1677	1951 Aug. 21	1:36	3.486	+ 92	+111	.....	.....
1678	21	2:56	3.542	+113	+103	.....	.....
84	1948 Apr. 21	5:31	3.544	+ 70	.....	+ 61	.....
1679	1951 Aug. 21	4:24	3.603	+106	+ 53	.....	.....
87	1948 Apr. 21	7:49	3.639	+ 63	+ 56	.....	.....
88	21	8:31	3.669	+ 73	+ 29	.....	.....
S 475	1947 Mar. 11	8:17	3.765	+106	.....	.....	.....
476	11	9:04	3.798	+118	.....	.....	.....
I 139	1948 June 18	2:53	3.908	+141	.....	.....	.....
1674	1951 Aug. 17	3:42	3.999	+ 44	.....	.....	.....
141	1948 June 18	5:07	4.001	+106	.....	.....	.....
1402	1950 Aug. 6	1:15	4.028	+ 45	+ 55	+ 24	.....
S 269	1946 July 20	2:46	4.064	+ 38	.....	.....	.....
I 1701	1951 Sept. 3	23:10	4.110	− 3	− 13	.....	.....
1403	1950 Aug. 6	3:30	4.121	+ 23	.....	.....	.....
1702	1951 Sept. 4	0:12	4.153	+ 41	.....	.....	.....
1703	4	1:20	4.200	+ 3	.....	.....	.....
1404	1950 Aug. 6	5:43	4.214	+ 18	+ 12	.....	.....
1431	Sept. 15	2:02	4.235	− 4	.....	.....	.....
S 459	1947 Mar. 7	9:22	4.236	+ 16p	.....	.....	.....
I 1704	1951 Sept. 4	2:38	4.254	+ 36p	.....	.....	.....
1418	1950 Aug. 23	23:46	4.266	− 11	0	.....	.....
1419	24	0:52	4.311	− 4	− 20	.....	.....
S 574	1947 July 27	2:34	4.350	− 4	− 7	.....	.....
I 163	1948 June 23	1:09	4.411	− 32p	.....	.....	.....
164	23	1:30	4.425	− 27	.....	.....	.....

‡ *Si* II yields −5 km/sec.

those from the core and much more negative than those from the red wings. At other times the red wing is practically absent. The behavior of the *H* lines at the phases under discussion suggests that we are observing a core produced in a mass of gas moving toward the observer and a wider and shallower line probably produced in the normal reversing layer of the primary star. Our belief that we are not dealing with two stellar lines arising from both components of the system finds confirmation in our failure to

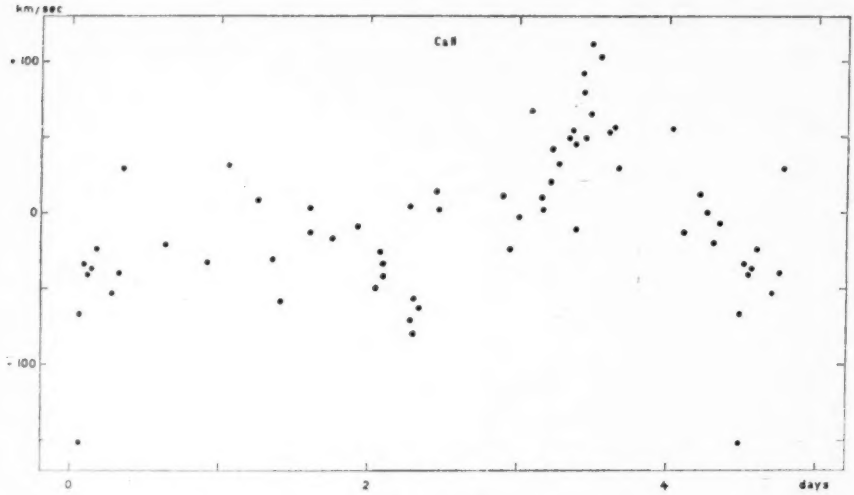

FIG. 3.—Radial velocities of R Arae from *Ca* II

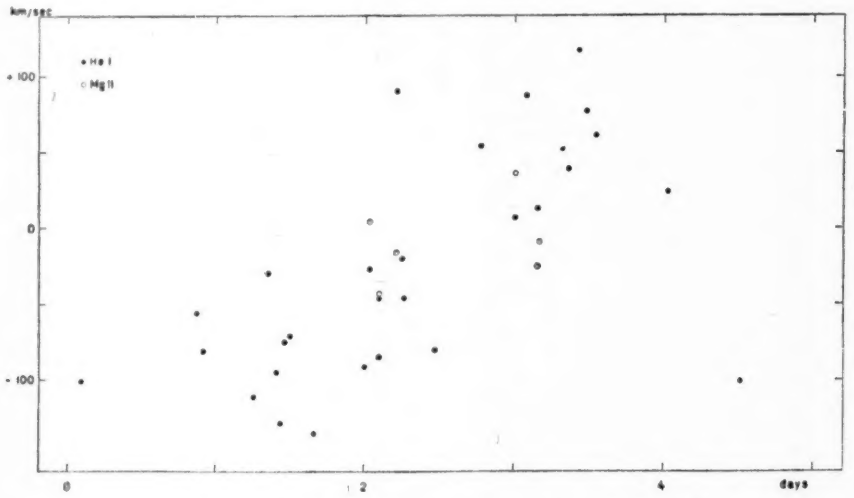

FIG. 4.—Radial velocities of R Arae from *He* I and *Na* II

observe double lines in the second half of the cycle, even at those phases where the measured velocities are strongly positive.

4. From about phase 2.4 days to about phase 3.3 days the *H* lines are fairly narrow; if any asymmetry affects them, it must be very small.

5. From about phase 3.3 days to about phase 4.0 days the radial velocities obtained are too positive, and the distribution of points is similar to the one characteristic of those systems with gaseous streams which belong to Struve's group III.[8] In the present case this distribution is rather peculiar, showing two "humps" which seem to be real. The *H* lines at the relevant phase interval are usually quite narrow, the impression being that the higher the velocity the fainter the lines. Furthermore, at the phases corresponding to the lowest values between the "humps" the lines are wider.

6. After phase 4.0 days, the lines usually are quite narrow and strong.

Let us try to clarify the nature of this important system by combining the available photometric data with our spectrographic observations. Considering Mrs. Gaposchkin's ranges for both minima of light and disregarding her ellipticity effect—which must be quite small in view of the Algol type of light-variation previously found by Roberts and in view of the values of the luminosities and radii of the components, namely, $L_P = 0.56$, $L_S = 0.44$, $a_P = 0.11$, $b_P = 0.10$, $a_S = 0.21$, $b_S = 0.20$, obtained by S. Gaposchkin[6] by assuming a "probably total" principal eclipse—and assuming spherical and uniformly illuminated stars, we deduce, by the well-known formula, that the ratio of the mean surface brightnesses is about 4.4. This suggests that the spectral type of the secondary star is early F. If the primary eclipse were total or nearly so, we would have $R_S/R_P \sim 1.8$ and $L_P/L_S \sim 1.3$ (the subscript "P" designating the primary B9 star and "S" the secondary component); therefore, this assumption implies that the spectrum at maximum must be double-lined and that at principal minimum we should observe only the secondary spectrum. Actually, we do not observe a double-lined spectrum at maximum, and the spectrum of the secondary star is not observed even at mid-eclipse, when the magnitude falls off by about 1 mag. Hence we must conclude that the primary eclipse is far from total and that $L_P \gg L_S$. The assumption of the secondary eclipse being total or nearly so leads to $R_S/R_P \sim 0.8$ and $L_P/L_S \sim 6.7$, values more in accordance with the spectrographic results, but the fact that the principal eclipse is far from total does not allow us to conclude that the secondary eclipse should be so.

Now the fact that even at mid-eclipse we do not observe the secondary spectrum requires that $L_P/L_S \gtrsim 2.5$, and this, assuming $J_P/J_S \sim 4.4$, leads us to a ratio $R_S/R_P \lesssim 1.3$. However, we must have $i \sim 90°$ (Gaposchkin's[6] solution gives $i = 85°.8$) because of the depth of the principal eclipse and because the spectral features observed are those usually associated with phenomena which are confined to a rather limited area about the orbital plane; and, if this assumption is a correct one, we cannot escape from the conclusion, in view of all the former considerations, that the secondary star has a radius smaller than the one of the principal component.

As far as the interpretation of the spectroscopic behavior of the system is concerned, we believe that we are dealing with a close binary system showing gaseous streams, with Kuiper's ejection mechanism of type B at work.[9] Let us refer to the *H* radial velocities. The mass of gas moving toward us, immediately after mid-eclipse, is interpreted as the escape of gas through the Lagrangian point L_2 of the *problème restreint*. And the negative displaced core which is clearly observed until about phase 2.4 days must be produced in an expanding ring formed by the material escaping through L_2, the velocity of expansion being of the order of 100 km/sec. After about phase 2.4 days the density of the expanding material must be such that we are not able to detect its absorption effects. The peculiar distribution of velocities after phase $0.75P$ should result from

[8] *Observatory*, **71**, 197, 1951.

[9] *Ap. J.*, **93**, 133, 1941; *McDonald Contr.*, No. 28.

the motion of gases inside the Jacobian critical equipotential surface as described by Struve[10] in his George Darwin Lecture. The rapid decline and recovery of the *H* velocities around phase 3.65 days, which remind us of a somewhat similar phenomenon observed by McNamara[11] in U Sagittae, may be connected with the actual shape of the critical equipotential surface along which the gases move. Within our interpretation we would expect to observe, before phase $0.25P$, a symmetrical behavior of the gases inside that equipotential surface; but our failure in observing this feature may mean only that we have here another case in which the two halves of the stream are not alike, as has already been found, and which may be due to differences in ionization.[12] Furthermore, the phenomenon described by Struve[13] of the behavior of the *H* lines near eclipse in systems such as U Cephei may also affect the spectrographic results around eclipse and may explain our failure in observing high positive velocities after about phase 4.0 days.

If our interpretation is correct, we should conclude that we are dealing with a system similar to β Lyrae,[14] and the differences in the spectroscopic behavior of both systems, such as the lack of "satellite" lines during eclipse in R Arae, should be attributed to differences in the relative dimensions of the systems. In the present case the ratio of the radii must be nearer unity than in the case of β Lyr.

Let us see whether or not we can uncover some further information from the spectrographic results. We may disregard the peculiar distribution of points after $0.75P$ and try to disregard the effect of the expanding ring; and, in doing so, we estimate K in around 60 km sec, which implies $a_1 \sin i \sim 3.6 \times 10^6$ km and $f(\mathfrak{M}) \sim 0.10\ \odot$. If we assume for the B9 star a mass of around 4 $\odot$, it results that the mass of the secondary star is of the order of 1.4 $\odot$, or that the mass ratio is nearly 3. The secondary star would, then, be of spectral type F. The eccentricity suggested by our *H* plot must certainly be spurious and produced by the effect of the expanding ring, but our conclusion is valid even for a value of e as large as 0.3.

Our system does not show strong emission lines; perhaps McNamara's[11] remark with respect to U Cephei may be also applied to R Arae.

The plot for *Ca* II seems to suggest that the expanding gases are very poor in *Ca* II, and, in the first three-quarters of the cycle, the stellar line may in some cases be blended with an interstellar line. The atoms of *Ca* II within the gaseous stream observed after phase $0.75P$ produce the same effect as the *H* atoms.

The results from *He* I are too few in number to enable us to draw any definite conclusion, but it seems that *He* I shares the behavior of *H*.

In short, all our conclusions place R Arae in Struve's group IV[8] of close binary systems, whose prototype is β Lyr. It would be formed by a B9 primary and an F secondary, with $L_B \gg L_F$, $\mathfrak{M}_B > \mathfrak{M}_F$, and $R_B > R_F$. But we are also led to the conclusion that an accurate photoelectric light-curve of R Arae and a solution from it should be highly desirable. With this information, we shall be able to decide whether our interpretation and conclusions are correct or whether they should be modified.

I am greatly indebted to Drs. E. Gaviola, J. Landi Dessy, and R. Platzeck for kindly securing for me several spectrograms of R Arae and also to Mr. Julio Albarracín for assisting in the computation of the radial velocities.

[10] *M.N.*, **109**, 487, 1949.

[11] *Ap. J.*, **114**, 513, 1951.

[12] Struve, *Pub. A.S.P.*, **60**, 160, 1948.

[13] Address of the retiring president of the American Astronomical Society, *Pop. Astr.*, **58**, 7, 1950.

[14] Struve, *Ap. J.*, **93**, 104, 1941. Our statement that R Arae seems to be a system similar to β Lyr does not imply, of course, the remarkable spectroscopic features which are characteristic of the spectrum of the latter.

THE SPECTRUM OF S VELORUM

JORGE SAHADE
Observatorio Astronómico de Córdoba, Argentina
Received, January 7, 1952

ABSTRACT

The system of S Velorum is a binary composed of an A5 V and a K5 III star, with gaseous streams similar to those previously found in several other eclipsing variables. The primary star displays double emission of *H*, each component of which undergoes eclipse by the secondary star. The latter, which is observed only during eclipse, displays central emission of *Ca* II. This seems to be another case in which one or both components depart from the mass-luminosity relation. The velocity of rotation suggested by the observations is larger than the orbital velocity. There is evidence that the scatter shown by the *H* radial velocities is produced by the effect of prominences in the A5 star. Struve's "peanut model" seems to hold for the streams of *Ca* II, but in the case of those of *H* we may be dealing with Kuiper's ejection mechanism of type A.

Among the southern eclipsing stars on the writer's observing program with the 154-cm Bosque Alegre reflector, S Velorum[1] was very promising because of the large difference between both minima of light. The spectrographic material for the present investigation—eighty-eight measurable plates—was obtained principally through the years 1950 and 1951, with the Wood-grating spectrograph, which gives a dispersion of about 42 A/mm, and, except on four occasions, with a projected slit-width of 0.038 mm. The star was usually trailed along the slit, its projected length being of 0.22 mm. Eighty-six of the plates secured were taken on Eastman 103*a*-O emulsion, and two on Eastman 103*a*-E emulsion. At maximum light, the exposure times on the O plates were of the order of 1 hour. The ratio of the exposures for obtaining the spectrum of the primary star and that of the secondary star was of the order of 1:9 or 1:10.

PHOTOMETRIC ELEMENTS

The variability in light of S Vel was discovered by Woods[2] in 1894 at the Cape Observatory and was confirmed the same year by Roberts,[3] at Lovedale. Roberts[4] found that "the variation [is] very regular, and of well defined [Algol] type." Furthermore: "the nearer to minimum stationary period the more rapid the variation. The passing into and from the stationary phase is abrupt; the form of the light-curve at these two points being practically a right-angle." His published elements, derived from 648 visual observations, are as follows:[4,5]

Period	$5^d22^h24^m21^s.1$ or 5.933577 days
Descending phase	4^h20^m
Stationary phase at minimum	6^h18^m
Ascending phase	4^h20^m
Epoch of middle of minimum	1900 Jan. $1^d3^h43^m12^s$ (G.M.T.) or JD 2415021.155

In his classical "study of the orbits of eclipsing binaries," Shapley[6] considered Roberts' published observations—173 in number—for the determination of the orbital elements of S Vel, which were classed among the "first-grade orbits." Shapley's elements[7] are given in Table 1.

[1] $\alpha = 9^h31^m4$; $\delta = -44°59'$ (1950.0). CD−44°5573 = CPD−44°3864 = HD 82829 (Sp. A0).
[2] Chandler, *A.J.*, **14**, 53, 1894.
[3] *A.J.*, **14**, 113, 1894.
[4] *A.J.*, **21**, 81, 1901.
[5] *Vierteljahrsschrift d. Astr. Gesellschaft*, **51**, 357, 1916.
[6] *Contr. Princeton U. Obs.*, No. 3, p. 17, 1915.
[7] *Ibid.*, pp. 82, 83.

A new photometric investigation of S Vel has recently been made on Harvard plates by S. Gaposchkin,[8] who was able to detect the secondary minimum. Gaposchkin's elements are the following ones:[9]

Period	5.933693 days	Light of brighter component	0.76
Maximum	8.35 mag.	Light of fainter component	0.24
Primary minimum	9.89 mag.	Radius of brighter component	0.12
Secondary minimum	8.38 mag.	Radius of fainter component	0.25

TABLE 1

SHAPLEY'S ELEMENTS OF S VEL

	Uniform Solution	Darkened Solution*	
Magnitude at maximum	7.85		mag.
Range of primary minimum	1.39	1.39	mag.
Range of secondary minimum	[0.06]	[0.12]	mag.
Semiduration of primary	0.322	0.343	days
Semiduration of totality	0.120	0.106	days
a_0	1.00	1.00	
Light of brighter component	0.722	0.722	
Radius of brighter star	0.104	0.121	a_1+a_2
Radius of fainter star	0.230	0.233	a_1+a_2
$\cos i$	0.000	(0)	
Ratio of equatorial radii	1.00	1.00	
Ratio of surface intensities	13.0	9.6	

* "The darkened solution is restricted by the necessity of a central eclipse" (Shapley, *Contr. Princeton U. Obs.*, No. 3, p. 96, 1915).

When this paper was being written, Dr. D. O'Connell, S.J.,[10] very kindly communicated to the author some of his unpublished results from photographic observations of S Vel. They are as follows:

Epoch of minimum (heliocentric)	JD 2430786.862
Period	5.93367 days
Maximum	8.03 mag.
Primary minimum	10.50 mag.
Secondary minimum	8.06 mag.
Duration of primary	0.576 days
Duration of totality	0.236 days
Ratio of radii both stars	$\sim$ 0.55
Ratio of surface brightnesses	$\sim$30
Indication of slight ellipticity	

The photometric observations of S Vel, therefore, agree in indicating that we are dealing with a binary system in which the fainter component—that is, the star which is in front during primary minimum—has a radius about twice the radius of the brighter star and that the distance between their centers is nearly 4.5 times the former's radius.

In view of the ratio of the surface brightnesses which is suggested by the light-elements, it is safe to conclude that the spectrum taken at maximum light cannot be noticeably blended with light from the larger and fainter star.

[8] *Harvard Ann.*, 115, 197, 1950.

[9] Private communication of May 24, 1950.

[10] Private communication of October 3, 1951.

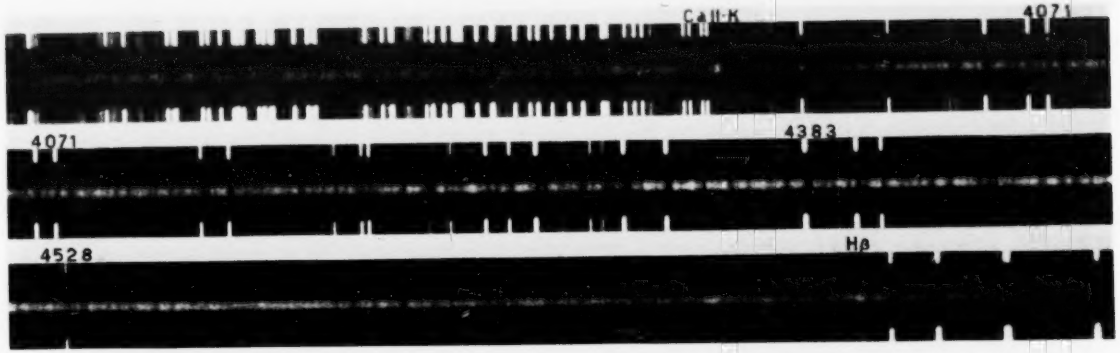

FIG. 1.—Spectrum of S Velorum at phase 0.018 days (plate I 1688) (positive enlargement)

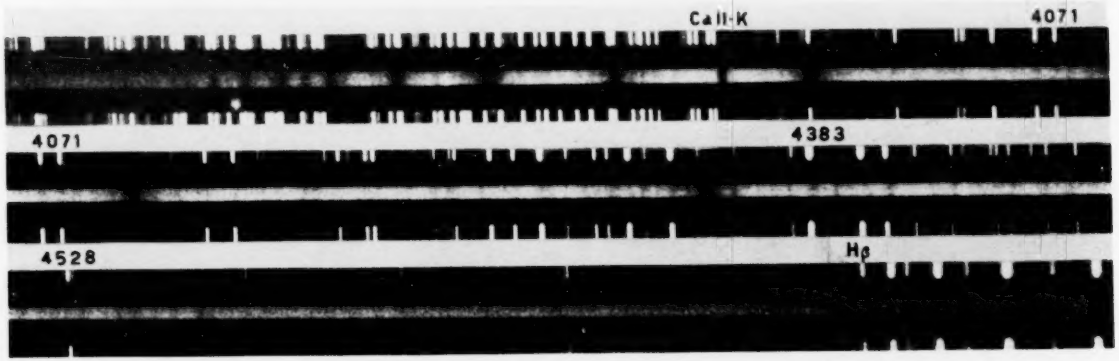

FIG. 2.—Spectrum of S Velorum at phase 2.178 days (plate I 1115) (positive enlargement)

As far as the orbital eccentricity is concerned, O'Connell[10] states that "the secondary minimum is so very shallow that there seems no hope of learning anything about the eccentricity of the orbit from the light-curve." However, from his mean light-curve, he "would take secondary minimum of S Vel as halfway between primary minima, but the minimum is so shallow that a displacement of, say, 0^d01, or perhaps even more, would be consistent with my observations."[11]

There is a discrepancy between Gaposchkin's and O'Connell's photographic depths for primary minimum, of nearly 1 mag. Roberts' visual range and the spectral type of the secondary star suggest that O'Connell's value is in order.[12]

THE TIME OF MID-ECLIPSE

The estimations of the star's brightness at the finder of the telescope suggested that the time of mid-eclipse actually falls too late when one computes it by means of Roberts' period and too early when one computes it by means of Gaposchkin's period—in both cases by taking as the starting point Roberts' value for the epoch of primary minimum. This was corroborated by the consideration of the spectral features as recorded on different plates, of the effective times of exposure, and of the distribution of the radial velocities at some critical phases which led to the conclusion that the time of mid-eclipse corresponds to about phase 5.78 days, as computed with Gaposchkin's period.

O'Connell's time for primary minimum does fit the Bosque Alegre observations, and, accordingly, the phases of the different spectrograms for the tabulation and plotting of the measured radial velocities have been computed with the expression

$$\text{JD } 2430786.862 + 5.93367E \text{ days};$$

and, in the discussion of results, phases 5.646, 5.816, 0.118, and 0.288 days will be considered to correspond to the times of beginning of eclipse, beginning of totality, end of totality, and end of eclipse, respectively, as indicated by O'Connell's elements.

Father O'Connell also mentions[10] that his period "fits my observations (from 1936 to 1951). Gaposchkin's period in *Harvard Annals* **115** definitely does not fit my observations. Roberts' minimum does not fit my elements. Perhaps the period is changing."

THE SPECTRUM

The spectroscopic features shown by S Vel outside principal eclipse and during total phases suggest that we are dealing in this case with a system of two stars, one of A5e V type, the other of K5e III type (Figs. 1 and 2), the latter being in front during primary minimum. The spectrographic observations agree with the photometric ones in indicating that the principal eclipse is total.

At maximum light we see only the A5 spectrum with strong and relatively narrow lines of *Ca* II and *H* and faint metallic lines.[13] The Balmer series is seen up to *H*16 or *H*17, which locates the star in the main sequence.[14]

The K line of *Ca* II undergoes changes throughout the cycle of light-variation. At the phases following eclipse, the line either shows a sharp core or is narrow with a flat bottom

[11] Private communication of October 25, 1951.

[12] After this paper was sent to press, the Library of the Córdoba Observatory received a copy of the 1951 Kukarkin and Parenago *Supplement* to their *General Catalogue of Variable Stars*, in which reference is made to a photographic photometric study of S Vel by Van Houten (*Leiden Ann.*, Vol. **20**, No. 7, 1950), who obtained the following results: Max. = 8.0 mag.; min. I = 10.8 mag.: JD 2429784.113 + 5.93366*E* days; $D = 0.10P$; $d = 0.044P$.

[13] Previous references to the spectral type at maximum light describe it as A0 (*Henry Draper Catalogue*, etc.) or A1 (Kukarkin and Parenago's 1948 *General Catalogue of Variable Stars* and Plaut's catalogue in *Pub. Kapteyn Astr. Lab.*, No. 54, 1950).

[14] Unsöld and Struve, *Ap. J.*, **91**, 365, 1940; Miczaika, *Zs. f. Ap.*, **25**, 268, 1948.

or sometimes even gives the impression that it is somewhat shaded shortward. Around 0.5 *P* the line is asymmetric, shaded toward the red, shows a sharp violet core, or is flat-bottomed. Afterward, it is deep and fairly narrow. At the phases following 0.75 *P* the line widens again slightly, and on some plates the line looks shaded toward the violet. At the partial phases the *Ca* II line becomes less strong, and it is sharper in the ascending than in the descending branch of the light-curve. The *H* lines are narrow and strong, but at some phases, especially after 0.75 *P*, they are slightly wider. The metallic lines of the A5 spectrum are faint, sometimes extremely faint. *Mg* II 4481 is diffuse at times; its intensity suggests that some dilution effect is present.

The A5 spectrum displays double emission lines of *H*, which were detected at *Hα* on two E plates; possibly the violet component is stronger than the red one. At the partial phases the emission components undergo eclipses: before mid-eclipse the presence of only a red component at *Hβ* is suspected on two rather underexposed spectrograms, and, after mid-eclipse, only a violet component is present at *Hβ*. The *Ca* II lines of the A5 component seem to share the same characteristics of the *H* lines, since violet bright components are present on the very good plates taken at phases 0.018 and 0.091 day.

The spectrum of the secondary star, which is observed alone during total phases, also displays emission lines. The K5 spectrum shows central bright cores of *Ca* II H and K. Furthermore, at the total phases, the spaces corresponding to the H and K absorption lines of *Ca* II seem to be almost entirely filled with emission. The classification of this spectrum was made by taking into consideration the criteria indicated by Morgan, Keenan, and Kellman in their *Atlas of Stellar Spectra*. The luminosity criteria indicate giant characteristics.

THE RADIAL VELOCITIES

The radial velocities of S Vel were determined by measuring, whenever it was possible, the lines listed by element and wave length in Table 2. *Hβ* and *Hα* were measured

TABLE 2

WAVE LENGTHS USED FOR THE DETERMINATION OF THE RADIAL VELOCITIES

H	*Ca* II	*Fe* I	*Fe* II	*Ca* I
3797.90	3933.66	4045.82	4233.17	4226.73
3835.39	3968.47	4063.60	4351.76	
3889.05		4071.74		
4101.74		4132.06		
4340.47		4325.76		
4861.33		4415.12		
6562.82				

just occasionally—three times and once, respectively—and on several plates the lines of *Fe* I, *Fe* II, and *Ca* I were not strong enough for measurement. The individual values obtained are tabulated in Table 3 and plotted in Figs. 3, 4, 5, 6, and 7. When measuring an asymmetric *Ca* II K line with a sharp core, the setting wire of the measuring machine was set upon the core.

In the tabulation and plotting of the *H* radial velocities, we have not included the results from plates at phases 5.751, 5.788, 5.810, 0.119, 0.163, and 0.163 days, respectively, that is, immediately before and after totality, for the reason which will be given below.

The double *H* emission lines suggest velocities of the order of 200 km/sec.

TABLE 3

RADIAL VELOCITIES OF S VELORUM

DATE	U.T.	PHASE (DAYS)	RADIAL VELOCITIES (KM/SEC) FROM				
			Ca II	*H*	*Ca* I	*Fe* I	*Fe* II
1951 May 5	0:23	0.018	+ 66*	+45	+ 75	+ 39	+ 62
Jan. 18	6:48	0.091	+ 54*	+49	+ 40	+ 45	.....
Jan. 30	4:16	0.119	− 47	†	+ 13	+ 22	.....
1950 Oct. 27	6:48	0.163	− 18	†	+ 12	− 8	+ 36
Feb. 8	4:51	0.163	− 42	†	− 15	− 12	− 10
1949 Feb. 11	6:04	0.168	− 14	+32	+ 34	+ 21	+ 18
Feb. 11	7:08	0.212	− 3	+24	+ 75	+ 17	+ 39
1950 Feb. 8	6:18	0.223	+ 22	+39	+ 32	− 20	+ 17
June 6	22:41	0.233	+ 43	+32	.....	.....	.....
Feb. 8	7:31	0.274	+ 38	+41	+ 47	+ 47	+ 47
June 6	23:55	0.284	+ 47	+40	.....	.....	.....
June 12	23:03	0.314	+ 50	+35	.....	.....	.....
Feb. 8	8:38	0.321	+ 52	+53	+ 67	.....	+ 87
June 7	1:06	0.333	+ 60	+70	.....	.....	.....
June 13	~ 0:25	~0.371	+ 42	+77	.....	.....	.....
June 13	1:33	0.418	+ 48	+75	.....	.....	.....
1951 Jan. 19	1:45	0.881	+ 17	.....	.....	.....	.....
1950 Jan. 28	1:50	0.905	+ 33	+43	+ 31	+ 21	+ 77
Jan. 16	7:21	1.002	+ 35	+38	.....	+ 29	.....
Feb. 3	2:54	1.015	+ 30	+52	+ 57	− 34	+ 37
May 9	2:18	1.052	+ 37	+52	+ 26	+ 76	+ 10
1951 Jan. 25	5:24	1.099	+ 39	+31	.....	.....	.....
1950 Feb. 3	6:30	1.165	+ 54	+31	+ 17	.....	+ 37
Mar. 5	3:10	1.358	+ 42	+34	.....	.....	.....
Mar. 11	2:12	1.384	+ 29	.....	.....	.....	.....
Jan. 17	1:24	1.754	+ 26	+35	+ 38	+17	+ 78
Jan. 11	8:06	1.967	+ 16	+60	+ 86	.....	+108
Jan. 20	5:14	2.026	+ 24	+19	.....	.....	.....
Feb. 10	5:13	2.178	+ 3	+ 1	.....	+ 1	.....
Feb. 28	0:58	2.200	+ 17	+28	+ 46	+ 17	+ 46
Feb. 4	7:46	2.218	+ 34	+36	+ 58	+ 17	+ 57
Mar. 6	2:34	2.333	+ 32	+48	+ 19	.....	+ 34
Jan. 12	1:44	2.702	+ 37	+18	+ 44	.....	+ 50
1951 July 11	23:41	2.718	+ 40	+36	.....	.....	+ 69
1950 Apr. 28	23:20	2.795	+ 49	+65	+ 67	+ 2	+ 12
Apr. 29	0:22	2.839	+ 57	+28	− 10	.....	+ 35
Apr. 29	1:34	2.889	+ 16	+42	+ 44	.....	+ 33
Jan. 12	6:39	2.906	+ 28	+32	+ 43	.....	+ 23
Feb. 5	1:00	2.936	+ 53	+33	+ 56	+ 57	+ 42
Apr. 29	2:55	2.945	+ 54	+64	+ 54	.....	+ 49
Jan. 18	6:22	2.961	+ 26	+34	+ 66	+ 4	− 5
1951 Jan. 21	6:26	3.076	+ 25	+22	.....	.....	.....
1950 Feb. 5	7:58	3.227	+ 23	+16	.....	+ 34	+ 9
Mar. 7	3:02	3.353	+ 31	+20	+ 41	.....	+ 26
Jan. 13	1:40	3.699	+ 43	+17	.....	.....	.....
Jan. 19	0:56	3.734	+ 50	+18	.....	+ 41	.....
Apr. 29	23:09	3.788	+ 31	+47	.....	.....	.....
Apr. 30	0:22	3.839	+ 66	+48	.....	.....	.....
Jan. 13	6:22	3.895	+ 62	+41	+ 67	.....	.....
Feb. 6	2:54	4.015	+ 66	+66	+106	.....	+ 81
Feb. 6	4:51	4.097	+ 61	+56	.....	+ 38	+ 63
June 4	22:38	4.164	+ 66	+83	.....	.....	.....
Feb. 6	~ 8:16	~4.239	+ 58	+51	.....	.....	.....
Mar. 8	1:36	4.293	+ 48	+38	.....	.....	.....

* Central emission.

† See p. 40, under "The Results."

TABLE 3—*Continued*

Date	U.T.	Phase (Days)	Radial Velocities (Km/sec) from				
			Ca II	*H*	*Ca* I	*Fe* I	*Fe* II
1950 June 16	23:13	4.321	+ 60	+49	.....	.....	.....
Jan. 14	1:45	4.702	+ 42	.....	.....	.....	.....
1951 Apr. 16	2:11	4.828	+ 61	+51	.....	.....	.....
Jan. 17	~ 2:30	~4.846	+ 44	.....	.....	.....	.....
Apr. 16	3:14	4.871	+ 46	+64	.....	.....	.....
1950 May 7	1:00	4.931	+ 84	+48	.....	.....	+108
May 7	2:16	4.984	+ 95	+83	+ 87	.....	+ 87
June 5	22:32	5.160	+ 83	+91	.....	.....	.....
Oct. 26	8:40	5.174	+ 96	+77	.....	.....	.....
June 5	23:45	5.211	+ 83	+73	.....	.....	.....
June 17	22:36	5.296	+ 93	+65	.....	.....	.....
1951 June 8	23:54	5.329	+103	+82	.....	.....	.....
1950 June 18	0:00	5.354	+120	+84	.....	.....	.....
June 23	22:35	5.361	+112	+65	.....	.....	.....
June 23	23:40	5.406	+ 96	+74	.....	.....	.....
Mar. 9	4:54	5.430	+114	+76	.....	.....	+ 49
June 24	0:48	5.453	+116	+86	.....	.....	.....
Mar. 9	6:10	5.483	+117	+97	.....	.....	.....
July 5	22:23	5.485	+ 84	+46	.....	.....	.....
Mar. 9	7:30	5.539	+111	.....	+101	.....	.....
July 11	22:50	5.571	+ 95	+79	.....	.....	.....
1951 Apr. 4	23:48	5.596	+ 97	+61	.....	.....	.....
1950 July 12	0:14	5.629	+118	+82	+ 13	.....	+ 88
1951 Apr. 5	0:46	5.636	+115	+78	+ 71	.....	.....
Apr. 5	1:49	5.680	+118	+93	+ 97	+ 82	.....
Apr. 16	23:20	5.709	+ 96	+69	+ 44	.....	.....
1950 July 23	23:17	5.722	+ 85	.....	.....	.....	.....
1951 Apr. 5	3:08	5.735	+110	+75	+103	+102	.....
Apr. 17	0:20	5.751	+106	†	+ 69	+ 52	.....
1950 Jan. 15	3:48	5.788	.....	†	+ 40	+ 74	.....
1951 Apr. 17	1:46	5.810	.....	†	+ 57	+ 17	.....
Jan. 18	3:40	5.895	+ 68*	+48	+ 37	+ 34	+ 55
Jan. 12	5:32	5.906	+ 38*	+46	+ 72	+ 63	+ 32
Apr. 17	4:12	5.912	+ 45*	+53	+ 9	+ 28	+ 38

THE RESULTS

The spectrographic results obtained for S Vel can be summarized as follows:

a) The distribution of the *Ca* II radial velocities, which show a large scatter, resembles strikingly the velocity-curve of RZ Scuti, investigated by Neubauer and Struve[15] several years ago. We have here another case similar to half-a-dozen others in which the eclipse effect suggests a velocity of rotation larger than the orbital velocity: RZ Sct, RY Per,[16] U Cep,[17,18] U Sge,[19] AQ Peg,[20] and SW Cyg[21]—all of them Algol systems composed of a dwarf early-type primary and a subgiant or giant late secondary.

[15] *Ap. J.*, **101**, 240, 1945; *Lick Obs. Contr.*, Ser. II, No. 10; *McDonald Contr.*, No. 107.

[16] Hiltner, *Ap. J.*, **104**, 396, 1946; *McDonald Contr.*, No. 129.

[17] Struve, *Ap. J.*, **99**, 222, 1944; *McDonald Contr.*, No. 87.

[18] Hardie, *Ap. J.*, **112**, 542, 1950; *McDonald Contr.*, No. 197.

[19] Struve, George Darwin Lecture, *M.N.*, **109**, 487, 1949; McNamara, *Ap. J.*, **114**, 513, 1951.

[20] Struve, *Ap. J.*, **103**, 76, 1946; *McDonald Contr.*, No. 121.

[21] Struve, *Ap. J.*, **104**, 253, 1946; *McDonald Contr.*, No. 126.

Besides a large rotational disturbance, the *Ca* II K velocities also show the peculiar concentration of too positive values after phase 0.75 P which is characteristic of those systems in which gaseous streams are present. If we disregard this peculiarity and assume that in the mean the radial velocities do represent orbital motion, we have a semi-amplitude of the order of 15 km/sec, which implies $a_1 \sin i \sim 1.4 \times 10^6$ km (since $i \sim 90°$ and the eccentricity is practically 0 and cannot be greater than 0.2) and $f(\mathfrak{m}) = 0.0031\ \odot$. From this mass function we may try to derive a reasonable set of values for the individual masses by assuming different mass ratios α. In doing this, we obtain the values given in Table 4.

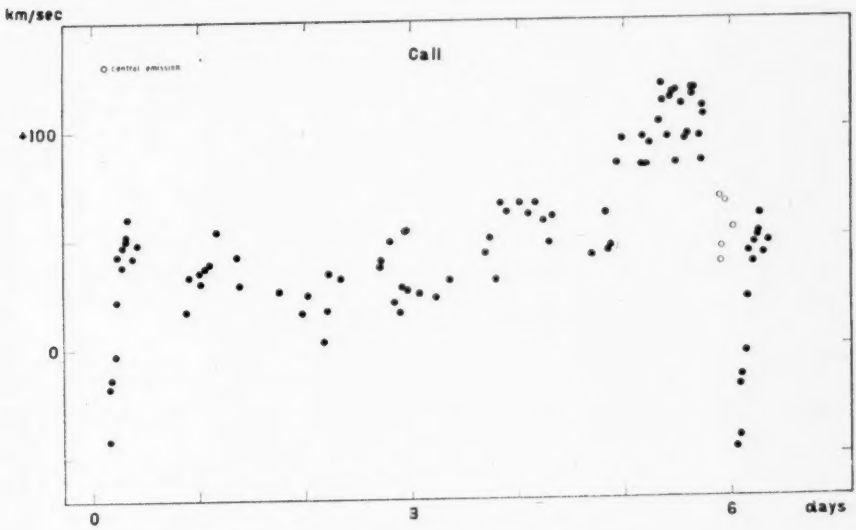

FIG. 3.—Radial velocities of S Velorum from *Ca* II

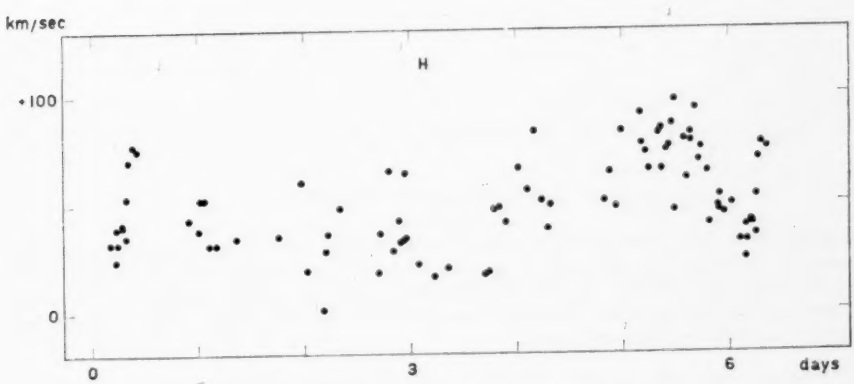

FIG. 4.—Radial velocities of S Velorum from *H*

Now the absolute magnitude for a dwarf A5 star is about +2 and, if it follows the mass-luminosity relation, its mass should be around 2 ⊙. If this is true, the luminosity of the secondary star must correspond to that of a subgiant, and hence its mass should be of the same order as that of the primary star. The tabulation made for different values of a suggests that, on the assumption that in the mean the *Ca* II velocities do represent orbital motion, reasonable values of the masses require that a be, say, of the order of 15

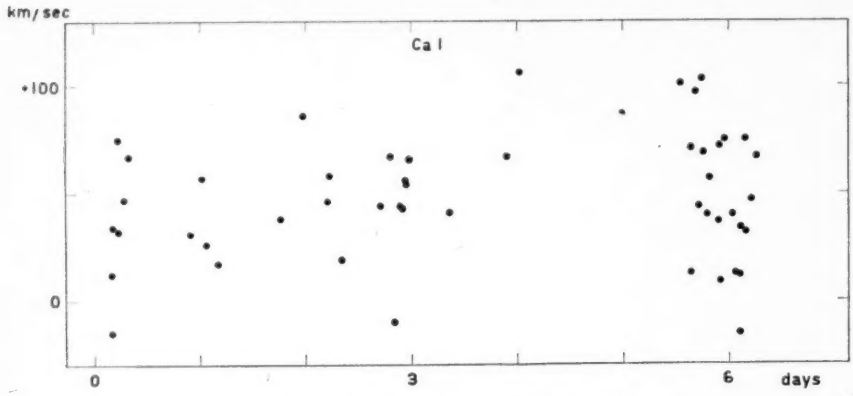

FIG. 5.—Radial velocities of S Velorum from *Ca* I

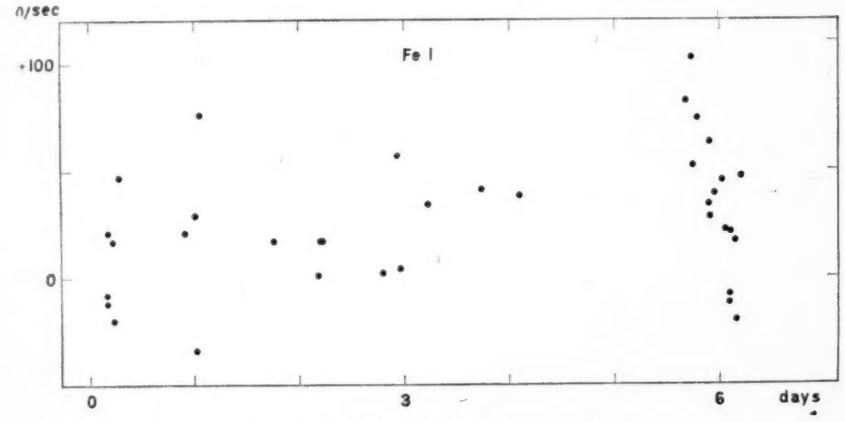

FIG. 6.—Radial velocities of S Velorum from *Fe* I

and that the stars—one or both—depart from the mass-luminosity relation. Otherwise, we must conclude that the velocity-curve is distorted and that we cannot rely upon the radial velocities to derive orbital elements. In view of the results obtained in other systems, such as XZ Sagittarii,[22] in which no evidence of distortion was found, probably the first conclusion is the correct one.

[22] Sahade, *Ap. J.*, **102**, 474, 1945; *McDonald Contr.*, No. 116; Sahade, *Ap. J.*, **109**, 439, 1949; *Obs. de Córdoba, Tirada aparte*, No. 23; Struve, *Ann. d'ap.*, **11**, 117, 1948.

The distribution of velocities during the partial phases after totality, which are interpreted as a rotational disturbance, is not reproduced before totality, partly because the corresponding velocities at the phases at which we have plates must be of the same order as those of the peculiar distribution after phase 0.75 P, and partly because we have not been able to measure the K line of *Ca* II, because of underexposure, on the plates between phases 5.75 and 5.82 days—that is, immediately before totality.

b) The velocities from H are characterized by a larger scatter than the one shown by *Ca* II and by an inconspicuous—relative to the case of *Ca* II—peculiar distribution after 0.75 P, which results in the distribution of points corresponding to a velocity-curve of

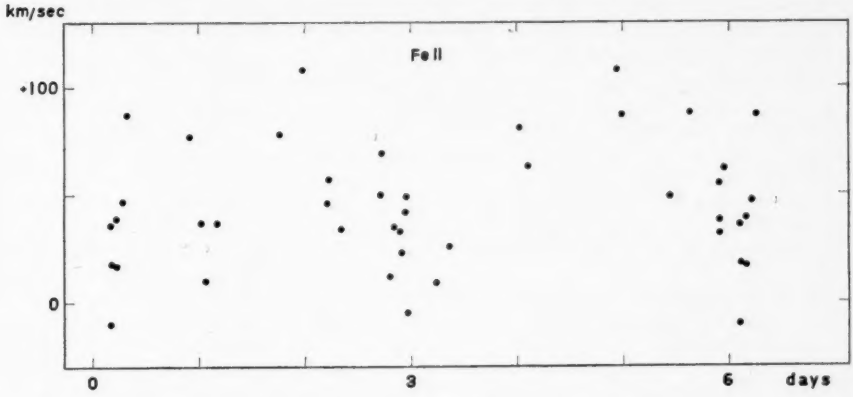

FIG. 7.—Radial velocities of S Velorum from *Fe* II

TABLE 4

α	m_1	m_2	α	m_1	m_2
1	0.01	0.01 ⊙	8	2.0	0.25 ⊙
2	0.06	0.03	10	3.8	0.38
4	0.31	0.08	20	27	1.4
5	0.56	0.11	30	89	3

small amplitude and large eccentricity. On the whole, the distribution of points is similar to the one found in systems such as RX Cassiopeiae,[23] in which the existence of gaseous streams seems to be established beyond doubt.

The large scatter of the radial velocities can be traced to erratic fluctuations probably produced by the action of prominences. The existence of such fluctuations of the radial velocities is clearly shown by two consecutive plates—at phase 2.795 days; exposure, 49 minutes, and at phase 2.839 days; exposure, 63 minutes—which yielded $+65 \pm 2.3$ and $+28 \pm 1.6$ (p.e.) km/sec, respectively, as means of four lines in each case. And the hypothesis that these irregular variations of radial velocity are related to prominence action has already been advanced by Struve in the case of UX Monocerotis.[19,24]

The rotational disturbance shown by H deserves special mention. At the partial

[23] Struve, *Ap. J.*, **99**, 295, 1944; *McDonald Contr.*, No. 94.

[24] *Ap. J.*, **106**, 255, 1947; *McDonald Contr.*, No. 138.

phases, except around second and third contacts, the radial velocities are absolutely smaller than for *Ca* II, showing a behavior similar to the one found in U Cep,[17,18,19,25] RZ Sct,[15] and RW Tau.[26] But immediately before second contact and after third contact, the radial velocities from the different members of the Balmer series show a trend as though they are affected by an emission component, the influence of which becomes less and less effective as we consider higher members. Near second contact the emission component affecting the results seems to be a red one; near third contact, a violet one, just as it must be according to the eclipses which each of the emission components of *H* undergoes, as described above. Table 5 gives the individual radial velocities for different members of the Balmer series from plates at phases near second and third contacts. Clearly, if we consider the radial velocities from the higher members of the series, which must be the less affected by the emission, the maximum value for the rotational disturbance is of the same order for *Ca* II and for *H*.

TABLE 5

Phase (Days)	Radial Velocities (Km/Sec) from					
	$H\theta$	$H\eta$	$H\zeta$	$H\delta$	$H\gamma$	$H\beta$
5.751	+125	+93	+84	+80	+64	.....
5.788	.....	.....	.....	.....	+64	.....
5.810	.....	.....	.....	+50	+30	.....
0.119	.....	.....	.....	+29	+57	.....
0.163	.....	.....	−12	+30	+52	.....
0.163	.....	.....	−64	− 8	+17	+35

Immediately after fourth contact, the radial velocities from *H* also behave like in U Cep, etc., in the sense that the velocities are too positive. The smaller velocities—positive and negative, respectively—obtained from *H* at the partial phases and immediately after fourth contact, can be interpreted, according to Hardie,[18] who followed a suggestion by Struve,[20] by assuming that we actually measure an asymmetric line resulting from the blending of a Stark-broadened line coming from the main body of the star and a narrow line displaced by rotation coming from the tidal bulge facing the secondary star. The observational fact that, at the partial phases near second and third contacts, the velocities are no longer smaller than those from the other elements would be in agreement with this theory, since we then observe only the tidal bulge of the primary star.

The relatively inconspicuous peculiar distribution of too positive velocities after phase 0.75 *P*, shown by *H*, may be explained by one of two hypotheses: either the profiles of the stellar and the stream components are such that we actually measure an average velocity between that of the star in its orbit and that of the stream, or the stream *H* velocities as seen projected upon the A5 disk are smaller than those of the *Ca* II stream. A third possibility could be that the velocities from the *H* stream are modified by those from a field of prominences with predominantly negative velocities. The visual inspection of the *H* lines on the available plates inclines us in favor of the second hypothesis, but there is no conclusive evidence for either one.

c) The radial velocities derived from the rest of the elements are too small in number for us to be able to infer much from them. Nevertheless, we can mention that the three elements show the rotational disturbance, but the velocity of rotation suggested is smaller

[20] Struve, address of the retiring president of the American Astronomical Society, *Pop. Astr.*, **58**, 1, 1950.

[26] Hiltner and Hardie, *Ap. J.*, **110**, 438, 1949; *McDonald Contr.*, No. 180.

than in the case of *Ca* II because the metallic lines from the A5 star, at the relevant phases, are blended with the lines from the secondary star.

The distribution for *Fe* II is rather peculiar, especially in the first half of the cycle, but the scatter is such that we cannot draw any conclusion.

CONCLUSIONS

We are concerned, in the present investigation, with another close binary system, formed by a dwarf primary of early spectral type and a giant late-type secondary, in which (1) one or both stars of the system seem to depart from the mass-luminosity relation; (2) the velocity of rotation of the primary star is larger than its orbital velocity; (3) the primary star displays prominence action; and (4) gaseous streams are present.

The central emission of *Ca* II which characterizes the spectrum of the secondary star suggests, according to the conclusions reached by Struve[27] from the study of the behavior of emission in some especially suited eclipsing variables, that the secondary star is "surrounded by a very extensive calcium chromosphere which is tidally elongated along the radius vector of the orbit to a much greater extent than is the photosphere of the star itself."[28] Our observations of the *Ca* II central emission are limited to the total phases, and the velocities obtained show a large scatter; however, since the mean value does not greatly differ from the value which seems to correspond to the systemic velocity, perhaps we can also say for S Vel that "the emitting mass which produces the *Ca* II lines belongs dynamically to one of the components of the binary [the secondary star in our case] and is carried with the latter in its orbital motion."[29]

Now the behavior of the absorption *Ca* II K line observed outside eclipse—in profile as well as in radial velocity—and the fact that, during the total phases, the spaces corresponding to *Ca* II in absorption in the spectrum of the secondary star are filled with emission suggest that Struve's "peanut model"[19] holds also for S Vel.

In the case of *H*, the smaller—relative to *Ca* II—velocities corresponding to the peculiar distribution after phase 0.75 *P* may mean that the direction of motion of the stream when we see it projected upon the A5 disk at the relevant phases, prior to eclipse, is different than for *Ca* II; and this seems to suggest that in the case of the *H* stream we may be dealing with Kuiper's ejection mechanism of type A.[30] This would imply different initial conditions for the *Ca* and *H* ejected material, such that *H* moves around the A star and *Ca* moves along a Jacobian equipotential external to both stars.

I am greatly indebted to Dr. L. Gratton and Mr. D. McLeish for allowing me to observe S Vel at some critical phases during observing time of theirs. Also to the former and to Drs. J. Landi Dessy and R. Platzeck for kindly obtaining for me several spectrograms used in this investigation, and to Mr. Julio Albarracín for assistance in the reduction of the plate measurements.

Note added in proof.—After reading a copy of the manuscript of this paper, Dr. O. Struve called my attention to a further detail of the structure shown by *Ca* II during the emission stage. Actually, to the violet of the emission features described under "The Spectrum" (see Figs. 1 and 2), *Ca* II H and K also show the presence of a faint negative displaced absorption (radial velocity of -380 km/sec), a phenomenon similar to the one found by Struve in UX Mon, which was interpreted as evidence of rapidly approaching prominences from the star facing the observer (the late-type secondary in both cases). In our case the reported absorption feature is shown only on the plate taken at phase 0.018 day.

[27] *Ann. d'ap.*, **9**, 1, 1946.

[28] *Ibid.*, p. 5.

[29] *Ibid.*, p. 2.

[30] *Ap. J.*, **93**, 133, 1941; *McDonald Contr.*, No. 28.

THE SPECTRUM OF U CYGNI (MINIMUM) IN THE VISUAL AND INFRARED REGIONS

YOSHIO FUJITA
Yerkes Observatory
Received November 1, 1951

ABSTRACT

Glass positives of spectrograms of U Cygni at its light-minimum, obtained by R. F. Sanford with the coudé spectrograph of the Mount Wilson Observatory, have been measured in the visual and infrared regions. Attention is called to the remarkable intensity increase of the lines of some elements which originate from the lowest excitation level. A table of wave lengths and identifications is given.

Spectra of stars of classes R and N with dispersion of 10 A/mm in the photographic region and 20 A/mm in the visual and infrared regions have been obtained by R. F. Sanford with the 100-inch telescope and its coudé plane-grating spectrograph. A general description of the spectrograms of these stars has been given by him.[1]

Of these stars, U Cygni is a particularly interesting object, because its spectrum has been taken at its light-minimum; at that time it showed the late spectral type of $C9_2$—the coolest type, according to the classification of Keenan and Morgan.[2] As suggested by Sanford, it seems worth while to investigate the details of the spectrum of the star; the results of the detailed study of U Cygni in the visual and infrared regions are given here.

The spectrograms investigated are positive copies on glass of coudé spectrograms obtained by R. F. Sanford, the details of which are given in Table 1.

TABLE 1

DATA ON SPECTROGRAMS

Star	Coudé Pl. No.	Date	Exposure (Minutes)	Emul.
U Cygni (minimum)	3485	1944, July 5	170	103*a*-F
	5742	1949, July 10	260	I-N*

* Hypersensitized with NH_3.

The spectral region between 5940 A and 8830 A has been measured. However, there are some small regions in this interval where the accurate determination of wave lengths is impossible, owing to underexposure.

The identification of the lines was aided by the *Revised Multiplet Table*[3] and *M.I.T. Wavelength Tables*;[4] in addition, the table of the infrared solar spectrum by Babcock and Moore[5] facilitated the recognition of the telluric bands of water vapor and oxygen.

[1] *Ap. J.*, **111**, 262, 1950.

[2] *Ap. J.*, **94**, 501, 1941.

[3] C. E. Moore, *Contr. Princeton U. Obs.*, No. 20, 1945.

[4] G. E. Harrison, *Massachusetts Institute of Technology Wavelength Tables* (New York: John Wiley & Sons, Inc., 1939).

[5] *The Solar Spectrum, λ 6600 to λ 13495* (*Pub. Carnegie Inst. Washington*, No. 579 [1947]).

The intensities of the star lines were estimated on a scale where 0 represents the faintest and 10 the strongest lines. After the identifications were made, ninety-five atomic lines which are sensibly free from blends and are comparatively sharp features were selected for the purpose of determining the radial velocity of the star. The result is + 10.4 km/sec, which is in good agreement with the results of Sanford.[6]

As the equivalent widths of some of the atomic lines have been given by Sanford,[1] it seemed worth while to compare our visual estimation of intensities with them. The re-

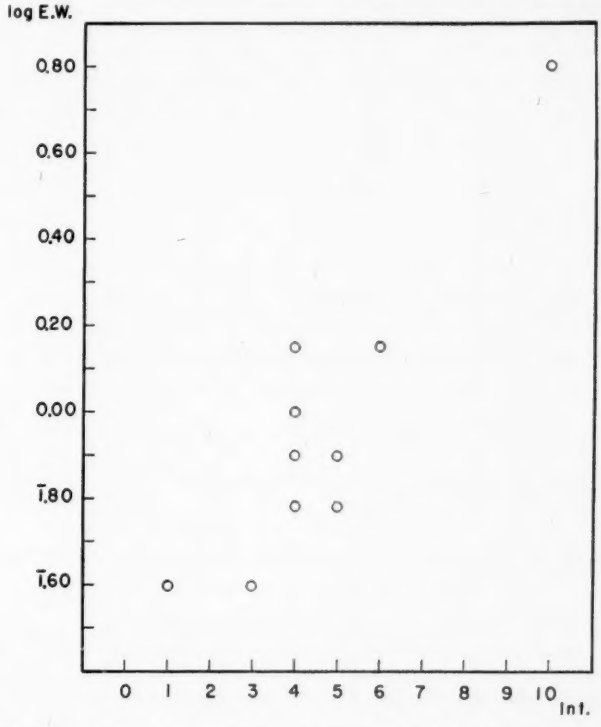

FIG. 1.—Relation between visual intensity and equivalent width of some lines in U Cygni

sults are shown in Figure 1. From this figure we can roughly estimate the equivalent width of any lines corresponding to our visual intensity.

The presence of the following elements is confirmed from our identifications: *Li*, *Na*, *K*, *Ca*, *Sc*, *Ti*, *V*, *Cr*, *Fe*, *Co*, *Ni*, *Rb*, *Sr*, *Y*, *Zr*, *Cs*, *Ba*, *La*, *Ca* II, *Sc* II, *Ba* II, and *La* II. The presence of *Y* II and *Zr* II is also probable; however, as the lower-level lines of *Al* are in the shorter-wave-length region and the low-level line of *Mg* is 4571.10, it is impossible to make sure of the existence of these two elements.

The most interesting result is that all lines which originate from the lowest energy level are present. If we plot the visual intensity of each atomic line against its lower excitation potential, the results are shown in Figure 2. It will be noted from this figure that the elements *La* and *K* have very strong lines and that the tendency for the decrease of

[6] *Op. cit.*, p. 270.

the intensity of the lines with the increase of the lower excitation potential is marked.[7] Thus the limiting excitation potential for the elements which are observed in this star can be estimated. The figure also indicates that U Cygni at its light-minimum is near the coolest stage.

In addition to the atomic lines, many lines of *CN* and C_2 have been identified. C_2 $^3\Pi \rightarrow {}^3\Pi$ and *CN* $^2\Pi \rightarrow {}^2\Sigma$ are present, and the new red system $^1\Pi_u$–$^1\Sigma_g^+$ of C_2 which has been found by J. G. Phillips[8] seems also to be present. However, there still remain many lines which are doubtful in identification because of blending and diffuse appearance. For the investigation of these lines, higher dispersion is needed.

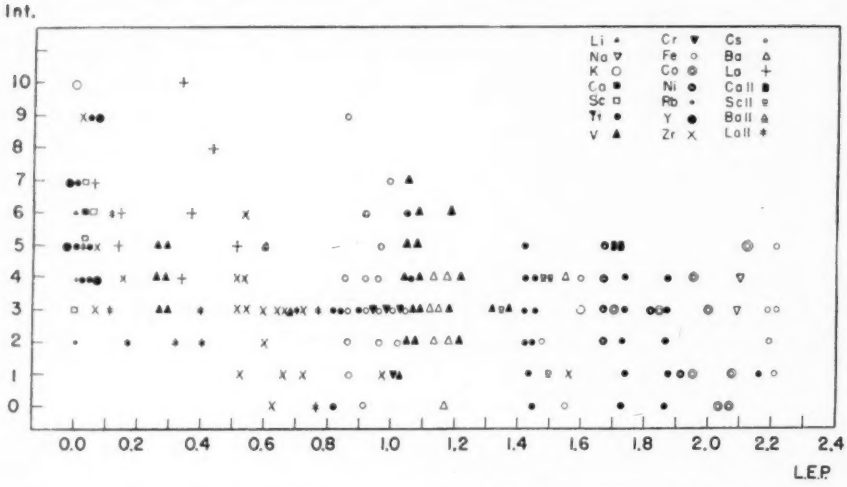

FIG. 2.—Relation between visual intensity and lower excitation potential of unblended lines in U Cygni.

All the lines which have been identified are listed in Table 2, with the estimated intensities and with multiplet numbers from the *Revised Multiplet Table* by C. E. Moore. Numbers in parentheses after the wave lengths refer to notes at end of table. Telluric and unidentified lines have been also included, as it was believed they would be of help in the identification of lines in the future.

In conclusion, the writer expresses his hearty thanks to Dr. W. W. Morgan, who kindly arranged for him to study the copies of the spectrograms of the Mount Wilson Observatory and gave him advice and many suggestions during the course of this investigation.

[7] The lines of *La* I in the spectrum of U Cygni and two other carbon stars were originally recognized by Sanford (*Pub. A.S.P.*, **59**, 333, 1947).

[8] *Ap. J.*, **107**, 389, 1948.

TABLE 2

WAVE LENGTHS AND INTENSITIES.

Wave Length	Intensity	Identification	Wave Length	Intensity	Identification
5944.87	5	.65 Ti 2	6008.81	3	.65 V 49
46.99	2		9.41	3	.45 Fe 64
47.75	2		10.01	1	
48.48	2		10.66	2	
49.51	3	.35 Fe 14	11.54	2	
51.24	2		12.55	1	.21 Fe 64
52.15	1		13.49	2	
53.17	1	.16 Ti 154	14.48	3	C_2 ?
54.54	3	.68 C_2	15.08	3	.25 Fe 63
55.36	4	.37 Zr 3	17.01	2	
57.07	3	.70 Fe 14	18.45	3	7.90 V 49, .62 Ti 70
58.26(1)	3d	.23 Fe 14, .34 Fe 63, C_2	19.60	3	.47 Ba 7
59.44	2		20.70	2	
60.37	3		21.82	2	
61.42	1		23.30	4	.41 Y 3
63.33	3	.25 Fe 63	24.50	3	
65.97	4	.83 Ti 154	25.39	3	
66.84	2		26.35	4	.14 C_2
67.53	1		27.30	3	
68.16	0		28.94	3b	.62 .77 C_2
69.19	4b		29.66	1	
70.14	2		31.50	5	.68 Ti 2
71.84(2)	3b	.70 Ba 7, 2.01 2.41 C_2	32.31	2	.12 C_2
73.33	1		33.79	2	
74.50	3	.13 .54 C_2	34.75	2	
75.99	2		36.62	2	
76.84	1		37.49	2	
78.52	3	.54 Ti 154	38.61	1	
79.33	4b		39.68	3d	.69 V 34
80.80	3	.75 V 49, .91 C_2	41.32	2	
81.18	4	0.89 Ti 72	42.35	2	
82.86	3		42.87	2	
83.23	3		43.51	1	
83.81	3	4.09 Co 37	45.42	3	.76 C_2
84.65(3)	7b	.59 Ti 2, .60 V 49	46.16	2	
86.63	2		47.21	3	
87.48	1		48.39	4	.64 V 49
88.77	4vb	.56 Ti 154, 9.08 C_2	49.51	3	
90.68	3		50.66	2	
91.60	0		51.88	3	.71 C_2
92.80	1		52.61	2	
93.48	1		53.84	2	
94.34	2		55.08	2	
95.35(4)	3	.09 C_2	56.92	3	
97.81	2		58.18	4	.11 V 34, C_2 ?
98.50	2		59.16	4d	8.76 Ti 70, .25 ScII 20, C_2 ?
99.91	3				
6001.33	3b	.53 ScII 20, 0.91 C_2	60.30	3	C (2,4)
2.25	2b	.27 V 49, 1.89 C_2	61.29	2	
2.85	3	.60 V 34	62.07	2	
3.53	1	.39 C_2	63.10(5)	4d	.12 Ba 7, 2.88 Zr 3, 2.89 Fe 63
4.31	3	C_2 ?			
5.33	3	.03 Co 37	64.50	4	.63 Ti 69
6.30	3		66.10	2	
7.40	3d	.31 Ni 42	66.77	3	7.13 LaII 48
			68.58	2	
			69.33	2	

TABLE 2-Continued

Wave Length	Intensity	Identification	Wave Length	Intensity	Identification
6070.13	3		6151.70	3b	.51 V 33, .62 Fe 62
72.15	3		53.13	2b	
73.56	2		54.23	3	.23 Na 5
74.99	3b		55.08	2b	
77.18	5		56.51(7)	2	
78.23	2		57.91	2	
79.59	2		59.13	3	
80.14	2		61.07	4	0.75 Na 5
81.72	7	.42 V 34	62.09	4	.17 Ca 3
82.63	5	.72 Fe 64	63.46	3	.56 Fe 64
84.14	3		6212.60(8)	3	3.06 Zr 24
85.13	4	.23 Ti 69	13.91	3vb	.87 V 20
86.90	5b	.55 V 49, 7.49 V 33, C_2 ?	15.05	2	
88.12	2		16.00	2	
89.31	4	.47 V 33	16.72	5b	.37 V 19
90.42	4b	.54 V 33, .18 V 34, C_2 ?	18.16	3b	.05 CN
91.58	2		19.46	2	.29 Fe 62
92.96	3b	3.14 Co 37, .81 Ti 153	20.44	2	
95.98	0		21.34	3	.66 Fe 13
96.60	0		22.80	5	.59 Y 2
97.47	2	.42 V 33, .08 Fe 64	24.70	5b	.51 .26 V 20
98.92	3	9.09 C_2	28.48	2	
99.78	2		29.34	0	
6101.51	2	$C^{12}C^{13}$(1,3)	30.20	0	
3.15	4b	2.72 Ca 3, .64 Li 4, .21 C_2	30.91	3d	.74 V 19, .97 Co 37
4.49	0		31.86	3	.76 Sc 3
5.48	0		32.85	0	
6.41	0	.47 ZrII 106 ?	33.43	3	.19 V 20
7.27	3	6.97 V 60	35.44	1	
7.92	2	8.12 Ni 45	37.46	4	.45 CN
9.00	3		39.50	6	.41 Sc 2, .78 Sc 3
10.64	4	.78 Ba 7	40.32	4	.24 V 20
11.83	4	.62 V 34	42.06	4	
13.73	1		43.16	4	.11 V 19, 2.80 V 19
15.15	3	4.78 Zr II 93	44.94	3	5.21 V 20, .51 Sc 3
16.53	1	.99 Co 37 ?	45.78	4	.63 ScII 28
17.75	2		46.53	2	
18.96	4d	9.21 C_2	48.24	2	
19.68	4	.51 V 34, 0.25 Fe 14	49.27	2	
20.76	3	.86 Zr 24, 1.01 Ti 153, 1.23 C_2	50.16	5b	9.92 La 7
22.26	6	.22 Ca 3	51.83	4	.83 V 19
24.85	4	.86 Zr 24	53.80	3	
25.51(6)	1		55.07	2	
27.36	4	.49 Zr 2	56.64	3d	.91 V 19, .37 Ni 43
28.47	4	.30 V 33, .99 Ni 42	57.79	4	.72 Ti 1
29.48	0	.57 LaII 47	58.90	4	.60 V 19, .96 Sc 3
31.95	2		59.89	4	C^{13}_{N} 14
33.46	2		61.19	3	.24 V 20, .10 Ti 104
34.36	4	.58 Zr 2	62.43	2	.30 LaII 33
35.47	2	.36 V 34, .07 V 60	64.01	1	
36.70	2	7.00 Fe 62	65.11	4	4.83 Ti 144, .14 Fe 62
38.39	4	.44 Y 3	65.89	3	6.02 Ti 144
39.36	1		66.52	4	.32 V 20
40.49	3	.50 Zr 24	68.73	4	.84 V 20, .50 Ti 103
41.66	3	.72 BaII 2	70.15	5	.34 V 20
43.09	5	.23 Zr 1	73.67	5	.39 Ti 1, .76 LaII 131
46.57	4b	.23 Ti 153, .38 Co 80	74.85	4	.67 V 19
47.89	2		75.56(9)	3	
48.93	3b		76.53	4	.31 Sc 2
50.06	4	.13 V 20	78.78(10)	1	.88 Atm O_2

TABLE 2-Continued

Wave Length	Intensity	Identification	Wave Length	Intensity	Identification
6281.10	4	0.63 Fe 13	6364.89	4	.92 Ti 1
82.08	3		66.48	1	.35 Ti 103
85.14	4	.19 V 19	67.58	1	
86.03	3		69.02	1	
86.74	2		70.41	2	
87.69	3		71.64	1	
88.91	0		72.76	2	
90.36	1		74.41	3	
91.81	2		76.06	2	
93.34	4b	2.86 V 19, .00 Ti 103, 2.97 Atm O_2 .57 La	77.43	1	
95.51	4b	.25 Ti 1, 144, .19 4.97 Atm O_2	78.92	5	.82 Sc 1
			81.49	4	.42 Ti 196
96.84	4	.65 Ti 1, .52 V 19	82.94	3	
98.29	1	.08 Ti 144	84.28	2	
6300.58	3	.70 ScII 28	85.02	3	
2.19	1		86.20	2	
3.11	0		87.06	4	
4.14	3	.35 Zr 24, 3.75 Ti 104	88.62	4	
5.90	5b	.67 Sc 2, 6.05 Sc 3, .82 Atm O_2	90.41	4	.48 LaII 33
			92.11	4	
6.87	2		93.24	3	
9.13	2		94.09	8	.23 La 7
10.45	4b	.48 CN, 9.90 ScII 28	96.20	5	
12.18	3	.24 Ti 104	97.75	5b	
13.12	3	.05 Zr 65	6400.30	6	.34 Fe 13
14.59	1		0.95	4	
15.87	0		2.15	4	.01 Y 2
17.18	2		3.18	3	
18.31	3	.03 Ti 103	4.84	2	
19.03	2		5.46	2	
20.45	2		7.05	4	.03 Zr 2
21.13	3b	0.85 ScII 28	8.11	7	.15 CN
22.18	0		9.60 (11)	0	
23.89	2		10.71	7b	.52 CN, .98 La 7
25.16	5	.22 Ti 1	13.20	9b	.13 Ti 1, .35 Sc 1
26.02	5	5.90 La 2	14.39	2	
27.57	5	.60 Ni 144	15.95	1	
30.26	3	.10 Cr 6	19.26	6	.15 Ti 196
31.12	1		20.78	2	
33.15	5b	.33 CN (5,1)	21.94	5	
35.67	3	.34 Fe 62	24.23	6	.09 C_2 ?
36.31	2	.10 Ti 103	25.04	5	
37.10	3		26.10	5b	
38.35	2		28.39	3	
39.61	2		30.22	5	9.91 Co 81
40.76	2		30.71	3	.85 Fe 62
42.03	3	1.68 Ba 6, .08 ScII 28	32.06	6	1.91 CN
44.75	3	.83 Sc 1	34.90	9	5.02 Y 2
45.76	2		36.60	3	
47.32	3		37.87	4	8.03 CN
48.42	1		39.11	3	.07 Ca 18 ?
49.78	2		40.00	2	
51.11	2		41.52	0	
52.21	2		42.40	2	.3 C_2
53.79	3	.84 Fe 13	46.02	1	5.76 Zr 57
55.26	1		47.01	0	
56.95	3	7.10 Zr 2	48.24	7	.10 Sc 1
57.98	3	8.12 LaII 47	48.85	3	
58.85	2	.69 Fe 13	50.08	4	9.81 Ca 19 ?, .23 Co 37, .09 Co 80
59.87	4	.90 Ti 1	50.65	4	.23 Co 37, .85 Ba 6
61.65	1	.41 Ti 196			
62.74	4	.87 Cr 6, .29 Sc 1			

TABLE 2-Continued

Wave Length	Intensity	Identification	Wave Length	Intensity	Identification
6451.63	3		6511.63	2	
52.36	3	.35 V 48	43.38(14)	10	.17 La 7, .51 Y 48
54.45(12)	6	.53 La	45.53	3	
56.11(13)	6b	5.99 La 1, 5.60 Ca 19 ?	46.42	2	.28 Ti 102
56.95	2		47.65	4	.58 Fe 13
58.39	4		50.13	3	.24 Sr 12
60.93	0		51.85	1	.68 Fe 13, .47 Co 54
62.63	5	.57 Ca 18 ?, .72 Fe 13	53.07	3	
64.52	5	.67 Fe 13, .70 Ca 19 ?	54.19	4	.22 Ti 102
65.85	2		56.07	2	.07 Ti 102
66.93	5	.97 V 32	57.52	5	.40 Y 1
68.44	1		58.21	5	.02 V 59
69.40	0		59.15	1	
70.03	1	.25 Zr 65	60.90	1	
71.51	4	.66 Ca 18 ?	62.34	0	
72.40	0		63.50	4	.40 Co 80
73.59	3		65.73	6	.88 V 48
74.12	2		69.03	3	
75.10	4b		71.04	4	0.96 LaII 47
78.66	5	.71 CN	72.84(15)	6	.78 Ca 1, .90 Cr 16
80.60	2	.51 C_2	74.39	7	.24 Fe 13
81.47	5	CN (6,2)	76.66	6	
83.86	2	.95 Fe 34	78.68	4	.51 La 1
85.92	4		79.15	4	8.96 V 32
86.64	3		81.25	3	.22 Fe 34, 0.96 Cr 16
87.87	1		83.47	2	
88.52	2		84.99	4	.89 Y 1
90.08	3	9.68 Zr 65, .34 Co 81	87.19(16)	1	
90.89	0		89.22	2	
92.20	0		90.63	0	
93.75	3	.78 Ca 18 ?	91.89	2	
97.02	5	6.90 BaII 2	92.80	0	.91 Ti 102
98.82	4	.76 Ba 6, .95 Fe 13	93.66	3	
99.85	1	.65 Ca 18 ?	95.41	3	.33 Ba 6
6500.84	3	1.21 Cr 16	96.78	3	
2.48	2		99.07	5	.11 Ti 49, .25 C_2
3.89	4	4.16 V 48	6600.25(17)	5	.17 La
5.42	1		2.61	1	
6.47	1		4.72	2	.60 ScII 19
7.48	1		6.16	4	5.98 V 48
9.10	4	8.74 Ca 18 ?	7.64	3	.82 V 59
9.92	1		9.76	3	.68 Fe 13
10.58	1		10.91	0	
12.33	1		13.71	2	.74 YII 26, .83 Fe 13
14.84	2		14.98	0	
15.83	2		16.99	2	
17.18	3		18.25	1	
18.88	3		19.72	1	
21.20	2		21.17	1	
22.75	4	.79 CN	23.72	1	
25.05	2		24.93	3	5.04 Fe 13, .86 V 48
26.09	2		28.85	3	
28.19	4		30.22	3	.02 Cr 16
29.33	1		32.40	0	.44 Co 111 ?
31.26	4	.44 V 48	34.24	1	
32.92	1	.89 Ni 64	38.32	1	
33.58	1	.68 C_2	40.10	2	
37.18	5	6.99 CN	41.32	0	
38.10	1	7.92 Cr 16	43.56	4	.64 Ni 43
39.82	0		48.12	2	.08 Fe 13

TABLE 2-Continued

Wave Length	Intensity	Identification	Wave Length	Intensity	Identification
6649.20(18)	1		6751.95	3	.94 Ti 152
50.91	7	.80 La	53.15	6	.00 V 31
53.54	1		54.52	1	
55.16	2		55.38	2	
57.52	3		57.34	2	
59.06	1		58.57	1	
60.08	1		59.75	3	
61.57	2		60.96	0	
63.48	2		62.47	5	.38 Zr 1
64.80	2		64.80	3	
65.56	3	.43 Fe 34	66.61	5	.49 V 31
66.63	3	.55 Ti 101	67.80	3	.78 Ni 57
69.40	1		69.53	3	
71.36	3	.41 LaII 33, .31 C_2	71.02	4	.04 Co 54
72.56	2		74.34	4	.28 LaII 2
75.40	4	.27 Ba 6	75.72	0	
78.78	2	.82 Co 54	77.04	0	
80.01	1		78.84	4b	
81.68	2		80.79	0	
83.25	2		82.17	0	
85.26	0		83.12	0	
86.14	1		85.10	3	4.98 V 31
87.70	7	.57 Y 1	87.48	2	
88.60	1		88.71	0	
89.47	2		90.00	1	
92.89	2	.89 CN	91.09	3	.02 Sr 3
93.93	2	.84 Ba 6	92.87	1	
95.51	1		93.69	4	.71 Y 1
96.35	0		95.44	2	.41 YII 26
97.88	2	.76 CN	96.93	3	
6700.93	2		98.01	2	
2.53	2		98.99	2	
4.15	1		6800.60	1	
5.75	1		1.67	4	.87 Fe 34
7.83	6	.74 Li 1	3.42	4	
10.03(19)	6b	9.49 La 6, .31 Fe 34	7.39	1	
13.25	0		8.24	1	
15.72	1		9.06	3	8.88 LaII 1
17.56	3		10.05	1	
19.53	1		12.53	3	.40 V 31
20.64	1		14.75	4	.95 Co 54
22.37	4		17.05	2	
23.50	1		18.37	1	
24.72	1		19.97	1	
25.86	3		21.14	1	
28.27	3		23.02	0	
29.33	1		24.17	2	
30.73	2		25.55	1	
31.80	1		27.18	3	
33.13	1		28.43	3	
34.67	2		30.14	3	9.94 V 31, 9.92 Co 81
35.72	1		32.46	2	.44 V 31, .49 YII 26
36.79	2		33.03	9	2.93 Zr 1
37.95	1		34.71	2	
39.39	3	.54 Fe 34	35.59	3	
41.68	1		36.86	1	
42.93	3	3.12 Ti 48	38.10	2	7.91 LaII 33
44.07	2		40.05	1	
50.00	2		41.78	3	.89 V 31
50.87	1		44.70	2	.67 Fe 34

TABLE 2-Continued

Wave Length	Intensity	Identification	Wave Length	Intensity	Identification
6847.23	6b		6947.73	3	.45 .64 Atm
49.71	2		49.06	4b	.09 8.98 Atm
51.55	4	.64 Fe 34	50.85	2	.75 1.24 Atm
56.63	3		51.68	3	.68 YII 33
58.22	3	.25 YII 26	52.48	2	.52 LaII 18
59.91	2		53.90	3	4.54 LaII 1, .58 .78 Atm,CN
61.18	2		55.67	2	.64 Atm
62.44	2		56.57	2	.40 .49 Atm
63.62	1		57.89	3	
64.94	1		59.35	3	.45 Atm
66.45	2		61.21	4	.26 Atm
68.58	6vb	.11 .24 .92 9.10 Atm O_2	64.45	4	.18 .69 K 7, .54 Atm
70.02	4	9.89 .01 Atm O_2	66.73	3	
70.97	5b	.95 1.29 Atm O_2	68.07	2	
72.63	4	.32 Co 54, .25 .84 Atm O_2	68.83	2	
74.52	5	3.80 .65 Atm O_2	71.05	4	0.87 Atm
76.10	5	5.59 .72 Atm O_2	74.77	4	
77.56	4	.64 Atm O_2	77.94	3	
78.89	4	.31 Sr 3, 9.04 Atm O_2	79.65	3	
80.15	5b	9.93 Atm O_2	81.85	3	
81.15	4		82.88	1	
82.11	2		84.59	1	
83.88	5	.83 Atm O_2	86.54	4	.58 Atm
85.84	7	.75 Atm O_2	87.77	1	.87 Atm
86.90	7	.74 Atm O_2	88.94	0	.99 Atm
87.62	2		89.78	4	CN (3,0)
88.40	1		90.66	2	.37 1.03 Atm, CN
89.10	2	8.95 Atm O_2	91.77	3	.80 Atm
90.02	6	9.90 Atm O_2	92.72	3	.85 3.52 Atm
92.55	9b	.57 Sr 1, .37 Atm O_2	97.08	1	
93.39	9	.31 Atm O_2	97.96	1	8.01 .72 Atm
94.84	2		99.21	3	8.96 Atm, $C^{13}{}_2N^{14}$
95.85	4	6.00 YII 26, 6.04 Atm O_2	7001.56	1	.57 Ni 64
97.10	4	6.97 Atm O_2	4.18	4	
98.60	4		4.88	2	.81 Co 89, .75 Atm
99.87	6	.95 Atm O_2	6.37	2	
6900.98	6	.87 Atm O_2	8.01	2	7.81 Ti 100
2.52	5		9.88	2	
3.44	4		11.80	2	
4.83	7	.12 5.02 Atm O_2	14.70	2	
6.27	3		16.61	3	.60 Co 54, .44 Atm
7.39(20)	2		18.21	1	
8.61	5	.53 9.43 Atm O_2	20.96	2	
16.67	4b		21.94	1	
18.53	5	.12 9.00 Atm O_2	23.67	2	.50 Atm
19.65	5	CN (2,0)	24.71	2	
20.58(21)	3		26.01	2	
29.47	3	.31 .60 .84 Atm O_2	27.16	3	.48 6.94 Atm
32.07	3	1.77 .04 .15 Atm	28.88	2	
33.62	3	.55 Y 1, .61 .82 Atm	30.91	2	
35.60	2	.28 .81 Atm	32.32	2	
36.30	3	.27 K 7	33.63	3	
37.53	3	.70 Atm	37.50	3	.04 Fe 61, .53 Atm
39.50	3	.61 Atm	39.81	3	.79 Atm
40.38	1	.19 Atm	43.78	1	
41.37	1	.22 Atm	45.86	4	.96 La 6
42.41	1	.37 .15 Atm	47.01	3	6.86 Atm
43.69	4	.80 Atm	49.26	2	
45.22	2		50.91	3	.85 Atm
46.45	2	.31 Co 110	52.79	4	.87 Co 54, .78 Atm

TABLE 2-Continued

Wave Length	Intensity	Identification
7054.90	1	
57.06	1	.00 Atm
58.13	1	
59.95	4	.94 Ba 5
60.97	1	.45 1.51 Atm
62.33(22)	1	
64.72	0	
65.45	1	.15 Ti 100, .64 Atm
66.41	5	.24 LaII 1
68.33	5	.37 La 1
70.05	0	.07 Sr 3
71.82	0	
72.85	1	
74.59	2	
76.29	3	
79.23	2	8.84 .59 Atm
82.68	2	
84.93	3b	.97 Co 54, .25 Ti 99, .98 Atm
87.30	3	.35 Zr 42
88.11	3	.15 Atm
90.53	3	CN (3,1)
92.90	3b	
94.30	2	
95.07	1	
95.78	2	
96.30	2	
97.72	1	.78 Zr 42
98.73	1	
7101.33	4	.28 Fe 61
3.38	3	.77 2.95 Zr 42
4.70	0	
5.93	2	
7.08	3b	
10.08	4	CN (4,1)
11.49(23)	4	.71 Zr 23, 0.91 Ni 64
13.23	2	
14.93	1	
17.08	2	
20.05	3	
22.24	3	
24.50	2	.47 Co 53
26.33	1	
27.31	1	
28.34	3	.15 9.13 Atm
30.31	3	.34 Ti 100
31.82	3b	
35.77	2	
37.95	0	8.05 Ti 98
39.14	3	8.91 Ti 99
40.00	2	
41.42	2	
43.10	2	
45.20	2	
47.34	1	
48.11	2	.15 Ca 30
49.91	3	
51.36	4	.18 ScII 27
53.33	1	
54.51	0	.69 Co 89
55.77	3	

Wave Length	Intensity	Identification
7156.98	0	
58.09	3	
59.88	1	
60.50	5	.33 Ti 98
63.72	2	
65.47	2	
67.65	2	.36 .90 Atm
68.97	1	9.14 Zr 42
70.42	5	.57 .09 Atm
72.70	2	.71 Atm
74.06	1	3.42 3.77 .15 Atm
76.08	3	5.96 .15 Atm
77.14	3	.11 .37 .62 Atm
78.46	1	.33 ScII 27, .42 Atm
80.21	3	.02 Fe 33
81.73	4	.52 .76 Atm
83.69	2	
84.67	3	.53 Atm
87.34	4b	.01 .39 Atm
88.45	3	.55 Ti 99
91.68	4	.50 .87 Atm
93.82	4	.74 YII 33, .56 .77 Atm
95.70	1	.24 Ba 10, .80 .04 Atm
97.11	3	.07 Ni 62, .23 Atm
98.25	3b	7.87 .44 Atm
7200.94	3vb	.56 1.20 Atm
4.11	3	3.85 .31 Atm
6.33	4	.42 Atm
7.92	2	
9.54	3	.44 Ti 99, .50 Atm
13.52	3	.35 Ti 143
15.02	1	
16.22	1	.20 Ti 98, .53 Atm
18.20	1	.02 Atm
20.98	2	
23.75	3	.64 Atm
27.34	0	.49 Atm
28.58	1	
30.44	1	
32.98	4	.90 Atm
34.81	3	.74 Atm
36.14	2	.14 Atm
37.83	3	.95 Atm
38.91	1	9.04 Atm
40.77	4	.62 .82 Atm
43.45	2	.48 .72 Atm
44.72	2	.86 Ti 99
45.83	3	.68 Atm
47.14	2	.21 Atm
49.03	1	8.92 Atm
50.10	1	.12 Co 53, .22 Atm
52.14	2	1.74 Ti 99, .37 Atm
52.97	5	3.76 Ti 143, .85 3.12 3.73 Atm
54.99	3	
57.42	1	.10 .37 .93 Atm
59.57	0	.56 Atm
60.55	0	.73 Atm
61.51	2	.94 Ni 162, 0.73 .45 2.01 Atm
64.31	3	.19 YII 33, .39 .60 Atm
66.10	3	.29 Ti 143, 5.59 Atm

TABLE 2-Continued

Wave Length	Intensity	Identification	Wave Length	Intensity	Identification
7266.91	1	7.00 Fe 61	7386.26	1	
69.98	2	.75 0.13 Atm	88.55	4	.46 YII 37
71.37	1	.43 Ti 97	90.72	3	.24 1.27 Atm
72.95	3	.97 Atm	92.37	4	.41 Ba 10
75.40	2	.40 Atm	93.08	4	
77.70	4b	.40 8.09 Atm	94.82	1	
79.63	3	.70 Atm	97.39	5	
80.44	2	.30 Ba 5, .67 Atm	98.63	2	
82.33	3	.36 LaII 1, .30 Atm	7401.12	1	
83.68	2		1.91	2	
85.04	2		3.15	2	
87.68	3	.38 8.13 Atm	5.99	4	6.23 YII 25
89.24	1		6.60	2	
90.83	4b	0.02 Ti 143, 1.48 Ni 63, .42 1.10 Atm	8.33	1	
			9.77	1	
92.52	3	.17 .70 Atm			
93.87	0		10.98	3	
95.35	4b	.03 .61 Atm	14.56	5	.51 Ni 62
99.58	2	.67 Ti 97 CN	17.18(27)	1	.38 Co 89, .06 Ti
7303.01	2	.20 Atm	19.59	3	
4.05	2	.13 .21 Atm	20.64	3	
6.11	2	5.87 Ti 143	22.14	4	
9.04	3	8.76 .52 Atm	22.95	3	3.17 Ti 97
11.20(24)	4	0.91 .08 .27 Atm	23.99	4	
13.15	4	.18 Atm	24.81	4	
15.56	1	.73 Co 89, .52 Atm	27.59	0	
16.99	1	.86 7.29 Atm	28.97	2	
18.40	3	.09 .38 .69 Atm	30.68	3	
20.71	3	.69 .85 Atm	31.83	2	.98 Ti 142
24.03	2	3.97 Atm	32.96	5	
27.37	2	.37 Atm	34.89	0	
29.03	1		37.17	4	.16 Co 53
30.91	1	.97 Ti 143, .86 Atm	38.56	1	
32.57	1	.26 Ti 143, .97 YII 25	40.02	6	9.89 Zr 23
34.07(25)	6	.17 La	42.39	5	
35.78	1	6.03 Zr 23, .34 Atm	44.21	2	
44.41	4	.72 Ti 97, 3.94 .76 Atm	45.60	2	
45.34	1		50.23	0	.32 YII 25
46.73	1		53.90	1	
48.76	1		56.37(28)	3	.35 Ti
50.12(26)	3	.09 Atm	57.38	2	
52.07	0		58.94	1	
54.70	2	.58 Co 53	60.92	3	CN (6,3)
57.02	2	.10 Atm	64.00	4	
57.62	1	.74 Ti 97	65.76	2	
60.29	3	.35 Atm	66.61	2	.44 Ti 142
62.41	0		67.55	1	
63.88	2	4.11 Ti 97, .74 Atm	68.78	2	
65.17	1		69.97(29)	3	0.05 Ti
66.70	4	.60 Ti 96	71.23(30)	2	.34 Ti
69.02	6b	8.47 .21 Atm	72.28	2	
69.87	2		73.32	2	
71.45	2	.50 Atm	75.06	4	4.94 Ti 142
72.30	4		78.69	4	.77 Co 53
74.20	5		79.57	2	
75.99	0		81.59	1	
77.51	1		83.45	6	.48 LaII 1
80.67	1		87.95	0	8.08 Ba 5
81.83	1		89.57	2	
83.61	0	.72 Atm	93.99	2	
85.22	0		94.81	0	.72 Fe 33

TABLE 2-Continued

Wave Length	Intensity	Identification
7496.21	1	
98.79	1	
7500.30	2	
1.45	1	
2.87	2	
5.02	2	
6.24	1	
7.36	2	
9.73	1	
10.70	1	
14.24	1	
15.16	1	
16.29	2	
18.65	2	
20.68	0	
22.95	1	
24.51	0	
27.03	1	
30.65	0	
33.26	2	
37.52	0	
39.18	3	
43.12	1	
46.44	2	
48.28	1	
51.01	2	
52.79	1	
54.62	3	.73 Zr 23
55.27	1	
58.70	2	
61.90	1	
62.60	3	
65.29	1	
70.28	0	
74.75	0	
77.78	0	
79.96	1	
86.12	2	
88.49	1	
90.63	0	.57 Co 89
91.87	1	
93.71	3	.70 4.00 Atm O_2
94.80	4b	.51 .97 5.24 Atm O_2
96.15	7b	5.77 .23 .50 Atm O_2
97.39	4	.44 Atm O_2
98.67	5	.65 .85 Atm O_2
7600.31	9b	.07 .49 Atm O_2
2.01	8b	1.70 .36 Atm O_2
3.52	5b	.56 Atm O_2
4.22	5b	.45 Atm O_2
5.47	4b	.64 Atm O_2
6.76	5b	.77 Atm O_2
7.85	5b	.93 Atm O_2
9.24	7b	.30 Atm O_2
10.51	7b	.46 Atm O_2
12.06	5b	.06 Atm O_2
13.13	5b	.19 Atm O_2
15.06	6b	.06 Atm O_2
16.00	5b	.15 Atm O_2
19.28	0	

Wave Length	Intensity	Identification
7621.04	7b	.00 Atm O_2
23.17	7b	.29 Atm O_2
24.48	7b	.50 Atm O_2
27.07	7b	.05 Atm O_2
28.20	8b	.23 Atm O_2
29.56	1	
31.01	7b	.02 Atm O_2
32.02	7b	.17 Atm O_2
35.06	6b	.19 Atm O_2
36.30	6b	.33 Atm O_2
37.21	5	.18 Atm O_2
39.54	9b	.59 Atm O_2
40.44	9b	.46 .71 Atm O_2
41.98	0	.54 2.65 Atm O_2
42.71	0	.65 Atm O_2
44.17	7b	.20 Atm O_2
45.37	7b	.31 Atm O_2
48.90	3	
49.79	4	.0b 0.14 Atm O_2
51.86	0	
54.02	5	.09 Atm O_2
55.19	4	.18 Atm O_2
59.39	3	.37 Atm O_2
60.44	3	.45 Atm O_2
63.39	1	
64.91(31)	10b	.91 K 1, 5.95 Atm O_2
68.41	2	
70.72	4	.60 Atm O_2
71.75	4b	2.09 Ba 5, .67 Atm O_2
73.40	1	
76.56	2	.57 Atm O_2
77.73	2	.62 Atm O_2
81.59	1	
83.65	2	2.76 .80 Atm O_2
90.10	2	9.68 .22 Atm O_2
93.27	2	
95.73	3	.84 Atm O_2
96.94	2	.87 Atm O_2
98.93	10	.98 K 1
7702.54	2	.74 Atm O_2
3.86	1	.76 Atm O_2
5.85	0	
9.15	0	
14.37	3b	.27 Ni 62, .56 C_2 (3,0)
16.71	1	.56 C_2 ?
17.62	1	.48 C_2
20.51	1	.76 C_2
23.70	1	
27.73	2	.56 C_2
32.11	1	.12 C_2
33.16	1	
35.52	0	
37.75	0	.90 C_2
38.86	1	.76 C_2
45.53	1	
46.91	1	7.05 C_2
52.95	0	3.16 C_2
56.77	1	.61 C_2
59.17	1	
62.71	1	

TABLE 2-Continued

Wave Length	Intensity	Identification	Wave Length	Intensity	Identification
7764.13	1		7911.35 (32)	3	.34 Ba 1
65.50	2		13.26	9b	2.89 Fe 12, .80 CN
67.34	0	.38 C_2	15.53	4b	.3 CN (2,0), .44 C_2, .63 Atm
75.54	1				
77.00	2		17.95	5	.78 8.38 CN, .71 C_2
			20.41	4	.24 CN, .67 Atm
79.52	1	.44 C_2			
80.43	2	.48 Ba 5	22.82	4	.98 CN
82.68	0		24.14	4	.35 Atm
86.50	0		26.35	3	.29 CN
88.84	1	.95 Ni 62	28.05	5	7.93 CN, .62 Atm
			29.87	4	.81 CN
7800.11	2	.23 Rb 1			
5.87	2		30.56	2	
9.32	0	.24 Co 79	33.23	5	.12 .48 CN
10.53	0		34.82	2	
19.54	0		36.02	1	
			37.56	3	.65 CN
28.96	0				
32.65	0		38.98	5	.53 Ti 151, .61 9.23 CN
36.96	0		40.19	2	
40.19	0		42.15	5	.00 CN
42.22	2		44.21	5	.38 CN
			45.14	3	4.65 Zr 40, CN (2,0)
45.10	1				
49.30	0	.38 Zr 40	46.55	3	.74 CN
50.41	3	CN (2,0)	47.71	2	.60 Rb 1
52.85	2	.74 Ti 34, CN	49.24	3	.17 Ti 125
55.14	1		50.51	2	.42 CN
			51.76	3	.73 CN
56.91	3				
59.10	2		53.96	3	
61.55	0		54.59	3	.57 CN
62.96	1		56.62	5b	.69 Zr 41, .71 CN
64.30	2	.44 Atm	58.37	3	.21 CN, .49 Atm
			59.76	2	
65.89	2	6.08 Atm			
69.99	1	0.00 Zr 41, .94 Atm	60.67	3	.73 Atm
72.93	6	.79 CN, Atm	62.64	4	.61 CN
73.50	0	.34 .96 CN	63.25	4	.13 CN Atm
74.79	1	CN (2,0)	65.06	6b	4.97 CN Atm
			67.15	3	.10 CN
75.94	2	6.11 CN			
77.23	3	.53 CN, 6.57 Atm	68.67	2	.47 CN, .12 Atm
78.93	3	.89 CN	70.20 (33)	4	.11 CN
80.76	4	.85 CN, .70 Atm	72.11	4	
82.01	4	1.90 YII 32	73.64	0	.79 CN
			74.61	1	.69 CN
82.87	0				
84.32	1		77.14	3	.22 CN
85.13	4	.01 CN, .00 Ti 34	78.51	3	.56 CN, .68 Ti 151
86.76	1		79.68	2	
87.61	2	.78 CN, .12 Atm	81.10	4	.15 CN
			84.80	4	.62 CN
89.39	4	.34 CN Atm			
91.96	1	.90 CN Atm	87.75	5	.36 Co 89, .97 CN
94.10	9b	.15 3.62 CN, 3.51 Atm	92.18	3	.32 CN
95.15	9b	.13 .52 CN, .50 Ti 34, .52 Atm	94.88	4	5.02 CN
			95.71	2	.63 CN
96.56	3	7.06 CN, .04 Atm	96.88	0	.80 Co 79
98.53	5	.38 .6 CN	98.22	1	.25 Atm
99.71	4	.86 CN	99.87	5	.88 0.30 CN, 0.30 Atm
7900.70	1	.80 CN Atm	8002.28	5	.40 CN
1.57	4	.78 CN Atm	3.75	3	
3.20	2		4.80	2	
4.18	3		7.69	3	.47 CN, .47 .72 Atm
5.56	2	.75 Ba 10, .60 CN	8.52	3	.46 CN
6.60	1		10.09	3	.09 CN
8.58	7	.75 CN Atm, .60 C_2 ?	11.67	2	
10.50	3	9.61 CN, .80 C_2 ?, .66 Atm	13.08	3	2.94 Atm

TABLE 2-Continued

Wave Length	Intensity	Identification
8015.35	1	
16.87	2	7.04 CN
18.23	2	.04 CN
20.65	2	.71 Atm
24.09	2	.18 CN
25.54(34)	4	4.84 Ti 151, .87 CN
27.34	3	.36 V 30
28.52	3	.54 Atm
30.76	2	
32.64	2	.77 CN
33.79	1	.61 4.29 Atm
35.03	2	4.96 CN
36.28	1	.46 Atm
38.01	1	
40.03	4	.28 CN, 9.60 Atm
41.74	1	.77 CN
44.05	7b	3.87 .40 CN, 3.17 Atm
45.52	2	.53 Atm
47.83	1	.60 Fe 12
49.78	2	.90 CN
50.81	5	
52.98	2	3.10 CN
54.20	2	.31 CN
55.38	1	
56.43	0	
57.99	2	8.14 Zr 41
60.43	5	.25 CN
62.64	5	3.10 Zr 40, .59 CN
64.11	0	.11 CN
66.04	0	.05 Ti 151, .20 YII 31
67.30	2	.26 CN (2,1)
68.27	1	.24 Ti 151
70.41	1	.12 Zr 40, .62 CN
72.38	3	.38 CN
74.24	1	.43 CN
75.02	0	
76.92	0	
79.05	0	
80.70	3	.55 Ti 195
81.53	3	.52 CN
82.51	2	.54 CN
84.96	3	5.18 CN
89.83	3	
91.23	2	
92.85	5	.64 3.04 CN
93.62	5	.48 V 30
95.98	3	6.02 CN, 6.58 Atm
97.77(35)	1	
99.39	1	
8100.92	2	
2.22	2	
3.95	3	
5.26	3	
7.23(36)	0	.12 CN
8.50	0	.17 .54 C_2
9.72	5	.84 CN
10.33	2	.09 CN, .18 C_2
11.59	2	.47 C_2
12.97	2	3.24 C_2
14.68	5	.89 CN
8116.87	4	.80 V 30
18.79	2	.91 CN
20.11	4	
22.08	1	.19 C_2
25.24	5	CN (3,1), .45 Atm
26.07	5	.23 CN
27.02	3	6.52 Li 3, .19 C_2, 6.85 Atm
27.81	2	
29.20	0	
30.49	5	.46 CN Atm
32.87	0	3.00 Zr 40
33.67	3	.53 C_2, .36 Ti 195, .78 Atm
35.15	0	.05 Atm
36.64	5	.53 Atm
37.45	4	
40.57	5	.67 Atm
41.93	5	.94 Atm
44.20	4	.58 V 30, 3.79 Atm
46.71	4b	.21 7.19 Atm
48.47	3	.08 .39 Atm
49.74	5	.88 CN, .69 Atm
52.48	4	.50 Atm
54.82	6	.67 Atm
57.84	3	8.02 CN Atm
61.83	9b	.06 V 30, .43 CN, .43 .97 2.35 Atm
64.55	6	.54 Atm
69.50	4	8.82 .39 0.00 Atm
70.86	1	
72.49	1	
74.51	4	.68 Atm
77.11	4	6.98 Atm
78.97	2	.49 9.06 Atm
80.20	1	
81.90	4	.85 Atm
83.11	3	.26 Na 4
86.49	2	.73 V 30, .37 Atm
84.65	2	
87.84	3	
89.21	4	.27 Atm
92.87	6	3.11 Atm
95.04	4	4.79 Na 4
97.55	4	.70 Atm
99.01	1	8.87 V 30
8200.57	5b	9.99 .69 Atm
4.11	0	.10 Fe 12
4.82	0	.93 Fe 12, .83 Atm
6.81	1	
8.20	2	
9.56	3	.56 Atm
11.12	0	
12.46	4	.59 Zr 40, .13 Atm
14.87	3	
18.19	3	.11 Atm
21.37	2	.55 Atm
22.40	1	
24.10	2	3.99 Atm
25.45	1	
26.85	3	.96 Atm
28.18	7b	7.99 .32 .76 Atm
29.90	1	.76 Atm

TABLE 2-Continued

Wave Length	Intensity	Identification	Wave Length	Intensity	Identification
8231.59	5	.29 .70 Atm	8349.05	4	.05 Fe 12, .16 .38 Atm
34.17	4	3.91 Atm	50.83	1	
37.38	4	.34 Atm	53.47	3	.15 Ti 33, .64 Atm
41.79	4	.61 V 30	57.20	3	.04 .44 Atm
43.54	4	.49 Atm	59.86	1	
44.99	0		62.32	2	.00 .30 Atm
47.02	3		64.02	3	.24 Ti 33
50.94	2		67.52	1	.33 Atm
52.70	4	.73 Atm	70.07	3	.21 Zr 40
53.48	2	.51 V 30	73.64	1	.71 Atm
54.20	1		76.25	3	.38 Atm
56.33	4	5.90 V 30, .52 Atm	77.79	3	.90 Ti 33
58.10	2		81.01	0	
59.76	1	.69 Atm	82.59	4	.23 Fe 12, .54 .82 Ti 33
60.61	1		83.38	2	
63.38	3	.45 Atm	86.28	2	
66.37	1		87.85	1	.78 Fe 60
68.11	1		89.23	2	.42 Zr 40
71.87	3	2.04 Atm	90.26	1	
72.26	1	.47 CN (3,2)	94.25	2	.02 Atm
74.15	5b	.35 Atm	96.79	3	.93 Ti 33
76.44	3	.54 .69 Atm	98.18	0	
79.51	1	.60 Atm	8405.23	2	
82.20	4	.02 Atm	6.95	0	
83.23	2		8.35	2	
85.09	0		9.70	2	
87.85	3	.94 Atm	11.33	2	
89.40	3	.54 Atm	12.31	3	.36 Ti 33
92.30	0		13.84	3	4.00 Zr 40
94.18	4b	3.52 .16 .54 Atm	15.47	1	.45 Atm
96.17	0		17.03	1	
98.32	3b		18.51	0	
8300.34	2	.41 Atm	19.93	2	
2.62	1		20.76	2	
4.13	1	.30 Atm	23.15	0	.10 Ti 150
5.16	4	.09 Atm	26.37	4b	5.89 Fe 12, .50 Ti 33
6.10	0	5.94 Zr 40	31.23	0	
7.43	3	.61 Fe 12, .41 Ti 33	32.96	1	
9.63	2		34.98	3	.98 Ti 33
11.86	2	.96 Atm	43.77	0	
13.89	1	.87 Atm	45.92	1	
16.04	3	.22 Atm	47.60	2	.63 Fe 12
17.99	3	8.14 Atm	50.37	2	
20.16	1		54.05	0	
21.29	5	.24 .59 Atm	56.12	2	
23.26	0		57.21	1	.10 Ti 141
24.35	2		60.20	2	.25 Atm
26.13	2		64.63	3	.65 Zr 40
27.08	2	.06 Fe 60	68.44	2	.46 Ti 150, .42 Fe 60
28.49	0		69.52	0	
29.83	1	.68 Atm	70.96	1	
31.55	1		73.92	0	
33.41	2	.58 Atm	76.59	3	
34.33	0	.37 Ti 33	78.06	1	
35.68	3	.51 Atm	80.10	2	
37.82	3		81.82	2	
38.92	5	9.03 Atm	82.99	2	3.16 Ti 150
42.30	0		84.87	2	
43.68	2		86.21	1	
45.76	0		87.94	3	

TABLE 2-Continued

Wave Length	Intensity	Identification	Wave Length	Intensity	Identification
8491.34	0		8594.12	1	
93.30	1		98.33	1	
94.55	0	.42 Ti 141	8601.03	0	0.98 Ti 141
95.71	2		2.50	2	
97.34	2		3.92	1	
98.09	4	.02 CaII 2, .44 Zr 40	5.47	1	
8502.40	1		7.35	0	
3.45	1		9.92	2	
4.63	1		11.27	1	
6.27	0		13.00	3	2.91 Ti 141
10.00	0		15.58	1	
13.95	2	4.08 Fe 60	16.83	0	
18.25	1	.37 Ti 150	21.52	0	
19.18	0		23.05	1	
21.07	4	.10 Cs 1	26.32	1	
22.79	2		29.08	1	
25.25	2		31.83	2	
26.97	1		33.96	1	
28.38	0		35.04	1	
29.94	1		36.44	2	
31.45	1	.36 Ti 141	38.08	1	
37.84	2		39.54	2	
39.66	1	CN (5,3)	41.91	2	
42.14	5b	.09 CaII 2	42.73	1	
46.56	0		44.45	2	
48.06	1	.07 Ti 150	62.12	5b	.14 CaII 2, 1.91 Fe 60
49.14	0		75.45	2	.38 Ti 68
50.67	4	.54 Ti 141	88.76	3	.63 Fe 60
55.32	3		92.29	3	.34 Ti 68
56.89	0		8734.57	2	.70 Ti 68
60.91	2		51.04	3	0.82 C_2 (2,0)
64.37	1		51.62	3	.44 .65 C_2
65.60	0	.45 Ti 141	52.10	0	3.92 C_2
67.21	1		57.06	2	.10 C_2
68.90	1		61.09	0	.16 C_2
70.72	1		63.87	3	.70 C_2
72.04	0		66.76	6	.64 Ti 68
74.58	1		67.87	0	.71 C_2
75.99	1		72.94	4	3.18 C_2
78.31	2	.40 Ti 141	78.62	4	.66 Ti 140
79.83	1		82.15	4	.04 C_2
81.97	2		92.37	3	.31 C_2
82.80	2		8804.90	3	.70 C_2
84.22	1		19.58	1	.39 Ti 68
91.09	1		24.24	1	.23 Fe 60

b = broad
d = diffuse
vb = very broad

NOTES TO TABLE 2

1. Contribution to the intensity by 5958.23 *Fe* 14 predominates.
2. Contribution to the intensity by 5971.70 *Ba* 7 predominates.
3. Contribution to the intensity by 5984.59 *Ti* 2 predominates.
4. The trace of 5996.01 *Ti* 154 is seen close to this line.
5. Contribution to the intensity by 6062.88 *Zr* 3 predominates.
6. The trace of 6116.99 *Co* 37 is seen close to this line.
7. The region between 6164 A and 6212 A was impossible to measure.
8. 6213.44 *Fe* 62 may be blended.
9. The trace of 6277.53 *Ti* 144 is seen close to this line.
10. The trace of 6279.76 *Sc* II 28 is seen close to this line.
11. Contribution to the intensity by 6410.98 *La* 7 predominates.
12. Not listed in *R.M.T.* It was identified from the *M.I.T. Tables*.
13. Contribution to the intensity by 6455.99 *La* 1 predominates.
14. Contribution to the intensity by 6543.17 *La* 7 predominates.
15. Contribution to the intensity by 6572.78 *Ca* 1 predominates.
16. The trace of 6586.33 *Ni* 64 is seen close to this line.
17. Not listed in *R.M.T.* It was identified from the *M.I.T. Tables*.
18. Not listed in *R.M.T.* It was identified from the *M.I.T. Tables*.
19. Contribution to the intensity by 6709.49 *La* 6 predominates.
20. The region between 6909 A and 6916 A was impossible to measure.
21. The region between 6921 A and 6929 A was impossible to measure.
22. The trace of 7062.97 *Ni* 64 is seen close to this line.
23. Contribution to the intensity by 7111.71 *Zr* 23 predominates.
24. 7312.62 Atm is not seen.
25. Not listed in *R.M.T.* It was identified from the *M.I.T. Tables*.
26. 7349.49 Atm may be blended.
27. 7417.06 *Ti* is not seen in *R.M.T.* In the table of infrared solar spectrum its lower excitation potential is 1.06 e.v.
28. Not seen in *R.M.T.* In the table of infrared solar spectrum its lower excitation potential is 0.81 e.v.
29. Not seen in *R.M.T.* In the table of infrared solar spectrum its lower excitation potential is 0.83 e.v.
30. Not seen in *R.M.T.* In the table of infrared solar spectrum its lower excitation potential is 0.81 e.v.
31. 7665.95 Atm O_2 is weaker than 7660.44 Atm. Therefore, contribution to the intensity by 7664.91 *K* 1 predominates.
32. Contribution to the intensity by 7912.89 *Fe* 12 predominates.
33. 7971.52 Atm may be blended.
34. The trace of 8026.38 *CN* is seen close to this line.
35. The trace of 8098.50 *Ti* 195 is seen close to this line.
36. The trace of 8107.84 Atm is seen close to this line.

RADIAL VELOCITIES AND MASSES OF DOUBLE GALAXIES*

THORNTON PAGE
Yerkes and McDonald Observatories†
Received July 23, 1951

ABSTRACT

With a grating spectrograph at the prime focus of the 82-inch reflector, spectra have been obtained of 20 double galaxies at approximately 330 A/mm dispersion. For each exposure, the slit was placed across both members of a pair and guided accurately so that two spectra appear side by side between the comparison spectra on each film. These films were measured both for the mean radial velocity of each pair, V, values of which range from 900 to 6700 km/sec, and for the difference in radial velocity between the two members of each pair, ΔV, which ranges from 0 to 360 km/sec. Measurement was facilitated by the emission lines, $H\alpha$ and [O II] λ 3727, which appear in many of the spectra. The errors are estimated to be about ± 100 km/sec in V and ± 30 km/sec in ΔV.

Using the measured values of V, the velocity-distance relation, and the angular separations, the projected linear separation of each pair is derived. From this and the measured value of ΔV, and assuming circular orbits, a "double-angled mass function" is obtained for each pair. The mean of these mass functions yields as a mean mass for the components of double nebulae, the value 8×10^{10} solar masses with an estimated observational error less than ± 40 per cent.

Although the observations do not yet permit an accurate determination of the frequency distribution of masses among these nebulae, there is good evidence in these and other data that many individual masses are over twice the mean, and many others are one-tenth the mean or less. In fact, these limited data indicate a sharp division between heavy-weight and light-weight galaxies of 1.5×10^{11} and 0.5×10^{10} solar masses, respectively.

INTRODUCTION

In principle, there appear to be at least four distinct methods for estimating masses of the galaxies: (*a*) from internal rotational motions in individual systems, as applied by Babcock[1] to M31, by Mayall and Aller[2] to M33 and to observational data of Pease and Humason[3] for NGC 3115 and 4594, and by Oort[4] to the galaxy; (*b*) from orbital motions of double galaxies as proposed by Holmberg;[5] (*c*) from the spread of velocities in clusters of galaxies, as applied by Sinclair Smith[6] and modified by Tuberg;[7] and (*d*) from a suitable mass-luminosity ratio.[8]

Since the outer regions of a galaxy may be too faint to record, the first method (*a*) yields a lower limit only; it is time-consuming and can be applied with accuracy only to near-by objects of large angular dimensions. The third (*c*) is limited to cluster nebulae, which may differ from the field nebulae due to the collisions studied by Spitzer and Baade;[9] this method may also be subject to theoretical criticism.[7, 10] The last (*d*) will not be applicable until a good deal of detailed mass data are obtained by the other dynamical methods.

The method applied here, (*b*) above, can, in principle, yield an accurate average value of the masses of galaxies involved in pairs without neglecting their outer parts. It de-

* *Contributions from the McDonald Observatory, University of Texas*, No. 204.

† On the staff of the Operations Research Office, The Johns Hopkins University, Chevy Chase, Maryland, since September, 1951.

[1] *Lick Obs. Bull.*, **19**, 41, 1939.
[2] *Ap. J.*, **95**, 5, 1942.
[3] *Proc. Nat. Acad. Sci.*, **2**, 520, 1916; Humason, *Ann. Rep. Dir. Mt. W. Obs.*, 1936–37, p. 31.
[4] *B.A.N.*, **3**, 275, 1927; **4**, 79, 1927.
[5] *Lund Ann.*, **6**, 1937.
[6] *Ap. J.*, **83**, 23, 1936.
[7] *Ap. J.*, **98**, 501, 1943.
[8] Hubble, *Ap. J.*, **79**, 8, 1934.
[9] *Ap. J.*, **113**, 413, 1951.
[10] G. C. Omer, Jr., private communication; Holmberg, *Ap. J.*, **92**, 265, 1940.

pends on measurement of ΔV, the difference in the radial velocities of two galaxies, which is assumed to be a projected orbital velocity in a circular orbit. The projected linear separation is obtained from the angular separation, S, and the distance, D; the latter is determined from the mean radial velocity of the system, V, and the velocity-distance relation, $V = kD$.

The application of this procedure to determine the average mass of a galaxy, and thence the mean density of matter in the universe, may appear to suffer from four weaknesses:

1. The double galaxies may differ statistically from the field galaxies.
2. The determination of mass is unreliable for wide pairs and for very close pairs moving within one another. It does not apply if the relative motion is hyperbolic.
3. Tidal effects and other second-order effects may greatly increase the complexity of reducing mean masses from observed radial velocities.
4. Because of the projection, a relatively large number of pairs must be studied to obtain a reliable mean mass, even with simplifying assumptions.

However, Holmberg has shown[5] that the double galaxies have roughly the same dimensions and absolute magnitudes as the field nebulae. The 827 double and multiple systems listed in his catalogue are so much more numerous[11] than the computed number of chance optical pairs among nebulae brighter than his limiting magnitude of 14.5, that virtually all these pairs can certainly be considered as physical systems. Holmberg derives a mean separation of 4000 psc.

It seems unlikely that the double galaxies are in the process of collision; that is, it is likely that they are moving in closed orbits. For, if they were moving in hyperbolic orbits, the number of pairs of field nebulae expected to be in random collision at any one time would be smaller by several orders of magnitude than the number of pairs actually observed.

Tidal effects have been neglected here, on the evidence of Carpenter's photographs, some of which are reproduced in Figures 1 and 2. As Carpenter[12] points out, many of these pairs ignore each other, tidally speaking; the major axes of the individual galaxies being perpendicular to the line joining the pair. If tidal coupling were complete, we would expect orbital and rotational angular momenta to be parallel; a plan view would then show two spirals of the same sense; and an oblique view would show the major axes parallel.

In the analysis of Section II below, the two galaxies in a pair are considered to behave as point masses. Such an approximation seems appropriate in view of the presently limited observational material and the complex dynamics of extended fluid disks. For the same reasons, the effects of one or more distant members on a close pair involved in a multiple system are neglected.

In criticism of this approximation, it may be noted that six, or possibly seven, of Carpenter's photographs show pairs of spirals formed in the same sense (i.e., both S or both Z), while only two (NGC 1241-3 and NGC 5278–9, both doubtful) show spirals possibly of reversed senses. This evidence of coupling between orbital and rotational motion in spiral pairs deserves further study.

Professor E. F. Carpenter has kindly provided the photographs reproduced in Figures 1 and 2, together with the following information:

> These photographs of some of the double galaxies which you are studying spectrographically are part of a collection of plates of more than 150 such objects having apparent separation of centers not exceeding the apparent diameter of the larger member. These photographs were for the most part made before World War II in a continuing systematic survey of this type of object. The original negatives have a scale of 45″ per mm. They were made with the 36-inch Steward

[11] Holmberg, *op. cit.*, Fig. 2, p. 13; *Ap. J.*, **92**, 200, 1940.

[12] Address of the retiring president, Section D, AAAS, Dec. 1950.

FIG. 1.—*a*, NGC 3395–6 (see Pease, *Ap. J.*, **51**, 280, 1920); *b*, NGC 3786–8 (see Pease, *Ap. J.*, **51**, 280, 1920); *c*, NGC 3799 3800; *d*, NGC 4647–9. South is indicated by an arrow on each photograph; enlarged approximately 7 times.

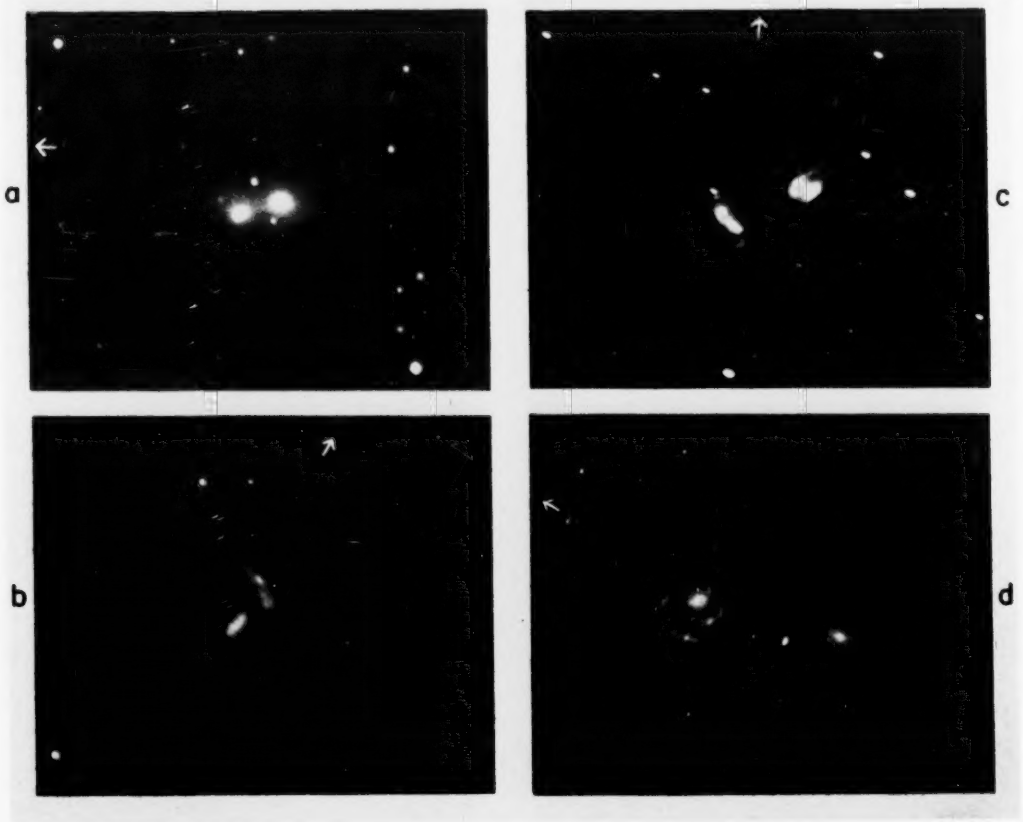

FIG. 2.—*a*, NGC 4782–3; *b*, NGC 4809–10; *c*, NGC 5257–8 (see Pease, *Ap. J.*, **51**, 280, 1920); *d*, NGC 5426–7. South is indicated by an arrow on each photograph; enlarged approximately 7 times.

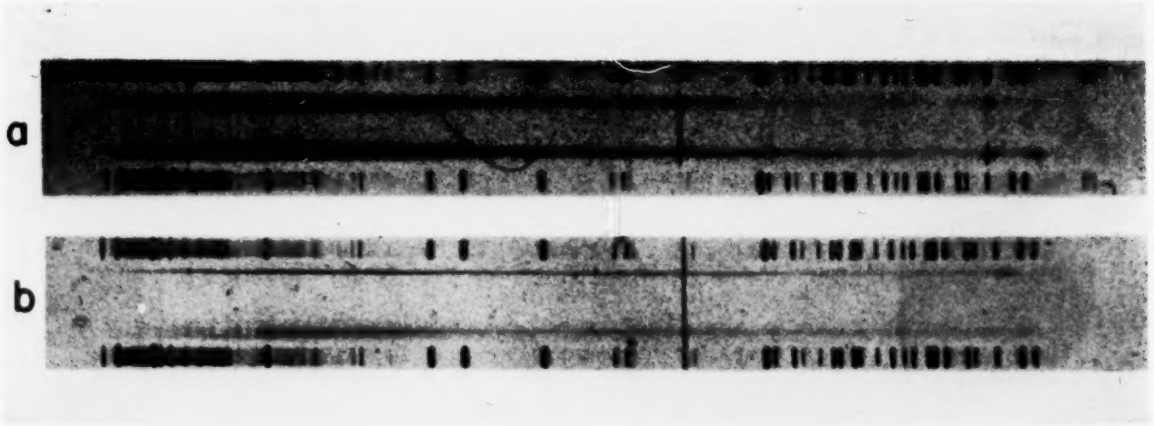

FIG. 3.—Spectra of double galaxies, enlarged 10 times. *a*, NGC 3395–6; *b*, NGC 3786–8. In each case the spectrum at the top is of the first nebula listed, and red is to the right. The comparison spectrum is from a cadmium-lead spark in the blue and from a neon lamp in the red. The night-sky lines, λλ 4477, 5890, and 6300, extend across both spectra. In NGC 3395–6 the forbidden line of *O* II, λ 3727, extends from one nebula to the other. These spectra were taken with the Babcock grating, exposure 4 hours.

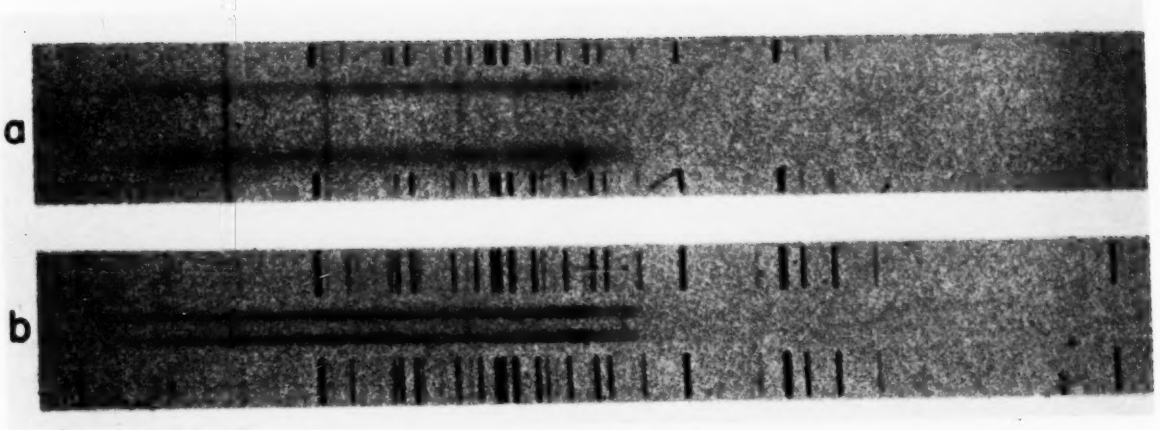

FIG. 4.—Spectra of double galaxies, enlarged 10 times. *a*, NGC 3799–3800; *b*, NGC 5929–30. In each case the spectrum at the top is of the first nebula listed, and red is to the right. The comparison spectrum is from a neon lamp. The night-sky lines, λλ 5577, 5890, 6300, and 6360, extend across both spectra. *Hα* and [*N* II] emission lines are present in all four nebular spectra and are strongly inclined, owing to rotation, in NGC 3800. These spectra were taken with the new Bausch and Lomb grating, which has lower efficiency in the blue, exposure 2 hours.

Reflector, usually with exposures of about an hour on Eastman *IIa*-O plates or an equivalent. The observing list was based largely on a ms. compilation generously given me a number of years ago by Professor Knut Lundmark.

I. THE OBSERVATIONAL MATERIAL

Spectra were all obtained with the B spectrograph attached at the prime focus of the 82-inch reflector. This spectrograph was originally designed by H. W. Babcock and modified by the author. Light passes through the slit and a central hole in the grating behind the slit to fall on an $f/4$ Pyrex paraboloid collimator of 2 inches aperture, whence it is reflected down on the grating and reflected again into an $f/0.65$ thick-mirror type UV-glass Schmidt camera of 2.5 inches aperture. The grating first used was one ruled in aluminum on Pyrex by H. D. Babcock at Mount Wilson in 1940, with 15,000 lines per inch and blaze at λ 5000 in the first order. This grating deteriorated with age and was replaced in March, 1951, with an aluminized Bausch and Lomb replica grating[13] of 15,000 lines per inch and blaze at λ 6500, which increased the speed at *Hα* by a factor of 3.

The scale at the prime focus of the 82-inch telescope is 25″.4/mm. The maximum slit length used was 11.4 mm (4′.8 at the prime focus), and the reduction factor in the spectrograph is 5.7. The scale perpendicular to dispersion on the spectrograms is 2′.4/mm. The dispersion varies linearly with the wave length on any one spectrogram and with the wave length centered on the spectrogram by adjustment of the grating. The two grating settings used were designated *G* (green centered) and *α* (*Hα* centered); for the former the dispersion was 330 A/mm at *Hα* and 415 A/mm at λ 3727; for the latter, 370 A/mm at *Hα*.

In order to obtain spectrograms in good focus from λ 3727 to *Hα*, the emulsion was curved to the 2.6-inch radius of curvature of the solid Schmidt camera face. All spectra were taken on Eastman 103*a*-F film, hypersensitized in a cool ammonia bath, dried quickly, cut to size $\frac{9}{16} \times \frac{9}{16}$ inch, and constrained to the proper curvature between a convex disk and a ring. The concave glass surface of the solid Schmidt camera face was oiled with clear kerosene (to provide good optical contact) and the emulsion pressed firmly against this surface during exposure. Before development, the kerosene was cleaned off the emulsion with methalene. Measurements of over 30 test films and other spectrograms have shown no evidence of film distortion or emulsion "creeping," within the errors of measurement. Several of the spectra are shown unretouched in Figures 3 and 4.

The curvature of the slit image was determined accurately from test spectra and found to be symmetrical, though not circular. The curvature varies systematically with wave length. A correction for curvature is applied to all the following measurements, although such correction is less than 1μ for the differential measurements of ΔV between spectra of two galaxies symmetrical to the optical axis. The correction for curvature between comparison lines and galaxy lines for measurement of V is generally less than 3μ.

Accuracy of measurement was limited by the slit width (0.20 mm, corresponding to 14 A at *Hα*); by the grain of the hypersensitized 103*a*-F emulsion, by the broadening of the lines, and by the inclinations of the lines in some of the spectra. In order to get the highest accuracy possible, all spectra were measured twice, once direct and once reversed; three settings were made on each comparison line and 10 or more on each galaxy line, there being roughly three near-by comparison lines for each galaxy line measured. Differential velocities were determined from the average differences between settings made on the galaxy lines in rapid succession, a procedure which certainly improves, for this purpose, upon separate individual measurements relative to comparison lines.

Great care was exercised in adjusting the micrometer run parallel to the dispersion and the micrometer wire perpendicular thereto in each measurement. Settings on the

[13] I am grateful for a Research Corporation grant which made this purchase possible.

TABLE 1
THE OBSERVATIONAL MATERIAL

NGC	Holmberg	No. of Films	Est. Line Intensities						Δy (Mm.)	V' (Km/Sec)	Weight (V')	ΔV (Km/Sec)	Weight (ΔV)
			N II	$H\alpha$	3727	D	H	K					
2814	124*	1	...	...	+5	...	...	...	1.59	1590	1.0	+ 7	1.0
2820	...	...	...	...	+2	...	...	...					
2872	130*	2	...	...	...	...	−4	−4	0.54	3280	2.6	−640	2.9
2875	...	...	...	...	...	...	−4	−3					
An 9:44a	143*	2	+½	+1	...	...	...	...	0.65	6070	1.8	+ 80	3.8
An 9:44b	...	...	+½	+2	...	...	...	...					
3395	215	4	+1	+4	+4	†	...	...	0.53	1643	16.5	− 4	25.8
3396	...	...	+5	+8	+8	†	...	...					
3769	270	2	+½	+1	+3	...	...	...	0.50	730	3.7	+ 36	4.0
Anon.	...	...	...	+½	+1	...	...	...					
3786	272*	1	+3	+5	+5	†	...	...	0.61	2550	1.0	+410	0.3
3788	...	...	...	...	...	...	−3	...					
3799	...	2	+2	+3	...	...	...	...	0.57	3540	5.3	− 44	5.0
3800	...	...	+3	+5	...	...	...	...					
4038 (S)	...	4	+2	+4	+4	†	...	...	0.44	1650	13.3	50 (S faster)	16.8
4039 (N)	...	...	+1	+4	+2	†	...	...					
4278	369	1	...	+1	...	−3	−5	†	1.50	925	0.6	−450	1.3
4283	...	...	...	+½	...	−2	−2	...					
4485	414	1	...	...	+1	†	...	...	1.435	720	1.0	+155	0.5
4490	...	...	...	...	+8	†	...	...					
4567	427	3	+½	+1	...	...	−3	−3	0.51	2200	2.9	+56	5.9
4568	...	...	+½	+2	...	...	−3	−3					
4647	448	1	...	+½	...	...	−1	−2	1.06	970	0.5	+260	0.5
4649	...	...	...	...	...	†	−2	−2					
4782	485	1	...	...	...	−2	−5	−2	0.29	4300	0.6	+630	1.0
4783	...	...	...	...	...	−2	−2	−4					
4809	486	1	...	+2	...	...	...	...	0.29	920	1.0	+ 60	2.0
4810	...	...	...	+2	...	...	...	...					
5194	526	1	†	+3	+5	...	−5	−3	1.85	515	1.0	+ 90	1.0
5195	...	...	†	+1	...	−5	−5	−3					
5257	532	1	+½	+2	+1	...	...	...	0.57	6720	0.4	+175	1.1
5258	...	...	+½	+½	+½	...	...	...					
5426	573	2	+½	+1	+1	...	−2	−4	0.97	2540	3.6	− 96	2.9
5427	...	...	...	...	+1	...	−2	−5					
5544	...	1	...	...	...	...	−½	−½	0.25	3170	1.5	− 10	0.1
5545	...	...	1	2	...	...	...	...					
5929	710	2	+1	+3	+3	...	...	...	0.20	2610	5.7	−185	10.0
5930	...	...	+3	+5	+1	...	...	...					
5953	714	3	+3	+5	+3	...	...	...	0.33	2120	12.1	+ 40	12.0
5954	...	...	+1	+3	+1	...	...	...					

* Known to be multiple systems rather than simple pairs.

† Other lines were measured as follows:

NGC 3395: λ 5007, Int. +3, $H\beta$ + 2, $H\gamma$ + 1
NGC 3396: λ 5007, Int. +5, $H\beta$ + 4, $H\gamma$ + 5
NGC 3786: λ 5007, Int. +8
NGC 4038(S): $H\beta$, Int. +2
NGC 4038(N): $H\beta$, Int. +2
NGC 4278: G, Int. −1
NGC 4485: $H\gamma$ through H_7 in absorption
NGC 4490: $H\gamma$ through H_7 in absorption
NGC 4649: G, Int. −2
NGC 5194: λ 5007, Int. +3
NGC 5195: $H\beta$, Int. −2, $H\gamma$ − 1, $H\delta$ − 2
NGC 5427: λ 5007, Int. +5.

comparison lines on either side of the galaxy spectra determined an average deviation from perpendicularity at each galaxy line, which was applied as a correction to the differential measurements (generally less than 1 μ).

As a result of these precautions, the unit mean error of a differential measurement of one emission line is believed to be about 2 μ, or 30 km/sec at $H\alpha$, and the mean unit error of an absolute measurement, about 4 μ, or 60 km/sec at $H\alpha$. These estimates are roughly confirmed by the internal errors derived in Section III below.

The early spectrograms taken in 1948–1949 indicated that a remarkably large proportion of the double galaxies show λ 6584 of [*N* II], $H\alpha$ and λ 3727 of [*O* II] in emission. In some cases, λ 5007 of [*O* III] and other hydrogen lines also appeared in emission. Another paper is in preparation on these emission features; it is sufficient to note here that practically all irregular and Sc type nebulae show emission lines and that the proportion decreases through Sb and Sa to some 20 per cent of E nebulae. Since the emission lines are generally sharper, more definitely identified, and more easily measured, there is a natural selection of emission-line objects in this study. However, the H, K, G, and D absorption lines were also measured on many spectra and these values combined at lower weight (see Sec. III).

TABLE 2

MEASURED RADIAL VELOCITIES

NGC	Humason	Mayall	Page	Weight
3395	.....	+1751 km/sec	+1641 km/sec	(16.5)
3396	.....	+1643	+1645	(16.5)
4038–9	+1636 km/sec	.....	+1625	(13.3)
			+1675	(13.3)
4278	+ 630	.....	+ 700	(0.6)
4283	+1070	.....	+1150	(0.6)
4485	+ 625	.....	+ 640	(1.0)
4490	+1370	.....	+ 795	(1.0)
4567	.....	+2284	+2228	(2.9)
4568	.....	+2413	+2172	(2.9)
4647	.....	+1448	+1100	(0.5)
4649	+1389	+1244	+ 840	(0.5)
5194	+ 438	.....	+ 470	(1.0)
5195	+ 542	.....	+ 560	(1.0)

The pairs of galaxies were chosen primarily from Holmberg's *Catalog of Double and Multiple Galaxies*,[5] limiting the selection to pairs of separation less than 4.'4 and mean surface brightness, *H*, generally brighter than 13.5 mag. per square minute of arc. Pairs with large differences in *H* were avoided. It was found that an emission-line object of $H = 13$ mag. required an exposure of at least 4 hours with the Babcock grating, or 2 hours at $H\alpha$ with the Bausch and Lomb grating.

In all, some 55 spectra were obtained of 25 different pairs, of which 36 spectra of 20 different pairs were chosen for measurement. These 20 pairs are listed by NGC numbers in Table 1, together with Holmberg's catalogue number, number of films, estimated line intensities, separation of the two spectra Δy, measured mean velocity V', measured differential velocity ΔV, and weights. For 13 of the nebulae in this list, velocities have been measured separately by Mayall and by Humason, who obtained the values given in Table 2, kindly made available to me in advance of publication. With a few exceptions, mainly the values of low weight, the agreement is satisfactory.

The measured mean velocities, V', have been corrected for galactic rotation by means of the relation

$$V = V' + 250 \cos\beta \cos(\lambda - 55°),$$

where β and λ are galactic latitude and longitude, respectively. Values of V are given for the 20 pairs in Table 3.

TABLE 3

DATA FOR 20 DOUBLE GALAXIES

NGC	Type	Em.*	A	H	S	d (Psc)	V (Km/Sec)	ΔV† (Km/Sec)	F (10^9 Suns)	F Range (10^9 Suns)	L (10^7 Suns)
2814	E	+	0.8	12.1	4.0	740	1680 ± 100	+ 7 ± 50	0.021	0 — 1.5	4.5
2820	E	+	3.0	13.4		2780					6.5
2872	E	—	0.6	12.5	1.35	1050	3150 ± 50	−640 ± 40	111.	92. −137.	16.5
2875	E	—	2.5	14.1		4350					12.5
An. 9:44a	E	+	2.0	13.7	1.62	6540	5910 ± 50	+ 80 ± 30	4.	1.42 — 8.0	50.
An. 9:44b	E	+	1.0	12.9		3270					41.
3395	Sc	+	1.3	12.1	1.32	1150	1610 ± 30	− 4 ± 15	0.002	0. — 0.05	15.5
3396	Irr	+	1.5	12.7		1330					6.2
3769	SBc	+	2.7	12.6	1.25	1150	770 ± 50	+ 36 ± 20	0.086	0.01 — 0.22	3.0
Anon	Sa	+	0.5	11.6		220					0.6
3786	S	+	1.7	13.0	1.52	2380	2540 ± 80	+410 ± 80	42.0	24.5 — 65.0	14.0
3788	S	—	1.7	12.2		2380					25.
3799	SBa	+	0.7	12.2	1.42	1340	3460 ± 50	− 44 ± 40	0.61	0.01 — 2.42	25.
3800	Sb	+	1.8	12.0		3440					43.
4038	Sc	+	(1.0)	13.0	1.10	(820)	1480 ± 30	50 ± 15	0.26	0.11 — 0.49	20.
4039	Sc	+	(1.0)	13.0		(820)		(S faster)			18.0
4278	E1	+	2.0	13.1	3.7	1020	920 ± 80	−450 ± 60	44.0	29.5 — 63.0	8.2
4283	E0	—	0.9	12.5		460					2.7
4485	Sc	+	1.1	11.6	3.5	460	760 ± 90	+155 ± 90	4.1	0.62 — 11.8	4.3
4490	Sc	+	4.3	12.3		1810					30.
4567	Sb	+	1.8	12.3	1.27	2120	2130 ± 50	+ 56 ± 25	0.55	0.15 — 1.3	23.
4568	Sb	+	3.2	12.6		3760					25.
4647	Sc	—	1.6	12.4	2.8	800	910 ± 100	+260 ± 90	11.1	4.0 — 23.0	9.9
4649	E2	—	2.7	12.5		1360					27.
4782	E0	—	0.5	11.4	0.71	1150	4170 ± 100	+630 ± 50	76.	52. −102.	57.
4783	E0	—	0.4	10.7		920					39.
4809	Irr	+	2.0	13.3	0.73	930	840 ± 100	+ 60 ± 40	0.14	0.01 — 0.50	1.7
4810	Irr	+	0.6	11.7		280					1.6
5194	Sc	+	10.4	(14.8)	4.4	3480	605 ± 70	+ 90 ± 50	1.38	0.23 — 3.8	10.8
5195	Irr	+	2.0	13.4		670					2.1
5257	Sb	+	0.6	11.8	1.42	2220	6660 ± 70	+175 ± 50	18.5	8.7 — 33.0	130.
5258	Sb	+	1.1	12.6		4050					90.
5426	Sbc	+	2.1	13.7	2.6	2880	2480 ± 60	− 96 ± 30	3.8	1.7 — 6.9	27.
5427	Sbc	+	2.0	13.1		2740					62.
5544	E	—	0.7	13.2	0.6	1190	3090 ± 70	− 10 ± 100	0.012	0. — 1.77	13.0
5545	E	+	1.2	12.9		2050					13.0
5929	E0	+	0.5	12.6	0.5	760	2750 ± 50	−185 ± 20	3.0	1.5 — 4.5	7.5
5930	E2	+	0.6	12.5		910					11.9
5953	E	+	0.3	10.7	0.8	360	2190 ± 30	+ 40 ± 20	0.185	0.04 — 0.47	10.8
5954	Sc	+	0.9	12.1		1090					11.9
Mean				12.5	1.83	1780			16.05	10.85 — 23.35	23.0

* Under "Em.," + indicates that emission lines are observed.

† ΔV is reckoned positive when the first nebula listed in the pair has the larger velocity of recession.

II. DYNAMICS

For two galaxies, here considered as point masses M_1 and M_2 moving in a circular relative orbit, we have the following relationships:

$$M_1 + M_2 \equiv 2M = \frac{a\,v^2}{(9.48\pi)^2}, \tag{1}$$

$$\Delta V = v \cos \phi\,, \tag{2}$$

$$S = \frac{a \sin \psi}{60\,D}, \qquad \text{and} \tag{3}$$

$$D = \frac{V}{k}, \tag{4}$$

where a is the radius of the relative orbit in astronomical units, v is the circular velocity in km/sec, ϕ is the angle between v and the line of sight, S is the angular separation in minutes of arc, ψ is the angle between the radius vector and the line of sight, D is the distance to the pair from the earth in parsecs, and k is[14] 5.26×10^{-4} km/sec/psc.

Since v is perpendicular to a, we have

$$\cos \phi = \sin i \cos \Omega\,, \qquad \text{and} \tag{5}$$

$$\cos \psi = \sin i \sin \Omega\,, \tag{6}$$

where i is the inclination of the orbit to the plane of the sky, and Ω the angle of the secondary galaxy from the receding node. Combining these expressions, we obtain

$$F \equiv \frac{60}{2k\,(9.48\pi)^2}\,S\,V\,(\Delta V)^2 = M \sin^2 i \cos^2 \Omega\,(1 - \sin^2 i \sin^2 \Omega)^{1/2}, \tag{7}$$

or

$$F \equiv 64.1 S\,V\,(\Delta V)^2 = M f\,, \tag{8}$$

where F is a double-angled mass function, analogous to the mass functon derived for spectroscopic binary stars, and $f \leq 1$. An observed value of F, therefore, sets a lower limit to the mean mass of any one pair of galaxies. The calculation of F for each of the 20 pairs is set forth in Table 3.

If, as seems quite likely, the orbits are inclined at random and the secondary galaxies of various pairs are at random angles from the node, the average value of f for a number of pairs is

$$\bar{f} = \frac{\displaystyle\int_0^{\pi/2} d\Omega \int_0^{\pi/2} \sin^3 i \cos^2 \Omega\,(1 - \sin^2 i \sin^2 \Omega)^{1/2} di}{\displaystyle\int_0^{\pi/2} d\Omega \int_0^{\pi/2} \sin i\; di} = 0.295\,, \tag{9}$$

where the integration has been performed by expanding the radical to three terms. From equations (8) and (9) we find the mean mass per single galaxy for a number of pairs to be $\bar{M} = \bar{F}/0.295$.

For random i and Ω we can also determine the distribution function $N(f)$, defined as the fraction of all values of f which lie between f and 1.0, by integrating under curves of constant f in the Ω cos i plane (cos i is used in order to provide the weighted interval sin $i\,di$). The integration has been done graphically, with an accuracy of 1 or 2 per cent, yielding the results given in the second column of Table 4.

We see from Table 4 that the distribution of f is sharply peaked at $f = 0$; that is, a given set of randomly oriented pairs of galaxies, all of the same mass, will yield values of

[14] Hubble, *Ap. J.*, **84**, 517, 1936.

F mostly near zero, with decreasing percentages for values of F up to the limit of $F = M$. It is this geometrical weakness of the present method which limits the accuracy of determining $\bar{M}$, the average mass; in effect, all but a quarter of the observations are lost in the projection; only a quarter of the observations are effective in determining $\bar{M}$.

One of the possible effects of selection treated in Section VI below may arise from the underrepresentation of wide pairs in these data. The average projected separation of the 20 pairs in Table 2 is 1.″83 and, although the average projected separation of the pairs listed in Holmberg's catalogue[5] is about 1.″5, there is reason to believe[15] that the average for all dynamical systems of about 13 mag. is considerably larger.

In the following paragraphs a correction for this selection will be derived. Later the theory will be applied to a second group of data in which much wider pairs are represented, with results that confirm those derived from the data of Tables 1 and 3.

The major effect of a selection of pairs closer than average is to favor small ψ (the angle between the line of centers and the line of sight) and hence to alter the expected distribution function, $N(f)$, from the values given in the second column of Table 4. Now

TABLE 4

THE THEORETICAL DISTRIBUTION FUNCTION $N(f)$

f	$N(f)$			f	$N(f)$		
	No Selection	$S<5'$	$S<2'$		No Selection	$S<5'$	$S<2'$
0	1.000	1.00	1.00	0.50	0.241	0.19	0.15
0.01	0.870	0.81	0.80	0.60	0.182	0.145	0.112
0.02	0.815	0.77	0.71	0.70	0.1295	0.102	0.078
0.05	0.725	0.66	0.58	0.80	0.0825	0.064	0.049
0.10	0.617	0.54	0.45	0.90	0.0393	0.030	0.022
0.20	0.486	0.41	0.34	1.00	0.0000	0.000	0.000
0.30	0.386	0.33	0.26				
0.40	0.308	0.25	0.20	$\bar{f}=$	0.295	0.25	0.21

lines of constant ψ can readily be drawn in the $\Omega \cos i$ plane, using equation (6); a set of modified distribution functions, $N(f, \psi < \psi_0)$, can be obtained by excluding the area of $\psi > \psi_0$ from the integration. However, for a given "cutoff" of projected separations, $S \leq S_0$, the angle ψ_0 will depend on the average space separation, $\bar{a}$, being considered:

$$\sin \psi_0 = \frac{S_0}{\bar{a}}. \tag{10}$$

Hence the modified $N(f)$ will depend on the "cutoff" of the projected separation, S_0, and also on the frequency function of space separations, $N(a)$.

The latter has been determined by Holmberg[15] from a statistical discussion of projected separations. He derives the logarithm of the number of secondary galaxies per unit volume at radius vector a (the primary galaxy of each pair being taken at the origin). For a given "cutoff," S_0, the distribution function $N(f)$ will be normal for $a \leq S_0$ and modified in varying degree for $a > S_0$. For the pairs of separation between a and $a + da$ the modified $N(f)$ will be $N(f, \psi_0 = \sin^{-1} S_0/a)$, and the number of such pairs is $4\pi a^2 N(a) da$. The effective distribution function for these conditions will be:

$$N_{S_0}(f) = N(f) \int_0^{S_0} 4\pi a^2 N(a)\, da + \int_{S_0}^{\infty} 4\pi a^2 N(a)\, N(f, \psi_0)\, da. \tag{11}$$

[15] Holmberg, *Ap. J.*, 92, 200, 1940.

The integration of equation (11) has been performed graphically to give the values in the third and fourth columns of Table 4 for two values of S_0.

Holmberg's values of $N(a)$ are for a in units of one minute of arc at the standard distance corresponding to apparent magnitude 13. All projected separations, S, were therefore reduced to S_R, corresponding to the standard distance, by the relation

$$S_R = S \times 10^{0.2(m-13)}, \tag{12}$$

where m is the magnitude of the brighter nebula in the pair. For the 20 pairs listed in Table 1 we find $\bar{S}_R = 1'.28$, whence the effective cutoff is taken to be between $2'$ and $3'$ (at 13 mag.). For the data on 15 pairs in Table 5, $\bar{S}_R = 7'.9$ and for all 35 pairs $\bar{S}_R = 4'.1$. The "cutoffs" $S_0 = 2'$ and $S_0 = 5'$ were used in calculating $N_{S_0}(f)$ in Table 4; the change

TABLE 5

MASS DATA FOR 15 OTHER DOUBLE GALAXIES

NGC	Source*	S	V (Km/Sec)	ΔV (Km/Sec)	F (10^9 Suns)
205–24	Hu	37'.0	158†	28	0.29
221–24	Hu	24.0	158†	47	0.54
247–53	Ho II	276.	(200)†	35	4.3
2366–2403	Ho II	210.	(300)†	5	1.0
3190–93	Hu	6.0	1270	52	1.3
3226–27	Hu	2.3	1140	227	8.7
3379–84	Ho I	7.3	720	40	0.54
3623–27	Hu	20.4	725	39	1.44
4382–94	Ho I	7.5	630	350	36.
4467–72	Ho I	4.3	1150	750	178.
5236–53	Ho II	114.	475	50	8.7
5457–61	Hu	4.3	410	2	0.00
5574–76	Hu	2.8	1600	188	10.2
5982–85	Ho I	7.6	2920	300	128.
6027a–b	Sey	0.37	4330	384	15.1
Mean		49.3			26.2

* Hu = Humason, unpublished; Ho I = Holmberg, *Lund Ann.*, **6**, 101, 1937; Ho II = Holmberg, *Ap. J.*, **92**, 257, 1940; Sey = Seyfert, *Pub. A.S.P.*, **63**, 72, 1951.

† These values of V are determined from estimated distances; the measured V' are small or negative.

from $S_0 = 2'$ to $5'$ being roughly equal to that from $S_0 = 5'$ to $S_0 = \infty$ (no selection). The effect on $\bar{f}$, and hence on $\bar{M} = \bar{F}/\bar{f}$, is 40 per cent between $S_0 = 2'$ and $S_0 = \infty$. In calculating $\bar{M}$ and the distribution of masses, the distribution function $N_{2'}(f)$ will be used with the observational data for the 20 pairs of Table 1 and $N_{5'}(f)$ for all 35 pairs for which data are available.

III. ERRORS

In Section IV below, we will derive information about $\bar{M}$ and the distribution of M from observed values of the mass function F. However, it is first necessary to determine how the observational errors in F will affect these conclusions; in fact, how the observed values of F should be combined with due regard to their errors. Unfortunately, the data are not homogeneous; some values of V and ΔV are of higher weight than others, owing to more and sharper lines, better exposure, more spectrograms, etc. A rough root-mean-square error was derived for each observed value of V and ΔV in the following way: weights were assigned to each line measured, giving unit weight for a sharp $H\alpha$ emission line, and half-weight for $\lambda < 4800$ A, for a diffuse line, a slanted line, or an absorption

line, for a slit-curvature correction greater than 3μ or a case where less than three nearby comparison lines were measured. The individual measures of V and ΔV for each pair of galaxies were then combined in the standard manner to determine weighted means, and the deviations and squared deviations computed. The error of unit weight was determined from the root mean square of *all* deviations and the r.m.s. error of the weighted means (some of which had weight less than unity and were based on but one measurement) were derived in the usual manner. The result of this procedure is that the error of a single measurement of unit weight is ± 50 km/sec in ΔV and ± 100 km/sec in V.

From equations (8) and (9) we will find the mean mass, $\bar{M}$; but the error in $\bar{M}$ is obviously not the error of the weighted mean of F, since the distribution function of f is so far from normal. In order to get an estimate of the error in $\bar{M}$ due to the known errors of measurement, a minimum and a maximum value of $\bar{F}$ were determined by applying all errors first in the positive sense and then in the negative sense, replacing negative values of F with zero. The error is probably overestimated by this procedure. The error

TABLE 6

THE OBSERVED DISTRIBUTION, $N(F)$

$F/10^9\odot$	$N(F)$		$F/10^9\odot$	$N(F)$	
	20 Pairs in Table 2	35 Pairs		20 Pairs in Table 2	35 Pairs
0	1.00 ± 0	1.00	100	0.046 ± .020	0.073
0.5	0.64 ± .02	0.72	140	0.000 ± .020	0.034
1.0	0.57 ± .04	0.62	180	0.000	0.019
2.5	0.46 ± .06	0.51	220	0.000	0.006
5	0.33 ± .06	0.40	260	0.000	0.001
10	0.29 ± .05	0.33			
15	0.25 ± .04	0.27	$\bar{F}/10^9\odot =$	16.05 ± 7	20.4
20	0.218 ± .035	0.22	$S_R =$	1.′28	4.′1
30	0.194 ± .035	0.19	$S_0 =$	2′	5′ or ∞
40	0.175 ± .030	0.17	$f =$	0.21	0.25 or 0.295
60	0.100 ± .025	0.114	$M/10^9\odot =$	77 ± 30	81.6 or 68.0
80	0.060 ± .022	0.086			

in S was taken to be $\pm 0.'1$. An upper limit to the error in $\bar{M}$ is thus determined to be ± 40 per cent.

In the study of the distribution of the mass functions F, it was necessary to take into account the fact that the values of F determined from the observations are subject to errors in differing amounts, despite the requirement that each value of F must enter the distribution function with unit weight. On this basis each value of F was considered to be spread out over the range of values between its maximum and minimum value, with a peak at its normal value. Thus, the single value of F for NGC 5257–8, probably at 18.5×10^9 with low weight (so that its value may be as high as 33.0 or as low as 8.7×10^9), was considered to lie 50 per cent in the interval $15\text{–}20 \times 10^9$; 13 per cent each in the intervals 5–10 and $10\text{–}15 \times 10^9$; and 8 per cent each in the intervals 20–25, 25–30, and $30\text{–}35 \times 10^9$.

In this manner the observed distribution function, $N(F)$, defined as the fraction of all values of F lying between F and 1.0, was derived, listed in the second column of Table 6, and plotted as crosses in Figures 5 and 6. (Two figures are necessary to show the distribution function with the required accuracy over the range $F = 0$ to 160×10^9 suns.) A smoothed curve through these crosses is taken as the best estimate of the true distribution function $N(F)$ for a large number of doubles. Statistical fluctuations are expected to

introduce errors in the observed distribution function of the order $\pm\sqrt{N'}$, where N' is the actual number of values of F observed in the interval, except that the curve must obviously pass through the value $N(0) = 1.0$. This effect of statistical fluctuations is shown as an error in the second column of Table 6 and by the two lines bounding all crosses on Figures 5 and 6. A curve which fits the observed $N(F)$ must lie between these lines of error.

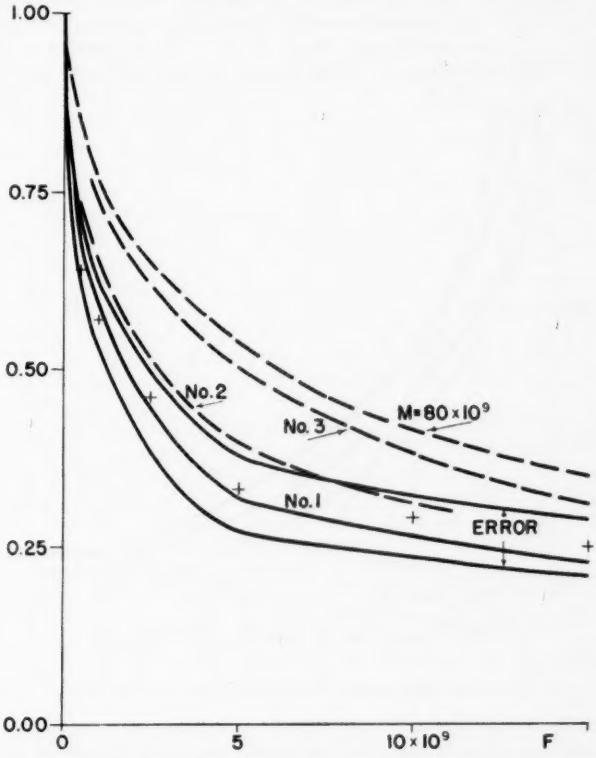

FIG. 5.—The distribution function, $N(F)$, for small F. The ordinate is the fraction of all values of F which lie between F and 1.0. The crosses represent observed values of $N(F)$, and the two continuous lines labeled "Error" indicate the estimated statistical fluctuations in these values. The remaining lines show the expected $N(F)$ for four different distributions of mass.

At this point it is appropriate to consider errors introduced by approximations in the dynamical analysis of Section II. In order of importance, four approximations are involved: (*a*) disk-shaped galaxies are treated as point masses; (*b*) in several cases the presence of more distant members in multiple systems has been ignored; (*c*) relative orbits are treated as circles; and (*d*) the mean radial velocity, V, has been taken as an accurate indicator of distance, in accordance with equation (4). No estimate can be given here of the effects of (*a*) and (*b*).

If the orbits are not circular, the error due to (*c*) above can be calculated by a treatment analogous to Russell's for common proper-motion stars,[16] which shows that the

[16] *Ap. J.*, 38, 89, 1928.

derived mass functions must be increased. Since no reliable estimate can be made of the distribution of orbital eccentricities for the double nebulae, it will only be noted here that the correction to $\bar{F}$ and $\bar{M}$ can at the most be of the order of +70 per cent (for eccentricities all near 1.0) and that, if the mean eccentricity is 0.5, the correction will be only +11 per cent, well within the estimated error in $\bar{M}$ of ±40 per cent.

Deviations from the velocity-distance law among field nebulae are generally[14] less than ±0.1 in log V, this value including errors in the distance criteria used by Hubble. Such errors, of ±25 per cent in D, enter F directly. However, the errors in F allowed in calculating $\bar{M}$ and $N(F)$ are considerably larger than ±25 per cent in all but one case (NGC 2872-5). Hence, the effect of (d) above can be neglected.

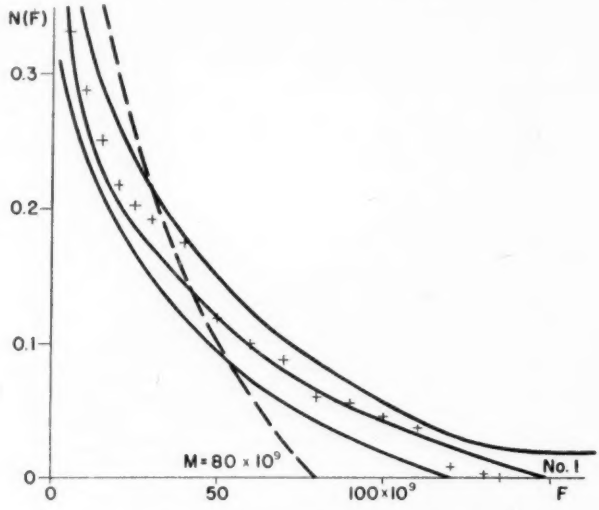

FIG. 6.—The distribution function, $N(F)$, for large F

IV. MASSES OF THE DOUBLE GALAXIES

As shown in Section II above, the mean mass per galaxy in a number of pairs can be determined from the mean of the observed mass functions; that is, $\bar{M} = \bar{F}/\bar{f}$, where $\bar{f}$ can be determined analytically if the orbital inclinations and angles from the node are randomly distributed. The selection of close pairs requires a correction to $\bar{f}$ based on the cutoff at $S_0 \simeq 2'$ and on the mean space separations of double galaxies. For the 20 pairs listed in Table 3 we find:

$$\bar{M} = (77 \pm 30) \times 10^9 \text{ solar masses},$$

where the error has been estimated in the liberal manner described in Section III.

Confirmation of the correction to $\bar{f}$ for selection of close pairs is obtained by adding to these data those for 15 other pairs observed previously and listed in Table 5. Four of these are early radial-velocity measurements cited by Holmberg,[5] and three refer to very wide pairs which were identified as physical systems by their common radial velocities. I am indebted to Mr. Milton Humason for permission to include data for 8 of these pairs not previously published. Since the individual radial velocities were measured separately in each of these pairs, the errors in ΔV may be quite large. Because of this fact and the

heterogeneous nature of these data, no estimate of the error in $\bar{F}$ or $N(F)$ derived from them can be given. However, the mean mass derived as above, assuming no cutoff (since separations as large as 276′ are included, and $\bar{S}_R = 7'.9$) is

$$\bar{M} = 89 \times 10^9 \text{ solar masses} .$$

Combining the data for all 35 pairs and assuming an effective cutoff at $S_0 = 5'$,

$$\bar{M} = 82 \times 10^9 \text{ solar masses} .$$

The agreement between the determinations for two independent selections of pairs lends considerable weight to the conclusion that $\bar{M}$ is near 80×10^9 solar masses for the double galaxies, although at least 3 of the pairs—NGC 2872–5, 4467–72, and 5982–5—have masses considerably larger than this (since M is greater than F observed for any pair, and the observed values of F are 111, 178, and 128 for these three pairs).

However, the observed distribution of F, listed in Table 6 and plotted on Figures 5 and 6, gives further evidence of a wide range in M. In principle, it is possible to derive the distribution of M from the observed distribution of F, using the appropriate theoretical distribution, $N(f)$. However, as noted by Chandrasekhar and Münch[17] in another connection, the solution of an integral equation of the type required to obtain $N(M)$ from $N(F)$ depends on the derivative of $N(F)$, which is poorly determined by the data. For this reason several discrete frequency functions of M were assumed, and the distribution functions $N_n(F)$ constructed for comparison with the observed $N(F)$. Each assumed frequency function can be expressed in the form $n_1(M_1) + n_2(M_2) + \ldots + n_i(M_i) + \ldots$, where $\Sigma n_i = 1$ and $\Sigma n_i M_i = \bar{M}$.

The simplest of these is the case of $n_1 = 1$, $M_1 = \bar{M} = 80 \times 10^9 \odot$, all masses equal to the mean, for which $N_0(F) = N(f)$, and $F = \bar{M}f$. As shown in Figures 5 and 6, $N_0(F)$ does not fit $N(F)$ within the lines of error.

In the more general case, the constructed $N_n(F) = n_1 N(f_1) + n_2 N(f_2) + \ldots + n_i N(f_i) + \ldots$, where $f_i = F/M_i$. $N(f)$ is taken from Table 4; $N(f) = 0$ for $f \geq 1.0$. The frequencies and masses used in four separate trial fits are listed in Table 7 and shown graphically in the top part of Figure 7.

The derived distribution functions, $N_n(F)$, from these trials are plotted in Figures 5 and 6. Trial No. 2 coincides with No. 1 for large values of F, but is too high between $F = 1$ and 7×10^9 suns. No. 3 is too high for $F < 20 \times 10^9$.

The distribution function for No. 1 lies everywhere within the lines of error and fits the observed $N(F)$ (shown by crosses in Figures 5 and 6) as accurately as the significance of these data will allow.

The significant result of this fit No. 1 is that two sharply separated masses of about 5×10^9 suns (representing about half of these galaxies, which may be termed "light weights") and about 150×10^9 suns (representing the other half, which may be termed "heavy weights") are required.

The terms "giant" and "dwarf," referring to luminosity, have been applied to the galaxies before, but the sharp distinction in mass has not previously been demonstrated. From the mass and luminosity data for six galaxies assembled by Mayall and Aller[2] (reproduced here in Table 8), they identified three or possibly four giants. Two of these, the Galaxy and M31, are comparable in mass with the "heavy-weight" double galaxies. The two dwarfs are comparable in mass with the "light-weight" double galaxies. It is possible that the intermediate masses of NGC 4594 and NGC 3115 are underestimated and that these objects are heavy weights as well as giants in luminosity.

The observed distribution of F for all 35 pairs of galaxies lies for the most part close to $N(F)$ for the 20 pairs in Table 3 (see Table 6). As partial confirmation of the methods

[17] *Ap. J.*, 111, 142, 1950.

used above it is to be noted that Trial No. 4 (Table 7), the best fit to $N(F)$ for all 35 pairs, yields a mass frequency very similar to that of Trial No. 1, except that 20 per cent of intermediate masses can be included.

As a further check on the sharp separation between heavy weights and light weights, trials No. 2 and No. 3 were made: No. 2 consisting of equal groups of dwarfs, intermediates, and giants, and No. 3 an approximation to a uniform spread in masses. The fact that No. 2 yields $N(F)$ too high from $F = 1$ to 7×10^9 suns is taken to indicate that masses intermediate between giants and dwarfs are rare among the double galaxies.

TABLE 7

ASSUMED MASS FREQUENCIES

$N_a(F)$ has been calculated using $N(f)$ for $S_0 = 2'$, except in Trial No. 4

n_i	M_i
Trial No. 1	
0.5	150×10^9
0.5	5
1.00	$\bar{M} = 77.5 \times 10^9$
Trial No. 2	
0.333	150×10^9
.333	80
0.333	5
1.000	$\bar{M} = 77.3 \times 10^9$
Trial No. 3	
0.0625	160×10^9
.0625	150
.0625	140
.0625	130
0.0625	120
0.0625	110
.0625	100
.0625	90
.0625	80
.0625	70
.0625	60
.0625	50
.0625	40
.0625	30
.0625	20
0.0625	10
1.0000	$\bar{M} = 85.0 \times 10^9$
Trial No. 4 (For 35 Pairs, $S_0 = 5'$)	
0.34	200
.20	50
0.46	5
1.00	$\bar{M} = 80.3$

Trial No. 3 indicates the same fact; it contains too many intermediate masses to fit the observed $N(F)$.

It is therefore concluded that the average mass of the 40 galaxies listed in Tables 1 and 3 is about 80×10^9 suns, and that they may be divided into two groups: light weights of individual masses about 5×10^9 suns and heavy weights of individual masses about 150×10^9 suns, with possibly one or two pairs of intermediate mass. Unfortunately, it is not possible to specify explicitly which of the pairs are light and which heavy, although NGC 2872–5, with $F > \bar{M}$, is undoubtedly a pair of heavy weights. If these 40 galaxies in double systems are a fair sample, some 50 per cent of the field nebulae are light and about 50 per cent heavy.

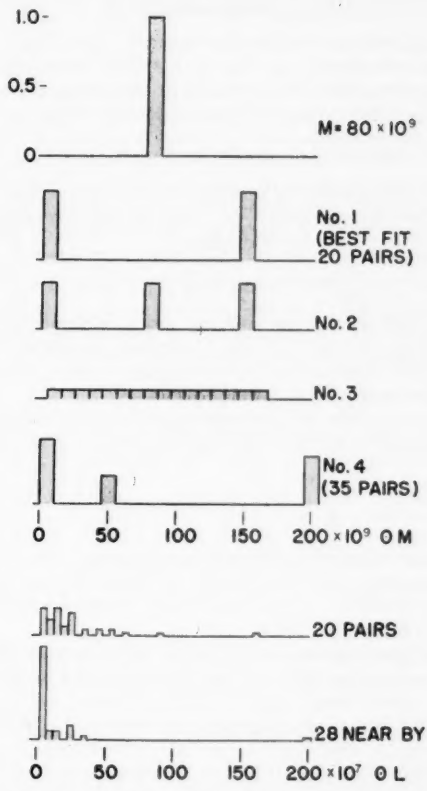

FIG. 7.—Distributions of mass and luminosity. Ordinates represent numbers of galaxies. The histogram "No. 1" represents the best fit to the present mass data for 20 pairs of galaxies.

TABLE 8

MASSES AND LUMINOSITIES OF SINGLE GALAXIES

Object	Type	M (10^9 Suns)	L (10^9 Suns)	Designation
Galaxy	(Sc)	200.	.....	Giant
M33	Sc	1.7	9.1	Dwarf
M31	Sb	95.	100.	Giant
NGC 4594	Sa	28.	250.	Giant
NGC 4111	Sa	(1.8)	6.3	Dwarf
NGC 3115	E7	15.	30.	Giant?

V. LUMINOSITIES

It is of interest to determine whether the luminosities of these nebulae also show a separation into giants and dwarfs. To this end Table 3 lists absolute luminosities in terms of the sun derived from Holmberg's[5] magnitudes, using the mean radial velocities given in Table 3 to determine distances by equation (4). Thus

$$\log L = 0.4\,(16.39 - m' + 5 \log V)\,, \tag{13}$$

where L is the absolute luminosity in terms of the sun, the constant term includes the absolute magnitude of the sun taken as 5, and the constant k from equation (4), and m' is corrected for galactic obscuration by the relation

$$m' = m - 0.25 \csc \beta\,. \tag{14}$$

The error in L due to estimated errors in k, m, and V is found to be ± 95 per cent. The error in m has been assumed to be ± 0.5 mag., based on comparison of Holmberg's magnitudes with those of Shapley and Ames.[18] Such large errors limit the conclusions which can be drawn from the luminosity data.

The arithmetic mean of these 40 luminosities in Table 3 is 23.0×10^7 suns. Combining this with the mean mass from Section IV above, the mean ratio of mass to luminosity is found to be

$$\frac{\bar{M}}{\bar{L}} = 3.48 \text{ (in solar units)}\,,$$

a figure considerably in excess of previous determinations.[8] The error in $\bar{L}$ derived from the random 95 per cent errors in L, is ± 5 suns; for these 40 galaxies, therefore, it is probable that $171 < \bar{M}/\bar{L} < 620$. Even the lower limit of the mass-luminosity ratio is very much larger than previous estimates.[19]

The distribution of these luminosities is plotted at the bottom of Figure 7. There is no indication of a sharp separation between giants and dwarfs in luminosity, although observational errors in L may have obscured such a separation. For comparison, the distribution of L among 28 near-by galaxies recently studied by Holmberg[20] is also plotted in Figure 7 (lowest graph). The single large value refers to M31. Errors in Holmberg's magnitudes are probably less than 0.1. The differences in luminosity distribution between the 20 pairs and the 28 near-by galaxies is probably also a result of the large errors involved in the former. This interpretation is partly borne out by the means and dispersions given in Table 9.

Since the errors in L are large and the classification of elliptical, irregular, and spiral types doubtful among the double nebulae in Table 3, little significance can be attached to the means for different types of double nebulae in Table 9. However, the total mean and dispersion of the double galaxies appear to be sufficiently similar to that for the 28 near-by galaxies to support the contention that these doubles form a similar sample of the field nebulae. At the same time, the large dispersions in Holmberg's more accurate luminosities of the near-by galaxies and the wide differences between spirals and the other types bear the warning that any small sample can easily be biased.

It is concluded that the 40 galaxies studied here have luminosities similar in their mean and dispersion to the 28 near-by galaxies studied more accurately by Holmberg and that the mean mass-luminosity ratio for these double galaxies is greater than 170, in solar units.

[18] *Harvard Ann.*, Vol. **88**, No. 2, 1932.

[19] Hubble, *The Realm of the Nebulae* (London: Oxford University Press, 1936); Wyse and Mayall, *Ap. J.*, **95**, 24, 1942.

[20] Holmberg, *Lund. Medd.*, Ser. II, No. 128.

VI. EFFECTS OF SELECTION

This study of the double galaxies was undertaken in order to gain information about the average masses of all galaxies, an aim which can be realized only if the objects studied represent a fair sample. The criteria for a fair sample, in this case, must be based on one or more of the following observable characteristics of galaxies: (*a*) membership in groups, (*b*) luminosity, (*c*) form, (*d*) size, (*e*) spectral characteristics, and (*f*) surface brightness. Distance (and radial velocity, proportional thereto) has been omitted from this list since nonhomogeneities of the universe are beyond the scope of this paper.

As for (*a*), Holmberg has shown that the double galaxies listed in his catalog[5] are a fair sample of the field nebulae—better, certainly, than the cluster galaxies. It would therefore be sufficient to show that the 20 pairs studied here are a fair sample from Holmberg's catalog. On the basis of mean separation, $\overline{S}$, this is very nearly true (see Sec. II).

With reference to (*b*), it has been shown in Section V above that the rather inaccurate luminosity data are at least consistent with the assertion that the 40 galaxies studied here are a similar sample to the 28 near-by galaxies. Table 9 shows that irregular forms may be

TABLE 9

MEAN ABSOLUTE LUMINOSITIES IN UNITS OF 10^7 SUNS

	20 PAIRS			28 NEAR-BY GALAXIES		
	No.	Mean	Dispersion	No.	Mean	Dispersion
Elliptical nebulae	16	20.1	16.7	6	1.1	0.9
Spirals	20	29.4	30.8	10	28.2	49.
Irregular nebulae	4	2.9	1.9	12	4.0	6.1
Local group	.....	.....	.....	13	18.4	46.
Total	40	23.0	25.5	28	12.0	32.4

underrepresented by a factor of 1/4.5, and spirals overrepresented by a factor of 1.3. However, the classification of forms among the double galaxies is not reliable, and this apparent defect in the sample may not be significant.

In order to use criterion (*d*) above, linear diameters, *d*, have been calculated from the expression

$$d = D \sin A = A\,V/1.81 \text{ parsecs}, \tag{15}$$

where A is the angular diameter in minutes of arc given by Holmberg[5] and the constant includes k from equation (4). The mean diameter of these 40 objects is 1780 psc. The mean of log *d*, and its dispersion, agree closely with the values derived by Holmberg[21] for 145 field galaxies, as indicated in the accompanying tabulation.

	40 Double Galaxies	145 Field Galaxies
$\overline{\log d}$	3.13	3.17 ± 0.03
Dispersion	0.34	0.34 ± 0.02

[21] *Lund Ann.*, **6**, 41, 1937.

As shown in Table 3 (third column), all but 9 of the 40 spectra show emission lines. This proportion, which depends primarily on the proportions of elliptical and early-type spirals included in the sample, is not significantly different from the proportion of field nebulae showing emission lines. There is no evidence that the spectra of double galaxies differ systematically from those of field nebulae; no further analysis of spectral types has been undertaken here.

With reference to criterion (*f*), it must be noted that the surface brightness varies widely over each image and that a mean surface brightness depends critically on the dimensions used. The dimensions available, those listed in the Holmberg[5] and Shapley-Ames[18] catalogues, were generally measured roughly on small-scale plates; accurate photometry has led to increases in these dimensions[20] by as much as a factor of 2. In order to make a rough comparison, the average surface brightness, defined as

$$H \equiv m + 2.5 \log (A \cdot B), \tag{16}$$

where A and B are the major and minor axes, has been computed for the double galaxies and for the 28 near-by galaxies, using Shapley and Ames's values[18] of A and B. There was a natural selection of objects of high surface brightness in the present observations, confirmed by the comparison of mean H and dispersions given in the accompanying tabulation. Individual values of H are listed in Table 3.

	40 Double Galaxies	28 Near-by Galaxies
$\bar{H}$	$12^m.5$	$13^m.9$
Dispersion	$0^m.82$	$1^m.38$

VII. CONCLUSIONS

On the basis of the assumptions and approximations listed in Section III above, the measured radial velocities and angular separations of 20 pairs of galaxies lead to a mean individual mass of 8×10^{10} suns, with an uncertainty much less than ± 40 per cent. Although more data are needed to determine the distribution of masses accurately, it can be stated with confidence that the distribution is not normal about this mean. Rather, there appear to be two groups among the 40 galaxies studied: light weights, of mass about 5×10^9 suns, and heavy weights, of mass about 150×10^9 suns, about equal in frequency. Intermediate masses cannot be present in appreciable number.

Luminosity data are too poor to allow identification of luminous giants with massive heavy weights. However, the over-all mean mass-luminosity ratio for these 40 galaxies is in the range 170–600 solar units.

The 40 galaxies studied appear to be a fair sample of the field nebulae (excluding only the cluster nebulae) on the basis of similar luminosities, sizes, and special characteristics. However, they are systematically of higher surface brightness than both the average near-by single galaxies and the average double galaxies. There is imperfect evidence that the 40 galaxies studied include more spiral types and fewer irregular types than the average.

There is no reliable observational evidence to indicate that the double galaxies differ systematically from the mean of all galaxies in mass, luminosity, or other characteristics. Pending further information, therefore, it is suggested that these conclusions apply to all field nebulae: (*a*) the average mass is about 8×10^{10} suns, and (*b*) in any group of galaxies chosen at random there are roughly equal numbers of light weights of mass 5×10^9 suns and heavy weights of mass 150×10^9 suns or more. The latter conclusion is consistent with measurements of individual masses from internal rotations.

THE RADIAL VELOCITY OF 16 LACERTAE*

O. STRUVE, D. H. MCNAMARA, R. P. KRAFT, S. M. KUNG, AND A. D. WILLIAMS

Berkeley Astronomical Department, University of California

Received February 11, 1952

ABSTRACT

Individual velocity-curves were obtained on 26 nights from 442 Mount Wilson and Lick spectrograms. These curves are represented as the sum of three periodic oscillations: $P_2 = 0.16916$ day ($4^h3^m35^s4$), $P_1 = 0.17085$ day ($4^h6^m1^s0$), and $P_3 = 12.097$ days. The corresponding semi-amplitudes are $K_2 = 14.8$ km/sec, $K_1 = 4.5$ km/sec, $K = 23.4$ km/sec. The absorption lines vary slightly in contour, probably in phase with P_2. They are sharpest on the ascending branches of the velocity-curves. The periods P_1 and P_2 combine to produce a beat period of $P_3 = 17.15$ days.

Merle Walker's discovery,[1] in August, 1950, at the Lick Observatory, of a 4-hour variation in the light-velocity and radial velocity of 16 Lacertae has inspired the present investigation. Walker's own photometric observations, obtained in 1951, appear in a separate article. Through a fortunate coincidence, G. R. Miczaika secured numerous photoelectric observations of 16 Lacertae at Heidelberg, also in 1951. Thus, for the first time, there is available for discussion a large amount of data secured simultaneously with photoelectric photometers and with powerful spectrographs. It has seemed best to carry out

TABLE 1

LIST OF STAR LINES

Wave Length	Element	Plate*	Wave Length	Element	Plate
3911.96	*O* II	C	4101.74	*Hδ*	γ
3918.98	*C* II	C	4120.81	*He* I	γ
3919.29	*O* II	C	4143.76	*He* I	γ
3920.68	*C* II	C	4267.17	*C* II	γ
3933.66	*Ca* II	C, γ	4340.47	*Hγ*	γ
3945.05	*O* II	C	4387.93	*He* I	γ
3954.37	*O* II	C	4471.48	*He* I	γ, L
3964.73	*He* I	C, γ	4481.23	*Mg* II	γ, L
3995.00	*N* II	C	4552.65	*Si* III	L
4009.27	*He* I	C, γ	4567.87	*Si* III	L
4026.19	*He* I	C, γ	4574.78	*Si* III	L
4069.79	*O* II	C, γ	4590.97	*O* II	L
4072.16	*O* II	C	4596.18	*O* II	L

* C = Mt. Wilson coudé spectrograph on the 100-inch telescope. γ = Mt. Wilson cassegrain, on the 60-inch telescope. L = Lick three-prism spectrograph on the 36-inch refractor.

the discussions separately, without attempting to iron out the small remaining discrepancies.

Table 1 gives a list of the star lines used in this work. The *Ca* II line K was not used in forming the mean values for each plate. This line is partly stellar and partly interstellar. On several high-dispersion plates it is completely resolved into two components. Table 2 gives the individual plate velocities. No heliocentric corrections have been ap-

* The observational material used in this investigation was obtained at the Mount Wilson and Lick Observatories.

[1] *Pub. A.S.P.*, **63**, 35, 1951.

TABLE 2

RADIAL VELOCITIES

Plate	Time (U.T.)	JD 2433+	Phase (Day)	Velocity (Km/Sec)
	August 11, 1951			
γ	4h35m	869.691	0.103	−27.4
	5 12	.717	.129	−19.6
	6 00	.750	.162	−10.4
	13	.759	.002	− 7.3
	25	.767	.010	− 1.6
	38	.776	.019	− 9.6
	7 04	.794	.037	−19.3
	17	.803	.046	−18.0
	29	.812	.055	−22.8
	41	.820	.063	−27.9
	53	.828	.071	−35.5
	8 11	.841	.084	−24.7
	37	.859	.102	−36.4
	50	.868	.111	−24.4
	9 02	.876	.119	−21.4
	16	.886	.129	−19.0
	27	.894	.137	−14.3
	39	.902	.145	−15.5
	51	.910	.153	− 7.8
	10 03	.919	.162	− 2.9
	15	.927	.001	− 3.5
	43	.947	.021	− 9.2
	55	.955	.029	−13.7
	11 07	.963	.037	−17.6
	19	.972	.046	−25.6
	30	.979	.053	−25.4
	41	.987	.061	−35.2
	52	.994	.068	−37.1
	12 03	870.002	0.076	−37.2
	August 12, 1951			
γ	5 45	870.740	0.137	− 8.7
	57	.748	.145	− 4.9
	6 11	.758	.155	+ 0.6
	24	.767	.164	+ 3.5
	36	.775	.003	− 8.6
	49	.784	.012	+ 1.0
	7 03	.794	.022	− 3.7
	16	.803	.031	− 8.9
	29	.812	.040	−12.6
	43	.822	.050	−16.7
	59	.833	.061	−24.5
	8 14	.843	.071	−27.7
	42	.862	.090	−30.1
	56	.872	.100	−26.5
	9 23	.891	.119	−21.4
	36	.900	.128	−16.1
	48	.908	.136	−13.5
	10 02	.917	.145	− 8.5
	17	.928	0.156	− 5.2
	August 12, 1951—*Continued*			
γ	10h31m	870.938	0.166	− 2.7
	44	.947	.006	− 4.4
	57	.956	.015	− 4.3
	11 11	.966	.025	− 3.1
	24	.975	.034	− 9.6
	37	.984	.043	−10.4
	51	.994	.053	−18.5
	12 04	871.003	.062	−23.6
	17	.012	0.071	−24.8
	August 13, 1951			
γ	4 36	871.692	0.074	−22.2
	49	.701	.083	−18.5
	5 03	.710	.092	−19.6
	16	.719	.101	−15.8
	29	.728	.110	−16.8
	42	.738	.120	−10.2
	55	.747	.129	− 8.3
	6 08	.756	.138	− 2.7
	22	.765	.147	+ 5.6
	35	.774	.156	+ 3.9
	47	.783	.165	+ 7.2
	7 02	.793	.006	+ 9.4
	15	.802	.015	+ 6.1
	29	.812	.025	+ 2.3
	42	.821	.034	+ 1.3
	55	.830	.043	− 7.0
	8 08	.839	.052	− 9.9
	22	.849	.062	−14.9
	35	.858	.071	−16.3
	48	.867	.080	−21.8
	9 02	.876	.089	−19.1
	16	.886	.099	−18.8
	27	.894	.107	−15.4
	38	.901	.114	− 2.5
	50	.910	.123	−10.4
	10 01	.917	.130	− 5.4
	12	.925	.138	− 3.0
	24	.933	.146	+ 0.7
	35	.940	.153	+ 5.1
	47	.949	.162	+ 9.8
	58	.957	.001	+ 6.9
	11 09	.965	.009	+10.3
	22	.974	.018	+ 9.8
	34	.982	.026	+ 3.8
	46	.990	.034	+ 1.2
	57	.998	.042	− 4.8
	12 09	872.006	.050	− 6.3
	20	.014	0.058	− 9.9

TABLE 2—*Continued*

Plate	Time (U.T.)	JD 2433+	Phase (Day)	Velocity (Km/Sec)
	August 14, 1951			
γ....	4h28m	872.686	0.053	+ 3.7
	42	.696	.063	− 2.9
	55	.705	.072	− 5.8
	5 09	.715	.082	− 8.2
	38	.735	.102	− 4.5
	52	.744	.111	− 5.5
	6 06	.754	.121	+ 3.2
	20	.764	.131	+ 4.7
	33	.773	.140	+12.6
	50	.785	.152	+13.3
	7 04	.794	.161	+18.4
	18	.804	.002	+21.2
	32	.814	.012	+19.4
	47	.824	.022	+15.2
	8 00	.833	.031	+14.7
	14	.843	.041	+ 7.1
	27	.852	.050	+ 4.8
	41	.862	.060	− 2.5
	54	.871	.069	− 0.8
	10 38	.943	.141	+ 6.1
	52	.953	.151	+12.7
	11 06	.962	.160	+16.4
	19	.972	.001	+18.1
	33	.981	0.010	+20.2
	August 15, 1951			
C....	7 24	873.808	0.160	+22.2
	39	.819	.002	+21.9
	50	.826	.009	+22.4
	8 11	.841	.024	+19.4
	22	.849	.032	+17.8
	32	.856	.039	+14.2
	43	.863	.046	+10.6
	54	.871	.054	+ 9.9
	9 05	.878	.061	+ 5.5
	15	.885	.068	− 0.4
	25	.892	.075	− 0.7
	35	.899	.082	− 0.1
	45	.906	.089	− 1.0
	55	.913	.096	+ 0.5
	10 05	.920	.103	+ 2.1
	15	.927	.110	+ 2.3
	25	.934	.117	+ 5.8
	35	.940	.123	+10.8
	45	.948	.131	+12.6
	56	.956	0.139	+17.1
	August 16, 1951			
C....	7 07	874.797	0.135	+10.4
	31	.813	.151	+14.1
	50	.826	0.164	+19.0
	August 16, 1951—*Continued*			
C....	8h12m	874.842	0.010	+19.2
	35	.858	.026	+17.3
	9 00	.875	.043	+ 5.7
	27	.893	.061	− 0.6
	54	.912	.080	− 3.0
	10 23	.933	.101	− 1.7
	50	.951	.119	+ 5.6
	11 18	.971	.139	+12.5
	47	.991	0.159	+18.7
	August 17, 1951			
C....	5 22	875.724	0.047	+ 1.8
	49	.742	.065	− 5.4
	6 16	.761	.084	− 7.2
	26	.768	.091	− 5.2
	7 09	.798	.121	− 0.1
	34	.815	.138	+ 5.9
	8 00	.833	.156	+11.8
	25	.850	.003	+14.2
	52	.869	0.022	+ 7.3
	August 18, 1951			
C....	8 23	876.849	0.157	+ 1.9
	9 16	.886	.024	− 5.2
	46	.907	.045	−16.7
	10 17	.928	.066	−22.2
	47	.949	.087	−23.2
	11 18	.971	0.109	−14.6
	August 25, 1951			
L....	5 28	883.728	0.100	−22.8
	6 16	.761	.133	− 1.5
	45	.781	.153	+ 7.8
	7 15	.802	.005	+ 7.6
	43	.822	.025	+ 1.0
	8 13	.842	.045	−12.8
	9 07	.880	.083	−24.3
	36	.900	.103	−17.9
	10 04	.919	.122	− 6.6
	39	.944	0.147	+ 6.4
	August 31, 1951			
L....	6 36	889.775	0.057	−27.0
	7 01	.792	.074	−32.0
	28	.811	0.093	−35.2

TABLE 2—*Continued*

Plate	Time (U.T.)	JD 2433+	Phase (Day)	Velocity (Km/Sec)
	August 31, 1951—*Continued*			
L....	7h55m	889.830	0.112	−31.2
	8 43	.863	.145	−17.1
	9 31	.897	.010	− 9.7
	10 05	.920	.033	−15.4
	37	.942	0.055	−29.0
	September 8, 1951			
L....	5 15	897.719	0.051	− 3.8
	45	.740	.072	− 8.2
	6 27	.769	.101	− 3.2
	7 07	.797	.129	+11.0
	8 05	.837	.000	+22.2
	36	.858	.021	+14.3
	9 05	.878	.041	+ 2.7
	34	.899	.062	− 7.6
	10 16	.928	0.091	− 5.9
	September 15, 1951			
L....	5 10	904.715	0.111	−46.4
	39	.735	.131	−33.0
	6 08	.756	.152	−26.4
	49	.784	.011	−21.0
	7 38	.818	.045	−35.3
	8 07	.838	.065	−48.0
	35	.858	.085	−51.8
	9 01	.876	.103	−48.7
	28	.894	.121	−44.1
	53	.912	.139	−32.3
	10 21	.931	0.158	−23.3
	September 21, 1951			
L....	3 20	910.639	0.115	+ 6.7
	50	.660	.136	+16.0
	4 20	.681	.157	+20.2
	50	.701	.007	+16.7
	5 20	.722	.028	+10.6
	55	.747	.053	+ 2.1
	6 30	.771	.077	− 2.1
	7 15	.802	.108	+ 2.8
	47	.824	.130	+10.3
	8 18	.846	0.152	+14.0
	September 28, 1951			
L....	3 32	917.647	0.018	−23.0
	4 06	.671	0.042	−36.6
L....	4h38m	917.693	0.064	−46.9
	5 10	.715	.086	−48.3
	40	.736	.107	−43.6
	6 10	.757	.128	−27.5
	49	.784	.156	−13.7
	7 20	.806	.008	−15.1
	48	.825	.027	−27.0
	8 20	.847	0.049	−39.4
	October 6, 1951			
L....	5 47	925.741	0.161	− 7.4
	6 22	.765	.016	− 4.6
	49	.784	.035	−12.5
	7 19	.805	.056	−21.4
	46	.824	.075	−29.2
	8 11	.841	.092	−30.8
	9 02	.876	.127	−20.5
	29	.895	.146	−12.6
	56	.914	.165	− 9.6
	10 24	.933	0.015	− 9.5
	October 18, 1951			
γ....	6 23	937.766	0.007	+11.6
	37	.776	.017	− 2.2
	51	.785	.026	− 2.8
	7 04	.794	.035	−12.6
	18	.804	.045	−14.2
	32	.814	.055	−29.6
	45	.823	.064	−29.9
	58	.833	.074	−41.2
	8 19	.847	.088	−36.4
	35	.858	.099	−39.0
	48	.867	.108	−34.5
	9 02	.876	.117	−26.8
	15	.885	.126	−16.8
	29	.895	.136	−12.5
	43	.905	.146	− 4.2
	56	.914	.155	− 5.8
	10 11	.924	.165	− 2.2
	24	.933	0.005	+ 3.3
	October 19, 1951			
γ....	5 39	938.735	0.130	−29.3
	53	.745	.140	−23.8
	6 07	.755	.150	−24.9
	21	.765	.160	−13.1
	35	.774	.000	−13.6
	49	.784	0.010	− 7.7

TABLE 2—*Continued*

Plate	Time (U.T.)	JD 2433+	Phase (Day)	Velocity (Km/Sec)
	October 19, 1951—*Continued*			
γ....	7h02m	938.793	0.019	−12.5
	16	.802	.028	−14.5
	29	.812	.038	−20.1
	42	.820	.046	−24.2
	57	.831	.057	−35.7
	8 10	.840	.066	−41.6
	23	.849	.075	−37.2
	37	.859	.085	−47.9
	50	.868	.094	−47.6
	9 04	.878	.104	−44.3
	18	.888	.114	−33.5
	31	.896	0.122	−32.3
	October 20, 1951			
γ....	5 19	939.722	0.102	−48.6
	34	.732	.112	−43.9
	48	.742	.122	−42.4
	6 01	.751	.131	−35.6
	15	.760	.140	−31.1
	28	.769	.149	−19.4
	42	.779	.159	−19.9
	54	.788	.168	−18.3
	7 08	.797	.008	−19.6
	21	.806	.017	−18.8
	35	.816	.027	−25.0
	48	.825	.036	−28.2
	8 02	.834	.045	−39.0
	16	.844	.055	−36.8
	30	.854	.065	−46.6
	44	.864	.075	−45.9
	58	.874	.085	−59.3
	9 11	.883	0.094	−51.4
	October 21, 1951			
γ....	5 11	940.716	0.081	−53.5
	25	.726	.091	−51.9
	38	.735	.100	−53.5
	52	.744	.109	−41.9
	6 06	.754	.119	−45.6
	19	.763	.128	−34.2
	32	.772	.137	−32.7
	45	.781	.146	−32.6
	58	.790	.155	−29.1
	7 11	.799	.164	−20.9
	25	.809	.005	−23.3
	37	.817	.013	−23.1
	52	.828	.024	−26.2
	8 05	.837	.033	−26.2
	18	.846	.042	−31.9
	32	.856	.052	−37.5
	46	.865	.061	−39.1
	59	.874	.070	−54.2
	9 13	.884	0.080	−47.2

Plate	Time (U.T.)	JD 2433+	Phase (Day)	Velocity (Km/Sec)
	October 22, 1951			
γ....	2h29m	941.603	0.122	−41.5
	42	.612	.131	−34.3
	56	.622	.141	−32.5
	3 11	.633	.152	−25.3
	29	.645	.164	−31.3
	43	.655	.005	−16.0
	56	.664	.014	−17.0
	4 10	.674	.024	−17.9
	24	.683	.033	−27.9
	37	.692	.042	−32.2
	51	.702	.052	−33.2
	5 08	.714	.064	−39.4
	22	.724	.074	−41.9
	35	.733	.083	−42.0
	49	.742	.092	−40.1
	6 02	.751	.101	−36.3
	16	.761	.111	−39.9
	30	.771	.121	−35.0
	43	.780	.130	−36.2
	57	.790	.140	−24.5
	7 10	.799	.149	−25.1
	23	.808	.158	−24.2
	36	.817	0.167	−19.5
	November 11, 1951			
γ....	2 28	961.603	0.161	− 1.0
	41	.612	.001	− 1.4
	55	.622	.011	+ 3.4
	3 08	.631	.020	+ 3.6
	21	.640	.029	− 4.1
	34	.649	.038	− 9.7
	47	.658	.047	−21.8
	4 01	.667	.056	−21.5
	15	.677	.066	−18.4
	28	.686	.075	−22.3
	41	.695	.084	−20.0
	54	.704	.093	−19.0
	5 07	.713	.102	−21.1
	20	.722	.111	−13.0
	33	.731	.120	−12.5
	46	.740	.129	− 9.5
	6 01	.751	.140	− 7.3
	14	.760	.149	− 7.1
	28	.769	.158	− 1.8
	41	.778	.167	− 3.4
	54	.788	.008	− 3.0
	7 07	.797	0.017	− 4.3
	November 12, 1951			
γ....	6 07	962.755	0.129	−24.6
	21	.765	.139	−25.9
	34	.774	.148	−19.1
	47	.783	0.157	−21.1

TABLE 2—*Continued*

Plate	Time (U.T.)	JD 2433+	Phase (Day)	Velocity (Km/Sec)
	November 12, 1951—*Continued*			
γ	7h01m	962.792	0.166	− 7.9
	14	.801	.006	−12.9
	28	.811	.016	− 9.8
	42	.821	.026	−10.1
	55	.830	0.035	−18.5
	November 13, 1951			
γ	3 13	963.634	0.163	−22.8
	27	.644	.003	−22.1
	40	.653	.012	−22.2
	53	.662	.021	−23.6
	4 07	.672	.031	−25.9
	20	.681	.040	−30.6
	33	.690	.049	−35.6
	46	.699	.058	−40.6
	5 15	.719	.078	−40.9
	30	.729	.088	−39.9
	50	.743	0.102	−39.4
	November 14, 1951			
γ	2 23	964.599	0.113	−37.8
	36	.608	.122	−38.2
	49	.617	.131	−29.8
	3 02	.626	.140	−25.5
	15	.635	.149	−24.0
	28	.644	.158	−22.2
	41	.653	.167	−16.6
	54	.662	.006	−24.1
	4 07	.672	.016	−27.3
	20	.681	.025	−28.3
	33	.690	.034	−34.6
	46	.699	.043	−39.3
	5 00	.708	.052	−44.8
	13	.717	.061	−46.8
	26	.726	.070	−52.4
	39	.735	.079	−50.4
	52	.744	.088	−44.1
	6 05	.753	.097	−48.4
	18	.762	.106	−41.4
	31	.772	.116	−38.9
	45	.781	.125	−33.0
	58	.790	.134	−27.9
	7 11	.799	.143	−24.3
	25	.809	0.153	−21.6
	November 15, 1951			
γ	2h20m	965.597	0.096	−43.7
	33	.606	.105	−43.6
	46	.615	.114	−36.0
	3 00	.625	.124	−33.6
	13	.634	.133	−23.9
	26	.643	.142	−24.8
	39	.652	.151	−24.1
	52	.661	.160	−24.1
	4 05	.670	.000	−22.6
	18	.679	.008	−19.4
	31	.688	.017	−18.0
	44	.697	.026	−22.8
	58	.707	.036	−28.8
	5 11	.716	.045	−32.4
	24	.725	.054	−38.0
	37	.734	.063	−43.6
	50	.743	.072	−40.1
	6 03	.752	.081	−40.0
	16	.761	.090	−43.1
	30	.771	.100	−41.2
	43	.780	.109	−38.3
	56	.789	.118	−33.7
	7 09	.798	0.127	−29.4
	November 16, 1951			
γ	2 20	966.597	0.081	−37.2
	33	.606	.090	−35.9
	46	.615	.099	−40.4
	59	.624	.108	−31.2
	3 12	.633	.117	−28.8
	25	.642	.126	−28.7
	36	.650	.134	−14.3
	51	.660	.144	−18.7
	4 04	.669	.153	−14.4
	17	.678	.162	−12.0
	30	.688	.002	−10.2
	43	.697	.011	−16.0
	56	.706	.020	−16.4
	5 10	.715	.029	−20.4
	23	.724	.038	−26.1
	36	.733	.047	−29.0
	49	.742	.056	−41.4
	6 02	.751	.065	−46.9
	15	.760	.074	−42.6
	28	.769	.083	−42.3
	41	.778	.092	−44.4
	54	.788	.102	−38.1
	7 07	.797	0.111	−23.7

plied to the dates or the phases. Figures 1–5 show the individual velocity-curves on 26 nights, between August 11 and November 16, 1951. These curves immediately reveal: (*a*) a periodic change of $2K$ and (*b*) a periodic change of γ.

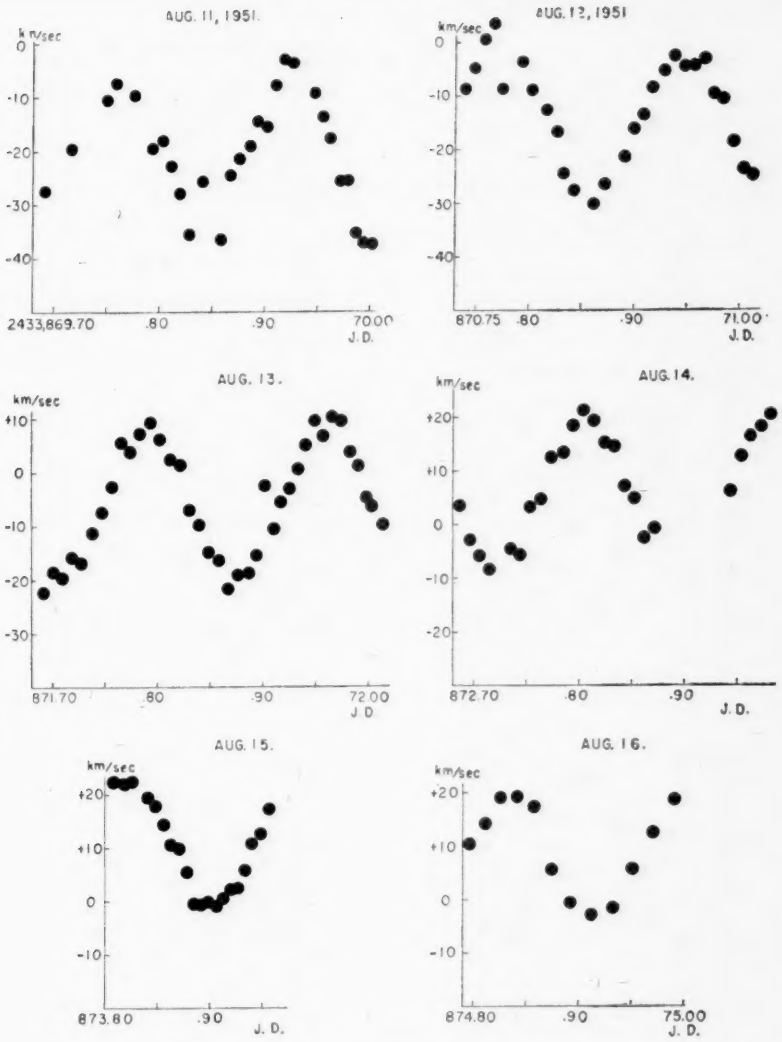

FIG. 1.—Radial velocities of 16 Lacertae

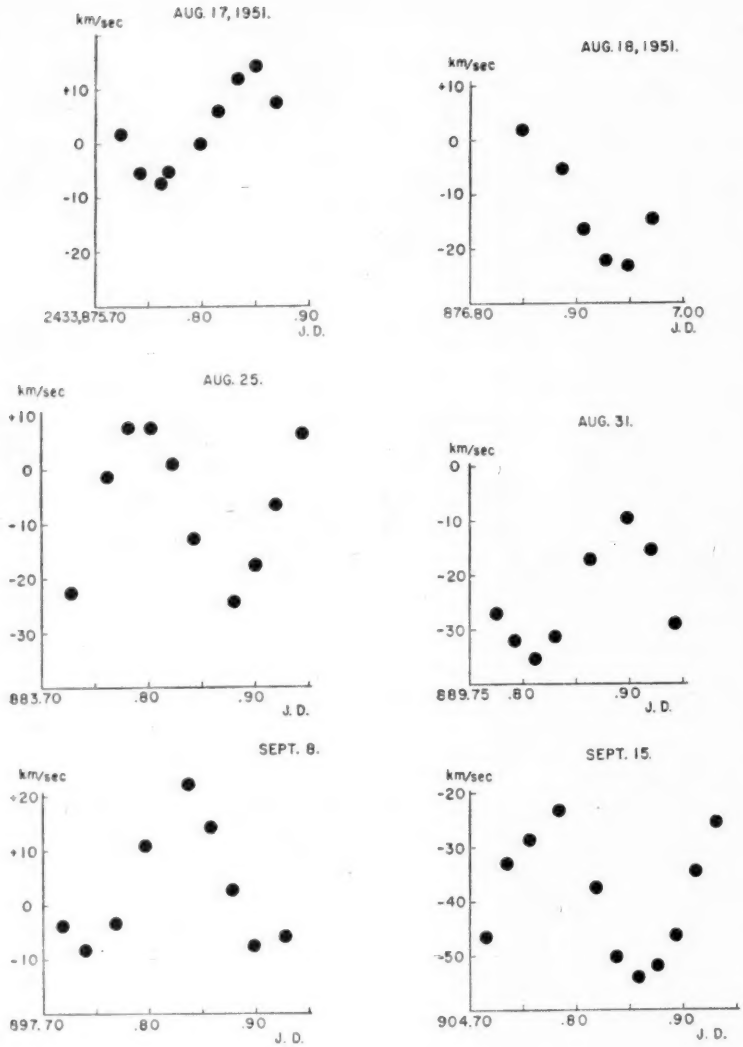

FIG. 2.—Radial velocities of 16 Lacertae

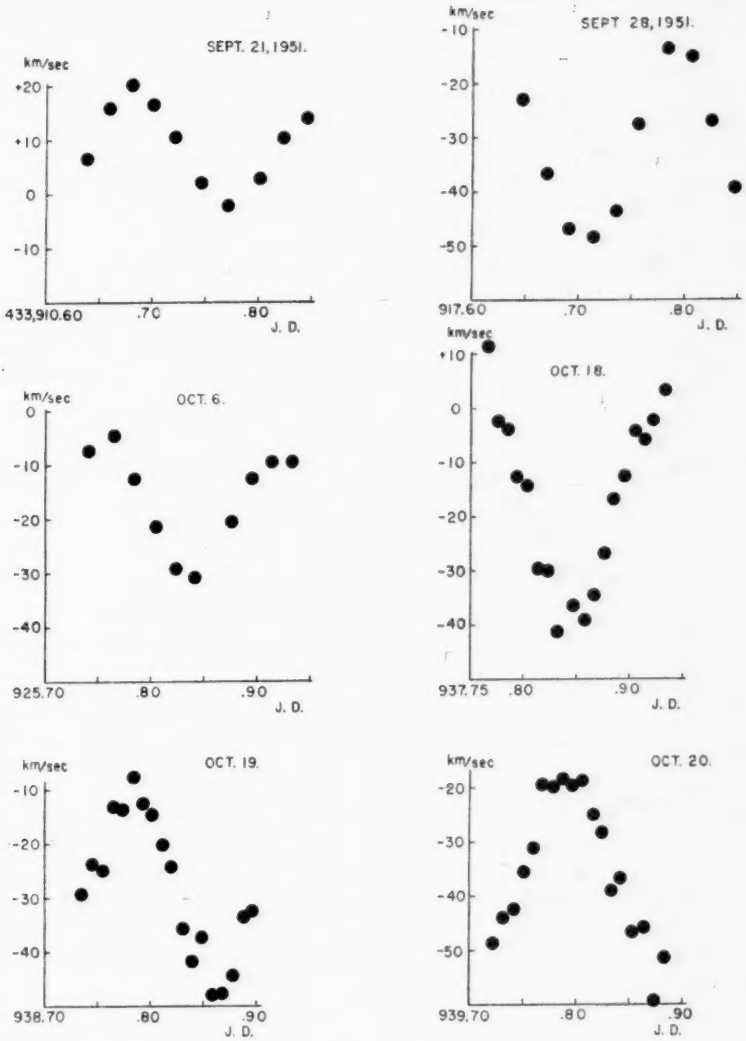

FIG. 3.—Radial velocities of 16 Lacertae

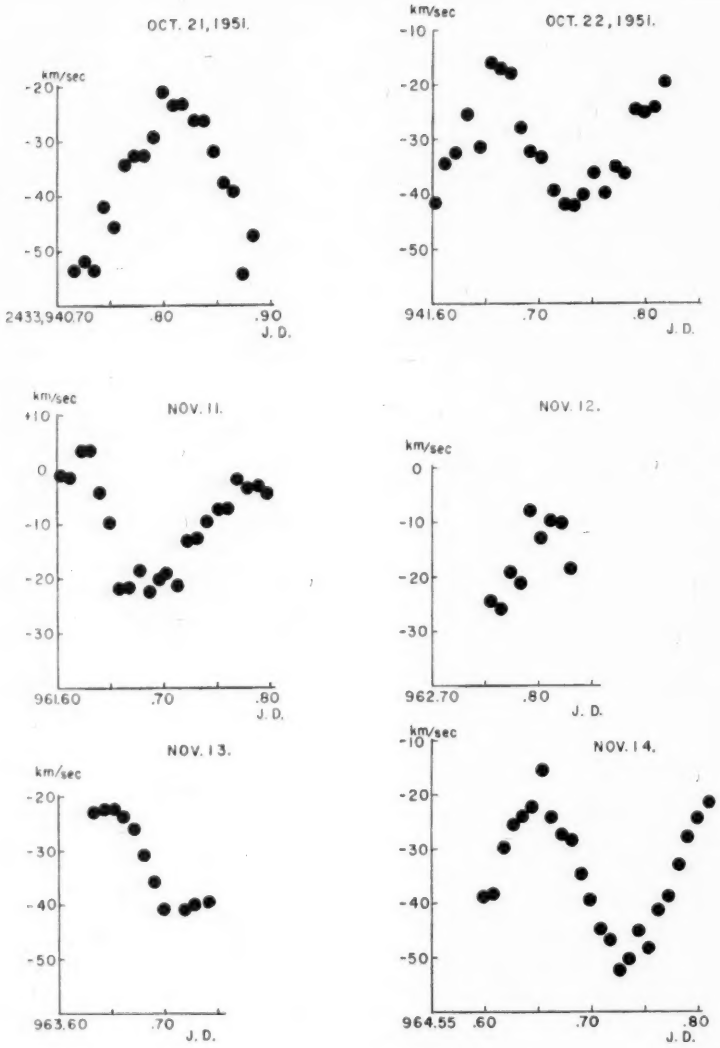

FIG. 4.—Radial velocities of 16 Lacertae

The observed values of $2K$ are listed in Table 3. The major obstacle in the determination of the period of variation of $2K$ is the lack of a well-observed minimum or maximum. The November observations appear to be best suited for choosing an epoch, in spite of the fact that they have a great deal of scatter. The best choice is JD 2433962.70. If Walker's 1950 observation is ignored, a value of 17.4 days gives the least amount of scatter for the majority of the observations which fall on the descending part of the curve.

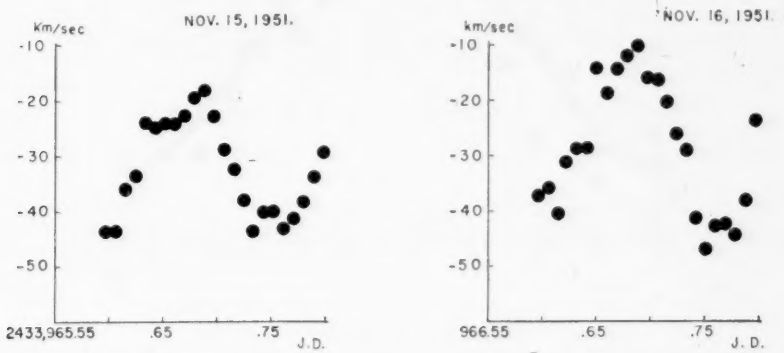

FIG. 5.—Radial velocities of 16 Lacertae

TABLE 3

DETERMINATION OF THE BEAT PERIOD FROM THE AMPLITUDES

JD 2433+	$2K$ (Km/Sec)	Phase* (Days)	Phase† (Days)	JD 2433+	$2K$ (Km/Sec)	Phase* (Days)	Phase† (Days)
527.92	39.	10.79	0.22	917.75	37.0	7.32	7.25
869.89	34.	10.76	11.59	925.83	25.0	15.40	15.33
870.82	32.	11.69	12.52	937.87	40.	10.34	9.97
871.83	30.	12.70	13.53	938.82	36.5	11.29	10.92
872.77	27.	13.64	14.47	939.83	34.0	12.30	11.93
873.87	22.	14.74	15.57	940.76	30.0	13.23	12.86
874.87	22.	15.74	16.57	941.81	25.0	14.28	13.91
875.86	20.	16.73	0.16	961.73	21.0	0.0	16.43
883.83	36.	7.6	8.13	963.68	19.5	1.95	0.98
889.85	26.5	13.62	14.15	964.68	28.	2.95	1.98
897.78	31.0	4.45	4.68	965.71	23.	3.98	3.01
904.81	31.0	11.48	11.71	966.72	29.	4.99	4.02
910.73	23.5	0.30	0.23				

* Epoch = 961.73; P = 17.15 days.
† Epoch = 962.70; P = 17.40 days.

The 1950 observation, however, falls at an impossible position on the curve, as indicated in Figure 6. In order to put this observation at a reasonable position with respect to the other observations, it is necessary to change the beat period from 17.4 days to either 17.15 or 17.75 days. Of these two values, 17.75 days is preferred, since it gives a smaller dispersion in the observations. The 17.75 period also appears to displace the August observations too far to the right.

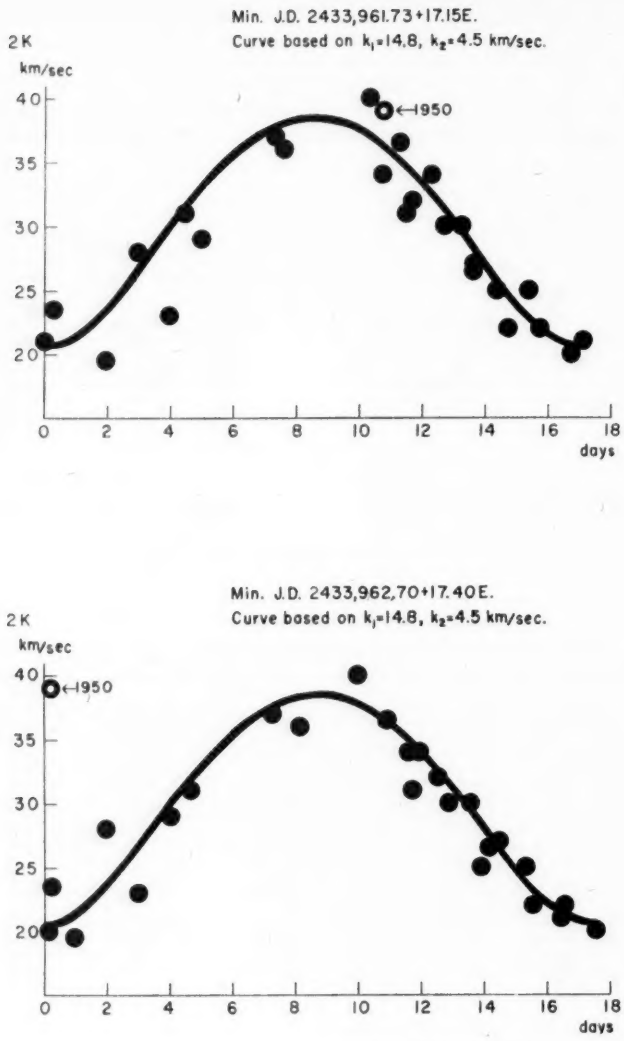

FIG. 6.—The beat period in the amplitudes of the velocity-curves

The two calculated curves given in Figure 6 were based upon the formula:[2]

$$K = \sqrt{\left[\left(K_2 - K_1 \cos \frac{2\pi}{P} t\right)^2 + \left(K_1 \sin \frac{2\pi}{P} t\right)^2\right]}. \quad (1)$$

The appropriate values of K_1 and K_2 were determined from the maxima and minima of the curves. The best epoch associated with the 17.15-day period is JD 2433961.73. The 1950 observation was purposely shifted to the right of center by choosing a period of 17.15 days, since Walker's light-curves indicate that it was obtained a few days after maximum light-amplitude. Apparently, this choice of period and epoch gives the best results when all the factors are considered. We shall adopt the following values for the beat period:

$$\text{Epoch of minimum} = \text{Zero phase} = \text{JD } 2433961.73 ,$$

$$P_3 = \text{Beat period} = 17.15 \text{ days} , \qquad K_2 = 14.8 \text{ km/sec} , \qquad K_1 = 4.5 \text{ km/sec} .$$

If this beat phenomenon is the result of the superposition of two harmonic oscillations, then there should also be present a periodic oscillation of the observed times of maxima (or minima) from their mean positions.

TABLE 4

EPOCHS FOR MAXIMUM VELOCITY*

Observed JD 2433+	Computed JD 2433+	O−C (Days)	Phase (Days)	Observed JD 2433+	Computed JD 2433+	O−C (Days)	Phase (Days)
869.926	869.826	0.000	10.76	917.790	917.798	−0.008	7.2
870.772	870.772	.000	12.5	925.765	925.749	+ .016	15.3
871.963	871.956	+ .007	13.5	938.785	938.774	+ .011	10.9
872.807	872.802	+ .005	14.5	939.787	939.789	− .002	11.9
873.824	873.817	+ .007	15.6	940.812	940.804	+ .008	12.9
874.840	874.832	+ .008	16.6	941.660	941.650	+ .010	13.9
875.850	875.847	+ .003	0.2	961.615	961.611	+ .004	16.4
883.791	883.797	− .006	8.2	963.657	963.641	+ .006	1.0
889.890	889.887	+ .003	14.2	964.652	964.656	− .004	2.0
897.830	897.837	− .007	4.7	965.670	965.671	− .001	3.0
904.780	904.773	+ .007	11.7	966.682	966.686	−0.004	4.0
910.685	910.694	−0.009	0.2				

* Maximum vel. = JD 2433869.926 + 0.16916E.

In Table 4 the epochs for maximum velocity are given. The computed epochs are based upon the formula

$$\text{Max. vel.} = 2433869.926 + 0^d16916E . \quad (2)$$

The 0.16916-day period, P_2, represents Walker's 1950 observation as well as the present observations. The difference in days (O − C) is given in the third column of Table 4. The phases are based upon the 17.15-day period. They were taken directly from the $2K$ material in Table 3.

The formula used to calculate the shift of the observed maximum is[2]

$$\phi = \text{arc } tg \frac{K_1 \sin X}{K_2 + K_1 \cos X}, \quad (3)$$

[2] O. Struve, *Ap. J.*, **112**, 520, 1950.

where $X = (2\pi/P)t$. Here t was assumed to be equal to 0 at phase 10.76 days, corresponding to the observation on JD 2433869.926 from which the epochs for maximum velocity were calculated in formula (2). The solid line in Figure 7 gives the resulting theoretical variation. The agreement is as good as could be expected.

An attempt to correlate the (O − C) data of Table 4 with a period of 12.1 days, which is an improved value for the orbital period originally found by Struve and Bobrovnikoff in 1925,[3] gave no results.

The value of the 4-hour period derived in equation (2), viz., $P_2 = 0.16916$, rests upon the observed maxima of the observed velocity-curves (Figs. 1–5) and therefore represents that value of P which is associated with the oscillation of larger amplitude, $K_2 = 14.8$ km/sec.

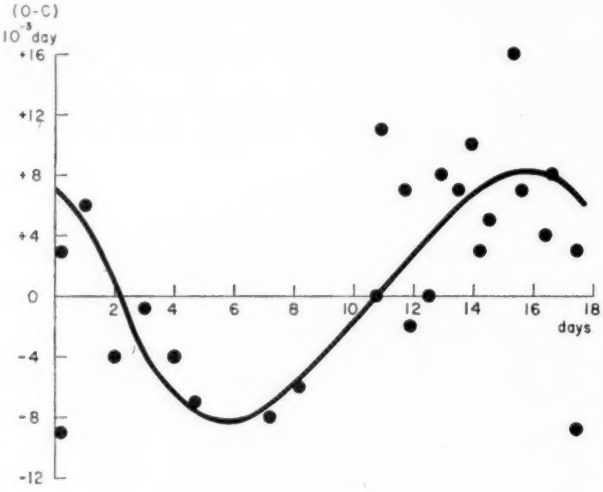

FIG. 7.—Periodic shifts of phase

We know that the period P_1, associated with the smaller-amplitude oscillation, $K_1 = 4.8$ km/sec, is related to the beat period in the following way:

$$\frac{1}{P_3} = \pm\frac{1}{P_2} \mp \frac{1}{P_1}. \tag{4}$$

There is an uncertainty in the signs which cannot be resolved from the values of P_3 and P_2 alone. It will be recalled that in the case of β Canis Majoris this uncertainty was easily resolved by the observations of the line profiles. These varied with the period P_2—the longer of the two—which was, in β CMa, associated with the oscillation of smaller amplitude. Thus the phase of maximum line width appeared to slide along the observed 6-hour oscillation. The shape of the observed velocity-curve was caused mainly by the (P_1, K_1) oscillation, but the line contours obeyed the longer value, P_2.

In the case of 16 Lac, as we shall see, the variation in line contour, though unmistakably present, is too small to be of value in finding the corresponding period. We are therefore uncertain as to whether P_1 is longer or shorter than P_2, the latter having been defined in the case of 16 Lac as the period associated with the larger amplitude.

[3] *Ap. J.*, **62**, 139, 1925.

But, if we turn to Figure 7 and Table 4, we find that, when the two oscillations are exactly in phase, at JD 2433869.926, the value of O − C is zero. As we move toward later dates the (O − C) become at first positive. Only after a lapse of 8 or 9 days, or half the beat period, do they become negative. This means that P_1 is longer than P_2, and the correct expression for computing P_1 is

$$\frac{1}{P_3}=\frac{1}{P_2}-\frac{1}{P_1} \quad \text{or} \quad \frac{1}{P_1}=\frac{1}{0.16916\ \text{day}}-\frac{1}{17.15\ \text{days}}.$$

This gives

$$P_1 = 0.17085\ \text{day}.$$

If we next turn our attention to the line contours, we recognize, first of all, that their variation is much smaller than in σ Scorpii, 12 Lacertae, ν Eridani, and even β CMa. They are, however, more pronounced than in β Cephei, where they cannot ordinarily be seen even with a dispersion of 3 A/mm.

The spectrum of 16 Lac would at all times be considered as having narrow absorption lines. The type, as given by Jane Ramsey, is B2, and the presence of the forbidden *He* I line at λ 4470 relates this star to β Cep and σ Sco (but only when the lines of the latter are narrow) and to other main-sequence B stars.

Yet, with the dispersion of the Mount Wilson coudé spectrograph, the variation in line contour is unmistakable. The only high-dispersion spectrograms which we have obtained were taken on August 15, 16, 17, and 18. They fall upon the descending branch of the curves in Figure 6, about between phases 12 and 16 days. It is possible that the line contours would show a greater amount of variation at the maximum of the curves, near phases 8 and 9 days, but this cannot now be ascertained. On all four nights the lines were broadest on the descending branches of the individual curves of Figures 1 and 2, and they were sharpest on the ascending branches. It is not possible to decide definitely whether this variation is associated with P_1 or P_2, but the latter is the more probable case.

There is a strong indication that the variation of line contour is more conspicuous in the case of the stellar *Ca* II line than in the other lines, such as those of *O* II. The stellar line *Ca* II K is at times as strong and as sharp as the interstellar component. Our high-dispersion spectrograms show rapid changes in intensity and sharpness of this stellar line, which are not shared by the interstellar component. These changes occur most often near the middle of the ascending branch in the P_2 cycle. They are not correlated with any of the periodic effects found thus far and probably represent real and rather drastic variations in the physical conditions of the atmosphere of the star. The presence of a *Ca* II line of considerable strength in a star of class B2 is perhaps in itself somewhat unusual.

As we have already remarked, there is a conspicuous periodic variation of the mean or γ-velocity as determined from the curves in Figures 1–5.

In assembling the observations, an earlier period of 12.3106 days, determined by Struve and Bobrovnikoff,[4] was used, which yielded a systematic displacement of the September, October, and November observations relative to those of August. A plot based on this period is shown in Figure 8, *A*. A new period of 12.097 days was then adopted, and a plot based upon it is shown in Figure 8, *B*. The average values of the velocities and corresponding average phases from epoch JD 2433869.500 are listed in Table 5. The observations of 1909 and 1924–1925 must play a part in the determination of this period. These earlier observations have been assembled with the period 12.097 days, and the results are shown in Figure 8, *B*. The lower curve represents the average of the 1951 observations and engenders a curious feature: There is no noticeable systematic displacement in phase, but there is a rather strong one in velocity. If one adjusts this curve upward by a small amount, a much better fit can be obtained. The procedure adopted is as follows:

The residuals to the 1951 curve of each observation, regardless of weight, were read

[4] *Ibid.*

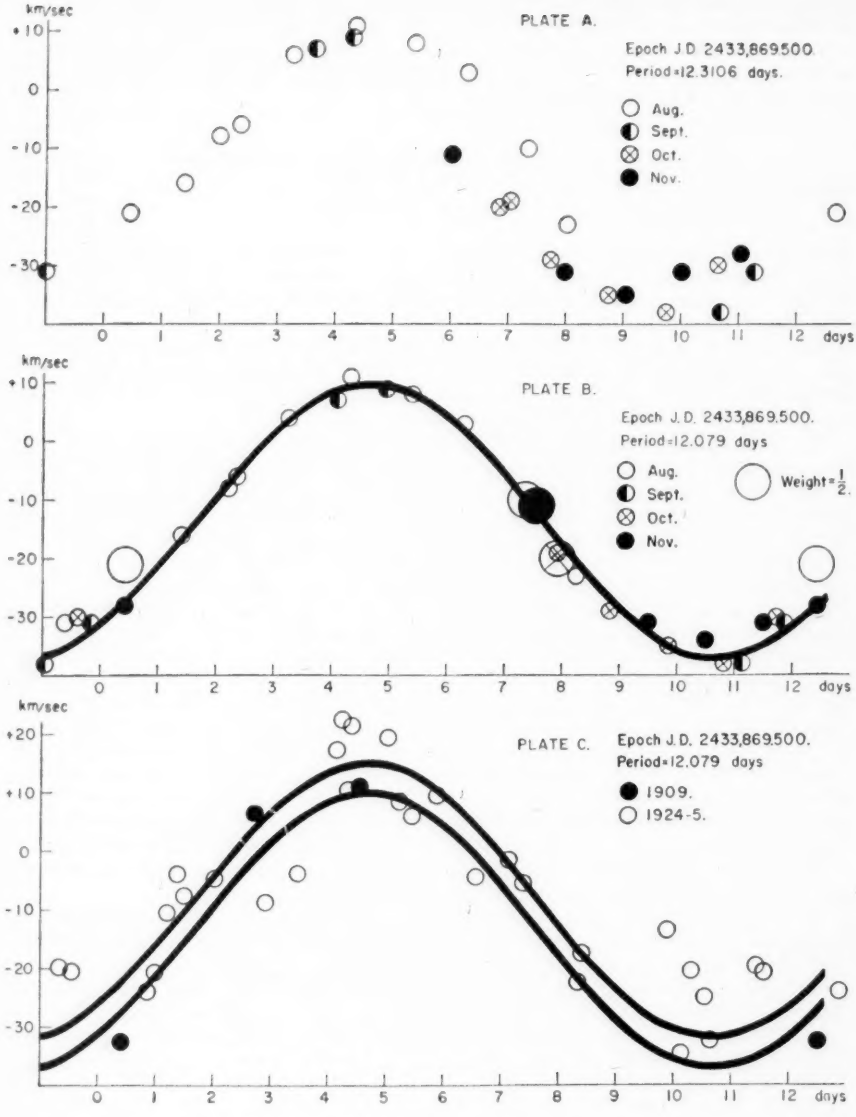

FIG. 8.—The 12-day oscillation of the mean velocities of the individual curves

off the plot of Figure 8, *C;* an unweighted average residual of +5.2 km/sec was obtained, and the 1951 curve was raised by this amount and drawn in. The need for this adjustment is difficult to explain as the result of the large secondary oscillation, because from 31 observations one would expect a uniform scatter of the points about the mean curve. Therefore, we must consider two possibilities, the first of which is the more probable: (*a*) there is a systematic difference between the Yerkes plates and those of the current series; (*b*) there is an additional long-period binary motion. An attempt was made to determine

TABLE 5

AVERAGE PHASES AND VELOCITIES OF THE 12.097-DAY PERIOD

Date	JD 2433+	Phase	V_0 (Km/Sec)	Weight	Date	JD 2433+	Phase	V_0 (Km/Sec)	Weight
Aug. 11...	869.925	0.425	−21	½	Sept. 28...	917.750	11.959	−31	1
12...	870.900	1.400	−16	1	Oct. 6...	925.800	7.912	−19	1
13...	871.850	2.350	− 6	1	18...	937.900	7.915	−20	½
14...	872.750	3.250	+ 6	1	19...	938.825	8.840	−29	1
15...	873.850	4.350	+11	1	20...	939.825	9.840	−35	1
16...	874.875	5.375	+ 8	1	21...	940.800	10.815	−38	1
17...	875.800	6.300	+ 3	1	22...	941.700	11.715	−30	1
18...	876.850	7.350	−10	½	Nov. 11...	961.725	7.546	−11	½
25...	883.825	2.228	− 8	1	12...	962.800	Insufficient observations		
31...	889.850	8.253	−23	1	13...	963.675	9.496	−31	1
Sept. 8...	897.800	4.106	+ 7	1	14...	964.700	10.521	−35	1
15...	904.825	11.131	−38	1	15...	965.700	11.521	−31	1
21...	910.725	4.934	+ 9	1	16...	966.700	0.424	−28	1

TABLE 6

Element	1925 Elements	1951 Preliminary Elements
P	(12.3106 days)	12.097 days
γ	− 6.9 km/sec	−13.6 km/sec
e	0.10±0.03	0.007
K	22.2±1.0 km/sec	23.4 km/sec
ω	7°8±8°5	28°
T	JD 2424063.894±0.016	JD 2433875.10
$a \sin i$	3.650×10^6 km	3.883×10^6 km

preliminary elements of the orbit from only the 1951 observations. Unfortunately, the eccentricity is nearly zero, and the Lehmann-Filhés method is not very effective.

Table 6 gives a set of elements which are consistent with the curve of Figure 8, *B*. The difference between the two γ-velocities is now 6.7 km/sec, which is close enough to the value determined from the residuals, 5.2 km/sec.

The final result of this investigation is of considerable interest. The periods P_1 and P_2 interfere as in β CMa[5] and ν Eri.[6] We have adopted the designations of the periods proposed by Struve.[7] The beat period is $P_3 = 17.15$ days $= 101.38\ P_2$. The fact that three

[5] V. P. Zessevich, *A.J.U.S.S.R.*, **21**, 94, 1944.

[6] *Ibid.*

[7] *Pub. A.S.P.*, **64**, 20, 1952.

stars are now known to have closely similar and interfering periods, P_1 and P_2, shows that this phenomenon is of fundamental importance in the stars of the β CMa or β Cep type.

Previous investigations have shown only the existence of P_2 in σ Sco and 12 Lac. This probably means that in these stars $K_2 \gg K_1$ and that, consequently, P_1 is not detectable. We do not yet know whether the beat phenomenon exists in β Cep. The absence of a variation in line profile would perhaps lead us to expect that only P_1 is present. But the star is certainly variable in light. Moreover, all previous investigators agreed that K is also variable. Thus our next task will be to find whether both P_1 and P_2 are present.

In the light of our work on 16 Lac, in which the variation in line profile was barely detectable with the highest dispersion, we should be prepared to find that P_2 may, after all, be present in β Cep, even though the change in line contour is not observable. Until this test has been made, it is futile to enlarge upon what has already been stated elsewhere concerning the physical interpretation of these phenomena.

Finally, in our proposed classification the 12.1-day period would be designated as P_5. There is no definite indication of a change in K_2, and consequently there is no P_4 (or I_4). But the fact that the lines change rapidly, and perhaps in an irregular manner, on the ascending branch of the 4-hour velocity-curve, suggests that we may have to investigate this question further.

The velocity obtained from the interstellar line *Ca* II K is -13.5 km/sec.

THE LIGHT-VARIABILITY OF 16 LACERTAE

G. R. MICZAIKA
Badische Landessternwarte, Heidelberg-Königstuhl
Received February 25, 1952

ABSTRACT

A total of 1821 photoelectric observations of the β Canis Majoris star 16 Lacertae during 28 nights in the autumn and winter of 1951 have been obtained. They revealed that the light-variation of the star is characterized by four periods. Two nearly equal periods P_1 and P_2 of about 0^d169 and 0^m07, respectively, 0^m04 amplitude, combine to produce a beat period $P_3 = 17^d6$. The observed amplitudes vary from 0^m03 to 0^m11. The residuals of the observed maxima and minima from uniform elements show a strong tendency to oscillate with the beat period. 16 Lacertae seems to be a spectroscopic binary consisting of a β Canis Majoris object and a second star with $P_4 = 12^d1$ as period of orbital motion. It is supposed that both short periods are induced in the atmosphere of the β Canis Majoris star.

I. INTRODUCTION

The early B star 16 Lacertae was announced as a spectroscopic binary by O. J. Lee[1] in 1910. O. Struve and N. T. Bobrovnikoff[2] derived a spectroscopic orbit from 31 spectrograms obtained in 1909 and 1924/25. They found a slightly eccentric orbit ($e = 0.10$, $\omega = 7°8$) with $P = 12.3106$ days and $K = 22.2$ km/sec. Merle F. Walker[3] discovered in 1950 that 16 Lacertae is also a β Canis Majoris star having a light-variation of 0.06–0.11 mag. and a radial-velocity variation of 40 km/sec in a period of nearly 4 hours.

Photoelectric observations of the star made at Heidelberg with a 12-inch refractor confirmed the period and character of the variability as found by Walker. I gave[4] the improved elements M = JD 2433505.926 + $0^d169012E$ derived from the maxima available until September 30, 1951. Through this note a particularly fortunate coincidence resulted, as Dr. Struve and Dr. McNamara had been observing the star at the Mount Wilson and Lick Observatories, while Mr. Walker had been getting photoelectric observations at the Lick Observatory during the same time. Hence there resulted frequent discussions by correspondence, mutual information, and the decision to publish all the papers together. A very large amount of material on the behavior of the star during the last season is available. At Heidelberg a total of 1821 photoelectric observations was secured during 28 nights between August 24, 1951, and January 7, 1952.

II. THE OBSERVATIONS

The observations were made with an RCA 1P21 photomultiplier and a 12-inch refractor. The electronic equipment built in the shop of the observatory and to be described elsewhere consists of a two-staged d.c. amplifier of the feed-back type and a power supply regulated by tubes. The output of the amplifier is given on a 0–1 milliammeter. The measurements were made in the way *aVaV*. . . . One observation of a star consisted of three readings of the deflection made within 30–60 seconds, preceded and followed by one reading of the intensity of the sky. A time constant of $RC = 4$ seconds was used. All the measurements were made without color filters, the corrections for differential extinction being based on $\Delta m = 0^m35\ \Delta \sec \zeta$. The coefficient 0^m35 is usually adopted for a 1P21 multiplier behind a refractor and is not critical, as Δm seldom surpassed 0.01 mag., owing to the short distance of the comparison star, 14 Lacertae, from 16 Lacertae.

All the observations are plotted in Figures 1 and 2. The scattering of the single points is rather different from night to night. In August and September the measurements had

[1] *Ap. J.*, **32**, 307, 1910.
[2] *Ap. J.*, **62**, 139, 1925.
[3] *Pub. A.S.P.*, **63**, 35, 1951.
[4] *Nachrichtenblatt AZ*, **5**, 32, 1951.

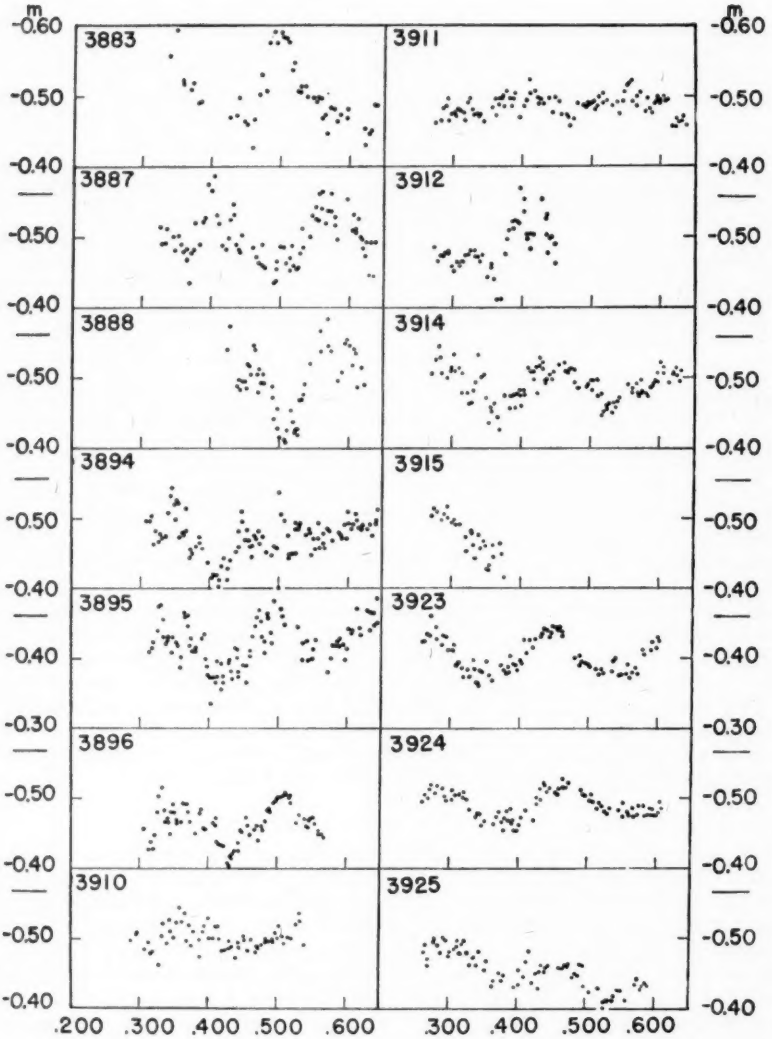

FIG. 1.—Light-curves of 16 Lacertae. The ordinates are magnitude differences, 16 Lacertae−14 Lacertae. The dates are given in abbreviated Julian days.

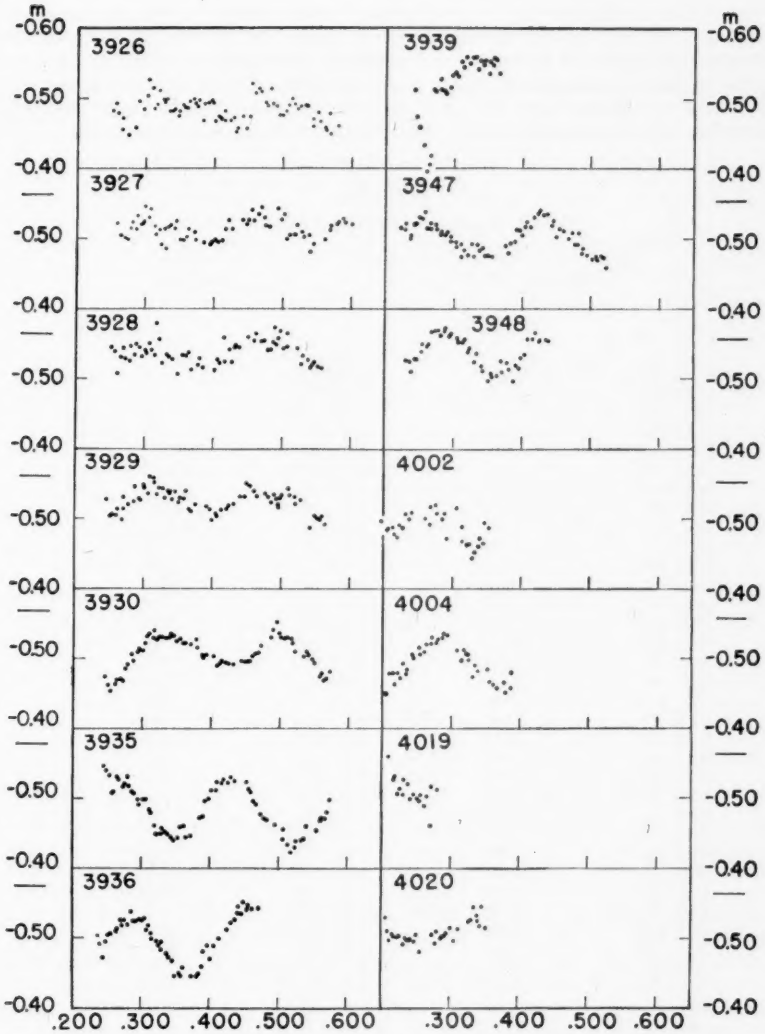

FIG. 2.—Light-curves of 16 Lacertae. For further explanation see Fig. 1

to be made on very humid nights, whose neighboring nights were heavily clouded. It is our experience that single clear nights lead, in general, to mean errors which are considerably larger than on nights of a long clear period. Such a series of nights occurred in October, 1951, when Mount Königstuhl lay in very dry air, rather high above a temperature inversion. Mean errors of ± 0.003 or ± 0.005 mag. are representative for these very rare nights. The light-curves secured at the favorable atmospheric conditions of October are by far the most regular ones. Hence it may be concluded that the light-variations of 16 Lacertae run in general without sudden disturbances or secondary waves.

TABLE 1

LIGHT-MAXIMA AND MINIMA OF 16 LACERTAE

MAXIMA			MINIMA		
243+	E	O−C	243+	E	O−C
3504.903*	−6	0	3504.806†	0	− 3
3505.762*	−1	+13	3504.988†	1	+10
3505.927*	0	+ 9	3505.834†	6	+10
3519.954*	83	− 5	3521.882†	101	−13
3521.976*	95	−13	3523.908†	113	−17
3523.831*	106	−19	3527.981†	137	− 4
3527.918*	130	+ 8	3883.425	2238	+14
3883.498	2232	+ 1	3887.492	2262	+20
3887.412	2255	+25	3888.509	2268	+22
3887.578	2256	+22	3894.413	2303	+ 5
3888.589	2262	+18	3895.425	2309	+ 2
3895.345	2302	+ 7	3896.432	2315	− 6
3895.501	2303	− 6	3914.371	2421	+ 1
3896.516	2309	− 6	3914.528	2422	−11
3912.428	2403	+ 4	3923.360	2474	+24
3914.446	2415	− 8	3923.532	2475	+27
3914.620	2416	− 3	3924.377	2480	+26
3923.273	2467	+22	3925.381	2486	+15
3923.448	2468	+28	3925.533	2487	− 2
3924.277	2473	+11	3927.390	2498	− 6
3924.452	2474	+17	3927.550	2499	−15
3925.292	2479	+11	3929.402	2510	−24
3926.304	2485	+ 8	3930.252	2515	−20
3926.460	2486	− 5	3930.417	2516	−24
3927.301	2491	−10	3935.354	2545	+ 7
3928.464	2498	−31	3935.520	2546	+ 4
3929.310	2503	−30	3936.369	2551	+ 7
3930.315	2509	−40	3947.349	2616	− 9
3930.491	2510	−34	3948.360	2622	−13
3935.428	2539	− 2	4002.331	2941	− 7
3936.285	2544	+ 9	4004.364	2953	− 4
3936.448	2545	+ 3	4019.255	3041	0
3939.322	2562	+ 1	4020.250	3047	−20
3947.258	2609	−14			
3947.426	2610	−15			
3948.288	2615	+ 1			
4002.274	2934	+23			
4004.290	2946	+ 9			
4020.355	3041	+ 3			

* Maxima derived by Walker, *Pub. A.S.P.*, **63**, 35, 1951.

† Minima determined from Walker's light-curves.

III. THE SHORT PERIOD OF THE LIGHT-VARIABILITY

From the plots of the observations, 32 light-maxima and 27 minima could be determined. They were used with 7 maxima derived by Walker in 1950 and 6 minima taken from his diagrams, to compute the elements of the short-period light-variability. The whole interval beginning with August 11, 1951, can be covered with uniform elements for both the maxima and the minima. The mean value of 0.169168 day of the periods of the maxima (0.169166 day) and the minima (0.169170 day) can be regarded as representative for the time from August 11, 1950, to January 7, 1952 (see Table 1).

TABLE 2

ELEMENTS OF 16 LACERTAE

Maxima	JD 2433505.918 + 0^d.169166
Minima	JD 2433504.809 + 0^d.169170
$M - m$	0.094 day

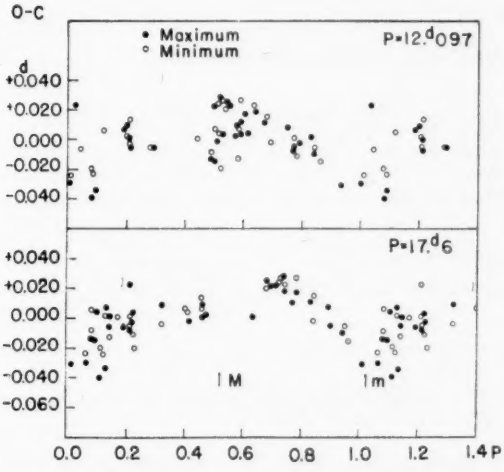

FIG. 3.—Phase shift of the light-curves, represented by $P = 12^d.097$ and $P = 17^d.6$. The maximum and minimum phases of the light-amplitude are marked by M and m, respectively. Phases are arbitrarily counted from JD 2433505.9.

The residuals O − C computed with the elements of Table 2 are represented in Figure 3, with the period found by Struve and Bobrovnikoff in the radial velocities some twenty-five years ago and now changed by the California observers to 12.097 days, as well as with the beat period, 17.6 days. Phases are counted from JD 2433505.9. The run of the residuals is obviously very much better with the beat period of 17.6 days than with the 12.097-day period. The material is not yet absolutely conclusive but speaks strongly in favor of the longer value. The scattering around the mean curve is probably due, to a large extent, to errors of the determination of the extremes in consequence of observational disturbances. The maxima and minima observed by Walker in 1950 are not given in the plot, as the beat period is not well enough known to combine both observational series. In the 17.6-day plot the phases are marked, when the variation of the light-amplitude reaches its maximum (M) and minimum (m) in the beat period, as discussed in Section IV.

IV. THE AMPLITUDE OF THE LIGHT-VARIABILITY

It was already suspected during the course of the observations that the amplitude of the light-variations is variable. The 12-day period seemed too short. If this variation was periodic at all, it required a little more than 15 days for one complete cycle. During the discussion I was informed by Dr. Struve[5] that the radial-velocity work under way in California revealed a period of 17.6 days in the amplitudes of the short-period velocity variations. It can be regarded as a beat period of two periods having nearly the same duration of 4 hours. A plot of the amplitudes (Fig. 4) against phases computed with $P = 17.6$ days immediately shows the beat phenomenon in the light-variation, too. This is beyond doubt, although the phase of maximum variability is only incompletely covered. The variations of the amplitude can be represented with the same period over the whole interval covered by my measures.

The photometric amplitudes of the two 4-hour periods producing observed light-amplitudes of 0.03–0.11 mag. were estimated to be 0.07 and 0.04 mag. A theoretical curve of the amplitude variation calculated with

$$A = \sqrt{[(A_1 + A_2 \cos x)^2 + (A_2 \sin x)^2]},$$
$$x = (\omega_1 - \omega_2)\, t - (\phi_1 - \phi_2),$$

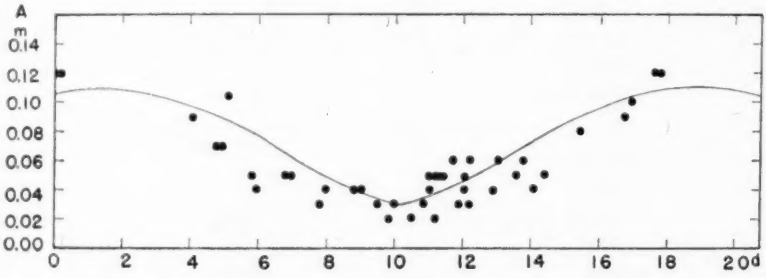

FIG. 4.—Variation of the photometric amplitude of 16 Lacertae with the beat period, $P_3 = 17^d6$. The phases are arbitrarily counted from JD 2433883.3.

is given in Figure 4. Maximum amplitude A occurs at JD $2433884.5 + 17^d6E$. The beat period is not so exactly known as is necessary to bridge the one-year interval between both observational series. If a conclusion can be drawn from Walker's 1950 curves and if the counting of the epochs elapsed is correct, an improvement of -0.3 day may perhaps be indicated. The maximum and minimum of the light-amplitude occur approximately at the phase of the largest positive or negative shift O − C of the light-curves.

The 12.1-day period could not be established in the amplitude variation.

V. DISCUSSION

The light-variability of 16 Lacertae is characterized by four periods:

a) Two nearly equal short periods P_1 and P_2, one of them lasting 0.169168 day, the other differing from that value by about 0.0016 day, as computed from

b) The beat period $P_3 = 17.6$ days of the amplitude variation, and very probably regulating the phase-shifting of the light-curves;

c) The period of the mean radial velocity, $P_4 = 12.097$ days.

[5] Later on, the California observers found from the 1951 data alone $P = 17.4$ days and preferred for their whole material $P = 17.15$ days. The difference means little for the present discussion, especially with regard to the value 17.4 days for 1951.

16 Lacertae differs from the other objects of the β Canis Majoris group discussed in detail, in so far as a fourth period, $P = 12.1$ days, is well established. The other stars do not show such a pronounced variation of the γ-velocity and a cyclic behavior of the light-curve. It is tempting to suggest the 12.1-day cycle as a real orbital motion of the β Canis Majoris component around a gravity center formed with a further component. Both the short periods may be evoked by oscillations of a rotating star, perhaps excited by a rapidly traveling stable satellite, lagging behind a strip of turbulence and waves in the adjoining layers of the B atmosphere and reinforcing one another with the beat period of 17.6 days. This picture follows the lines of the hypothesis of Struve[6] on the β Canis Majoris stars but approaches that of Ledoux,[7] in so far as both the 4-hour periods are assumed as properties of the atmosphere and are not ascribed to the exciting satellite. Of course, its revolution period may be identical or nearly identical with one of them.

The phase relation of both the 4-hour periods seems to be independent of the phase in the 12.1-day cycle. This period cannot be found in my photometric material. The explanation may be sought in the assumption that the orbital motion of the β Canis Majoris component with the 12.1-day period around the center of gravity is without appreciable influence on the light-changes and is probably not essential for the phenomenon of this type of light-variability.

More observations of 16 Lacertae and related objects must be awaited to solve the problems here involved.

In conclusion, the writer wishes to acknowledge his indebtedness to Dr. O. Struve for many discussions during the last phase of this work. Thanks are due to the Sigma Xi Society for a grant to cover the purchase of two RCA 1P21 photomultipliers through the kind intervention of Dr. H. Shapley, and to Mr. K. Bahner for assistance at the instrument.

[6] *Ap. J.*, **112**, 520, 1950; **113**, 589, 1951; *Pub. A.S.P.*, **62**, 263, 1950; **63**, 249, 1951.

[7] The original paper of P. Ledoux was not accessible to the author; information was taken from Struve's comment in *Pub. A.S.P.*, **63**, 249, 1951.

A PHOTOELECTRIC STUDY OF 16 LACERTAE

MERLE F. WALKER
Berkeley Astronomical Department, University of California
Received April 4, 1952

ABSTRACT

Photometric observations of 16 Lacertae in 1950 and 1951 have established the following periods: $P_2 = 0.169165$ day and $P_1 = 0.170845$ day, which combine to give a beat period $P_3 = 17.20$ days. The amplitudes of the two variations are approximately equal. Comparison with radial-velocity observations obtained simultaneously by O. Struve and D. H. McNamara shows that a well-defined relation exists between the amplitudes of the light- and velocity-curves. The light- and velocity-curves are "in phase," maximum light occurring at the time of maximum contraction of the star on the pulsation hypothesis. The fact that P_1 and P_2 have a ratio of velocity amplitudes of about 3 to 1 and a ratio of light-amplitudes near unity can be used to explain: (1) the observed periodicities in the times of maximum light and of maximum velocity; (2) the periodicity in the phase relationship between the light- and velocity-curves; and (3) the shape of the beat-curves. From an integration of the velocity-curves, the fractional change in radius is found to vary from 1.5 to 2.4 per cent. The temperature variation required to explain the observations on the pulsation hypothesis is less than the limit of observational detection.

The B2 star 16 Lacertae was discovered in 1950 to be a β Canis Majoris star with a 4-hour variation in light and velocity.[1] During the summer and fall of 1951 spectroscopic observations were carried out by O. Struve at Mount Wilson and D. H. McNamara at Lick.[2] Simultaneous photometric observations were obtained on 13 nights by the author at Lick. Additional photometric observations were secured by G. R. Miczaika at Heidelberg.[3] Each of these investigations is being reported separately, although, with the permission of the authors, I have made considerable use of the spectroscopic results in the later portion of this paper.

With the exception of one night, all the photometric observations were made with the 12-inch Lick refractor. The photometer employed a 1P21 photomultiplier tube and yellow and blue Corning filters 3385 and 5562. The output of the cell was connected to a d.c. amplifier, designed by Kron,[4] and the amplified signal was then fed into a Brown recorder. On August 13 the observations were made with a similar photometer on the Crossley reflector.

The observations have been reduced to no atmosphere by the use of extinction coefficients determined each night from the comparison star, 14 Lacertae. The magnitudes and colors have been left on the system defined by the telescope-filter-cell combination. The individual light- and color-curves for each night are shown in Figures 1–3. The ordinates of the curves are for the light-curves the blue-magnitude difference and for the color-curves the color difference, 16 Lacertae *minus* 14 Lacertae. Heliocentric corrections have been applied to the times of observation.

On several nights HD 217227 was used as an additional comparison star. This star gives a nearly constant magnitude difference for the mean light of 16 Lacertae. Thus it appears likely that 14 Lacertae is itself slightly variable and that this is the cause of the night-to-night changes in the magnitude difference between 14 Lacertae and the mean light of 16 Lacertae, which are evident in the illustrations. Observations of the Be star HD 217050 were also obtained and will be discussed in a subsequent paper.

[1] *Pub. A.S.P.*, **63**, 35, 1951.

[2] O. Struve, D. H. McNamara, R. P. Kraft, S. M. Kung, and A. D. Williams, *Ap. J.*, **116**, 81, 1952.

[3] *Ap. J.*, **116**, 99, 1952.

[4] *Ap. J.*, **115**, 1, 1952.

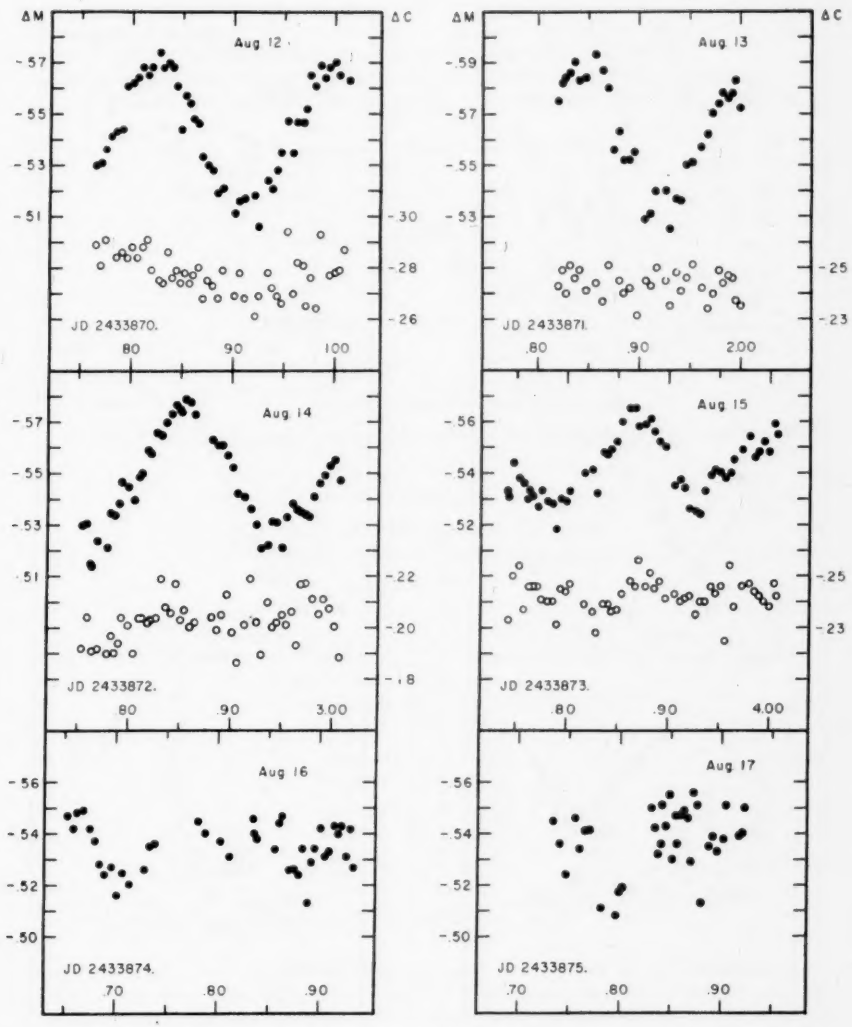

FIG. 1.—Photometric observations of 16 Lacertae in 1951. The dots represent blue-magnitude differences, and the circles color differences, 16 Lacertae *minus* 14 Lacertae, reduced to no atmosphere.

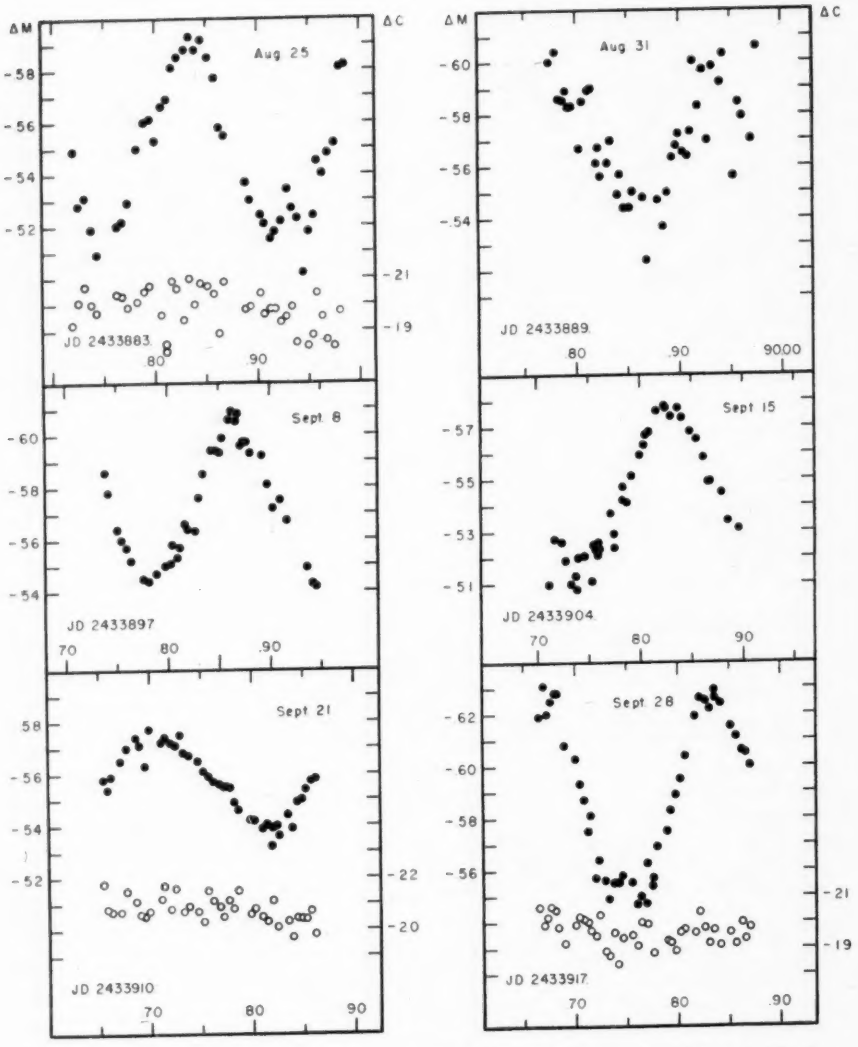

FIG. 2.—Photometric observations of 16 Lacertae in 1951. Ordinates and symbols as in Fig. 1

It is apparent from the color-curves that there is no definite change in the color of the star. Some of the curves seem to show a maximum blueness when the star is brightest, yet others, for light-curves having comparable amplitudes, do not. The color variation on August 12 is very likely the result of incomplete elimination of extinction; the color-curve is symmetrical about the time of meridian passage of the star.

Perhaps the most outstanding feature of the light-curves is the pronounced beat phenomenon which they exhibit. The maximum light-variation observed in 1951 was 0.079

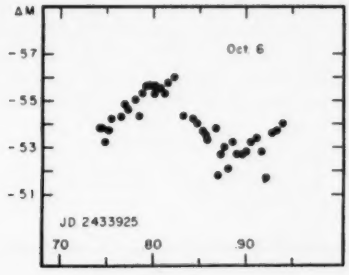

FIG. 3.—Photometric observations of 16 Lacertae in 1951. Ordinates and symbols as in Fig. 1

TABLE 1

THE BEAT PERIOD OF 16 LACERTAE

JD 2433+	Light-Range R (Mag.)	$2K$* (Km/Sec)	Phase $P=17.20$ Days	Phase $P=17.27$ Days	JD 2433+	Light-Range R (Mag.)	$2K$* (Km/Sec)	Phase $P=17.20$ Days	Phase $P=17.27$ Days
504.90	0.110	.....	0.722	0.809	873.88	0.036	22	0.174	0.173
505.88	.110	.....	.778	.865	874.80	.000	22	.227	.226
519.92	.079	.....	.595	.677	875.82	.025	20	.287	.285
521.90	.090	.....	.710	.792	883.85	.078	36	.753	.750
523.87	.060	.....	.824	.906	889.87	.056	26.5	.103	.099
527.92	.081	39	.060	.141	897.84	.065	31.0	.567	.561
535.90	.048	.....	.524	.603	904.81	.064	31.0	.972	.964
870.89	.056	32	.000	.000	910.76	.038	23.5	.318	.309
871.91	.060	30	.059	.059	917.77	.079	37.0	.726	.715
872.88	0.059	27	0.116	0.115	925.84	0.029	25.0	0.195	0.182

* Taken from Struve's paper (O. Struve *et al.*, *Ap. J.*, **116**, 81, 1952).

mag. Only one set of observations was obtained at a time of minimum range. Unfortunately, there were some difficulties with the photometer during this night, August 16, and, as a result, the observations are not too good. On the following night the atmospheric conditions were very poor, so that again the light-curve is very uncertain. However, on the basis of the predicted times of maximum and minimum light and the general appearance of the curves, I have considered that there was no light-variation on August 16 and a variation of 0.025 mag. on August 17. Thus, while it is uncertain just what the smallest light-amplitude is, it must be less than one or two hundredths of a magnitude. The light-variations observed in 1950 and 1951 are listed in Table 1.

The 1951 observations can be satisfied by a period between 17 and 17½ days. If we as-

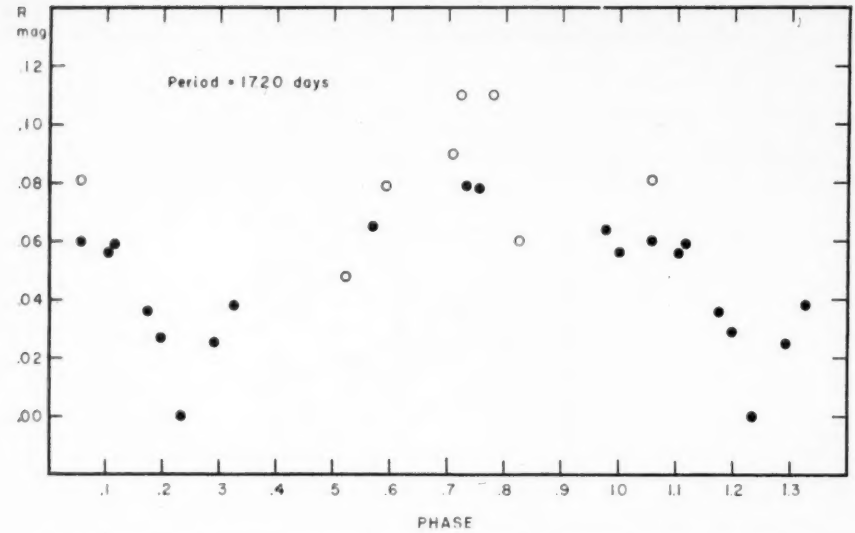

FIG. 4.—The beat period in the amplitudes of the light-curves. The ordinate is the light-variation, the abscissa is the phase computed from zero phase = JD2433870.89 + 17.20E days. Circles represent observations made in 1950.

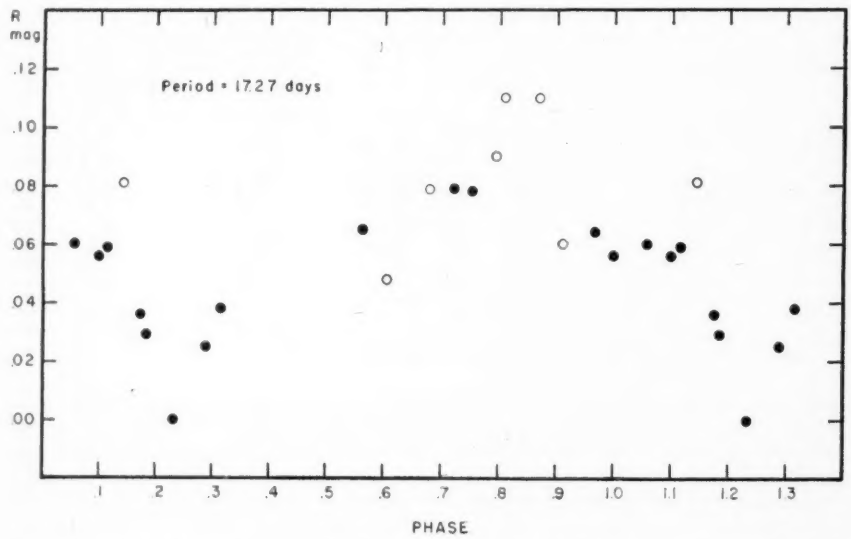

FIG. 5.—The beat period in the amplitudes of the light-curves. Ordinates and symbols as in Fig. 4, phases computed from zero phase = JD 2433870.89 + 17.27E days.

sume that the maximum amplitude occurs halfway between successive epochs of minimum amplitude, then the 1950 observations lead to a period of about 17.20 days, as shown in Figure 4. On the other hand, it might be that the maximum amplitude occurs later in time than the mid-point between the minima of the beat-curve, a region of the curve not covered by the photometric observations. In this case the observations could be satisfied by a period of about 17.27 days, as indicated in Figure 5. This latter supposition seems rather unlikely, since Struve *et al.* have additional measurements of velocity on this portion of the beat-curve and find no evidence of asymmetry. However, if the 17.20-day period is correct, there remains quite a large scatter in the observed amplitudes. In particular, the largest light-variations observed in 1950 are 0.03 mag. greater than those observed in 1951. This may be observational scatter, or it may be that the amplitude of the beat cycle is itself variable. Clearly, series of good photometric observations covering the entire 17-day cycle in different seasons are to be desired.

TABLE 2

OBSERVED MAXIMA OF 16 LACERTAE*

Helioc. JD 2433+	O−C (Day)	Phase (P=17.20 Days)	Helioc. JD 2433+	O−C (Day)	Phase (P=17.20 Days)
504.906	−0.013	0.826	871.849	+0.011	0.060
505.765	.000	.776	872.854	+ .001	.118
505.930	− .004	.786	873.868	.000	.177
519.957	− .018	.601	883.837	− .012	.757
521.795†	− .041	.708	889.930	− .009	.111
523.834	− .032	.827	897.864	− .025	.752
527.921	− .005	.064	904.828	+ .003	.977
535.830†	− .046	.524	910.701	− .045	.319
870.826	+ .003	.000	917.830	− .020	.733
870.996	+0.004	0.010	925.801	−0.001	0.197

* Max. light = Helioc. JD 2433505.765 + 0.169165E day.
† Low weight.

On the basis of the foregoing discussion, I have tentatively adopted the following elements for the beat period:

$$\text{Min.} = \text{JD } 2433874.80 + 17.20E \text{ days}.$$

Note that the zero phase in all of the figures has been arbitrarily taken at JD 2433870.89, the date of the first 1951 observations.

From the 1950 and 1951 observations of the time of maximum light, the following improved elements of the short-period variation have been derived:

$$\text{Helioc. max.} = \text{JD } 2433505.765 + 0.169165E \text{ day}.$$

This corresponds to the P_2 period in Struve's notation. These observed maxima and the residuals from the maxima computed with this formula are given in Table 2.[5] The epoch of maximum light in the above formula was arbitrarily taken as the observed time of one of the first well-determined maxima. The fact that the residuals are not symmetrical about zero indicates merely that we have not made a very good choice. It would probably have been better to decrease the epoch given above by about 0.02 day.

It is seen in Figure 6 that the residuals exhibit a periodic variation in the 17-day peri-

[5] The 1950 observations were originally published without having the heliocentric corrections applied. These have been added to obtain the times given in Table 1.

od. As pointed out by Struve,[6] this is to be expected if the beat phenomenon is caused by the superposition of two harmonic oscillations. If the amplitudes of the two component harmonic oscillations are equal, the largest residual should be one-quarter of the period, or about ± 0.04 day. The largest phase shift observed is about ± 0.025 day. While this is smaller than would be expected if the amplitudes were equal, it is much larger than the value of ± 0.008 day found by Struve for the phase shifts of the time of maximum velocity.

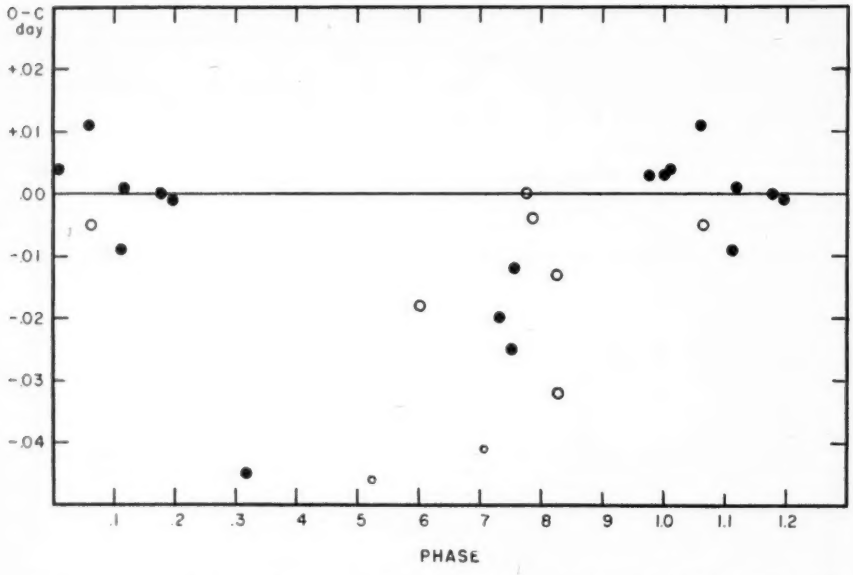

FIG. 6.—Periodic variations in the times of maximum light. The ordinate is the residual, observed maximum *minus* maximum predicted from the formula Hel. max. = JD 2433505.765 + 0.169165E day. The phases are computed from zero phase = JD 2433870.89 + 17.20E days. Circles represent observations made in 1950.

Since the residuals of the observed maxima from the mean period become more positive after the time of maximum beat amplitude, we may apply Struve's argument[2] to show that the other short period must be greater than the one given above, so that

$$\frac{1}{P_3} = \frac{1}{P_2} - \frac{1}{P_1},$$

where $P_2 = 0.169165$ day, $P_3 = 17.20$ days, and therefore $P_1 = 0.170845$ day, using Struve's notation. In view of the various uncertainties discussed above, I have hesitated to assign amplitudes to the two short periods. However, the general appearance of the beat-curve and the large phase shifts discussed above indicate that the values of these amplitudes are very nearly equal, much more so than the corresponding velocity-amplitudes determined by Struve. There appears to be no correlation of the photometric observations with the 12-day period of the gamma velocity found by Struve.[2]

Let us now consider the light- and velocity-observations together. Taking the ob-

[6] *Ap. J.*, 112, 520, 1950.

served light-ranges from Table 1 and the corresponding values of $2K$ from Struve's paper,[2] we see in Figure 7 that there exists a definite relationship between the amplitudes of the light- and velocity-curves. As we have pointed out earlier, the photometric observations on the two nights nearest to the epoch of minimum amplitude are rather uncertain. Thus the lower end of this curve is not well established. There is some indication that the relationship is nonlinear, but this depends rather heavily upon the observation of August 16. However, it seems fairly certain that the light- and velocity-amplitudes do not go to zero together. We shall return to this point in a moment.

Except for the deviation of the curve for light-variations less than 0.05 mag., our observations agree very closely with the amplitude-curve published by Hellerich,[7] which combined data from all the known class members for which observations were available.

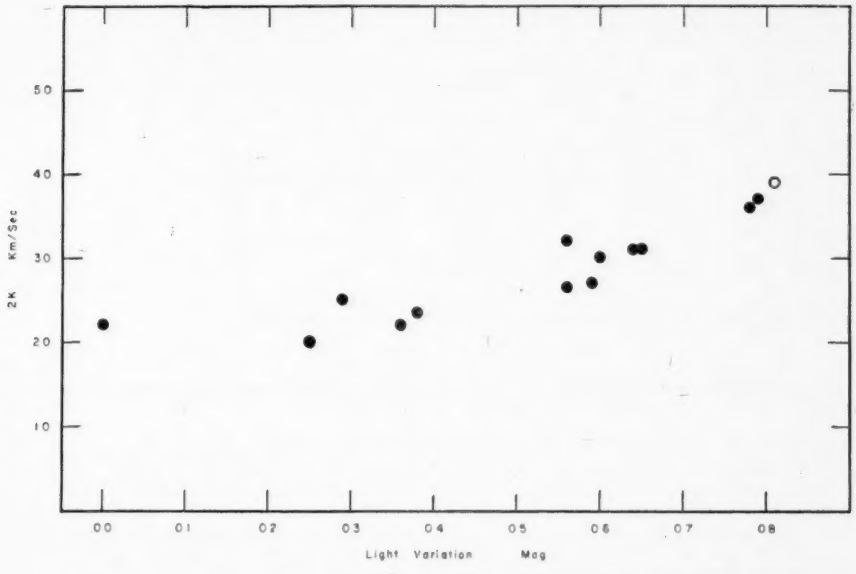

FIG. 7.—Relationship between the amplitudes of the light- and velocity-curves. The circle represents the 1950 observation.

The combined observations show that, as in ν Eridani[8] and 12 Lacertae,[9] the light- and velocity-variations are nearly "in phase." That is, the light-maximum occurs very nearly at the time when the velocity-curve crosses the gamma axis in going from positive to negative values, or at the time of maximum contraction on the pulsation hypothesis. Similarly, minimum light occurs at the time of maximum dilation of the star. Table 3 lists for each date the time difference between maximum and minimum light and the time of gamma velocity. Figure 8 shows that the phase relationship oscillates about the zero phase in the 17-day period. This also probably results from the difference in the size of the periodic shifts of the light- and velocity-curves discussed above.

If this is so, then obviously the amplitude of the phase-relationship-curve should be

[7] *A.N.*, **269**, 258, 1939.

[8] M. F. Walker, *Pub. A.S.P.*, **63**, 176, 1951.

[9] W. H. Christie, *Pub. Dom. Ap. Obs. Victoria*, Vol. **4**, No. 5, 1927.

the difference between the amplitudes of the curves of the phase shifts of the light- and velocity-maxima. As we have mentioned earlier, the amplitude of the curve of residuals of maximum velocity was found by Struve to be about 0.008 day. Comparing this with Figures 6 and 8, we see that within the observational error this does, in fact, appear to be the case. Thus the shape of the beat-curves and the size and shape of the various residual curves for both light and velocity can be interpreted as the combination of two harmonic oscillations having a ratio of velocity-amplitudes of about 3 to 1 and a ratio of light-amplitudes near unity.

Having available simultaneous light- and velocity-observations, it would be desirable

TABLE 3

PHASE RELATIONSHIP BETWEEN LIGHT AND VELOCITY

JD 2433+	ΔT* (Day)		Phase (P=17.20 Days)	JD 2433+	ΔT* (Day)		Phase (P=17.20 Days)
	1	2			1	2	
870.89	+0.003	+0.004	0.000	889.87	−0.008†	+0.017	0.103
71.91	+ .016	+ .003	.059	97.84	− .010	− .015	.567
72.88	+ .002	.000	.116	904.81	+ .006	+ .003	.972
73.88	− .001	− .020†	.174	10.76	+ .029	− .008	.318
74.80			.227	17.77	− .005	− .008	.726
75.82			.287	25.84	−0.001	+0.004	0.195
83.85	−0.003	−0.005	0.753				

* 1 = Maximum light *minus* gamma velocity; 2 = minimum light *minus* gamma velocity.
† Low weight.

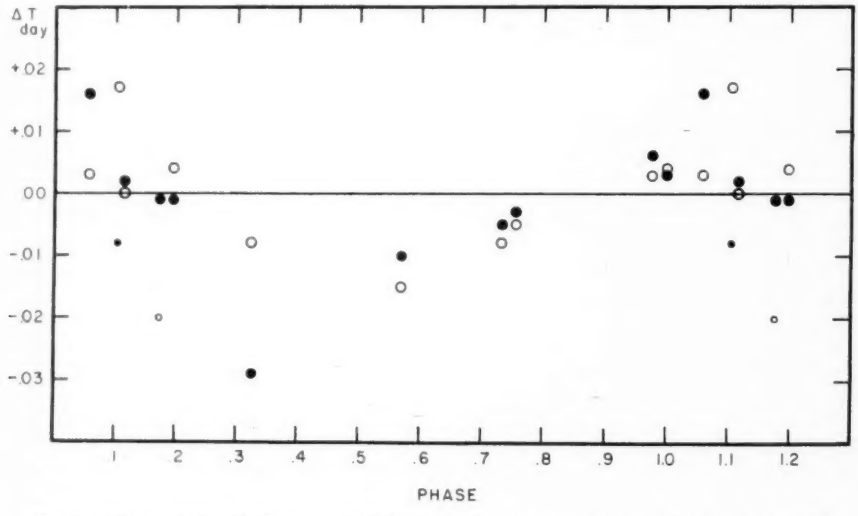

FIG. 8.—Phase relationship between the light- and velocity-curves. The ordinate is the time difference, maximum or minimum light *minus* gamma velocity. Dots refer to light-maxima, circles to light-minima. Small symbols indicate observations of lower weight. The phases are counted from zero phase = JD 2433870.89 + 17.20E days.

to employ them to ascertain whether or not the star is pulsating. The hypothesis of pulsation is particularly attractive in this case, since the light- and velocity-observations are in phase. A summary of the several semi-empirical tests which have been proposed has been given by S. Rosseland.[10] The basic idea involved in these tests is to separate out of the light-curve of the star the effect resulting from a change in temperature by making use of the change in the color index. The remaining light-variation is then assumed to be caused by the change in surface area produced by the pulsation. The change in radius computed from this light-variation should then agree with that computed from the velocity-curve.

Unfortunately, there is, as we have seen, no definitely established variation in the color of 16 Lacertae. Either the light- and velocity-variations have no accompanying change in temperature, or, more probably, the effect is too small to be detected. Struve,[11] on the basis of coudé spectra taken with the 100-inch reflector at Mount Wilson, believes that the spectral class of 16 Lacertae changes not more than one subdivision during the 4-hour period. Since the spectral class is B2, the temperature change must be less than about 1000° K. If we assume that the star radiates like a black body with a temperature of 20,000° K, then for the cell and filter system used in this investigation a change of

TABLE 4

VARIATION IN RADIUS AND TEMPERATURE OF 16 LACERTAE

DATE 1951	MAXIMUM			OBSERVED LIGHT-VARIATION (MAG.)	REQUIRED	
	ΔR (Km)	$\Delta R/R$ (Per Cent)	Δm_T (Mag.)		Δm_T (Mag.)	ΔT (° K)
Aug. 16	8.0×10^4	1.5	0.031	0.000	0.031	246
Sept. 28	13.0×10^4	2.4	0.052	0.079	0.131	1040

1000° will cause a change in blue magnitude of 0.126 mag. and a color change of 0.004 mag. It is thus obvious that, for a hot star such as this, the ordinary yellow-blue color system is too insensitive to variations in temperature. It may be possible to detect these small temperature effects by using an infrared to ultraviolet color base line. Until such observations can be carried out and the effect of temperature changes allowed for, it seems hopeless to attempt to apply the pulsation tests properly.

We can, however, see that the observations might be explained on this basis. The contributions to the light-curve from the change in the surface area and in the temperature will be out of phase by 180°. Thus, if the range of temperature variation changed properly with the changing amplitude of pulsation, one could have the observed case of the light-amplitude going to zero, or nearly to zero, while there remained an appreciable variation in radial velocity. Let us consider the two extreme cases: the observations of August 16, which show the smallest light- and velocity-amplitudes, and those of September 28, which show the largest amplitudes. The data in Table 4 have been computed in the following manner. On the assumption that the coefficient of limb darkening is 0.54,[12] the velocity-curves were integrated to give the maximum change in radius on each date, using the formula[10]

$$\Delta R = p\Delta D ,$$

[10] *The Pulsation Theory of Variable Stars* (Oxford: Clarendon Press, 1949), chap. ix.

[11] Private communication.

[12] H. N. Russell, *Centennial Symposia* (Cambridge, Mass.: Harvard College Observatory, 1948), p. 195.

where

$$p = \frac{6 - 2k}{4 - k};$$

k is the coefficient of limb darkening and ΔD is the displacement found by integrating the velocity-curves. Kopal and Treuenfels[13] have given the average radii of B- to K-type eclipsing binaries. From their data, the radius of 16 Lacertae has been assumed to be $R = 5.51 \times 10^6$ km. The light-variation resulting from the change in radius, Δm_r, was then calculated by the formula[10]

$$-\Delta m_r = 2.17 \frac{\Delta R}{R}.$$

The last two columns in Table 4 give the temperature change and the resulting variation in blue magnitude which would be required to produce the observed light-curves, assuming that the light-variation due to the change in surface area is given by Δm_r. It is evident that the percentage change in radius is not irreconcilable with the hypothesis of pulsation and that, as we have seen before, the temperature change required to produce the observed light-curves is consistent with the upper limits set by the spectroscopic observations.

Hellerich[7] has also applied a rather indirect test of pulsation in the β Canis Majoris stars. He finds that the relations between the amplitudes of the light- and velocity-curves which he derived for stars of the β Canis Majoris, RR Lyrae, RV Tauri, and cepheid classes reduce to the same curve if the various stellar temperatures are reduced to a standard temperature, and the effects of the temperature variations upon the light-curve are modified accordingly. From this he concludes that the same physical process is operating in all of these classes to produce the light- and velocity-variations. However, his analysis takes no account of the differences in the variations in the various classes, such as the degree of regularity or of the difference in the phase relationship between the light- and velocity-curves. Thus, while all of these stars may be undergoing pulsation of some sort, it seems likely that the details and perhaps the cause of the pulsation differ for each class.

So far there appears to be no evidence that the β Canis Majoris class includes any stars other than the very homogeneous group of early B stars. The F star δ Scuti, which is generally listed as a β Canis Majoris star, has a phase lag between the light- and velocity-curves similar to the cepheids.[14] Thus it would seem that a somewhat different physical process is operating in this star than in the B stars. No simultaneous observations have been made of the several short-period A stars which are sometimes listed as β Canis Majoris stars; it would be very worth while to study some of these stars in order to decide if they should be classed with the early B stars or with objects like δ Scuti.

It is a pleasure to thank Dr. C. D. Shane and the members of the staff of the Lick Observatory for making the facilities of the observatory available and for their interest in the observing program.

[13] *Harvard Circ.*, No. 457.

[14] E. A. Fath, *Lick Obs. Bull.*, **17**, 175, 1935; *Lick Obs. Bull.*, **18**, 77, 1937.

DWARF M STARS FOUND SPECTROPHOTOMETRICALLY
THIRD LIST

A. N. Vyssotsky and Betty Ann Mateer
Leander McCormick Observatory, University of Virginia
Received March 5, 1952

ABSTRACT

One hundred and thirty-three additional dwarf M stars are listed in Table 1. The 349 M dwarfs found at McCormick and published in the three lists include approximately 60 per cent of all dwarfs of type M0 and later between apparent magnitudes 8.5 and 9.9 in the northern sky. The percentage is smaller for the brighter and fainter magnitude ranges.

The list of M dwarfs presented in Table 1 is a continuation of two similar lists published previously.[1,2] The discovery procedure has already been described. These stars were all discovered prior to July 5, 1949; since that time, nearly 100 additional M dwarfs have been found on our plates which are not as yet included in our published lists because motions are not yet available for half of them. The third list is being published at this time because radial velocities for most of the stars are to be published soon by Dr. E. R. Dyer, Jr., from spectrograms taken at Mount Wilson Observatory.

The arrangement of Table 1 is similar to that of the second list.[2] As before, any star which has previously been included as a late dwarf in the published lists from Mount Wilson or McDonald Observatories is designated by boldface type in the first column. Wherever possible an effort has been made to improve on the relatively crude apparent magnitudes derived from the *Bonner Durchmusterung* by comparing the intensity of the spectrum with spectra of stars on the same plate whose magnitudes have been determined at McCormick, Bergedorf, Potsdam, or Harvard. This has been possible in about two-thirds of the cases.

Proper motions of sixty-four stars have been newly derived. The largest of these is that of No. 253, which exceeds one second of arc per year. In general, these were determined from a comparison of positions on a recent McCormick plate with positions given in the *Astrographic Catalogue*.[3] In a few cases when no AC positions were available, comparisons were made from pairs of McCormick plates separated by two- or three-year intervals. In two cases early positions have been measured on Harvard MC plates which Dr. Shapley kindly put at our disposal. We are also indebted to Director Haro of the Tonanzintla and Tacubaya Observatories for unpublished positions from the Tacubaya Astrographic Zones. Proper motions for two stars of the second list[2] not previously available are given in Table 2.

The spectral class of each star was assigned chiefly, but not exclusively, on the basis of the strength of the *TiO* bands; a secondary criterion frequently used was the contrast of the break at the G band. In eight cases the spectrum was noted as peculiar when these two criteria were contradictory; in these cases the break at the G band and the visibility of the individual lines in the interval between λ 4227 and λ 4310 indicated an earlier spectral class than did the *TiO* bands. With increasing experience, it becomes possible to include with confidence many more K8 stars and even a few classified as K5.

The estimated absolute magnitudes in the ninth column of Table 1 depend on four criteria which have been described in a previous paper.[4] Since the four criteria do not always agree, the estimated absolute magnitude is a compromise. Thus there is no one-to-

[1] *Ap. J.*, **97**, 381, 1943.
[2] *Ap. J.*, **104**, 234, 1946.
[3] *Pop. Astr.*, **54**, 499, 1946.
[4] *Ap. J.*, **104**, 239, 1946.

TABLE 1

DWARF M STARS

No.	BD or AC	1855.0 R.A.	1855.0 Decl.	m_v	μ_α''	μ_δ''	Sp.	M_v	π	Source of Proper Motion	Obs.
218	+41°19–173	0h25m2	+41° 12′	11 0	+0″.301	+0″.155	M0	7 8	+0″.058	McC–AC	H
219	−30 277	0 48 7	−30 28	9 3	+0 34	+ 14	K8	7:	.....	Luyten	V
220	−26 348	0 57 4	−26 23	10 0	−0 041	− 351	K8	7:	+ 039	Yale zone	V
221	+ 5 307	2 8 3	+ 5 56	9 0	−0 161	− 045	K8	7:	.....	E. B. Lex.	Ma
222	+ 4 2600–94	2 16 3	+ 4 11	10 0	−0 07	+ 04	M0	7 9	.....	McC–AC	Ma
223*	+ 7 385	2 19 8	+ 7 3	9 7	+0 092	− 179	K8	7:	.....	Toulouse	Ma
224*	+ 3 339	2 20 2	+ 3 46	8 6	+0 15	+ 21	M2	9 1	+ 070	Ci 18 319	Ma
225	−26 1207	3 8 5	−26 59	9 5	+0 252	+ 086	M0	7 9	+ 044	Yale zone	V
226	+53 2250–45	3 45 6	+53 9	10 5	+0 33	− 39	M0	8 2	+ 052	Ci 20 271	Ma
227*	+42 849	3 45 8	+42 57	10 0	−0 144	+ 032	M0	7 8	+ 020	Hls. ph. III 554	Ma
228	−15 728	4 2 8	−15 4	10 4	−0 078	+ 045	M0	8 3	.....	McC–AC	V
229	+47 977	4 10 9	+47 59	9 1	−0 030	+ 028	K8	7 5	+ 049	McC–AC	Ma
230	+26 10592	4 19 8	+25 54	10 7	+0 071	− 050	M0	8 8	.....	McC–AC	V
231*	+ 3 2328–36	4 24 8	+ 3 48	10 3	+0 033	− 167	M0	8 8	.....	McC–AC	Ma
232		4 48 6	+48 32	11 2	+0 096	− 337	M0	8 6	+ 020	McC–AC	Ma
233	+72 3130	5 49 9	+72 11	10 0	−0 042	+ 002	M0	7 9	.....	McC–AC	H
234	+67 1894	5 52 4	+67 59	9 0	−0 025	− 094	K8	7 5	.....	Green. Astr.	Ma
235*	+63 639	5 59 6	+63 26	9 0	+0 191	− 220	K8	7:	.....	McC–AC	Ma
236*	+10 1032	6 2 9	+10 23	10 3	+0 07	− 92	M5	12:	+ 101	Ci 20 375	Ma
237	+67 2080	6 14 5	+67 41	11 0	+0 034	− 080	M	7:	.....	Green. Astr.	Ma
238	+72 3338	6 27 3	+72 3	11 0	−0 111	− 544	M0	9 6	+ 040	Green. Astr.	H
239	+47 1355	6 40 7	+47 33	8 9	−0 244	− 721	K8	7 7	+ 075	E. B. Lex.	Ma
240*	+40 1758	6 46 5	+40 16	8 4	+0 13	− 41	K8	7 5	+ 032	Ci 18 837	Ma
241*	+16 222–203	6 52 9	+16 6	10 0	−0 018	− 007	K8	7:	+ 026	McC–AC	Ma
242*	+67 2334	6 53 0	+67 26	10 8	−0 259	− 077	M0	9 3	.....	Green. Astr.	Ma
243	+68 467	7 1 9	+68 41	9 7	+0 241	+ 030	K8	7 7	.....	Green. Astr.	Ma
244	+68 474	7 6 9	+68 31	9 7	+0 043	+ 134	K8	7 7	.....	Green. Astr.	Ma
245	+68 3124	7 16 9	+68 55	10 5	−0 178	− 121	M0	9 4	.....	Green. Astr.	V
246*	+36 1638	7 22 4	+36 32	10 4	−0 281	− 250	M2	10 2	+ 089	E. B. Lex.	Ma
247	+14 1684	7 22 9	+14 55	9 4	+0 057	− 294	K8	7:	.....	E. B. Lex.	V
248	+ 9 56–237	7 24 0	+ 9 6	10 2	−0 077	+ 073	K5	7:	.....	Toulouse	V
249	+33 213–242	7 53 9	+34 0	10 4	−0 150	+ 089	M0	7 9	+ 014	McC	Ma
250	+33 1646	7 59 7	+33 14	10 3	−0 048	− 192	M0	8 3	+ 033	McC	V
251	+33 1694	8 16 0	+33 6	9 6	0 00	− 64	K8	7 5	+ 036	Ci 20 473	V
252	+29 1754	8 18 4	+29 23	9 9	−0 234	+ 250	K8	7 7	.....	McC–AC	V
253	+36 28826	8 19 3	+35 31	10 8	−1 003	− 454	M0	10 2	.....	McC–AC	V
254	+67 552	8 23 2	+67 47	9 3	−1 073	+ 048	M0	9 8	+ 087	Green. Astr.	V
255*	+32 1769	8 29 5	+32 27	10 2	−0 078	− 102	K8	7:	.....	McC–AC	V
256*	+43 1844	8 30 8	+43 38	8 9	−0 170	− 297	K8	7:	.....	Hls. ph. II 1215	V
257	+10 1857	8 34 8	+10 6	9 6	+0 18	− 64	M2	9 4	+ 035	Ci 20 484	Ma
258	+35 1890	8 44 7	+35 47	8 9	−0 203	− 295	K8	7 9	.....	E. B. Lex.	Ma
259	+11 1940	8 46 9	+11 42	10 0	−0 14	− 05	K8	7 5	+ 038	McC–AC	Ma
260*	+12 1944	8 49 1	+12 12	11 0	−0 011	− 327	M5	11 8	.....	McC–AC	V
261	+21 1949	8 50 2	+21 6	9 1	+0 66	− 15	K8	7 5	+ 045	Ci 20 500	V
262	+ 2 2116	8 51 5	+ 2 25	10 6	−0 051	− 067	M0	8 5	.....	McC–AC	Ma
263*	+16 1877	8 52 1	+16 24	10 0	−0 126	+ 009	M0	8 7	.....	McC–AC	V
264*	+15 1957	8 53 3	+15 51	9 0	−0 096	− 313	M0p	8 8	+0 024	Ci 18 1066	Ma
265	+47 2368–79	9 1 8	+47 12	10 7	−0 38	− 02	M0	9 8	.....	McC–AC	V
266	+40 393–28	9 15 0	+40 41	10 2	−0 135	− 229	K8	7 9	.....	Hls. ph. I 83	Ma
267	+40 2208	9 18 3	+40 8	10 0	+0 143	− 139	K8	7 9	.....	E. B. Lex.	V
268	− 8 2689	9 21 7	− 8 38	10 8	+0 043	− 055	M0	9 4	.....	McC–AC	V
269*	+18 2213	9 22 7	+18 54	9 8	+0 185	− 290	K8	7:	.....	McC–AC	V
270	+23 2121	9 29 0	+23 21	9 2	−0 13	− 17	K8	7 7	.....	McC–AC	H
271	+23 2124	9 29 7	+23 10	9 8	−0 080	− 097	K8	7 7	.....	McC–AC	H
272	− 9 2895	9 32 2	− 9 33	9 2	+0 05	− 05	K5	7:	.....	McC–AC	V
273	+45 1791	9 53 4	+45 16	8 8	−0 240	− 075	K8	7:	.....	Hls. ph. I 256	Ma
274	+12 2201	10 14 6	+12 54	10 5	−0 287	− 026	K8	7 7	.....	McC–AC	Ma
275	+ 1 2013–63	10 45 2	+ 1 15	10 5	−0 082	− 030	M0	9 1	.....	McC–AC	V
276*	− 1 2457	10 45 3	− 1 18	10 0	−0 24	− 75	K8	7 9	.....	Luyten	Ma
277*		10 54 6	+17 18	(11 3) (11 5)	+0 08	− 18	(M0 M0	(10 2 10 2)	.....	Luyten	V
278	+16 2216	11 0 8	+16 33	9 2	+0 19	− 36	M0p	8 3	.....	Ci 20 611	V
279	+19 2423	11 1 6	+19 50	10 5	+0 004	+ 052	K8	7 5	.....	McC–AC	V
280	+22 1613–38	11 2 1	+22 24	10 8	+0 073	+ 005	M0	8 7	.....	McC–AC	V
281	+19 2427	11 4 2	+19 48	10 5	−0 160	− 099	K8	7 9	.....	McC–AC	Ma
282	+34 2214	11 12 9	+34 25	10 1	+0 10	−0 27	K5	7:	.....	E. B. Lex.	Ma

TABLE 1—*Continued*

No.	BD or AC	1855 0 R.A.	1855 0 Decl.	m_p	μ_α^*	μ_δ^*	Sp.	M_v	π	Source of Proper Motion	Obs.
283*	+48°1958	11h29m4	+48°15′	9 6	+0°132	−0°038	M0	8 6		McC–AC	Ma
284	+ 5 2529	11 34 3	+ 5 57	9 7	+0 21	−0 48	K8	7 9		Ross 911	V
285	+31 2290	11 37 1	+31 47	8 9	−0 06	−0 38	K8	7 5		Ci 18 1450	Ma
286		11 40 2	+ 1 37	11 2	+0 621	+1 364	M5	11 4	+0″294	McC	V
287	+30 2201	11 46 5	+30 22	10 9	−0 08	−0 08	K8	7 7		McC–AC	Ma
288	+ 3 2569	11 47 3	+ 3 57	9 5	−0 17	+0 08	K8	7:		McC–AC	V
289	+10 2374	11 56 9	+10 0	9 6	−0 30	0 00	K5	7:		Wolf 1427	H
290	+ *0 1514–64*	12 0 9	+ 0 19	11 0	−0 96	−0 08	M2	10 2	+ 060	Ci 20 684	V
291	+59 1428	12 4 8	+59 44	10 0	+0 102	+0 012	M0	9 2		McC–AC	V
292*	+ 6 2573	12 8 6	+ 6 28	9 5	−0 289	−0 085	K8	7 9		G. C. 16745	V
293*	+ 1 2684	12 13 0	+ 1 23	10 0	+0 091	−0 022	M0	9 4		McC–AC	Ma
294	+ *13 1308–25*	12 16 5	+13 23	10 2	+0 065	−0 173	M2	9 4	+ 050	McC–AC	H
295	+ 8 2599	12 18 6	+ 8 53	10 2	−0 122	−0 091	M0	8 8		McC–AC	H
296		12 28 2	+34 53	10 3	−0 047	+0 024	M0	8 3		McC–Harvard	Ma
297	+32 2274	12 40 3	+32 0	9 7	+0 05	−0 22	M0p	8 8		E. B. Lex.	Ma
298	+36 2322	12 50 9	+36 1	10 7	−0 27	−0 19	M0	9 8		McC–AC	Ma
299	+35 2406	13 0 8	+35 10	9 6	−0 127	−0 005	K8	7 8		E. B. Lex.	V
300	+10 2540	13 13 6	+10 41	9 7	−0 24	−0 11	K8	7:		McC–AC	Ma
301*	+29 2405	13 16 8	+29 59	8 5	−0 476	+0 244	M0	9 8	+ 065	Ci 18 1730	V
302	+39 2643	13 18 7	+39 41	9 5	−0 08	−0 04	K8	7:		E. B. Lex.	Ma
303*	+48 2138	13 31 9	+48 52	9 7	−0 21	−0 12	M0p	8 8		E. B. Lex.	Ma
304	+36 2397	13 32 6	+36 42	10 3	+0 03	−0 08	K8	7 8		McC–AC	Ma
305*	+46 1889	13 33 4	+46 56	10 5	−0 04	+0 39	M2	11 1		E. B. Lex.	Ma
306	+39 2675	13 37 0	+39 59	9 0	+0 095	−0 097	K8	7 5		E. B. Lex.	Ma
307	+18 2776	13 38 1	+18 34	9 6	+0 43	−1 81	M0	9 1	+ 086	Ci 18 1784	Ma
308	+15 2620	13 38 4	+15 41	8 5	+1 781	−1 457	M2	11 1	+ 193	G. C. 18602	Ma
309	+ *22 2632*	13 40 8	+22 10	11 0	+0 089	−0 086	M0	9 4		McC–AC	Ma
310*	+16 2565	13 43 0	+16 7	9 6	−0 094	−0 327	K8	7:		E. B. Lex.	Ma
311*	+18 2811	13 53 9	+18 47	10 2	−0 10	+0 28	M0	8 1		E. B. Lex.	Ma
312	+30 2512	14 15 7	+30 19	8 6	−0 662	−0 314	M0p	8 8	+ 071	G. C. 19374	H
313	+34 2541	14 29 0	+34 23	9 3	−0 73	+0 22	K8	7 8	+ 049	Ci 18 1920	Ma
314	+45 2247	14 55 7	+45 58	9 2	+0 26	+0 34	M0	9 4	+ 068	Ci 18 1996	H
315*	+40 2881	15 19 4	+40 9	9 9	+0 07	+0 13	K8	7 5		McC–AC	H
316	+ *32 105–80*	15 36 9	+32 23	10 8	−0 090	−0 025	K8	7 9		McC–AC	Ma
317	+36 2641	15 39 5	+36 24	10 5	+0 04	−0 06	K5	7:		McC–AC	Ma
318	+11 2874	15 45 3	+11 20	9 1	−0 258	−0 240	M0	9 1	+ 038	McC–AC	Ma
319	+39 3048	16 44 5	+39 33	10 2	+0 091	−0 282	M0p	8 6	+ 015	McC–AC	Ma
320	+38 2847	16 45 9	+38 33	9 6	+0 046	+0 070	K8	7:	+ 028	E. B. Lex.	Ma
321*	+ 5 3409	17 23 3	+ 5 40	9 5	+0 038	−0 262	M			Yale zone	Ma
322	+68 946	17 37 3	+68 28	9 1	−0 375	−1 280	M5	13:	+ 203	Ci 18 2354	Ma
323	+71 850	17 38 6	+71 58	8 6	+0 101	−0 059	K8	7 5	+ 045	Green. Astr.	Ma
324	+ *4 2510–357*	17 48 2	+ 3 49	10 0	−0 091	+0 045	M0	8 6		McC–AC	Ma
325	+10 3665	18 41 6	+10 36	8 0	+0 115	−0 449	K8	7 5	+ 056	Ci 18 2462	Ma
326	+ *9 148–85*	19 36 5	+ 9 46	9 6	+0 189	+0 099	M0	7 9		McC–AC	V
327*	−12 5594	19 49 3	−12 56	9 2	−0 079	−0 505	M0	8 1	+ 055	Yale zone	Ma
328	+ 6 4450	20 1 2	+ 6 16	10 0	+0 164	+0 181	K8	7 5		McC–AC	Ma
329	−14 5652	20 1 5	−14 42	9 ½	+0 110	−0 050	K8	7:	+ 048	Yale zone	Ma
330	−20 5833	20 1 9	−20 54	9 2	−0 438	−0 366	M0p	8 1		Yale zone	Ma
331*	+30 4155	20 37 9	+30 47	10 0	+0 015	0 000	K8	7 9		McC–AC	Ma
332	− 5 5480	21 1 2	− 5 1	9 4	−0 047	+0 005	K8	7 5		Yale zone	V
333	+24 4329	21 1 6	+24 36	9 8	−0 021	−0 160	K8	7:		McC–AC	Ma
334	−11 5581	21 14 3	−11 8	10 3	−0 036	−0 007	K8	7 8		McC–AC	V
335	+ 0 4810	21 54 8	+ 0 43	9 4	−0 48	−0 27	M0p	9 4	+ 102	Ci 20 1331	Ma
336	−21 6267	22 30 8	−21 22	9 3	+0 455	−0 067	M2	12:		Yale zone	V
337	−15 6290	22 45 5	−15 1	10 5	+0 96	−0 56	M5	13:	+ 206	Ross 780	V
338*	−12 6393	22 52 3	−12 9	10 8	+0 200	−0 057	M2	10 0		McC–Harvard	V
339	−23 17699	22 52 6	−23 18	7 6	−0 894	+0 039	M0	9 1	+ 125	Yale zone	V
340	−26 16420	22 52 6	−27 5	9 6	+0 112	−0 158	M0	8 8		McC–AC	V
341	−23 17748	22 59 3	−23 56	9 4	+0 161	−0 312	M0	8 3		Yale zone	V
342	−16 6218	23 0 7	−16 11	10 6	+0 054	+0 006	M0	9 4		McC–AC	V
343	+ *3 2781–116*	23 0 7	+ 2 32	10 8	+0 321	+0 282	M0	8 7		McC–AC	Ma
344	+ 4 4988	23 9 4	+ 4 54	10 2	+0 033	+0 021	M0	8 3		McC–AC	Ma
345	− 3 5691	23 34 8	− 3 22	10 5	−0 23	−0 28	M0	8 8		McC–AC	V
346	−20 6640	23 35 2	−20 41	9 9	−0 268	−0 270	K8	7:		McC–AC	V
347	+ *36 6443B*	23 38 5	+35 28	10 0	+0 333	+0 040	M0	8 5	+0 056	McC–AC	Ma
348	−22 6219	23 47 3	−22 36	10 6	−0 06	+0 16	M0	10 2		McC–AC	V
349*		23 49 7	−17 20	10 7	+0 37	+0 28	M0	9 1		Luyten	V
350	−17 6862	23 54 0	−17 45	10 7	+0 27	−0 19	M0	9 4		Luyten	V

[Note to Table 1 on following page]

NOTE TO TABLE 1

* In the next to the last column "Luyten" means *Pub. Minnesota Obs.*, Vol. **3**, No. 4; and "Toulouse" stands for *Ann. Obs. Toulouse*, Vol. **17**. In the last column "H" stands for K. G. Henize, a former graduate student of this observatory.

223. K5 on another plate.
224. ADS 1865, $d = 0''.6$, $\Delta m = 0.2$ mag.
227. ADS 2861, $d = 1''.6$, $\Delta m = 0.2$ mag.
231. Double (Alden, unpublished): $d = 2''.7$, $\Delta m = 1.0$ mag.
235. M0 on another plate.
236. M2 on another plate.
240. Mount Wilson gives spectra of two components as K5 and M1.5 and a combined spectrum as M0. Not in ADS.
241. K5 on another plate.
242. M2 on another plate.
246. Kuiper (*Ap. J.*, **95**, 201, 1942) lists Ross 989 as the faint companion to this star.
255. K5 on another plate.
256. K5 on another plate.
260. M2 on another plate.
263. Double, $d = 1''.6$, $\Delta m = 0.5$ mag. (Alden, unpublished).
264. ADS 7139, $d = 5''$, $\Delta m = 0.1$ mag.
269. K5 on another plate.
276. M0 on another plate.
277. L 1258–39 and L 1258–40: $d = 19''$, $\Delta m = 0.1$ mag.; common proper motion.
283. ADS 8242, $d = 2''.2$, $\Delta m = 0.2$ mag.
292. ADS 8486, $d = 2''$, $\Delta m = 1.5$ mag.
293. M2 on another plate.
301. The spectrum is composite: Mount Wilson observers give M0 for the brighter and K6 for the fainter components. ADS 8887, $d = 0''.7$, $\Delta m = 0.2$ mag.
303. ADS 8980, $d = 2''.8$, $\Delta m = 0.2$ mag.*
305. M0 on another plate.
310. K5 on another plate.
311. K8 on another plate.
315. K5 on another plate.
321. Spectrum overlaps with that of an A star. Dyer (unpublished) gives for the spectral class M1.
327. K8 on another plate.
331. Double: $d = 4''.4$, $\Delta m = 3$ mag. This star probably is Espin 366 = ADS 14230, although Espin originally identified it as BD+30°4159; the latter appears as a single star on our plates.
338. M0 on another plate.
349. According to Luyten, a 15th-magnitude companion at 31" shares the motion of this star.

TABLE 2

STARS FROM THE SECOND LIST

Star No.	μ_α	μ_δ	Source
90*	+0".392	−0".098	McC
135	−0.259	+0.256	McC

* Star No. 90 is a physical double (Alden, unpublished): $d = 15''.4$, $\Delta m = 2$ mag.

one correspondence between spectral subclass and estimated absolute magnitude. This may or may not indicate a real dispersion in absolute magnitudes across the sequence. Absolute magnitudes brighter than 7.5 and fainter than 12 are extrapolated values.

We are indebted to Miss Louise F. Jenkins for twenty-eight of the parallaxes in the tenth column; these have been taken from the forthcoming third edition of the *Parallax Catalogue* of the Yale Observatory. Fifteen additional parallaxes have been kindly supplied in advance of publication by Director H. L. Alden of this observatory. He has also furnished the data on double stars found by him on the parallax plates; these appear in the notes to the tables.

As regards the selectivity of the McCormick discoveries, Table 3 presents an array including all stars of the three lists. In this, the fainter components of double stars have been omitted and also star No. 69, which is not a dwarf.[2] It appears that the optimum range of apparent visual magnitude for the discovery of M dwarfs on McCormick plates is between 8.5 and 9.9. It is evident that we must have missed relatively more stars in

the brighter and fainter ranges. Moreover, the relative number of K8 stars is undoubtedly considerably greater than those we have been able to recognize with certainty. As stated above, most of these K8 stars are contained in the third list, only twenty having been discovered previously. Also it appears to be relatively more difficult to recognize the K8 stars in the fainter-magnitude ranges.

TABLE 3

COUNTS OF MCCORMICK DWARFS BY APPARENT MAGNITUDE AND SPECTRAL CLASS

m_v	K5	K8	M0	M2	M5	M	Total
7.5– 7.9	.....	.....	1	1	.....	.....	2
8.0– 8.4	.....	2	2	1	.....	.....	5
8.5– 8.9	.....	6	8	10	.....	.....	24
9.0– 9.4	1	18	24	9	1	.....	53
9.5– 9.9	1	26	36	17	.....	1	81
10.0–10.4	2	14	60	20	2	2	100
10.5–10.9	1	8	44	9	1	5	68
11.0–11.4	.....	.....	10	1	2	2	15
11.5–11.9	.....	.....	.....	.....	.....	1	1
Total	5	74	185	68	6	11	349

It appears that our three lists contain about 60 per cent of all the dwarfs of types M0 and later between apparent magnitudes 8.5 and 9.9 north of the equator. This estimate comes from a comparison of the McCormick lists with the two Mount Wilson lists in *Contributions*, Nos. 511 and 726. In the brighter and fainter magnitude ranges the percentage is smaller.

THE SPECTRA OF THE BRIGHT STARS OF TYPES F5–K5

NANCY G. ROMAN
Yerkes Observatory
Received March 1, 1952

ABSTRACT

Spectral types and luminosity classes have been obtained for 641 stars in the spectral range F5–K5 brighter than 5.50 visual magnitude and north of declination −20°. These types show the well-known absence of subgiants later than K1 and, in addition, show that the stars near zero absolute magnitude become plentiful extremely abruptly between G5 and G8. In the range G0–G5 we have 4 giants; at G8 we have 67. Color-magnitude diagrams show that this change occurs in a very small range of temperature.

New calibrations of the absolute magnitudes are made for all spectral types and luminosity classes which contain enough stars to yield significant results. For the most part these agree well with older determinations. A surprising result is that the K0 III–K2 III stars are about 0.8 mag. fainter, on the average, than the giants at G8 and in the classes K3–K5. That this is not merely a systematic effect in the classification is shown by the fact that the mean absolute magnitudes for all stars of luminosity classes II–IV show the same phenomenon.

Space velocities corrected for the solar motion have been computed for each star fainter than luminosity class II. In the spectral range G8–K1 it is found that spectroscopic differences exist among stars of the same spectral type and luminosity class. If these stars are separated spectroscopically, it is found that the velocity distributions within the different groups are also different. The two groups which contain 85 per cent of the stars are about equally numerous. They are separated by the fact that the G band and λ 4226 of *Ca* I are stronger relative to the remainder of the spectrum in one group than they are in the other. The velocity distributions indicate that the group with the stronger G band and λ 4226 is dynamically related to the group of weak-line stars in the earlier types and that the other group is dynamically related to the strong-line stars. In addition, two other groups exist which are characterized by peculiarities in the cyanogen absorption. One of these has fairly strong cyanogen which is characterized by a peculiar appearance of the region near λ 4150 and by a strengthening of the absorption in this region compared to that near λ 4120. Dynamically, these stars cannot be distinguished from the weak-line group. The fourth group is characterized by unusually weak cyanogen absorption. As has been known for some time, these stars are the "high-velocity" stars. Although some members of this group have fairly low velocities and some members of the weak-line group have fairly high ones, the mean velocities of the stars with weak *CN* is 95 km/sec, as compared to a mean of 41 km/sec for the weak-line group.

I. INTRODUCTION

As part of a program instigated some years ago by Dr. W. W. Morgan, covering all spectral types, spectra have been obtained of all nonvariable stars brighter than visual magnitude 5.50, north of declination −20°, and with Henry Draper spectral types in the range F0 to Ma. The revised types of 693 of these stars are in the interval F5–K5 inclusive. These spectra form an important collection of data for statistical studies of stars in this spectral range, both alone and combined with the large amount of additional data available for these stars. The majority have measured trigonometric parallaxes, all but a few binaries without orbits have published radial velocities, and all the stars have well-observed proper motions.

Of the 693 stars, 41 probably have composite spectra either because they are unresolved binaries or because they are visual binaries too close to separate on the slithead of the Yerkes 40-inch spectrograph. These have been omitted from this discussion. In addition, 11 of the stars do not appear to belong anywhere on the normal Hertzsprung-Russell diagram. These will be discussed individually in the notes to Table 4. For each of the remaining 641 stars a spectral type, luminosity class, spectroscopic parallax and absolute magnitude, and, except for the supergiants, a space velocity have been determined. In addition, new calibrations have been made of the absolute magnitudes in many parts of the spectral type–luminosity class diagram, and the distributions of the stellar speeds have been discussed.

II. SPECTRAL TYPES

Each of the stars has been classified on the system of the Yerkes spectral atlas,[1] except that two minor changes in that system have been suggested recently by Dr. Morgan.[2] The stars of types F5–F8, such as β Del and υ Peg, which were previously assigned to luminosity class III, have now been assigned to luminosity class IV, and the former class IV stars, such as α CMi, have been included in class IV–V. The reason for this change is the fact that spectra of the stars of the older class III resemble the stars of class V more closely than those of class I*b*. The class III stars of types G2–K1 have been reclassified using new criteria and a system of types for the standard stars which provides a better correlation of spectral type with color. Dr. Morgan prepared a new list of standards for the types G8–K1 about a year and a half ago, basing his classification primarily on the appearance of the G-band region and, to a lesser extent, on the strength of λ 4226 of *Ca* I. For reasons mentioned below, the present author has also considered the strength of the hydrogen lines as an indicator of spectral type at G8 and K0 after the luminosity class of the star has been accurately determined. The use of this additional criterion does not change the spectral type assigned to any of the standard stars, nor does it lessen the correlation of spectral type with color.

Figure 1 illustrates the correlation between the Henry Draper and the revised spectral types. On the average, the agreement is good. The most notable features are the concentration of the HD G5 stars at G8 on the present system, the widespread and almost uniform distribution of the HD type K0 stars over the revised range G8–K3, and the sparing use of the types F8 and K2 in the *Henry Draper Catalogue*. Also, the mean revised type for the stars which were classified K2 in this catalogue is almost as late as K4. As mentioned in the preceding paragraph, the colors confirm the revised type G8 for most of the HD G5 stars. The mean color for the G8 giants is very nearly four-fifths of the way from that of the G0 giant to that of the K0 giants, and a smooth progression in color from class V to class II is preserved for each spectral type on the revised system. The relative scarcity of K1 stars in the revised types is probably a systematic effect in the present classifications, since the decision to use this type was not made until after the preliminary classifications were finished. However, the accuracy possible in the classification seems to warrant the use of this type.

Figure 2 shows the number of stars in each region of the spectral type–luminosity class array as well as the divisions in luminosity used at each spectral type. Two supergiants have been omitted, HR 8752 at G0 I*a* and ψ^1 Aur at K5 I*ab*. The supergiants are distributed uniformly in spectral type, and the low-luminosity stars show their expected behavior. The latter are plentiful at F5 and gradually diminish in number toward later spectral types and, hence, toward lower absolute magnitudes. This behavior is due to the selection effect introduced by the bright limiting apparent magnitude. However, other features of the diagram cannot be explained this easily. The most striking of these is the very sudden onset of giants at G8. Even on the older system the onset was fairly sudden at G5 but the new classifications have sharpened the boundary appreciably. Between G0 and G5 we have 4 stars in luminosity class III (i.e., as we shall see later, with absolute magnitudes near 0.0 mag.), while at G8 we have 67. The strong concentration of giants persists to later spectral types also, thinning out only gradually by K5. The stars in luminosity classes III–IV, II–III, and even II indicate the existence of the same phenomenon. An equally striking feature is the lack of stars fainter than the class III stars and later than K1. This cannot be due solely to selection effect, since the absolute magnitudes of these stars would be no greater than those of the F dwarfs and certainly not sufficiently lower

[1] Morgan, Keenan, and Kellman, *An Atlas of Stellar Spectra* (Chicago: University of Chicago Press, 1943).

[2] Private communication.

than the absolute magnitudes of the stars of the same luminosity class at G8 to account for their complete disappearance at K2.

III. ABSOLUTE MAGNITUDES

The existence of good proper motions and trigonometric parallaxes for the stars brighter than 5.5 mag. makes these stars useful for calibrating the luminosity classes in terms of absolute magnitude. For this reason new values of the mean absolute magni-

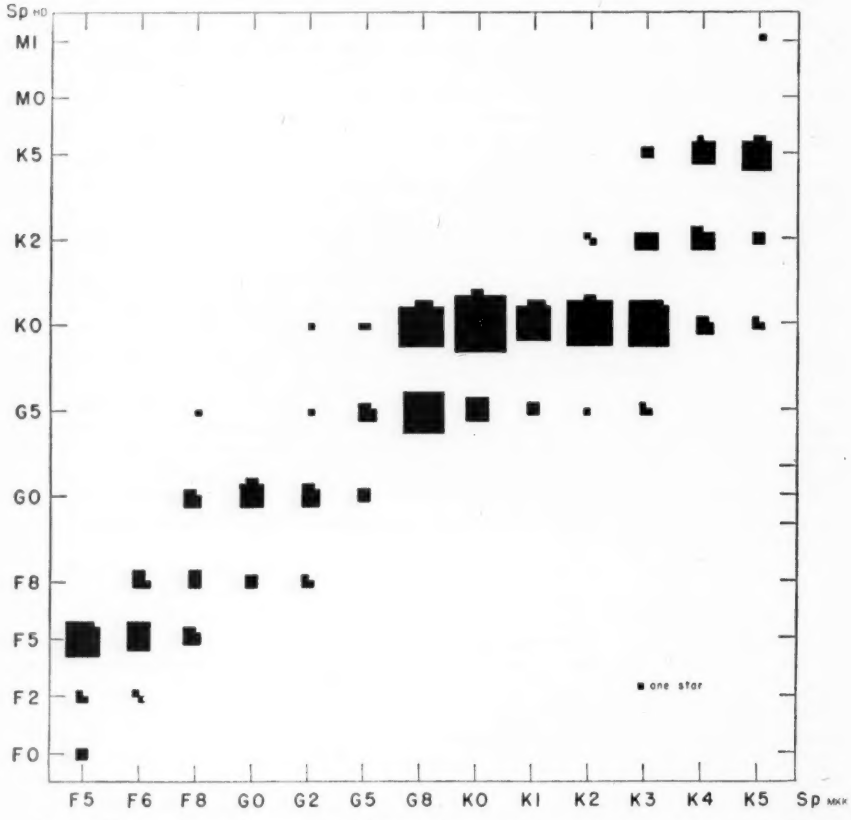

FIG. 1.—The correlations between the HD spectral type and the types on the system of the Yerkes spectral atlas. The area of each block represents the number of stars at that point on the diagram.

tudes have been determined for those classes which contain a sufficient number of stars brighter than this limit to make the new calibration useful.

For stars with appreciable trigonometric parallaxes, i.e., for stars in luminosity classes with mean absolute magnitudes fainter than -0.5 mag., the mean trigonometric parallax was computed for each group. For each star with more than one determination of its trigonometric parallax, individual values from Allegheny, Cape, Greenwich, McCormick, and Yale Observatories were averaged with equal weight, unless the probable

errors of the individual determinations differed considerably. These values were taken from the back of the *General Catalogue of Stellar Parallaxes* (Yale, 1935). The resulting value was then reduced to the parallax which the star would have if it had the apparent magnitude 5.00 instead of its actual apparent magnitude. Negative parallaxes were divided by the same factor by which they would have had to be multiplied if they had been positive. These values were then averaged, weighting the value for each star according to the number of independent determinations. Although the parallaxes of most of the stars are too small to be of any use individually, the agreement among the reduced parallaxes is surprisingly good. If anything, the mean errors given in Table 1, which

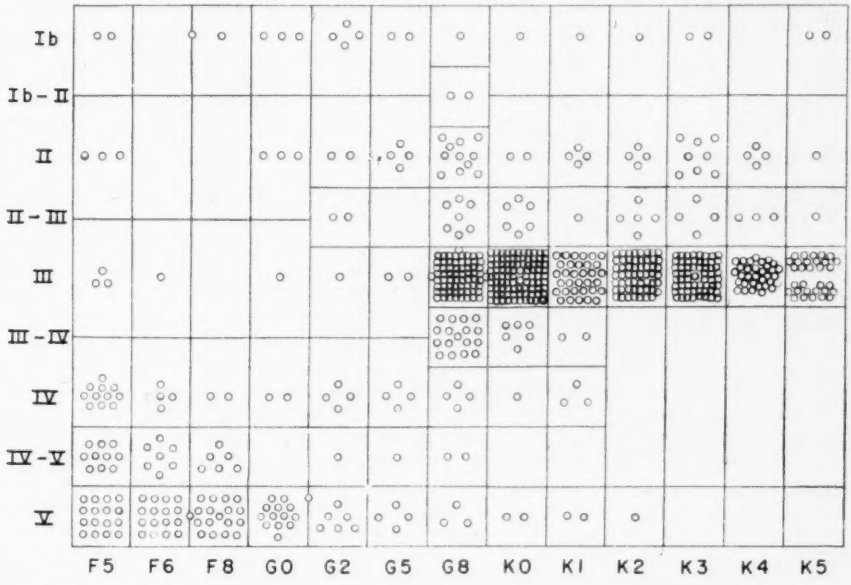

FIG. 2.—The spectral type–luminosity class array for the bright northern stars. Each circle represents one star. The lines indicate the number of types usually distinguished. Circles centered on a line indicate stars with in-between types.

have been computed on the assumption that one good determination of a trignonometric parallax has a mean error of 0".010, is overestimated. After this work had been completed, Dr. Strömgren pointed out[3] that it would be preferable to use the observed parallaxes directly. If an estimate is made of the mean absolute magnitude of a group of stars and is used to compute spectroscopic parallaxes, then a comparison of the mean unreduced trigonometric and the mean spectroscopic parallaxes will indicate the correction which must be applied to the assumed absolute magnitude. For three groups in different parts of the spectral type–luminosity diagram, this method was used. The results agreed with the first results within the mean errors of the determinations.

For groups with mean absolute magnitudes brighter than +3.0 the mean parallax was also computed from the proper motions. The observed motion for each star was also reduced to the value it would have if the star were actually of apparent magnitude 5.00. The sky north of declination −20° was divided into nine regions of approximately equal

[3] Private conversation.

TABLE 1

MEAN PARALLAXES

Spectral Type	Method	Number of Stars	π ($m=5.00$)	$10+5\log\bar{\pi}$	Adopted $\bar{M}$
F5 IV–F8 IV	π_{tr}	14	$0''.0227 \pm 0''.0018$ m.e.	$+1.8 \pm 0.2$ m.e.	+1.9
F5 IV–F8 IV	μ	19	.0287 .0032	+2.3 .2	
F5 IV–V—G2 IV–V	μ	26	.0357 .0025	+2.8 .2	
F5 IV–V—F6 IV–V	π_{tr}	15	.0390 .0020	+3.0 .1	+2.8
F8 IV–V; G0 IV–G2 IV	π_{tr}	9	.0421 .0023	+3.1 .1	+2.9*
F5 V	π_{tr}	13	.0463 .0020	+3.3 .1	+3.3
F6 V	π_{tr}	15	.0554 .0021	+3.7 .1	+3.6
F8 V	π_{tr}	17	.0546 .0016	+3.7 .1	+3.9
G0 V–G2 V	π_{tr}	19	.0786 .0016	+4.5 .0	+4.4*
G5 II–K5 II	μ	34	.0032 .0005	−2.5 .3	−2.6
G8, K0 II–III	μ	9	.0069 .0015	−0.8 .5	−0.9*
K1 II–III—K5 II–III	μ	14	.0066 .0018	−0.8 .6	−0.9*
G8 III	μ	65	.0088 .0010	−0.2 .2	0.0
G8 III	$\bar{v}$	65	.0057 .003:	−1.1	
G8 III	π_{tr}	49	.0114 .0012	+0.3 .2	
K0 III	μ	86	.0162 .0014	+1.0 .2	+0.7
K0 III	π_{tr}	71	.0136 .0010	+0.7 .2	
K1 III	μ	32	.0148 .0009	+0.9 .1	+0.8
K1 III	π_{tr}	22	.0155 .0017	+1.0 .2	
K2 III	μ	61	.0147 .0015	+0.8 .2	+0.9
K2 III	π_{tr}	46	.0166 .0012	+1.1 .2	
K3 III	μ	59	.0114 .0016	+0.3 .3	+0.1
K3 III	π_{tr}	42	.0106 .0012	+0.1 .2	
K4 III	μ	31	.0098 .0019	+0.0 .4	−0.1
K4 III	π_{tr}	25	.0106 .0015	+0.1 .3	
K5 III	μ	31	.0090 .0007	−0.2 .2	−0.2
K5 III	π_{tr}	26	.0095 .0016	−0.1 .4	
G5—K0 III–IV	μ	22	.0193 .0029	+1.4 .3	+1.3*
G5—K1 III–IV	π_{tr}	19	.0187 .0019	+1.4 .2	
G5—K0 IV	π_{tr}	6	.0526 .0044	+3.6 .2	+3.5*
K1 IV	π_{tr}	3	0.038 0.004	+2.9 0.2	+2.9

* Individual mean absolute magnitudes were adopted as shown below.

F8 IV–V	+3.0	G8 II–III	−1.0	K1 III–IV	+1.3
G0 IV	+2.6	K0 II–III—K2 II–III	−0.8	G5 IV	+3.2
G2 IV	+2.9	K3 II–III—K5 II–III	−1.0	G8 IV	+3.5
G0 V	+4.3	G8 III–IV	+1.3	K0 IV	+3.5
G2 V	+4.6	K0 III–IV	+1.4	K1 IV	+2.9

area, and the mean proper motion was determined in each region. These mean motions were then used to compute mean parallaxes according to the formulae given by Smart.[4] These formulae involve the assumptions that the two-stream picture of stellar motions is valid and that there are an equal number of stars in each stream. In addition, the amount of the solar motion and the stream constants are required for their application. A solar motion of 20 km/sec was adopted.[5] For the stream constants the values found by Smart and Tannahill[6] in their study of the Cape proper motions were used. These formulae have the advantage that they make use of the total proper motion rather than just one component of this motion. As the observational errors in the proper motions are relatively small, each star was given equal weight in the solution. The mean error of the results is computed from the agreement of the results from individual regions of the sky.

The results of the solutions for the mean parallaxes are given in Table 1. In this table, π denotes parallax; μ, the total proper motion; v, the component of the proper motion parallel to the solar motion; m, the visual apparent magnitude of a star; and M, the visual absolute magnitude of a star. It is evident that where the two methods of determining the mean parallax overlap the agreement between them is good. This table also gives the absolute magnitudes, found by assuming that all stars in each group have the same absolute magnitude, together with the approximate mean error of these values as indicated by the mean errors of the mean parallaxes. To obtain the true mean absolute magnitude, the correction $0.23\sigma_M^2$ must be applied where σ_M is the standard deviation of the absolute magnitudes of the stars in the group. It was estimated that this correction is about +0.1 mag., except for the dwarfs earlier than G0 for which the correction was ignored. This correction has been included in the adopted visual absolute magnitudes given in the final column of Table 1. A few values in this column, for the F stars and the class II–III stars in the range G8–K5, have been smoothed somewhat.

Figure 3 shows a plot of the adopted visual absolute magnitudes in this region of the H-R diagram. The points connected by dotted lines are from an article by Keenan and Morgan.[7] The remainder are from the new solutions. Of particular note is the sharp drop in absolute magnitude for the giants between G8 and K0, followed by the equally steep rise between K2 and K3. The results in Table 1 leave little doubt that this behavior is real. In addition, the second method of employing the trigonometric parallaxes mentioned above also supports the sharp drop between G8 and K0. Finally, at G8, an additional solution was made, using the upsilon components of the proper motion. This solution has decidedly less weight than that using the total proper motions, both because of the loss of one component of the motion and because of the varying weights in different parts of the sky and, hence, the low weight in some regions. However, it supports the high luminosity at G8 III. The point at K1 IV is uncertain, but it is definitely above the point for K0 IV.

Table 2 gives the mean absolute magnitude for each spectral type for all luminosity classes except class I and, for stars later than the sun, class V. The stars omitted are too few to have much real influence on the mean, but they lie far enough from the mean to cause spurious fluctuations from one spectral type to the next. Although these mean absolute magnitudes refer only to the stars in this study and may not be valid for other groups of stars, such as those in a particular galactic latitude or with fainter apparent magnitudes, they do illustrate the characteristics of this material. The mean absolute magnitudes for the stars earlier than G5 behave as one would expect. Among the later-type stars the same behavior can be noted as was found in the giants of these classes.

[4] *Stellar Dynamics* (Cambridge: At the University Press, 1938).

[5] Based on the results of Nordström, *Lund Medd.*, Ser. II, No. 79, 1936.

[6] *M.N.*, **100**, 30, 1939.

[7] *Astrophysics*, ed. J. A. Hynek (New York: McGraw-Hill Book Co., 1951).

Hence this behavior is not a product of the classification system. If we omit the dwarfs, the K0–K2 stars are definitely fainter as a group than are those stars either at G8 or later than K2.

The data shown in Figures 2 and 3 are combined in Figure 4, which illustrates a schematic color-magnitude diagram for the stars included in this study. The mean color for each spectral type and luminosity class was determined from the $B-V$ colors measured by H. L. Johnson.[8] The area of the color-magnitude diagram was then divided

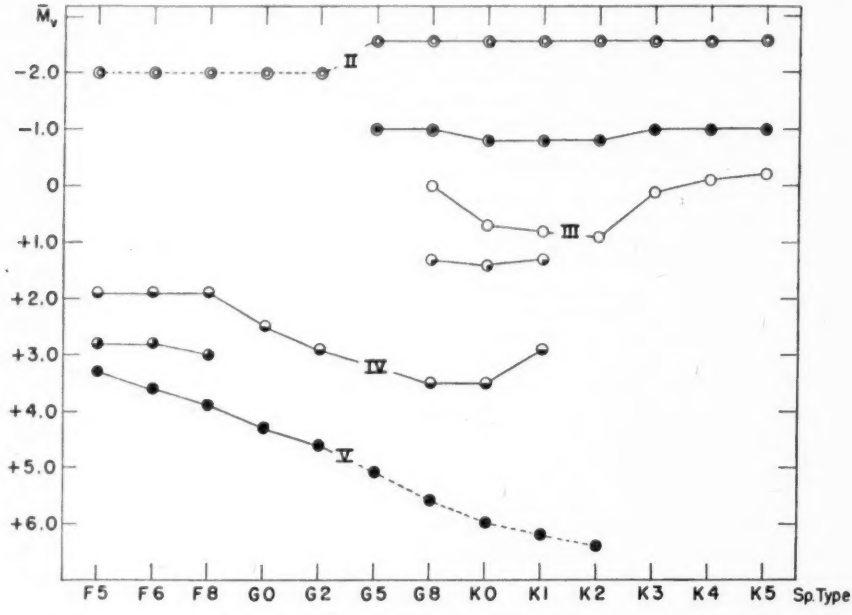

FIG. 3.—Mean absolute magnitudes for stars in the range F5–K5. Roman numerals indicate the main luminosity classes. The remaining lines are for luminosity classes II–III, III–IV, and IV–V. The dotted lines connect values given by Keenan and Morgan. The remaining points are based on new results.

TABLE 2

MEAN ABSOLUTE MAGNITUDES TO LIMITING MAGNITUDE 5.50 FOR MIXED LUMINOSITY CLASSES

Spectral Type	$\bar{M}$	Spectral Type	$\bar{M}$
Classes II–V:		*Classes II–IV:*	
F5	+2.2	G5	+0.7
F6	+3.0	G8	+0.1
F8	+3.5	K0	+0.6
G0	+3.2	K1	+0.6
G2	+2.1	K2	+0.5
		K3	−0.3
		K4	−0.4
		K5	−0.3

[8] *Ap. J.* (in press).

into cells, each centered on the mean $B-V$ and mean absolute magnitude, on the HRP system, for the stars in a given cell in the spectral type–luminosity class diagram and with the boundaries approximately midway between adjacent centers. In each of the cells constructed in this way, a circle was drawn for each star found to have the corresponding spectral type and luminosity class. Hence no circle on the diagram represents a particular star, but the result should be similar to that which we would obtain if we knew the color and absolute magnitude for each star individually. However, the width of the giant sequence for the late-type stars is indeterminate. Figure 4, again, shows the same features

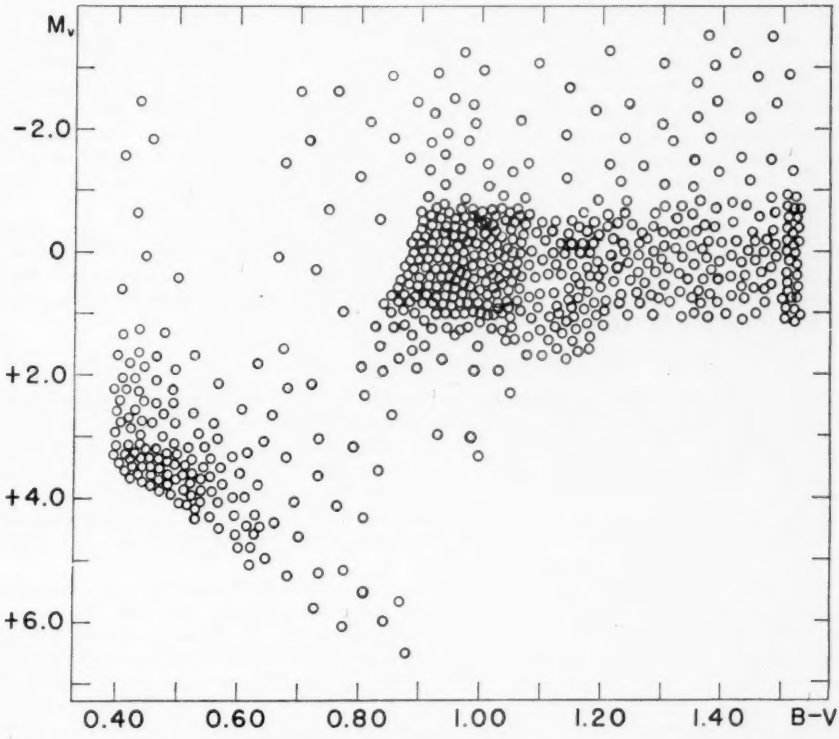

FIG. 4.—A schematic color-magnitude diagram for the bright northern stars. Each circle represents one star, but not a particular star.

as Figure 2. Stars with absolute magnitudes greater than +2.0 are entirely absent for colors greater than 1.4 mag., and stars with absolute magnitudes between −1.0 and +1.0 are scarce for colors between 0.45 and 0.82 mag. On this diagram the spectra merely form an intermediate step in obtaining the position of a given star. Hence the sharp onset for the late-type giants is probably real. If it is not real, then the giants are even more crowded at the color 0.85 or 0.86 mag., since the mean color of the stars cannot be changed appreciably.

The general features shown in Figure 4 are not new. In 1913 H. N. Russell made the statement: "It is further noteworthy that all the stars of classes K5 and M which appear on our diagram are either very bright or very faint. There are none comparable with the

Sun in brightness."[9] In 1922 H. D. Curtis[10] published an H-R diagram, based on all parallaxes available at the time and on the HD spectral types, which is surprisingly similar to the color-magnitude diagram shown in Figure 4. In the same year Hertzsprung[11] called attention to the fact that, if the quantity $m + 5 \log \mu$, where m is the apparent magnitude and μ is the total proper motion, is plotted against the reciprocal color temperature, then, for stars about 5 mag. brighter than the sun, there is a "marked gap" on the diagram between the red stars and the blue stars. Comparing his diagram with his table of the colors corresponding to each spectral type, we see that the gap is between stars of spectral type A5 and stars slightly later than G2 on the HD system. During the succeeding thirty years the edges of this gap have tended to become less well defined in the literature, and the red edge of the gap has progressed steadily toward the violet, until some modern authors have placed this edge near F5 or even earlier. Further evidence that the giants actually start abruptly near G8 is furnished in Figure 5, which shows two diagrams similar to Figure 4 but derived from independent sets of data. Figure 5*a* is a plot of the colors measured by Bottlinger[12] against the absolute magnitudes computed from the trigonometric parallaxes. Figure 5*b* is a plot of the infrared colors measured by J. S. Hall[13] against the absolute magnitudes which the stars would have if each had a tangential motion of 20 km/sec. That is, $P = m_v + 5 \log \mu + 1.87$. Both figures contain all the stars plotted in Figure 4 for which the necessary data are available, and the mean colors of G0 V and G8 III stars have been indicated on each. Since these diagrams are very similar to Figure 4, we may conclude that the Hertzsprung gap extends through G5 and has a very sharp boundary at a temperature between that of a G5 giant and a G8 giant.

IV. VELOCITY DISTRIBUTIONS

Nearly two years ago it was shown that among the late F- and early G-type stars two groups of stars could be distinguished in the same spectral type and luminosity class by small spectroscopic differences.[14] It was also shown that the members of these two groups, which occur in nearly equal numbers among the bright northern stars, have different velocity distributions. The stars in one of these groups have systematically weaker lines than those in the other group, and the two groups have been identified accordingly as the strong-line and the weak-line stars. β Vir is representative of the strong-line group, and ι Psc of the weak-line group.

In the course of classifying the remainder of the stars, it was found that spectroscopic differences also exist among stars of the same luminosity class and spectral type in the range G8–K1. Eighty-five per cent of these stars belong to one of two groups. In one of these, both the G band and *Ca* I 4226 are stronger than in stars of the same type in the other group. The two K0 III stars, HR 4126 and 2 Dra, are examples of the members of each group, and the differences between these stars are typical. Relative to the strength of *Fe* I 4045, λ 4226 is stronger in the spectrum of 2 Dra than it is in the spectrum of HR 4126. This alone might be explained if 2 Dra were later in type or lower in luminosity. However, the G band is also stronger in 2 Dra, and this would indicate an earlier type; the strength of the cyanogen and the ratio of λ 4077 to λ 4063 indicate that 2 Dra cannot be appreciably fainter than HR 4126. Figure 6 illustrates the velocity distributions for the stars in the two groups together with the velocity distributions

[9] *Pop. Astr.*, **22**, 275, 1914. The giant and dwarf sequences had been recognized by Hertzsprung nine years earlier, but Russell seems to have been the first to emphasize that there were no stars of intermediate absolute magnitude among the late K- and M-type stars, although such stars existed in earlier types.

[10] *Pub. A.S.P.*, **34**, 33, 1922.

[11] *Leiden Ann.*, **14**, Pt. 1, 1922.

[12] *Veröff. u. Sternw Berlin-Babelsberg*, Vol. **3**, No. 4, 1923.

[13] *Ap. J.* **79**, 145, 1934.

[14] N. G. Roman, *Ap. J.*, **112**, 554, 1950.

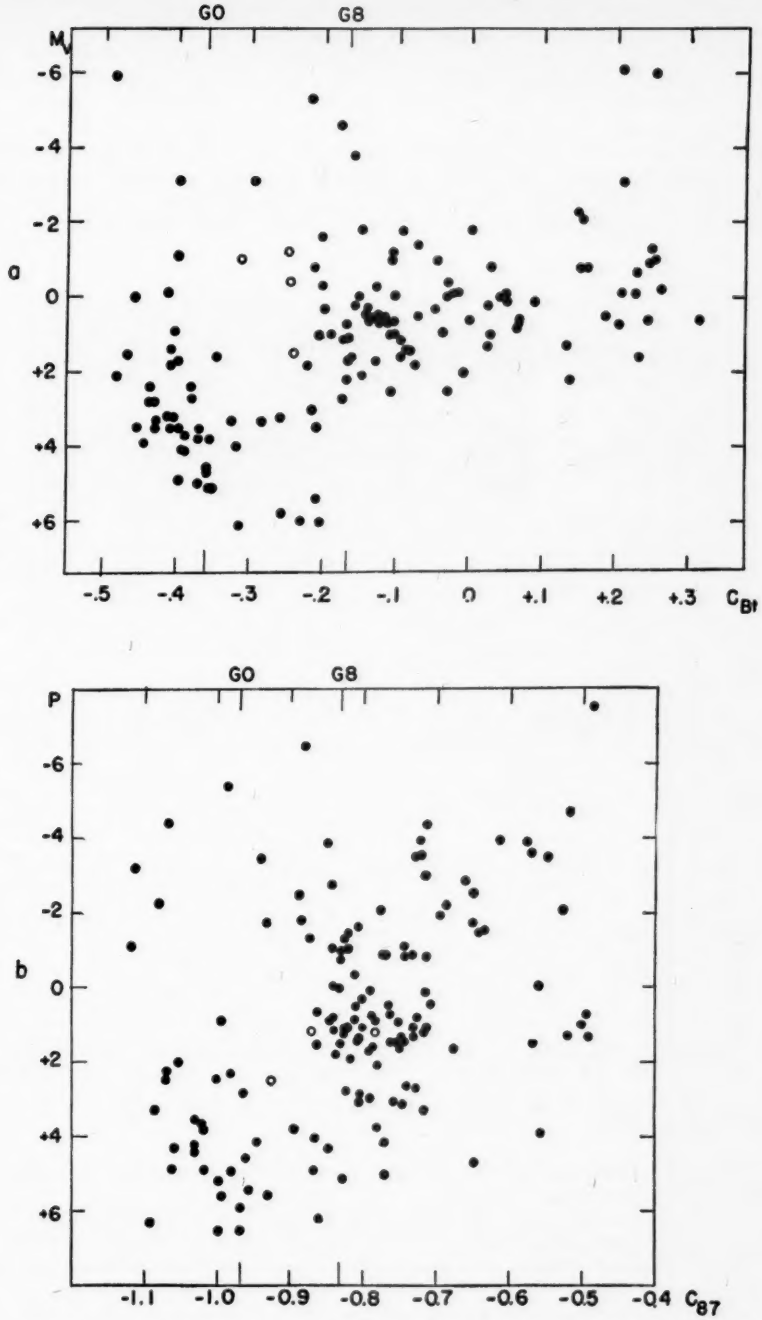

FIG. 5.—Color-magnitude diagrams for the bright northern stars: *a*, a plot of the visual absolute magnitudes determined from trigonometric parallaxes and the colors measured by Bottlinger; *b*, a plot of visual magnitudes determined from hypothetical parallaxes (i.e., the assumption that each star has a tangential velocity of 20 km/sec) and the colors measured by Hall.

for the strong- and weak-line groups in the earlier types for comparison. (Thirty-seven stars have been added to the diagrams shown in the earlier paper.) Table 3 contains, for each group, the number of stars, the mean velocity, and the standard deviation of the velocities. These show that one group of the late-type stars can be identified dynamically with the strong-line group in the earlier stars and the other with the weak-line group. For this reason, although the names are no longer descriptive, the group of stars resembling HR 4126, which appears similar dynamically to the strong-line stars of earlier type,

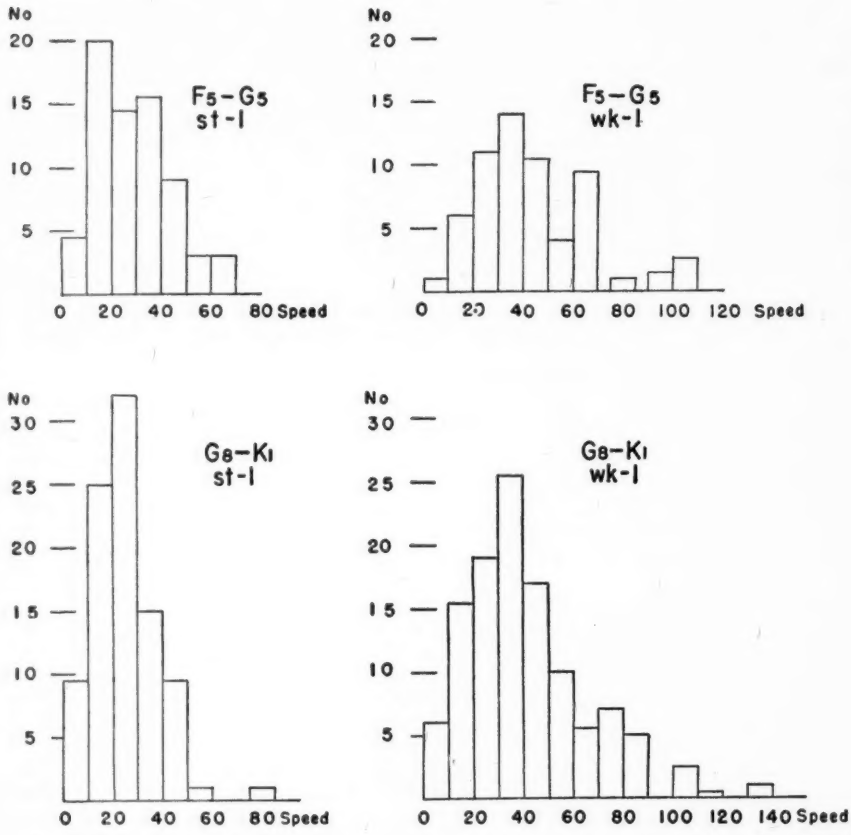

FIG. 6.—The frequency distributions of the speeds in the strong- and weak-line groups in the spectral ranges F5–G5 and G8–K1.

has been called the strong-line group and the group of stars resembling 2 Dra has been called the weak-line group.

The remaining 15 per cent of the stars of types G8–K1 appear to belong to neither of these groups spectroscopically but to one of the groups represented by the K0 III stars illustrated in Figure 7. Stars in these groups seem to share the characteristics of the weak-line group to the extent that the G band and λ 4226 tend to be strong compared with the remainder of the spectrum, but, in addition, the *CN* band is peculiar. In stars like

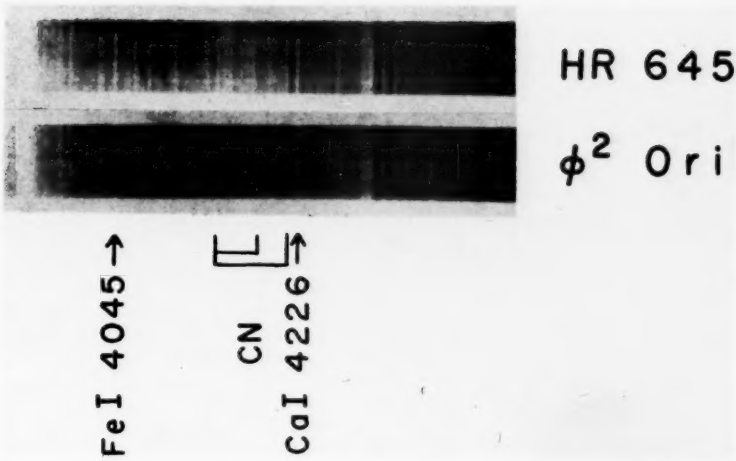

FIG. 7.—Two K0 III stars with peculiar *CN*. HR 645 belongs to the 4150 group. ϕ^2 Ori belongs to the group with weak *CN*. Both stars are high-velocity stars, and the two must be fairly similar in temperature and luminosity.

HR 645, not only is the absorption in the region between λ 4145 and λ 4175 stronger than in the region between λ 4175 and λ 4215, but also the appearance is different. Similar stars have been found on objective-prism plates at the Case Observatory by Dr. Nassau and his associates. They are recognized on low dispersion by the fact that the λ 4150 region of *CN* is too strong compared with the region more to the red. Hence they have been called "4150 stars." In addition, the entire *CN* band appears too strong for the strength of the hydrogen lines and of λ 4077. On the other hand, in stars like ϕ^2 Ori, the

TABLE 3

CHARACTERISTICS OF THE VELOCITY DISTRIBUTIONS

GROUP	NUMBER OF STARS	MEAN SPEED (KM/SEC)	STANDARD DEVIATION (KM/SEC)
	F5–G5 (except G2 and G5 III and IV)		
Strong-line	70	28.4± 1.7	14.5
Weak-line	61	42.7± 2.8	22.2
	G5–K1, II–III to IV		
Strong-line	91	24.7± 1.3	12.6
Weak-line	113	40.9± 2.3	24.1
4150	25	42.1± 8.3	41.6
Weak *CN*	12	95.6±13.7	47.4

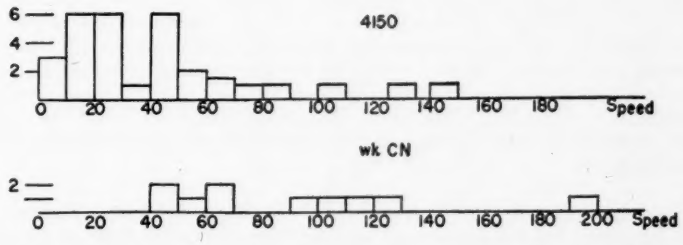

FIG. 8.—The frequency distributions of the speeds of the 4150 stars and of the stars with weak *CN*

CN is too weak for the strength of λ 4077 and for the luminosities indicated by trigonometric parallaxes.

Table 3 also gives the characteristics of the velocity distributions for these groups of stars, and Figure 8 illustrates these distributions. It is seen that the velocity distribution for the 4150 stars is similar to that for the weak-line stars, although spectroscopically they form a distinct group. The dispersion is higher, but for such a small number of stars this difference may not be significant. On the other hand, the stars with weak *CN* definitely form a separate group dynamically. The mean velocity is decidedly higher than that for the other groups, and the distribution of the velocities also appears differ-

ent, although it should be remembered that Figure 8 contains very few stars. This is definitely a high-velocity group of stars, and it has been recognized for some time both in globular clusters[15] and among the high-velocity stars.[1] More recently, both stars in globular clusters and the high-velocity stars have been recognized as objects belonging to Baade's population II, and the weak *CN* has been identified as a characteristic of this population.[16] It should be noted, however, not only that some members of this group have velocities lower than the 63 km/sec limit but also that stars in the weak-line and in the 4150 groups have velocities which are above this limit. For example, the velocity of HR 645 is 143 km/sec.

Spectroscopic differences exist also among stars later than K1. The 4150 stars seem to be fairly numerous at K2, and the stars with weak *CN* are also certainly present at this type (for example, α Boo).

Several lines of evidence support the above conclusions. The addition of 37 stars to the 98 previously discussed with spectral types in the range F5–G5 has had no appreciable effect on the velocity characteristics of the strong- and weak-line groups. Among the later-type stars, the velocity characteristics of each group show clearly in each spectral type separately. Hence the divisions are almost certainly real. Throughout the region of the H-R diagram included in this investigation, the mean reduced trigonometric parallaxes for the strong- and weak-line stars of the same spectroscopic absolute magnitude agree within their mean errors. In addition, in each group, the mean radial velocity agrees with the mean velocity from one component of the tangential motion in both the earlier and later spectral types. Thus the higher mean velocities for some groups cannot result from the use of values of the spectroscopic absolute magnitudes which are too high for these groups. The galactic concentration tells us nothing: all the stars seem to be fairly uniformly distributed in a direction perpendicular to the galactic plane up to the relatively small distances reached in this investigation.

Table 4 lists the stars brighter than 5.50 mag., north of declination $-20°$, with revised spectral types between F5 and K5, with the exception of variable stars, stars with composite spectra, and stars in three lists which have been published recently.[14, 17] The table includes the name or HR number of each star, its 1900 position, the visual apparent magnitude corrected for the light of the fainter component in close visual double stars and two-line spectroscopic binaries, the spectral type, the spectroscopic parallax and absolute magnitude, the group (strong-line, weak-line, 4150, or weak *CN*) to which the star belongs, and its space velocity corrected for the usual solar motion of 20 km/sec toward $\alpha = 18^h04^m$ and $\delta = +28°$. The abbreviations "st-l," "wk-l," and "wk CN" stand for "strong-line," "weak-line," and "weak *CN*," respectively; an "n" at the end of a line indicates a note on that star at the end of the table. The remaining symbols have their usual meanings.

I am indebted to Dr. W. W. Morgan not only for the use of a large number of plates but also for many helpful discussions and for lists of revised spectral types for the standard stars.

[15] B. Lindblad, *Ap. J.*, **55**, 85, 1922, and D. M. Popper, *Ap. J.*, **105**, 204, 1947.

[16] W. Baade, *Ap. J.*, **100**, 137, 1944, and Keenan, Morgan, and Münch, *A.J.*, **53**, 194, 1948.

[17] Morgan and Roman, *Ap. J.*, **112**, 362, 1950, and W. P. Bidelman, *Ap. J.*, **113**, 304, 1951.

Table 4

Spectroscopic Results

Name	α (1900)	δ	m	Spectral Type	M	Group	π sp	Speed (Km/Sec)
53 Psc	0h 0m.2	- 6°16'	4.68	K1 III	+0.8	4150	0".017	40
6 Cet	0 6.2	-16 1	5.05	F8 V	+3.6	wk-1	.051	32
HR 37	0 7.1	-18 30	5.47	K5 III	-0.2		.0073	26
ι Cet	0 14.3	- 9 25	5.75	K2 III	+0.9		.027	26
13 Cet	0 30.1	- 4 9	5.73	F8 V	+3.9	wk-1	.043	32
HR 152	0 51.3	+43 56	5.44	K5 III	-0.2		.0074	50
ε And	0 53.3	+28 46	4.52	G8 III	+0.0	wk CN	.0125	156
δ And	0 54.0	+30 19	3.49	K3 III*	+0.1		.021	18
α Cas	0 54.8	+55 59	2.47	K0 II-III	-0.8	st-1	.022	6
32 And	0 55.7	+38 55	5.42	G8 III	0.0	st-1	.0082	22
β Cet	0 58.8	-18 32	2.24	K0 III	+0.7	st-1	.049	15
φ' Cet	0 59.2	-11 9	4.93	K0 III	+0.7	st-1	.014	34
γ And	0 42.0	+23 45	4.30	K1 II	-2.6		.0042	
δ Psc	0 45.5	+ 7 2	4.55	K5 III	-0.2		.011	39
64 Psc	0 45.7	+16 24	5.23	F8 V	+3.9	st-1	.054	19
υ' Cas	0 49.1	+58 26	4.95	K2 III	+0.9		.0155	32
υ² Cas	0 50.7	+58 38	4.85	G8 III-IV	+1.3	wk-1	.020	56
φ² Cet	0 51.0	-11 49	5.49	K4 III	-0.1		.0076	42
η And	0 51.9	+22 53	4.62	G8 III-IV	+1.3	st-1	.022	24
HR 285	0 55.0	+65 43	4.52	K2 II-III	-0.8		.0086	54
ε Psc	0 57.9	+ 7 21	4.45	K0 III	+0.7	wk-1	.018	41
μ Cas	1 1.6	+54 26	5.26	G5 Vp*				n
η Cet	1 3.6	-10 43	3.60	K2 III	+0.9		.029	27
χ Psc	1 6.1	+20 30	4.89	K0 III	+0.7	st-1	.0145	17
τ Psc	1 6.2	+29 34	4.70	K0 III-IV	+1.4	st-1	.022	31
φ Psc	1 8.3	+24 3	4.64	K0 III	+0.7	st-1	.016	12
ξ And	1 16.5	+45 0	4.99	K0 III-IV	+1.4	st-1	.019	17
ψ Cas	1 18.9	+67 36	4.96	K0 III	+0.7	4150	.014	20
θ Cet	1 19.0	- 8 42	3.83	K0 III	+0.7	wk-1	.024	48
46 Cet	1 20.7	-15 7	5.19	K3 III	+0.1		.0095	31
49 And	1 24.1	+46 30	5.33	K0 III	+0.7	4150	.011	17
μ Psc	1 24.9	+ 5 38	5.12	K4 III	-0.1		.0090	144
η Psc	1 26.1	+14 50	3.72	G8 III*	0.0	st-1	.018	16
χ Cas	1 27.4	+58 43	4.38	K0 III	+0.7	wk-1	.0145	30
40 Cas	1 30.5	+72 32	5.50	G8 II-III	-1.0	wk-1	.060	25
50 Cet	1 31.1	-15 54	5.48	K2 III	+0.9		.012	22
51 And	1 31.9	+48 7	5.77	K3 III*	+0.1		.019	26
χ And	1 33.4	+43 52	5.17	G8 III	0.0	wk-1	.0092	32
HR 483	1 35.7	+42 7	5.10	G2 V*	+4.6	st-1	.079	32
ν Psc	1 36.2	+ 4 59	4.68	K3 III	+0.1		.012	26
107 Psc	1 37.1	+19 47	5.32	K1 V*	+3.2		.151	46
HR 500	1 37.7	- 4 12	5.27	K3 II-III	-1.0		.0056	48
τ Cet	1 39.4	-16 28	3.65	G8 V*	+5.6		.245	60
o Psc	1 40.1	+ 8 39	4.50	K0 III	+0.7	st-1	.017	26
ζ Cet	1 46.5	-10 50	3.92	K2 III	+0.9		.025	9
α Tri	1 47.4	+29 6	3.58	F5 IV*	+1.9	wk-1	.046	24
ξ Psc	1 48.4	+ 2 42	4.84	K0 III	+0.7	wk-1	.015	30
ι Ari	1 51.9	+17 20	5.16	K1 p				n
49 Cas	1 56.0	+75 38	5.30	G8 III	0.0	wk-1	.0086	26
γ And A	1 57.3	+41 51	2.28	K2 III	+0.9		.053	18
α Ari	2 1.5	+22 59	2.23	K2 III*	+0.9		.054	18
60 And	2 7.0	+43 46	5.08	K4 III	-0.1		.0092	52
HR 645	2 7.0	+50 36	5.40	K0 III	+0.7	4150	.0115	145
η Ari	2 7.2	+20 44	5.35	F5 V	+3.3	st-1	.039	15
ξ' Cet	2 7.7	+ 8 23	4.54	G8 II	-2.8		.0038	
64 And	2 17.8	+49 35	5.49	G8 III	0.0	st-1	.0080	16
65 And	2 18.9	+49 50	4.86	K4 III	-0.1		.010	7
14 Tri	2 26.0	+35 42	5.35	K5 III	-0.2		.0077	48
HR 737	2 26.3	+ 1 50	5.44	K3 III	+0.1		.0085	17
HR 745	2 28.5	+72 23	5.34	G8 III	0.0	wk-1	.0085	37

Table 4 (continued)

Name	α (1900)	δ	m	Spectral Type	M	Group	π sp	Speed (Km/Sec)
ν Cet	2h30m6	+ 5° 9'	5.02	G8 III	0.0	st-1	0".0099	28
ε Cet	2 34.7	-12 18	5.01	F5 IV-V	+2.8	wk-1	.036	25
39 Ari	2 42.0	+28 50	4.62	K1 III	+0.8	st-1	.017	42
17 Per	2 45.4	+54 39	4.87	K5 III	-0.2		.0105	19
20 Per	2 47.4	+37 56	5.32	F4 V	+3.3		.039	9
η Eri	2 51.5	- 9 18	4.05	K1 III-IV	+1.3	wk-1	.028	44
24 Per	2 52.9	+34 47	4.97	K2 III	+0.9		.0155	51
HR 918	2 58.0	+56 19	5.08	K0 II-III	-0.8	wk-1	.0066	85
κ Per	3 2.7	+44 29	4.00	K0 III	+0.7	wk-1	.022	42
ω Per	3 4.8	+39 14	4.82	K1 III	+0.8	st-1	.016	24
δ Ari	3 5.9	+19 21	4.53	K2 III	+0.9		.019	32
94 Cet	3 7.7	- 1 34	5.14	F8 V	+3.9	st-1	.057	8
HR 969	3 9.1	+50 34	5.29	G5 II	-2.3		.0030	
HR 991	3 12.5	+33 51	4.92	K2 II	-2.6		.0031	
HR 999	3 14.3	+28 41	4.72	K3 II-III	-1.0		.0072	15
63 Ari	3 17.0	+20 23	5.25	K3 III	+0.1		.0093	32
o Tau	3 19.4	+ 8 41	3.80	G8 III*	0.0	st-1	.017	45
σ Per	3 25.6	+47 39	4.55	K3 III	+0.1		.013	29
5 Tau	3 25.4	+12 36	4.28	K0 II-III	-0.8	st-1	.0095	13
56 Per	3 25.5	+45 43	5.35	F4 III*	+0.2		.0093	65
δ Eri	3 38.5	-10 6	3.72	K0 IV*	+3.5	wk-1	.091	55
32 Eri A	3 49.3	- 3 15	4.95	G8 III	0.0	st-1	.010	17
HR 1249	3 57.5	- 0 35	5.42	F8 V	+3.8	st-1	.043	19
37 Tau	3 58.3	+21 49	4.50	K0 III	+0.9	st-1	.019	13
HR 1257	3 58.9	+ 2 33	5.39	F6 IV	+1.9	wk-1	.020	46
39 Eri	4 9.6	-10 30	5.13	K3 III	+0.1		.0098	74
HR 1327	4 11.3	+64 54	5.40	G5 III	0.0	wk-1	.0082	33
54 Per	4 13.9	+34 20	5.10	G8 III	0.0	4150	.0095	41
γ Tau	4 14.1	+15 23	3.86	K0 III*	+0.7	st-1	.023	30
φ Tau	4 14.2	+27 7	5.06	K1 III	+0.8	wk-1	.014	20
δ Tau	4 17.2	+17 18	3.93	K0 III*	+0.7	st-1	.023	31
HR 1390	4 19.7	+31 13	5.33	K1 III	+0.8	wk-1	.012	42
ψ Tau	4 21.0	+14 29	4.94	G8 III	0.0	st-1	.010	20
75 Tau	4 22.7	+16 8	5.29	K2 III	+0.9		.013	25
ε Tau	4 22.8	+18 58	3.53	K0 III*	+0.7	wk-1	.026	51
θ' Tau	4 22.9	+15 44	4.04	K0 III*	+0.7	st-1	.022	32
45 Eri	4 26.3	- 0 16	4.97	K3 II-III	-1.0		.0064	6
HR 1452	4 29.4	- 9 11	5.50	K4 II-III	-1.0		.0050	116
α Tau	4 30.2	+16 19	1.06	K5 III*	-0.2		.056	41
3 Cam	4 32.0	+52 53	5.31	K0 III	-0.7	st-1	.012	44
53 Eri	4 33.6	-14 30	3.98	K2 III	-0.9		.024	41
HR 1523	4 41.6	+61 2	5.32	K3 III	+0.1		.0090	32
HR 1533	4 43.2	+37 19	5.10	K4 II	-2.6		.0029	
60 Eri	4 45.7	-16 23	5.16	K0 III	+0.7	wk-1	.013	34
ξ Aur	4 45.9	+36 32	5.04	K3 III	+0.1		.010	33
o² Ori	4 50.7	+13 21	4.28	K2 III	+0.9		.021	26
104 Tau	5 1.5	+18 31	5.79	G4 V	+4.9	st-1	.066	36
68 Eri	5 3.8	- 4 35	5.23	F5 V	+3.3	wk-1	.041	15
HR 1684	5 6.0	+15 55	5.36	K5 III	-0.2		.0077	28
HR 1686	5 6.1	+79 7	5.16	F8 V	+3.8	wk-1	.049	36
ρ Ori	5 8.1	+ 2 45	4.64	K3 III	+0.1		.0125	24
16 Aur	5 11.6	+33 16	4.81	K3 III	+0.1		.0115	64
109 Tau	5 13.3	+22 0	5.14	G8 III	0.0	wk-1	.0093	27
21 Ori	5 14.0	+ 2 30	5.45	F5 II	-2.0		.0052	
σ Aur	5 17.9	+37 18	5.22	K4 III	-0.1		.0086	30
111 Tau	5 18.6	+17 17	5.14	F8 V	+3.9	st-1	.057	33
29 Ori	5 19.1	- 7 54	4.21	G8 III	0.0	wk-1	.014	38
27 Ori	5 19.4	- 0 59	5.15	K0 III	+0.7	wk-1	.013	38
φ Aur	5 21.0	+34 24	5.26	K3 p				n

Table 4 (continued)

Name	α (1900)	δ	m	Spectral Type	M	Group	π sp	Speed (Km/Sec)
31 Ori	5^h24^m7	- 1°10'	4.97	K5 III	-0.2		0".0092	9
ϕ^2 Ori	5 31.4	+ 9 14	4.39	KO III	+0.7	wk CN	.018	109
51 Ori	5 37.3	+ 1 26	5.24	K1 III	+0.8	wk-1	.013	74
τ Aur	5 42.3	+39 9	4.64	G8 III	0.0	wk-1	.012	51
152 Tau	5 42.9	+24 32	5.02	G8 III	0.0	4150	.0099	4
ν Aur	5 44.6	+39 7	4.18	KO III	+0.7	st-1	.020	21
χ^1 Ori	5 48.5	+20 16	4.62	GO V	+4.3	st-1	.086	30
δ Aur	5 51.3	+54 17	3.88	KO III*	+0.7	wk-1	.023	19
HR 2113	5 55.1	- 3 5	4.69	K2 III	+0.9		.0175	14
37 Cam	6 1.2	+58 57	5.42	G8 III	0.0	wk-1	.0082	47
36 Cam	6 2.8	+65 44	5.39	K2 II-III	-0.8		.0058	9
κ Aur	6 9.0	+29 32	4.45	G8 III	0.0	wk-1	.013	83
71 Ori	6 9.0	+19 12	5.18	F6 V	+3.6	st-1	.048	25
γ Mon	6 10.0	- 6 15	4.09	K3 III	+0.1		.016	23
74 Ori	6 10.8	+12 18	5.11	F5 IV-V	+2.8	wk-1	.034	41
HR 2260	6 15.3	-16 47	5.28	K3 III	+0.1		.0091	29
45 Aur	6 15.7	+53 30	5.41	F5 III	+0.2	st-1	.0091	33
5 Lyn	6 18.1	+58 28	5.43	K4 III	-0.1		.0077	15
HR 2305	6 19.5	-11 28	5.39	K3 III	+0.1		.0088	55
HR 2379	6 26.7	-12 19	5.33	K3 III	+0.1		.0090	25
ψ^2 Aur	6 32.2	+42 35	5.09	K3 III	+0.1		.010	15
ν^2 CMa	6 32.3	-19 10	4.14	K1 IV	+2.9	st-1	.057	20
ν^3 CMa	6 33.5	-18 9	4.65	K1 III	+0.8	st-1	.017	22
HR 2450	6 34.7	-14 3	4.97	K2 II	-2.6		.0051	
ψ^4 Aur	6 35.8	+44 37	5.17	K5 III	-0.2		.0084	83
13 Lyn	6 38.5	+57 16	5.47	KO III	+0.7	wk-1	.011	20
30 Gem	6 38.4	+13 20	4.65	K1 III	+0.8	st-1	.017	4
56 Aur	6 39.5	+43 41	5.34	GO V	+4.3	st-1	.062	43
ψ^6 Aur	6 40.0	+48 54	5.28	K1 III	+0.8	st-1	.013	25
17 Mon	6 41.9	+ 8 9	5.00	K4 III	-0.1		.0104	33
18 Mon	6 42.7	+ 2 51	4.70	KO III	+0.7	st-1	.016	9
ψ^7 Aur	6 43.7	+41 54	5.04	K3 III	+0.1		.0102	69
HR 2527	6 45.5	+77 6	4.75	K4 III	-0.1		.0107	43
θ CMa	6 49.8	-11 55	4.25	K4 III	-0.1		.0135	90
HR 2649	6 58.1	+11 6	5.25	K3 III	+0.1		.0092	7
63 Aur	7 4.8	+39 29	5.07	K4 II-III	-1.9		.0061	57
τ Gem	7 4.8	+30 25	4.48	K2 III	+0.9		.019	14
20 Mon	7 5.3	- 4 5	5.02	KO III	+0.7	wk-1	.014	101
18 Lyn	7 7.2	+59 49	5.33	K2 III	+0.9		.013	83
65 Aur	7 15.4	+36 57	5.21	KO III	+0.7	wk-1	.0125	33
66 Aur	7 17.2	+40 52	5.28	KO III	+0.7	4150	.012	18
57 Gem	7 17.4	+25 15	5.08	G8 III	0.0	wk-1	.0096	28
ι Gem	7 19.5	+28 00	3.89	KO III	+0.7	wk-1	.023	19
ε CMi	7 20.2	+ 9 28	5.07	G8 III	0.0	st-1	.0097	24
63 Gem	7 21.8	+21 39	6.01	F5 IV-V	+2.8	st-1	.023	17
22 Lyn	7 22.3	+49 53	5.36	F6 V	+3.6	st-1	.044	36
γ CMi	7 22.7	+ 9 8	4.60	K3 III	+0.1		.013	41
65 Gem	7 23.6	+28 7	5.09	K2 III	+0.9		.015	23
6 CMi	7 24.2	+12 15	4.85	K2 III	+0.9		.016	31
HR 2896	7 28.8	+31 11	5.33	KO III	+0.7	wk-1	.0094	28
υ Gem	7 29.8	+27 7	4.22	K5 III	-0.2		.013	38
25 Mon	7 32.3	- 3 53	5.17	F5 III	+0.2	wk-1	.010	41
HR 2959	7 35.8	-15 2	5.15	K3 II	-2.6		.0028	
α Mon	7 36.5	- 9 19	4.07	KO III	+0.7	wk-1	.021	11
σ Gem	7 37.1	+29 8	4.26	K1 III	+0.8	st-1	.020	58
76 Gem	7 38.0	+26 1	5.40	K5 III	-0.2		.0075	10
κ Gem	7 38.4	+24 38	3.68	G8 III*	0.0	st-1	.018	9
β Gem	7 39.2	+28 16	1.21	KO III*	+0.7	wk-1	.079	33
81 Gem	7 40.3	+18 45	5.02	K5 III	-0.2		.0090	77
6 Pup	7 45.2	-16 59	5.54	K3 III	+0.1		.0081	76

Table 4 (continued)

Name	α (1900)	δ	m	Spectral Type	M	Group	π sp	Speed (Km/Sec)
HR 3075	$7^h46.^m2$	+74°11'	5.56	K3 III	+0.1		0P0081	41
14 CMi	7 53.2	+ 2 29	5.40	KO III	+0.7	wk-1	.0115	83
27 Mon	7 54.7	- 5 24	5.06	K2 III	+0.9		.015	47
28 Mon	7 56.1	- 1 7	4.38	K4 III	-0.1		.0105	46
HR 3145	7 57.1	+ 2 37	4.52	K2 III	+0.9		.019	58
χ Gem	7 57.4	+28 4	5.04	K2 III	+0.9		.015	20
55 Cam	8 2.9	+68 46	5.48	G8 II	-2.6		.0024	
19 Pup	8 6.6	-12 38	4.68	KO III	+0.7	wk-1	.016	21
HR 3212	8 6.7	- 7 28	5.36	G8 III	0.0	st-1	.0084	30
20 Pup	8 8.7	-15 29	5.05	G5 II	-2.3		.0034	
β Cnc	8 11.1	+ 9 30	3.76	K4 III	-0.1		.017	10
31 Lyn	8 16.0	+45 31	4.45	K5 III	-0.2		.012	50
HR 3306	8 20.6	+ 7 53	5.23	G8 II	-2.6		.0027	
η Cnc	8 26.9	+20 47	5.52	K3 III	+0.1		.0082	24
π^2 UMa	8 31.5	+64 41	4.76	K2 III	+0.9		.017	30
σ Hya	8 33.5	+ 3 42	4.54	K2 III	+0.9		.019	14
6 Hya	8 35.3	-12 7	5.15	K4 III	-0.1		.0089	41
9 Hya	8 37.1	-15 35	4.98	K1 III	+0.8	st-1	.0145	34
δ Cnc	8 39.0	+18 31	4.17	KO III	+0.7	wk-1	.020	42
ι Cnc	8 40.7	+29 8	4.20	G8 II	-2.6		.0044	
12 Hya	8 41.7	-13 11	4.44	G8 III	0.0	wk-1	.015	31
35 Lyn	8 45.3	+44 6	5.24	KO III	+0.7	wk-1	.012	37
ρ^2 Cnc	8 49.7	+28 19	5.25	G3 II-III	-1.0	st-1	.0056	17
ζ Hya	8 50.1	+ 6 20	3.30	KO III	+0.7	4150	.030	17
σ^1 UMa	8 59.8	+67 17	5.33	K5 III	-0.2		.0079	20
HR 3612	9 0.2	+38 51	4.71	G8 Ib-II	-3.6		.0022	
ω Hya	9 0.7	+ 5 30	5.41	K2 II-III	-0.9		.0058	16
τ Cnc	9 2.0	+30 3	5.38	G8 III	0.0	wk-1	.0085	24
τ UMa	9 2.7	+63 55	4.74	A7 m				n
ξ Cnc	9 3.8	+22 27	5.22	KO III	+0.7	st-1	.0125	27
17 UMa	9 8.4	+57 10	5.48	K5 III	-0.2		.0073	29
23 Hya	9 11.7	- 5 56	5.40	K2 III	+0.9		.0125	32
26 Hya	9 15.0	-11 33	4.94	G8 III	0.0	st-1	.010	18
27 Hya	9 15.6	- 9 8	4.97	G8 III-IV	+1.3	st-1	.018	16
κ Leo	9 18.8	+26 37	4.31	K2 III	+0.9		.018	23
α Hya	9 22.7	- 8 14	2.16	K3 III	+0.1		.039	24
HR 3751	9 22.9	+81 46	4.58	K3 III	+0.1		.013	9
24 UMa	9 25.6	+70 16	4.57	G5 IV	+3.2	st-1	.063	31
λ Leo	9 26.0	+23 25	4.48	K5 III	-0.2		.0115	21
6 Leo	9 26.6	+10 9	5.28	K3 III	+0.1		.0092	17
ξ Leo	9 26.6	+11 45	5.12	KO III	+0.7	wk-1	.013	34
10 LMi	9 28.1	+36 51	4.82	G8 III	0.0	st-1	.012	24
HR 3809	9 28.8	+40 4	4.99	KO III	+0.7	wk-1	.014	25
11 LMi	9 29.7	+36 16	5.48	G8 IV-V	+4.5		.067	37
10 Leo	9 31.9	+ 7 17	5.14	K1 III	+0.8	wk-1	.014	17
HR 3834	9 33.3	+ 5 6	4.78	K3 III	+0.1		.012	60
27 UMa	9 33.8	+72 42	5.39	KO III	+0.7	st-1	.012	12
ι Hya	9 34.8	- 0 41	4.10	K3 III	+0.1		.016	33
43 Lyn	9 35.8	+40 13	5.50	G8 III	+0.0	wk-1	.0079	34
υ^1 Hya	9 46.7	-14 23	4.29	G8 III	0.0	st-1	.014	36
μ Leo	9 47.1	+26 29	4.10	K2 III	+0.9		.023	31
31 Leo	10 2.6	+10 29	4.58	K4 III	-0.1		.0115	40
HR 3991	10 5.2	-12 19	5.42	F5 V	+3.3	st-1	.038	14
λ Hya	10 5.7	-11 52	3.83	KO III	+0.7	4150	.024	27
γ Leo	10 14.5	+20 21	2.61	KO III	+0.7	wk CN	.042	65
μ Hya	10 21.3	-16 20	4.06	K4 III	-0.1		.015	42
β LMi	10 22.1	+37 13	4.51	G8 III-IV	+1.3	st-1	.023	14
HR 4126	10 26.6	+76 14	5.04	KO III	+0.7	st-1	.014	26
48 Leo	10 29.6	+ 7 28	5.17	G8 II-III	-1.0	wk-1	.0059	87
37 LMi	10 33.1	+32 30	4.77	G2 II	-2.0		.0044	

Table 4 (continued)

Name	α (1900)	δ	m	Spectral Type	M	Group	π sp	Speed (Km/Sec)
φ Hya	10h35m.7	-16°21'	5.11	K0 III	+0.7	st-1	0".015	25
58 UMa	10 35.1	+66 14	5.17	K2 III	+0.9		.014	42
HR 4181	10 35.9	+69 36	5.23	K3 III	+0.1		.0094	16
ν Hya	10 44.7	-15 40	3.32	K2 III	+0.9		.035	49
44 UMa	10 47.5	+55 7	5.36	K3 III	+0.1		.0089	20
46 LMi	10 47.7	+34 45	5.92	K1 III	+0.8	wk-1	.024	59
46 UMa	10 50.2	+34 2	5.23	K1 III	+0.8	wk-1	.024	30
α Crt	10 54.9	-17 46	4.20	K0 III	+0.7	4150	.020	105
58 Leo	10 55.4	+ 4 9	5.05	K1 III	+0.8	wk-1	.014	25
61 Leo	10 56.7	- 1 57	4.97	K3 III	-0.2		.0092	34
α UMa	10 57.6	+62 17	1.95	K0 III*	+0.8	st-1	.055	8
ψ UMa	11 4.0	+45 2	3.15	K1 III	+0.8	wk-1	.034	11
HR 4365	11 10.6	+13 51	5.43	K3 III	+0.1		.0084	21
ν UMa	11 13.1	+33 38	3.71	K3 III	+0.1		.019	22
δ Crt	11 14.3	-14 14	3.62	G8 III-IV	+1.3	wk-1	.051	41
λ Crt	11 18.4	-18 14	5.15	F5 IV	+1.9	st-1	.022	48
ε Crt	11 19.6	-10 19	5.07	K5 III	-0.2		.0088	22
τ Leo	11 22.8	+ 3 24	5.18	G8 II-III	-1.0	st-1	.0058	40
87 Leo	11 25.2	- 2 27	5.07	K4 III	-0.1		.0092	34
2 Dra	11 30.2	+69 53	5.38	K0 III	+0.7	wk-1	.012	75
υ Leo	11 31.3	- 0 16	4.47	G9 III	+0.3	wk-1	.015	31
92 Leo	11 35.6	+21 54	5.43	K0 III	+0.7	wk-1	.012	13
3 Dra	11 36.9	+67 18	5.48	K3 III	+0.1		.0084	31
ζ Crt	11 39.7	-17 48	4.90	G8 III	0.0	st-1	.0105	39
χ UMa	11 40.8	+48 20	3.85	K0 III*	+0.7	wk-1	.024	17
HR 4521	11 41.6	+56 11	5.41	K3 III	+0.1		.0087	28
o Vir	12 0.1	+ 9 17	4.24	G8 III*	0.0	wk-1	.014	67
7 Com	12 11.3	+24 30	5.06	K0 III	+0.7	wk-1	.013	26
HR 4668	12 11.5	+33 37	5.08	K1 III	+0.8	st-1	.014	47
16 Vir	12 15.3	+ 3 52	5.10	K0 III	+0.7	wk CN	.013	96
11 Com	12 15.7	+18 21	4.91	G8 III	0.0	wk-1	.0105	75
HR 4699	12 15.8	-13 1	5.36	K1 III	+0.8	st-1	.012	30
5 CVn	12 19.2	+52 7	4.97	G7 III	0.0	st-1	.010	28
6 CVn	12 20.9	+39 34	5.22	G8 III-IV	+1.3	wk-1	.017	5
15 Com	12 22.0	+28 49	4.56	K1 III-IV	+1.3	4150	.022	14
HR 4783	12 28.7	+33 48	5.43	K0 III	+0.7	wk-1	.0115	31
χ Vir	12 34.1	- 7 27	4.78	K2 III	+0.9		.017	19
27 Com	12 41.7	+17 7	5.33	K3 III	+0.1		.0089	63
35 Com	12 48.4	+21 47	5.10	G8 III	0.0	st-1	.0095	6
37 Com	12 55.5	+31 20	5.08	K1 p				n
9 Dra	12 56.1	+67 8	5.50	G8 III	0.0	wk CN	.0079	69
ε Vir	12 57.2	+11 30	2.95	G9 III	+0.3	st-1	.030	29
41 Com	13 2.4	+28 10	4.90	K5 III	-0.2		.0094	46
49 Vir	13 2.7	-10 12	5.26	K1 III	+0.8	st-1	.013	27
HR 4997	13 9.2	+40 41	5.05	K0 III	+0.7	st-1	.0135	14
57 Vir	13 10.6	-19 25	5.32	K1 IV	+2.9	4150	.033	72
HR 5013	13 12.3	+14 12	5.45	K3 III	+0.1		.0085	43
63 Vir	13 17.7	-17 13	5.45	K0 III	+0.7	wk-1	.011	24
69 Vir	13 22.1	-15 27	4.89	K1 III	+0.8	4150	.015	29
76 Vir	13 27.7	- 9 39	5.43	K0 III	+0.7	wk-1	.011	8
89 Vir	13 44.4	-17 38	5.11	K1 III	+0.8	st-1	.014	40
υ Boo	13 44.7	+16 18	4.23	K5 III	-0.2		.0126	29
6 Boo	13 45.0	+21 46	5.06	K4 III	-0.1		.0093	32
90 Vir	13 49.6	- 1 1	5.30	K2 III	+0.9		.013	12
9 Boo	13 52.0	+27 59	5.18	K3 III	+0.1		.0096	45
κ Vir	14 7.6	- 9 48	4.31	K3 III	+0.1		.014	61
4 UMi	14 9.2	+78 1	5.00	K3 III	+0.1		.0104	23
15 Boo	14 10.0	+10 54	5.36	K0 III	+0.7	wk-1	.012	59
α Boo	14 11.1	+19 42	0.24	K2 III	+0.9		.135	69
HR 5361	14 13.3	+35 58	4.93	K1 III	+0.8	st-1	.016	21

Table 4 (continued)

Name	α (1900)	δ	m	Spectral Type	M	Group	π sp	Speed (Km/Sec)	
υ Vir	14^h14^m4	$-1°43'$	5.24	G8 III	0.0	4150	0"0089	56	
20 Boo	14 15.0	+16 46	4.97	K3 III	+0.1		.0106	58	
ϕ Vir	14 23.0	- 1 47	4.97	G2 III	+0.2		.011	45	
ρ Boo	14 27.5	+30 49	3.79	K3 III*	+0.1		.018	37	
5 UMi	14 27.7	+76 8	4.37	K4 III	-0.1		.013	28	
31 Boo	14 36.7	+ 8 35	5.03	G8 III	0.0	wk-l	.010	19	
9 Boo	14 40.6	+17 23	4.69	K0 III	+0.7	st-l	.016	10	
11 Lib	14 45.3	- 1 53	5.05	G8 III-IV	+1.3	wk-l	.018	103	
HR 5541	14 46.6	+37 41	5.50	K0 III-IV	+1.4	wk-l	.015	79	
β UMi	14 51.0	+74 34	2.24	K4 III*	-0.1		.034	31	
ω Boo	14 57.7	+25 24	4.93	K4 III	-0.1		.0098	56	
110 Vir	14 57.9	+ 2 29	4.62	K0 III	+0.7	st-l	.0175	13	
β Boo	14 58.2	+40 47	3.63	G8 II-III	-1.0	st-l	.012	13	
ψ Boo	15 0.2	+27 20	4.67	K2 III	+0.8		.018	34	
ν Lib	15 1.1	-15 52	5.29	K5 III	-0.2		.0080	13	
HR 5635	15 3.4	+54 56	5.21	G8 III	0.0	wk-l	.0090	52	
δ Boo	15 11.5	+33 41	3.54	G8 III*	0.0	wk CN	.0195	43	
HR 5691	15 13.5	+67 44	5.23	F8 V	+3.9	st-l	.054	63	
6 Ser	15 16.0	+ 1 4	5.43	K3 III	+0.1		.0083	56	
11 UMi	15 17.2	+72 11	5.14	K4 III	-0.1		.0090	18	
ι Dra	15 22.7	+59 19	3.47	K2 III*	+0.9		.051	14	
ν^1 Boo	15 27.3	+41 10	5.15	K5 III	-0.2		.0084	21	
37 Lib	15 28.7	- 9 43	4.83	K1 III	+0.8	wk-l	.013	151	
γ Lib	15 29.9	-14 27	4.02	G8 III-IV	+1.3	wk-l	.029	30	
16 Ser	15 31.7	+10 21	5.40	K0 p					n
ϕ Boo	15 34.2	+40 41	5.41	G8 IV	+3.5	st-l	.0078	20	
β UMi	15 34.4	+77 41	5.33	K5 III	-0.2		.0078	20	
κ Lib	15 36.2	-19 21	4.96	K5 III	-0.2		.0095	43	
α Ser	15 39.3	+ 6 44	2.75	K2 III*	+0.9		.043	34	
ω Ser	15 45.2	+ 2 30	5.35	G8 III	0.0	wk-l	.0085	35	
δ CrB	15 45.4	+26 23	4.73	G5 III-IV	+1.7	wk-l	.025	14	
ρ Ser	15 46.9	+21 17	4.38	K5 III	-0.2		.0096	49	
κ CrB	15 47.5	+35 58	4.77	K0 III-IV	+1.4	st-l	.021	80	
θ Lib	15 48.1	-16 26	4.34	G8 III-IV	+1.3	wk-l	.025	50	
ϵ CrB	15 53.5	+27 10	4.22	K3 III	+0.1		.015	28	
5 Her	15 56.3	-18 6	5.28	K0 III	+0.7	wk-l	.012	66	
ρ CrB	15 57.2	+33 37	5.45	G2 V	+4.6	wk-l	.068	64	
κ Her A	16 3.6	+17 19	5.34	G8 III	0.0	st-l	.0085	12	
HR 6016	16 4.6	- 3 12	5.41	K4 III	-0.1		.0079	18	
τ CrB	16 5.3	+36 45	4.94	K0 III-IV*	+1.4	wk-l	.020	77	
χ Sco	16 8.3	-11 35	5.50	K3 III	+0.1		.0082	14	
ϵ Oph	16 13.0	- 4 27	3.34	G8 III	0.0	wk-l	.022	33	
ξ CrB	16 18.2	+31 7	4.72	K0 III	+0.7	st-l	.016	41	
ψ Oph	16 18.3	-19 48	4.59	K0 III	+0.7	wk-l	.017	12	
ν^2 CrB	16 18.7	+33 56	5.28	K5 III	-0.2		.0080	40	
HR 6126	16 22.0	+69 20	5.44	K2 III	+0.9		.012	10	
η Dra	16 22.6	+61 44	2.39	G8 III*	+0.0	st-l	.026	7	
HR 6136	16 23.5	+ 0 53	5.47	K4 III p	-0.1		.0077	54	n
ϕ Oph	16 25.4	-16 24	4.40	G8 III	0.0	st-l	.013	24	
β Her	16 25.9	+21 42	2.81	G8 III*	0.0	st-l	.027	12	
HR 6152	16 26.2	+20 42	5.29	G8 p					n
29 Her	16 27.9	+11 42	4.92	K5 III	-0.2		.0094	89	
HR 6196	16 35.3	-17 33	5.04	G8 II	-2.5		.0030		
HR 6199	16 36.0	+56 13	5.44	K1 III	+0.8	st-l	.012	21	
η Her	16 39.5	+39 7	3.61	G8 III-IV	+1.3	st-l	.035	33	
18 Dra	16 40.2	+64 47	5.00	K1 p					n
43 Her	16 41.0	+ 8 46	5.38	K5 III	-0.2		.0076	18	
51 Her	16 47.5	+24 50	5.20	K2 II-III	-0.9		.0063	13	
23 Oph	16 49.3	- 6 0	5.35	K2 III	+0.9		.013	9	
HR 6287	16 50.5	+21 7	5.48	G8 III	+0.0	wk-l	.0079	43	

Table 4 (continued)

Name	α (1900)	δ	m	Spectral Type	M	Group	π sp	Speed (Km/Sec)
54 Her	16h51m0	+18°36'	5.56	K4 III	-0.1		0"0074	72
κ Oph	16 52.9	+ 9 32	3.42	K2 III*	+0.9		.031	65
30 Oph	16 55.9	- 4 4	5.00	K4 III	-0.1		.0096	34
ε UMi	16 56.2	+82 12	4.40	G5 III	+0.0	st-1	.015	18
HR 6388	17 6.5	+40 54	5.12	K3 III	+0.1		.0099	41
41 Oph	17 11.5	- 0 20	4.82	K2 III	+0.9		.016	18
HR 6435	17 15.9	+10 58	5.28	K4 II-III	-1.0		.0053	94
σ Oph	17 21.6	+ 4 14	4.44	K3 II	-2.6		.0039	
HR 6516	17 25.3	- 0 59	5.54	G8 IV-V	+4.6		.071	60
λ Her	17 26.7	+28 11	4.48	K4 III	-0.1		.012	15
27 Dra	17 32.4	+68 12	5.21	K0 III	+0.7	wk-1	.0125	72
β Oph	17 38.5	+ 4 37	2.94	K2 III*	+0.9		.039	28
μ Her	17 42.6	+27 47	3.48	G5 IV	+3.2	wk-1	.088	43
87 Her	17 44.8	+25 39	5.34	K2 III	+0.9		.015	13
90 Her	17 50.1	+40 1	5.12	K3 III	+0.1		.0099	28
ξ Dra	17 51.8	+56 53	3.90	K2 III*	+0.9		.025	23
ν Oph	17 53.5	- 9 46	3.50	K0 III	+0.7	st-1	.028	29
ξ Her	17 53.9	+29 16	3.82	K0 III	+0.7	st-1	.024	26
γ Dra	17 54.3	+51 30	2.42	K5 III*	-0.2		.050	14
93 Her	17 55.6	+16 46	4.71	K0 II-III	-0.8	4150	.0090	5
70 Oph	18 0.4	+ 2 31	4.28	K0 V*	+6.0		.220	24
71 Oph	18 2.5	+ 8 43	4.75	G8 III-IV	+1.3	st-1	.021	21
HR 6791	18 4.5	+43 27	5.11	K0 p				
36 Dra	18 13.3	+64 22	5.03	F5 V	+3.5	wk-1	.045	41
105 Her	18 15.1	+24 24	5.49	K4 II	-2.6		.0024	
74 Oph	18 15.9	+ 3 20	4.92	G8 III	0.0	st-1	.010	27
η Ser	18 16.1	- 2 55	3.42	G8 IV	+3.5	wk-1	.105	42
ξ Lyr	18 16.4	+36 1	4.34	K2 III	+0.9		.020	8
ζ Sct	18 18.2	- 8 59	4.83	K0 III	+0.7	wk-1	.015	29
HR 6885	18 18.4	+17 46	5.48	K3 III	+0.1		.0083	44
109 Her	18 19.4	+21 43	3.92	K2 III	+0.9		.025	67
χ Dra	18 22.9	+72 41	3.69	F8 V*	+3.6	st-1	.096	62
60 Ser	18 24.5	- 2 3	5.44	K0 III	+0.7	4150	.011	45
42 Dra	18 25.7	+65 30	4.99	K2 III	+0.9		.015	62
HR 6970	18 29.5	-11 3	5.25	G8 III	0.0	st-1	.0088	34
α Sct	18 29.8	- 8 19	4.06	K3 III	+0.1		.016	96
HR 6983	18 31.7	+52 16	5.42	K0 III	+0.7	st-1	.0115	7
ε Sct	18 38.0	- 8 22	5.09	G8 II	-2.6		.0029	
HR 7064	18 42.1	+26 33	4.92	K3 III	+0.1		.011	13
HR 7117	18 48.3	+73 58	5.33	K0 II-III	-0.8	wk-1	.0076	57
o Dra	18 49.7	+59 16	4.78	K0 II-III	-0.8	wk-CN	.0076	55
HR 7137	18 50.8	+50 35	4.97	G8 III	0.0	st-1	.010	32
η Sct	18 51.7	- 5 55	5.04	K2 III	+0.9		.015	81
HR 7162	18 53.3	+32 46	5.21	G0 V	+4.3	wk-1	.066	34
ε Aql	18 55.1	+14 56	4.21	K2 III	+0.9		.022	34
υ Dra	18 55.6	+71 10	4.91	K0 III	+0.7	wk-1	.014	15
HR 7181	18 55.7	+26 5	5.23	K2 III	+0.9		.013	28
λ Lyr	18 56.2	+32 0	5.11	K3 II	-2.6		.0029	
12 Aql	18 58.3	- 5 53	4.15	K1 III	+0.8	wk-1	.021	30
53 Dra	19 9.8	+56 41	5.24	G8 III	0.0	4150	.0069	25
43 Sgr	19 11.8	-19 8	5.05	G8 II	-2.6		.0050	
54 Dra	19 12.1	+57 32	5.28	K2 III	+0.9		.013	35
δ Dra	19 12.5	+67 29	3.24	G9 III	+0.3	wk-1	.026	17
23 Aql	19 13.5	+ 0 54	5.32	K2 II-III	-0.8		.0060	
κ Cyg	19 14.8	+53 11	3.98	K0 III*	+0.7	st-1	.022	28
26 Aql	19 15.2	- 5 36	5.10	G8 III-IV	+1.3	wk-1	.017	35
τ Dra	19 17.5	+73 10	4.63	K3 III	+0.1		.0125	66
31 Aql	19 20.2	+11 44	5.23	G8 IV	+3.5	4150	.045	130
4 Vul	19 21.1	+19 36	5.31	K0 III	+0.7	wk-1	.012	43
μ Aql	19 29.2	+ 7 10	4.65	K3 III	+0.1		.012	96

Table 4 (continued)

Name	α (1900)	δ	m	Spectral Type	M	Group	π sp	Speed (Km/Sec)
37 Aql	$19^h29^m.6$	-10°47'	5.24	G8 III	0.0	4150	0".0089	20
σ Dra	19 32.6	+69 29	4.73	K0 V*	+6.0		.175	74
ε Sge	19 32.8	+16 14	5.67	G8 III	0.0	st-l	.0074	22
HR 7468	19 33.5	+44 28	5.13	K0 III	+0.7	wk-l	.013	60
54 Sgr	19 35.0	-16 31	5.45	K2 III	+0.9		.012	50
φ Cyg	19 35.4	+29 55	4.79	G8 III-IV	+1.3	st-l	.020	27
β Sge	19 36.6	+17 15	4.45	G8 II	-2.6		.0039	
10 Vul	19 39.6	+25 32	5.45	G8 III	0.0	wk-l	.0080	17
56 Sgr	19 40.5	-20 0	5.06	K1 III	+0.8	wk-l	.014	62
15 Cyg	19 40.7	+37 7	5.02	G8 III	0.0	st-l	.0099	33
o Aql	19 46.2	+10 10	5.22	F8 V	+3.9	st-l	.054	22
20 Cyg	19 48.1	+52 44	5.17	K3 III	+0.1		.0096	39
ε Dra	19 48.5	+70 1	3.99	G8 III*	0.0	wk-l	.016	43
ξ Aql	19 49.4	+ 8 12	4.86	K0 III	+0.7	wk-l	.015	38
β Aql	19 50.4	+ 6 9	3.90	G8 IV*	+3.5	wk-l	.083	51
η Cyg	19 52.6	+34 49	4.05	K0 III	+0.7	wk-l	.021	18
HR 7633	19 54.0	+58 35	5.13	K5 II-III	-1.0		.0060	32
γ Sge	19 54.3	+19 13	3.71	K5 III	-0.2		.017	22
26 Cyg	19 58.5	+49 50	5.28	K1 II-III	-0.8	4150	.0061	21
η Sge	20 0.7	+19 42	5.26	K2 III	+0.9		.013	41
ρ Dra	20 2.4	+67 35	4.68	K3 III	+0.1		.012	11
66 Dra	20 4.0	+61 42	5.57	K3 III	+0.1		.0081	79
23 Vul	20 11.6	+27 30	4.73	K3 III	+0.1		.012	30
24 Vul	20 12.5	+24 22	5.45	G8 III	0.0	wk-l	.0080	34
α^2 Cep	20 12.5	-12 51	3.77	G9 III	+0.5	wk-l	.021	18
HR 7759	20 13.4	+40 3	5.50	K4 II	-2.6		.0024	
σ Cep	20 13.6	-19 26	5.46	K3 II	-2.6		.0024	
HR 7794	20 18.2	+ 5 1	5.41	G8 III-IV	+1.3	wk-l	.015	18
59 Cyg	20 19.9	+31 52	4.60	K3 III	+0.1		.0125	8
69 Aql	20 24.4	- 3 15	5.11	K2 III	+0.9		.014	18
70 Aql	20 31.5	- 2 54	5.22	K5 II	-2.6		.0027	
71 Aql	20 33.2	- 1 27	4.51	G8 III	0.0	st-l	.0125	8
κ Del	20 34.3	+ 9 44	5.23	G5 IV	+3.2		.039	48
1 Aqr	20 34.3	+ 0 8	5.39	K1 III	+0.3	wk-l	.012	42
30 Vul	20 40.6	+24 55	5.15	K2 III	+0.9		.014	76
52 Cyg	20 41.5	+30 21	4.34	K0 III	+0.7	wk-l	.019	22
ε Cyg	20 42.0	+33 36	2.64	K0 III*	+0.7	st-l	.041	49
HR 7956	20 43.2	+34 0	5.20	K3 III	+0.1		.0095	15
η Cep	20 43.3	+61 27	3.59	K0 III-IV	+1.4	wk CN	.086	124
31 Vul	20 47.9	+26 45	4.76	G8 III	0.0	st-l	.011	47
32 Vul	20 50.3	+27 41	5.24	K4 III	-0.1		.0085	26
17 Del	20 50.9	+15 20	5.39	K0 III	+0.7	wk-l	.0115	7
63 Cyg	21 3.2	+47 15	4.88	K4 II	-2.6		.0032	
ν Aqr	21 4.2	-11 47	4.52	G8 III	0.0	st-l	.0125	25
ι Cep	21 16.7	-17 16	4.30	G8 III	0.0	st-l	.014	25
1 Peg	21 17.5	+19 23	4.24	K1 III	+0.8	wk-l	.021	66
71 Cyg	21 25.3	+46 6	5.34	K0 III	+0.7	wk-l	.012	41
ρ Cyg	21 30.2	+45 9	4.22	G9 III	0.0	wk CN	.014	41
72 Cyg	21 30.7	+38 5	4.98	K1 III	+0.3	4150	.015	67
25 Aqr	21 34.5	+ 1 48	5.33	K0 III	+0.7	wk-l	.012	40
42 Cap	21 36.1	-14 30	5.29	G2 IV	+2.9	st-l	.033	46
κ Cap	21 37.1	-19 19	4.82	G8 III	0.0	wk-l	.011	51
46 Cap	21 39.7	- 9 32	5.29	G8 II-III	-1.0	4150	.0055	7
11 Cep	21 40.5	+70 51	4.35	K0 III	+0.7	wk-l	.015	44
12 Peg	21 41.5	+22 29	5.45	K0 Ib	-4.5			
HR 8324	21 41.9	+71 52	5.40	K1 III	+0.8	4150	.012	45
16 Cep	21 57.3	+72 42	5.15	F5 V	+3.3	st-l	.043	33
ν Peg	22 0.6	+ 4 34	4.90	K4 III	-0.1		.010	70
HR 8424	22 2.0	+44 32	5.32	K5 III	-0.2		.0078	17
20 Cep	22 2.0	+62 18	5.39	K4 III	-0.1		.0080	33

Table 4 (continued)

Name	α (1900)	δ	m	Spectral Type	M	Group	ϖ sp	Speed (Km/Sec)	
24 Cep	22h 7m9	+71°51'	4.99	G8 III	0.0	st-1	0".010	5	
HR 8472	22 8.2	+56 21	5.42	F8 V	+3.9	st-1	.050	14	
HR 8475	22 8.4	+34 7	5.42	K2 III	+0.9		.0125	16	
HR 8485	22 9.8	+39 13	4.64	K3 III	+0.1		.012	7	
1 Lac	22 11.6	+37 15	4.22	K3 II-III	-0.9		.0090	6	
θ Aqr	22 11.6	- 8 17	4.32	G8 III-IV	+1.3	st-1	.025	12	
β Lac	22 19.3	+51 44	4.58	G9 III	+0.3	wk-1	.014	67	
35 Peg	22 22.8	+ 4 12	4.93	K0 III	+0.7	wk-1	.015	110	
κ Aqr	22 32.6	- 4 45	5.35	K2 III	+0.9		.013	53	
11 Lac	22 36.1	+43 45	4.64	K3 III	+0.1		.0125	23	
66 Aqr	22 38.2	-19 21	4.38	K4 III	-0.1		.010	38	
13 Lac	22 39.5	+41 18	5.24	K0 III	+0.7	wk-1	.012	30	
λ Peg	22 41.7	+23 22	4.14	G8 II-III	-1.0	st-1	.0095	16	
μ Peg	22 45.2	+24 4	3.67	K0 III	+0.7	st-1	.028	26	
ι Cep	22 46.1	+65 40	3.68	K1 III	+0.8	st-1	.027	35	
HR 8702	22 47.9	+82 37	4.97	K3 III	+0.1		.0105	29	
HR 8748	22 55.2	+83 49	4.96	K4 III	-0.1		.0097	37	
HR 8779	22 59.7	+66 40	5.50	K3 III	+0.1		.0082	8	
3 And	22 59.7	+49 30	4.91	K0 III	+0.7	wk-1	.014	76	
56 Peg	23 2.2	+24 56	4.98	K0 IIp*					n
ψ¹ Aqr	23 10.7	- 9 38	4.48	K0 III	+0.7	wk-1	.018	86	
γ Psc	23 12.0	+ 2 44	3.85	G8 III*	0.0	wk CN	.017	197	
94 Aqr	23 15.9	-14 0	5.27	G5 IV	+3.2		.058	24	
o Cep	23 14.5	+67 34	4.90	K0 III	+0.7	wk-1	.0145	11	
11 And	23 14.8	+48 5	5.42	K0 III	+0.7	wk-1	.011	35	
7 Psc	23 15.3	+ 4 50	5.18	K2 III	+0.9		.014	48	
68 Peg	23 18.0	+11 46	5.28	K3 III	+0.1		.0091	2	
θ Psc	23 22.9	+ 5 50	4.45	K1 III	+0.8	4150	.019	48	
70 Peg	23 24.1	+12 15	4.67	G8 III	0.0	wk-1	.012	25	
14 And	23 26.4	+38 41	5.34	K0 III	+0.7	wk CN	.012	114	
72 Peg	23 29.0	+30 46	5.21	K4 III	-0.1		.0087	23	
λ And	23 32.7	+45 55	4.00	G8 III-IV	+1.3	wk CN	.029	80	
γ Cep	23 35.2	+77 4	3.42	K1 IV*	+2.9	4150	.105	39	
HR 8987	23 37.3	-16 0	5.44	K4 III	-0.1		.0078	8	
78 Peg	23 39.0	+28 48	4.98	K0 III	+0.7	wk-1	.014	10	
ψ And	23 41.1	+45 52	5.09	G5 Ib	-4.5				
τ Cas	23 42.2	+58 6	5.09	K1 III	+0.8	wk-1	.014	26	
27 Psc	23 53.5	- 4 7	5.07	G9 III	+0.3	st-1	.0115	40	
3 Cet	23 59.4	-11 4	5.16	K3 Ib	-4.5				

* These stars have been classified by Dr. W. W. Morgan and have been used as standards in this study.

μ Cas This star shows spectroscopic evidence of being fainter than other G5 V stars, such as κ Cet. The large trigonometric parallax supports this conclusion.

ι Ari The hydrogen lines and λ 4290 are strong enough to indicate a class II star, but the CN is barely strong enough for class III, and the Sr II line is not much stronger than this would require.

φ Aur CN is very strong, but Sr II is only slightly stronger than in class III stars, and the hydrogen lines are quite weak.

τ UMa A metallic-line star. See Roman, Morgan, and Eggen, Ap. J., 107, 107, 1948.

57 Com The hydrogen lines are strong, but the strontium line indicates that the star is no brighter than class II, and the CN indicates an even lower luminosity. CH is very weak. The remainder of the spectrum shows no evidence that it is composite.

16 Ser Sr II is very strong, but CN is only moderate in intensity, and the hydrogen lines are weak.

HR 6136 CN is too strong for a star later than K2 or K3, but the Ca I line, λ 4226, is as strong as it is at K5 III.

HR 6152 The hydrogen lines and Sr II indicate that this is a class II star, but CN is very weak or absent. CH is probably too strong for class II.

18 Dra CN and CH are weak. Otherwise, the star appears to be a normal giant.

HR 6791 CN and Sr II are weak. The hydrogen lines are strong enough to indicate a fairly high luminosity.

56 Peg The hydrogen lines are too weak for the strength of Sr II and CN.

A THEORY OF THE SPATIAL DISTRIBUTION OF GALAXIES*

J. NEYMAN AND E. L. SCOTT
Statistical Laboratory, University of California
Received February 18, 1952

ABSTRACT

A theory of the spatial distribution of galaxies is built, based on the following four main assumptions: (i) galaxies occur only in clusters; (ii) the number of galaxies varies from cluster to cluster, subject to a probabilistic law; (iii) the distribution of galaxies within a cluster is also subject to a probabilistic law; and (iv) the distribution of cluster centers in space is subject to a probabilistic law described as quasi-uniform. The main result obtained is the joint probability generating function $G_{N_1, N_2}(t_1, t_2)$ of numbers N_1 and N_2 of galaxies visible on photographs from two arbitrarily placed regions ω_1 and ω_2, taken with fixed limiting magnitudes m_1 and m_2, respectively. The theory ignores the possibility of light-absorbing clouds. The function $G_{N_1, N_2}(t_1, t_2)$ is expressed in terms of four functions left unspecified, which govern the details of the structure contemplated. Methods are indicated whereby approximations to these functions can be obtained and whereby the general validity of the hypotheses can be tested.

I. INTRODUCTION

The distribution of the numbers of galaxies as revealed by the data of Hubble,[1] Shapley,[2] and Shane[3] does not conform with the Poisson law and indicates the presence of a factor causing "contagion." In order to explain this phenomenon, two kinds of hypotheses are discussed in the literature. Hypotheses of one kind postulate that not only the apparent but also the actual spatial distribution of galaxies is clustered.[4] Indeed, some clusters of galaxies appear to be identified and are studied per se.[5] The hypotheses of the alternative type tend to explain the apparent clustering of galaxies by the effects of extinction of their light by interstellar clouds.[6] Undoubtedly both factors play a role.

The purpose of the present paper is to study the implications of a probabilistic model of spatial clustering of galaxies, ignoring the possibility of extinction by clouds. It is hoped that this model will fit the data relating to regions of the sky not affected by clouds. However, whether it does or not, the evaluation of the effects of clustering in space and the comparison with observations are likely to be helpful in understanding the machinery of the phenomena studied.

The probabilistic model considered is based on several postulates which we classify under two headings: postulates essential to the model, or structural postulates, on the one hand, and secondary postulates, on the other. All the postulates are described below in precise mathematical form. Here, however, it seems useful to characterize them in a manner which is less precise but which is likely to make a stronger appeal to the intuition.

The postulates labeled "structural" or "essential" are those reflecting the major properties of the universe contemplated. These are:

a) Galaxies occur only in clusters.

b) The number of galaxies varies from one cluster to another in a manner subject to a definite probabilistic law, the same for all clusters.

* This paper was prepared with the partial support of the Office of Naval Research

[1] *Mt. W. Contr.*, No. 485; *Ap. J.*, **79**, 9, 1934; *Mt. W. Contr.*, No. 557; *Ap. J.*, **84**, 517, 1936.

[2] *Harvard Ann.*, Vol. **88**, No. 2, 1932; Vol. **105**, No. 8, 1937; Vol. **106**, No. 1, 1938.

[3] In preparation; see also *Proc. Amer. Phil. Soc.*, **94**, 13, 1950.

[4] C. V. L. Charlier, *Ark. mat. astr. fys.*, Vol. **16**, No. 22, 1921; *Medd. Lunds Obs.*, Ser. II, No. 128, 1950.

[5] E. Hubble and M. Humason, *Mt. W. Contr.*, No. 427, 1931; *Ap. J.*, **74**, 43, 1931; H. Shapley, *Proc. Nat. Acad. Sci.*, **19**, 591, 1933.

[6] V. A. Ambartzumian, *Comm. Burakan Obs.*, issue VI, 1951.

c) The distribution of galaxies within a cluster is random and is subject to a probabilistic law which also is the same for all clusters.

d) The distribution of cluster centers in space is random and what we propose to call "quasi-uniform." To explain this term, we shall consider two cubes, k_1 and k_2, of equal volume arbitrarily placed in space but nonoverlapping. A distribution will be called "quasi-uniform" if it satisfies the following two conditions: (i) Whatever the integer $n \geqq 0$, the probability that there will be exactly n cluster centers in k_1 is always equal to the probability that there will be exactly n cluster centers in k_2. We emphasize that this equality persists regardless of the location of the two regions k_1 and k_2. (ii) The presence in k_1 of any particular number of cluster centers does not influence the probability that k_2 will contain exactly n cluster centers ($n = 0, 1, 2, \ldots$), and this is regardless of whether k_1 and k_2 are near by or distant, provided that they do not overlap.

e) Whatever may be the motions of the cluster centers and of the galaxies within the clusters, they can be neglected.

The last two postulates require some comments. Postulate *d* characterizes what we call "quasi-uniformity of a distribution." Ordinarily, when one speaks of statistical uniformity in space, one has in mind a distribution of points obtainable from a particular machinery of distributing these points. This machinery consists in dividing a bounded portion $\mathfrak{V}$ of the space into a finite but very large number N of elementary volumes $\mathfrak{v}$ of equal size. Then, in order to place a point P_1 in $\mathfrak{V}$, we select one of the elements $\mathfrak{v}$, with equal chance $1/N$ for each element, and place P_1 in the element selected. Once the point P_1 is placed, we proceed to place the next point, P_2, in exactly the same manner and without regard to the position assumed by P_1, etc. As is well known, if N and the number of points $P_1, P_2, \ldots$, are both large, then the distribution resulting from the above operations will conform with the law of Poisson: whatever be the volume $\mathfrak{V}^*$ partial to $\mathfrak{V}$, the probability that it will contain exactly n points P is given by the formula

$$e^{-\lambda}\frac{\lambda^n}{n!}, \tag{1}$$

where λ is a suitable constant. This machinery of distributing points P in the volume $\mathfrak{V}$ may be called the "Poisson machinery."

It will be seen that the Poisson machinery of distributing points possesses the characteristic of quasi-uniformity which we described. We discuss this point in some detail for the reason that the converse statement is not true, so that a quasi-uniform distribution of points need not necessarily be the Poisson distribution. In order to illustrate this circumstance, consider the following machinery of distributing points $P_1, P_2, \ldots$, in the volume $\mathfrak{V}$. As formerly, this volume $\mathfrak{V}$ is divided into a large number N of elements $\mathfrak{v}$ of equal size. Then a die is thrown, and the number d of dots on the upper face is noted. Further, out of the N elementary volumes, one is selected, with the probability of any particular selection equal to $1/N$. Then the first d points, $P_1, P_2, \ldots, P_d$, are put into the volume element selected. This process is then repeated many times. The machinery just described will satisfy postulate *d*. However, it is obviously not the Poisson machinery. It, and many similar machineries, produce what is known as *contagious* distributions of points—this in spite of the characteristic of quasi-uniformity.

The purpose of formulating postulate *d* in this particular form is to cover the possibility that the cluster centers are distributed in space independently of each other (that is, Poisson-wise) and also the possibility that they themselves are clustered. In the latter case the presence of a cluster center in a given volume would increase the probability that the volume includes some additional cluster centers.

Now we must comment on postulate *e*. Although not explicitly stated, postulates *a*–*d* refer to a particular moment of time, for example, to the moment of taking photographs. The galaxies photographed are generally at different distances from the observer and,

owing to the time spent by light in traveling to the observer, the positions and the apparent magnitudes of the individual galaxies photographed refer to different moments. Should the galaxies and/or the cluster centers have substantial velocities, then the distribution of their positions at these different times need not conform with postulates *a*–*d*, even though the distribution of simultaneous positions does. The purpose of postulate *e*, then, is to eliminate the consideration of this possibility. An alternative postulate might be one reflecting the hypothesis of an expanding universe.

The foregoing structural postulates are used below to obtain general forms of the distributions of galaxies on the photographic plate. In order to obtain these distributions numerically, it is necessary to adopt further hypotheses specializing the distributions mentioned in the structural postulates. These additional hypotheses are described as "secondary" postulates. They can be formulated in many different ways. Our attitude toward any particular function selected is that toward an interpolation formula. The final choice will depend upon comparison with observations. In the meantime, our preference is for as few parameters as possible combined with flexibility and simplicity in the formulae.[7]

II. PRELIMINARY REMARKS

Under this heading we combine certain known formulae of the calculus of probability which will be used frequently.

1. *Fundamental formula on conditional expectations.*—In the following we shall use frequently the fundamental formula connecting conditional and absolute expectations. Let X and Y be any two random variables. Let $E(Y \mid X = x)$ denote the conditional expectation of Y, given that the random variable X assumed a specified value x. Further, let $E(Y)$ denote the unconditional or absolute expectation of Y. We assume that both these expectations exist. Starting with $E(Y \mid X = x)$, we define a new random variable $E(Y \mid X)$ as follows: Whenever X assumes any value x, then $E(Y \mid X)$ assumes the value $E(Y \mid X = x)$. The fundamental formula mentioned is, then,

$$E(Y) = E\{E(Y \mid X)\}. \tag{2}$$

2. *Probability generating function.*—Let $X_1, X_2, \ldots, X_s$ be a set of s random variables, all capable of assuming only nonnegative integer values 0, 1, 2, ... Further, let $t_1, t_2, \ldots, t_s$ be arbitrary nonnegative numbers not exceeding unity. Then the probability generating function of $X_1, X_2, \ldots, X_s$ is defined as the expectation of the product $t_1^{X_1} t_2^{X_2} \ldots t_s^{X_s}$. The generic notation for the probability generating function is

$$\begin{aligned} G_{X_1, X_2, \ldots, X_s}(t_1, t_2, \ldots, t_s) &= E\left[\prod_{i=1}^{s} t_i^{X_i}\right] \\ &= \sum_{n_1=0}^{\infty} \sum_{n_2=0}^{\infty} \cdots \sum_{n_s=0}^{\infty} \prod_{i=1}^{s} t_i^{n_i} P\{(X_1 = n_1)(X_2 = n_2) \ldots (X_s = n_s)\}, \end{aligned} \tag{3}$$

where $P\{(X_1 = n_1)(X_2 = n_2) \ldots (X_s = n_s)\}$ denotes the probability that simultaneously $X_1 = n_1$, $X_2 = n_2, \ldots, X_s = n_s$ and where the multiple series in the right-hand side is uniformly convergent for $0 \leqq t_i \leqq 1$, $i = 1, 2, \ldots, s$.

A probability generating function is differentiable indefinitely with respect to all its arguments for $0 \leqq t_i < 1$, $i = 1, 2, \ldots, s$. The partial derivatives of the probability generating function are connected with the probabilities $P\{(X_1 = n_1)(X_2 = n_2) \ldots$

[7] The results obtained in connection with certain secondary postulates will be published in a subsequent paper by the authors and C. D. Shane.

$(X_s = n_s)\}$ and also with the moments and product moments of the variables $X_1, X_2, \ldots, X_s$. In fact, formula (3) implies that

$$P\{(X_1 = n_1)(X_2 = n_2)\ldots(X_s = n_s)\} = \frac{\partial^{n_1+n_2+\ldots+n_s}G}{\partial t_1^{n_1}\partial t_2^{n_2}\ldots\partial t_s^{n_s}}\Bigg|_{t_1=t_2=\ldots=t_s=0}\prod_{i=1}^{s}\frac{1}{n_i!}. \quad (4)$$

Also, if the derivative of the right-hand side of expression (4) exists at $t_1 = t_2 = \ldots = t_s = 1$, then

$$\frac{\partial^{n_1+n_2+\ldots+n_s}G}{\partial t_1^{n_1}\partial t_2^{n_2}\ldots\partial t_s^{n_s}}\Bigg|_{t_1=t_2=\ldots=t_s=1} = E\left\{\prod_{i=1}^{s}\frac{X_i!}{(X_i-n_i)!}\right\}. \quad (5)$$

Because of these properties, the study of distributions of random variables capable of assuming only nonnegative integer values is reducible to the study of the corresponding probability generating functions. This method was introduced by Laplace. A modern presentation referring to single variate distributions is given in a recent book by Feller.[8]

III. GENERAL STOCHASTIC MODEL OF THE SPATIAL DISTRIBUTION OF GALAXIES

In this section we restate in mathematical form the several structural postulates which underlie the stochastic model of the universe studied in this paper. However, it is convenient to change the order in which the postulates are listed.

POSTULATE 1.—*To every region* R *with volume* $\mathfrak{V}$ *there corresponds a random variable* $\gamma(R)$ *representing the number of cluster centers falling within* R. *The distribution of* $\gamma(R)$ *depends on the volume* $\mathfrak{V}$ *only.* It does not depend either on the shape of the region R or on its location.

The probability generating function of $\gamma(R)$ will be denoted $G_\gamma(t|\mathfrak{V})$.

POSTULATE 2.—*Whatever be the nonoverlapping regions* $R_1, R_2, R_3, \ldots$, *the corresponding random variables* $\gamma(R_j)$, $j = 1, 2, \ldots$, *are completely independent.*

Postulates 1 and 2 deal with the probability distribution of the *number* of cluster centers within any given region R in space. In the following it will be necessary to consider as random the position of a single cluster center, given that it is located in R. This appears to require a special postulate (postulate 3) to the general effect that, as far as their positions in R are concerned, all clusters are, in a sense, equivalent. Then postulates 1, 2, and 3 combine to imply that the position of any given cluster is random. This point is discussed in some detail in Section IV.

POSTULATE 3.—*Let* R *be an arbitrary region of positive volume* $\mathfrak{V} > 0$ *and* R_1 *an arbitrary part of* R. *If* R *is known to include exactly* $n > 1$ *cluster centers numbered* $C_1, C_2, \ldots, C_n$, *and if* $a_1 < a_2 < \ldots < a_m$ *is an arbitrary combination of* $m < n$ *numbers selected out of* $1, 2, \ldots, n$, *then the probability that* R_1 *will contain exactly* m *cluster centers and that these cluster centers will be* $C_{a_1}, C_{a_2}, \ldots, C_{a_m}$ *is independent of the combination* $a_1, a_2, \ldots, a_m$ *and is equal to the conditional probability that* $\gamma(R_1) = m$, *given that* $\gamma(R) = n$, *divided by the number of combinations of* m *objects out of the given* n.

We shall use the symbol $C_i \in R_1$ to denote that the cluster center C_i is included in R_1. Also the notation[9]

$$\prod_{i=1}^{m}(C_{a_i} \in R_1) = (C_{a_1} \in R_1)(C_{a_2} \in R_1)\ldots(C_{a_m} \in R_1) \quad (6)$$

[8] *Probability Theory and Its Applications* (New York: John Wiley & Sons, Inc., 1950).

[9] This notation is very convenient and was used in formula (3). The reader unaccustomed to it may wish to consult J. Neyman, *First Course in Probability and Statistics* (New York: Henry Holt & Co., 1950).

will denote the logical product of the m propositions $C_{a_i} \in R_1$ for $i = 1, 2, \ldots, m$. The meaning of this term is: All the cluster centers $C_{a_1}, C_{a_2}, \ldots, C_{a_m}$ are included in R_1.

With this notation, postulate 3 may be expressed by the formula

$$P\left\{\left[\gamma(R_1) = m\right] \prod_{i=1}^{m} (C_{a_i} \in R_1) \mid \gamma(R) = n\right\} = \frac{m!\,(n-m)!}{n!} P\{\gamma(R_1) = m \mid \gamma(R) = n\}. \tag{7}$$

POSTULATE 4.—*To every cluster center there corresponds a random variable ν, representing the number of galaxies belonging to this cluster. The distribution of ν is the same for all clusters.*

The probability generating function of ν will be denoted by $G_\nu(t)$.

POSTULATE 5.—*The random variables $\nu_1, \nu_2, \ldots, \nu_k, \ldots$, representing the numbers of galaxies in different clusters, are completely independent.*

Further below we shall need symbols to denote the co-ordinates of a cluster center and those of a galaxy, which we shall treat as a point. In cases where a *random cluster center* is considered, its co-ordinates will be treated as random variables and denoted by the capital letters U, V, W. The particular values assumed by these variables will be denoted by the corresponding lower-case letters u, v, w. Similarly, the random variables representing a *random galaxy* will be denoted by the capitals X, Y, Z, and the particular values of the variables by x, y, z. The co-ordinate axes will be assumed orthogonal, with their origin at the observer and with arbitrary directions.

POSTULATE 6.—*Given that the center of a cluster is at a specified point* (u, v, w), *the position of every galaxy belonging to this cluster is random and the probability density of its co-ordinates* X, Y, Z *is represented by a function* f (η) *depending only on the distance*

$$\eta = \{(x-u)^2 + (y-v)^2 + (z-w)^2\}^{1/2} \tag{8}$$

between the cluster center and the position of the galaxy. The function f(η) *is the same for all clusters and is continuous for all values of η.*

POSTULATE 7.—*Whatever be the galaxies* $g_1, g_2, \ldots, g_m, \ldots$, *whether belonging to the same cluster or not, the triplets of random variables* (X_m, Y_m, Z_m) *representing their co-ordinates,* $m = 1, 2, \ldots$, *are completely independent.*

The foregoing seven postulates determine what is considered to be the structure of the spatial distribution of galaxies. As such, of course, this distribution is unobservable. The following postulate 8 is meant to establish a link between the unobservable distribution of galaxies in space and what can be observed on photographic plates. It is convenient to make this link in two steps. First we consider an idealized photographic plate which, for any given observational setup, has a fixed limiting apparent magnitude, constant for the entire plate. If the apparent magnitude of a galaxy is less than this limiting magnitude, it will sometimes be convenient to say that this galaxy is "visible" in the observational setup considered. The relation between the numbers of galaxies visible on an idealized plate and the counts on actual plates is dealt with in a later paper by the authors jointly with C. D. Shane, in which empirical data are discussed.

POSTULATE 8.—*Given an observational setup, to every galaxy with co-ordinates* (x, y, z) *there corresponds a probability $\theta(\xi)$ that the apparent magnitude of this galaxy will be less than the limiting apparent magnitude of the idealized photographic plate. This probability depends only upon the distance*

$$\xi = \{x^2 + y^2 + z^2\}^{1/2} \tag{9}$$

to the galaxy and is continuous for all values of ξ.

It will be seen that, in order to obtain numerically the characteristics of the distribution of galaxies visible on photographic plates, many details of the foregoing general postulates will have to be specialized. Thus, for example, the probability $\theta(\xi)$ will have to be specialized in accordance with the limiting apparent magnitude of the idealized plate, with the assumed form of the distribution of absolute magnitudes of extragalactic nebulae, and with the effect of red shift. All these details are independent of the structural postulates. It is interesting, however, that postulates 1 and 2 do establish a limitation on the probability generating function $G_\gamma(t|\mathfrak{V})$ of the number of cluster centers falling in a region of volume $\mathfrak{V}$.

IV. IMPLICATIONS OF POSTULATES 1 AND 2

In this section we discuss briefly the general form of the probability generating function $G_\gamma(t|\mathfrak{V})$ as implied by the two postulates 1 and 2. Let R_1 and R_2 be two nonoverlapping regions of finite volumes $\mathfrak{V}_1$ and $\mathfrak{V}_2$, and let $R_1 \cup R_2$ be the union of R_1 and R_2. Finally, let γ_1, γ_2, and γ_3 stand for the numbers of cluster centers in R_1, R_2 and $R_1 \cup R_2$, respectively. Obviously, $\gamma_3 = \gamma_1 + \gamma_2$. Because of the independence of γ_1 and γ_2,

$$G_\gamma(t|\mathfrak{V}_1+\mathfrak{V}_2) \equiv G_\gamma(t|\mathfrak{V}_1)G_\gamma(t|\mathfrak{V}_2). \tag{10}$$

Equation (10), valid for all $\mathfrak{V}_1$ and $\mathfrak{V}_2$, is, then, a consequence of the assumption that the distribution of cluster centers is quasi-uniform. It is easy to see that the converse is also true and that every probability generating function depending on a parameter $\mathfrak{V}$, which satisfies condition (10), will determine a quasi-uniform distribution of cluster centers.

Distributions satisfying condition (10) were studied by Paul Lévy,[10] who termed them "infinitely divisible." It follows from Lévy's work that, for every $\mathfrak{V}$,

$$G_\gamma(t|\mathfrak{V}) = [G_\gamma(t|1)]^{\mathfrak{V}}, \tag{11}$$

so that, in order to know the probability generating function of $\gamma(R)$ corresponding to an arbitrary region of volume $\mathfrak{V}$, it is sufficient to know this distribution for $\mathfrak{V} = 1$.

It can be shown[11] that the function $G_\gamma(t|1)$ must be of the form

$$G_\gamma(t|1) = \exp\left\{-h_0+\sum_{k=1}^{\infty} h_k t^k\right\} = \exp\{h(t)\}, \text{ say}, \tag{12}$$

where $h_0, h_1, \ldots, h_k, \ldots$ are all nonnegative numbers subject to the restriction that the series $\sum_{k=1}^{\infty} h_k$ is convergent and that $\sum_{k=1}^{\infty} h_k = h_0$. Conversely, if the series formed by the nonnegative numbers $h_1, h_2, \ldots, h_k, \ldots$ is convergent and if its sum is equal to h_0, then the right-hand side of equation (12) represents a probability generating function such that, whatever $\mathfrak{V} \geqq 0$, the expression (11) is also a probability generating function. It will then satisfy equation (10). Incidentally, formulae (11) and (12) imply that, whatever $\mathfrak{V}$, the probability that the number of clusters $\gamma(R) = 0$ is necessarily a positive number.

If $h_2 = h_3 = \ldots = 0$, then equation (11) reduces to

$$G_\gamma(t|\mathfrak{V}) = e^{-\mathfrak{V}h_0(1-t)}, \tag{13}$$

which is the probability generating function of the Poisson distribution. On the other hand, if at least one of the h_k, for $k \geqq 2$, is positive, then, whatever $\mathfrak{V}$, the number of

[10] *Théorie de l'addition des variables aléatoires* (Paris: Gauthier-Villars, 1937).

[11] J. Neyman and E. L. Scott, in preparation.

cluster centers $\gamma(R)$ does not follow the Poisson law. However, it is interesting to notice that the most general distribution of $\gamma(R)$ is, in a sense, reducible to Poisson distributions.

To see this, denote by $\mu_1, \mu_2, \ldots, \mu_k, \ldots$ a sequence of completely independent Poisson variables with expectation of μ_k equal to $\mathfrak{V}h_k$ for $k = 1, 2, 3, \ldots$. Finally, let

$$\mu_0 = \sum_{k=1}^{\infty} k\,\mu_k . \tag{14}$$

Because of the independence of the μ_k, the probability generating function of μ_0 is equal to the product of the probability generating functions of products $k\mu_k$. Since the probability generating function of μ_k has the form (13), with h_k replacing h_0, it is obvious that the probability generating function of the product $k\mu_k$ is given by

$$e^{-\mathfrak{V}h_k(1-t^k)} . \tag{15}$$

It follows that the probability generating function of μ_0 is

$$\exp\Big[-\mathfrak{V} \sum_{k=1}^{\infty} h_k (1 - t^k) \Big] , \tag{16}$$

which, because of formulae (11) and (12) and because $h_0 = \sum_{k=1}^{\infty} h_k$, coincides with $G_\gamma(t|\mathfrak{V})$.

As a result of all this, we may state that the most general quasi-uniform distribution of cluster centers requires that the number $\gamma(R)$ be distributed as is the sum (15) of the Poisson variable μ_1 plus double the Poisson variable μ_2 plus triple the Poisson variable μ_3 and so forth.

Formulae (11) and (12) imply that, if the expectation of $\gamma(R)$ exists, then the function $h(t)$ is differentiable at $t = 1$ and $E[\gamma(R)] = \mathfrak{V}h'(1)$, so that the derivative $h'(1)$ represents the average number of cluster centers per unit volume.

As mentioned above, when it is given that an arbitrary region R of volume $\mathfrak{V} > 0$ contains exactly $n > 0$ cluster centers, postulates 1, 2, and 3 imply that the co-ordinates U_i, V_i, and W_i of the ith cluster center are random variables. The joint probability distribution of all such triplets has interesting properties, some of which depend on the function $h(t)$. One of the properties is needed in the present paper and will be quoted without proof as follows.

Whatever be the quasi-uniform distribution of cluster centers and whatever be the number $\mathrm{n} \geqq 1$ *of cluster centers known to be contained in a region* R *of finite volume* $\mathfrak{V} > 0$, *the conditional probability density function, given* n, *of the co-ordinates* U, V, W *of any one of these cluster centers taken separately is constant over the region* R *and, therefore, is equal to* $1/\mathfrak{V}$.

Another property of the distribution which is of particular interest may be stated as follows.

Given that the region R *of volume* $\mathfrak{V} > 0$ *contains exactly* $\mathrm{n} > 1$ *cluster centers, say* C_1, $C_2, \ldots, C_n$, *such that* $P\{\gamma(R) = n | \mathfrak{V}\} > 0$, *the conditional probability* π_k *that exactly* k *out of the cluster centers* $C_2, C_3, \ldots, C_n$ *will coincide with* C_1 *is given by the formula,*

$$\pi_k = \frac{(k+1)\,h_{k+1}P\{\gamma(R) = n-k-1 \,|\, \mathfrak{V}\}}{\sum_{m=0}^{n-1} (m+1)\,h_{m+1}P\{\gamma(R) = n-m-1 \,|\, \mathfrak{V}\}} , \tag{17}$$

$$\text{for} \qquad k = 0, 1, \ldots, n-1 .$$

It is seen that, if any of the numbers $h_2, h_3, \ldots, h_n$ is positive, then this probability may be positive. In particular, if $h_1 = h_2 = \ldots = h_{n-1} = 0$, but $h_n > 0$, then $\pi_{n-1} = 1$. This means that, in this case, all the n cluster centers present in R will coincide or, in other words, that, instead of n distinct cluster centers, there will be just one multiple cluster center of multiplicity n.

The final picture, then, of the quasi-uniform distribution of cluster centers is that, in the general case, it contains a Poisson distribution of *single* clusters with the expected number of cluster centers per unit volume equal to h_1. In addition, it contains a Poisson distribution, independent of the first, of *double* clusters with the expectation of the number of centers per unit volume equal to h_2. In addition, there will be Poisson distributions of cluster centers of *triple*, *quadruple*, etc., clusters, all completely independent. If $h_k = 0$, then there will be no clusters of multiplicity k. In particular, if $h_2 = h_3 = \ldots = 0$, then all the clusters will be single clusters.

Proofs of these properties of the general quasi-uniform distribution must be relegated to a separate publication in a statistical journal.[11] Some of these properties are foreshadowed in the work of Paul Lévy already quoted.

V. JOINT DISTRIBUTION OF THE NUMBERS N_1 AND N_2 OF GALAXIES VISIBLE WITHIN TWO ARBITRARY SOLID ANGLES

Consider two arbitrary regions, ω_1 and ω_2, overlapping or not, which will be photographed on idealized plates. The same letters ω_1 and ω_2 will be used to denote the two solid angles, with vertices at the observer, corresponding to these regions. The observational setups for the two regions may be the same or not, so that the limiting magnitude m_1 of the photograph of ω_1 need not be the same as the limiting magnitude m_2 of the photograph of ω_2. For convenience, we shall assume $m_1 \leqq m_2$.

Denote by N_1 and N_2 two random variables representing, respectively, the numbers of galaxies visible on photographs taken over ω_1 and ω_2. The purpose of this section is to deduce the joint probability generating function $G_{N_1, N_2}(t_1, t_2)$ of N_1 and N_2 as implied by the eight structural postulates enumerated above.

Briefly, the method used consists in dividing the whole space into an infinity of bounded regions of convenient shape. Each region will contain a certain number of cluster centers. Galaxies from the corresponding clusters may fall and be visible either in ω_1 or in ω_2 or in both. Thus N_1 and N_2 are represented as sums of contributions from each of the regions contemplated. Further, the contribution of each particular region is split into as many components as there are cluster centers in this region, so that N_1 and N_2 appear as double sums. The advantage of this procedure is that, according to the postulates adopted, the contribution to N_1 of any one particular cluster is independent of that of any other cluster, so that N_1 appears as the sum of completely independent components. The same applies to N_2. It is noteworthy, however, that the contributions to N_1 and N_2 from any one cluster are dependent.

After this general description, we may proceed to details. Let Δ be an arbitrary positive number which we shall later make tend to zero. Divide the whole space into an infinity of equal cubes $R_1, R_2, \ldots, R_j, \ldots$, of dimensions Δ, by passing three sequences of planes distant by Δ, each sequence parallel to one of the co-ordinate planes. The cubes R_j will be described as the elementary cubes of dimensions Δ. The order in which they are numbered is immaterial. Obviously, the volume is the same, equal to Δ^3.

Simplifying the notation adopted earlier, we shall use the symbol γ_j to denote the number of cluster centers in R_j. Assume for a moment that $\gamma_j > 0$ and consider the kth cluster center in R_j. Denote by N_{1jk} the number of galaxies visible in ω_1 which belong to the kth cluster centered in R_j. Similarly, N_{2jk} will denote the number of galaxies visible in ω_2 which belong to the same kth cluster centered in R_j. In further work it will be convenient to consider the variables N_{1jk} and N_{2jk} for $k = 0$. In order to do so, we shall adopt the convention $N_{1j0} = N_{2j0} \equiv 0$.

With this convention, N_1 and N_2 may be represented as sums of infinitely many components of the type, say,

$$N_{ij} = \sum_{k=0}^{\gamma_j} N_{ijk} \qquad \text{for} \qquad i = 1, 2 . \tag{18}$$

Obviously, N_{ij} represents the contribution to N_i of all the clusters centered in R_j and is equal to the sum on the right of formula (18), whether γ_j is zero or not. The postulates adopted imply that the couples of random variables (N_{11}, N_{21}), (N_{12}, N_{22}), . . . , (N_{1j}, N_{2j}), . . . are completely independent. Taking this into account and noting that

$$N_i = \sum_{j=1}^{\infty} N_{ij} , \qquad \text{for} \qquad i = 1, 2 , \tag{19}$$

we may write

$$G_{N_1, N_2}(t_1, t_2) = \prod_{j=1}^{\infty} G_{N_{1j}, N_{2j}}(t_1, t_2) . \tag{20}$$

Thus, in order to compute the joint probability generating function of N_1 and N_2, it is sufficient to compute that of the jth components (18) and to evaluate the infinite product on the right-hand side of equation (20).

In order to compute the probability generating function of N_{1j} and N_{2j}, we start with the definition and then apply formula (2), which connects absolute and conditional expectations:

$$G_{N_{1j}, N_{2j}}(t_1, t_2) = E(t_1^{N_{1j}} t_2^{N_{2j}}) = E[E(t_1^{N_{1j}} t_2^{N_{2j}} \mid \gamma_j)] . \tag{21}$$

If γ_j is zero, then $N_{1j} = N_{2j} = 0$. Otherwise, N_{1j} and N_{2j} are sums of the same number γ_j of components N_{1jk} and N_{2jk}, respectively. Each pair (N_{1jk}, N_{2jk}) represents the contributions to N_1 and N_2 from the kth cluster centered in R_j. The postulates adopted imply that all the γ_j pairs are completely independent. Also, the distribution of each of the γ_j clusters is exactly the same. Therefore, the joint distribution of each pair (N_{1jk}, N_{2jk}) must be the same, coinciding with that of (N_{1j1}, N_{2j1}), say. For these reasons, whether γ_j has a positive value or is zero,

$$E(t_1^{N_{1j}} t_2^{N_{2j}} \mid \gamma_j) = [G_{N_{1j1}, N_{2j1}}(t_1, t_2)]^{\gamma_j} ; \tag{22}$$

and formula (21) may be rewritten as

$$G_{N_{1j}, N_{2j}}(t_1, t_2) = E\{[G_{N_{1j1}, N_{2j1}}(t_1, t_2)]^{\gamma_j}\} . \tag{23}$$

Here $G_{N_{1j1}, N_{2j1}}(t_1, t_2)$ represents the joint probability generating function of the contributions N_{1j1} to N_1 and N_{2j1} to N_2 of any one of the clusters known to have its center in the elementary cube R_j. Referring to the definition of the probability generating function of the variable γ_j corresponding to R_j, it is easy to see that formula (23) implies

$$G_{N_{1j}, N_{2j}}(t_1, t_2) = G_\gamma[G_{N_{1j1}, N_{2j1}}(t_1, t_2) \mid \Delta^3] \tag{24}$$

or, using formulae (11) and (12),

$$G_{N_{1j}, N_{2j}}(t_1, t_2) = \exp\{\Delta^3 h[G_{N_{1j1}, N_{2j1}}(t_1, t_2)]\} . \tag{25}$$

Thus, in order to compute the joint probability generating function of N_{1j} and N_{2j}, it is sufficient to compute that of a single pair of components (N_{1j1}, N_{2j1}) and substitute the result for the argument of the probability generating function of γ_j.

Using formulas (20) and (25), we have

$$G_{N_1,\ N_2}(t_1,\ t_2)\ =\exp\{\Delta^3\sum_{j=1}^{\infty}h\,[G_{N_{1j1},\ N_{2j1}}(t_1,\ t_2)]\}. \tag{26}$$

The general form of $G_{N_{1j_1},\ N_{2j_1}}(t_1,\ t_2)$ will be obtained in the next section. Here we shall notice that the series on the right-hand side of formula (26) need not be convergent. However, the cases of divergence are easily interpreted. Owing to the particular meaning (3) of a probability generating function and because $h(t) \leqq 0$, if the series diverges at $t_1 = t_2 = 0$, this means simply that $P\{(N_1 = 0)(N_2 = 0)\} = 0$. If the same series diverges for $t_1 t_2 > 0$, then all the probabilities $P\{(N_1 = n_1)(N_2 = n_2)\} = 0$ for *all* values of $n_1, n_2 = 0, 1, 2, \ldots$. This is interpreted to mean that, in this particular case, the probability that there will be an infinite number of visible galaxies in at least one of the solid angles ω_1 and ω_2 is unity. While these and similar cases are theoretically possible, since they do not correspond to empirical facts, we shall consider only such functions $h(t)$, $G\gamma(t)$, $f(\eta)$, and $\theta(\xi)$ with which the series on the right is convergent for all values of t_1 and t_2, $0 \leqq t_1, t_2 \leqq 1$, and, therefore, formula (26) is different from zero.

VI. FINAL FORM OF $G_{N_1,\ N_2}(t_1,\ t_2)$

The probability generating function of the variables N_{1j1}, N_{2j1} is obtained by using certain considerations of a character somewhat different from those above. For this reason it was thought useful to treat the problem in a separate section. The elementary cube R_j may contain a number of cluster centers. However, we are now interested in only one of them, namely, the first. The letters U, V, W will be used to denote the co-ordinates of its center so long as these co-ordinates remain random. The letters u, v, w will be used to denote the particular values that U, V, and W may assume. The random variable representing the number of galaxies in the cluster will be denoted by ν. We begin with the definition of the probability generating function and apply formula (2) twice. First we write

$$G_{N_{1j1},\ N_{2j1}}(t_1,\ t_2)\ =E\,(t_1^{N_{1j1}}t_2^{N_{2j1}})\ =E\,[E\,(t_1^{N_{1j1}}t_2^{N_{2j1}}\,|\,U,\ V,\ W)\,]. \tag{27}$$

Next we consider a fixed system of values u, v, w and consider

$$E\,(t_1^{N_{1j1}}t_2^{N_{2j1}}\,|\,u,\ v,\ w)\ =E\,[E\,(t_1^{N_{1j1}}t_2^{N_{2j1}}\,|\,u,\ v,\ w,\ \nu)\,]. \tag{28}$$

In order to proceed further, we consider the mth galaxy of the cluster and two random variables α_m and β_m defined as follows: If the galaxy falls in the solid angle ω_1 and is visible in it, then $\alpha_m = 1$. Otherwise, $\alpha_m = 0$. If the mth galaxy falls in the solid angle ω_2 and is visible there, then $\beta_m = 1$. Otherwise, $\beta_m = 0$. Obviously, the random variables α_m and β_m are dependent. Because of postulate 6, the joint distribution of (α_m, β_m) is the same for all $m = 1, 2, \ldots, \nu$. Also, because of postulate 7, all the couples (α_1, β_1), $(\alpha_2, \beta_2), \ldots, (\alpha_\nu, \beta_\nu)$ are completely independent. Finally, given a fixed value of $\nu > 0$,

$$N_{1j1} = \sum_{m=1}^{\nu}\alpha_m\,, \qquad N_{2j1} = \sum_{m=1}^{\nu}\beta_m\,. \tag{29}$$

Repeating the reasoning which now must be familiar to the reader, we find that

$$E\,(t_1^{N_{1j1}}t_2^{N_{2j1}}\,|\,U,\ V,\ W)\ =G_\nu\,[G_{\alpha_1,\ \beta_1}(t_1,\ t_2\,|\,U,\ V,\ W)\,]. \tag{30}$$

In postulate 8 we introduced the probability that the apparent magnitude of a galaxy at distance ξ from the observer will be less than the limiting magnitude of the idealized

plate. Because the observational setups used to photograph the regions ω_1 and ω_2 need not be the same, it is necessary to make a distinction between $\theta_1(\xi)$ and $\theta_2(\xi)$ corresponding to the setups to be used for regions ω_1 and ω_2, respectively.

In order to compute the probability generating function of α_1 and β_1, given that the co-ordinates of the corresponding cluster are u, v, w, denote by $\omega_1\omega_2$ the common part of the solid angles ω_1 and ω_2 and introduce the following probabilities.

Let $p_1(u, v, w)$ denote the probability that a galaxy from a cluster centered at (u, v, w) will be visible on the plate taken over the region ω_1 but not on the plate taken over ω_2. Because we have assumed that the limiting magnitude $m_1 \leqq m_2$, we have

$$p_1(u, v, w) = \iiint_{\omega_1 - \omega_1\omega_2} f(\eta)\, \theta_1(\xi)\, dx\,dy\,dz\,. \tag{31}$$

Let $p_2(u, v, w)$ denote the probability that a galaxy from a cluster centered at (u, v, w) will be visible on the plate taken over ω_2 but not on that taken over ω_1. Obviously,

$$p_2(u, v, w) = \iiint_{\omega_2 - \omega_1\omega_2} f(\eta)\, \theta_2(\xi)\, dx\,dy\,dz + \iiint_{\omega_1\omega_2} f(\eta)\,[\theta_2(\xi) - \theta_1(\xi)]\, dx\,dy\,dz\,. \tag{32}$$

Finally, let $p_3(u, v, w)$ denote the probability that a galaxy from a cluster centered at (u, v, w) will be visible on both plates,

$$p_3(u, v, w) = \iiint_{\omega_1\omega_2} f(\eta)\, \theta_1(\xi)\, dx\,dy\,dz\,. \tag{33}$$

As mentioned, the present general statement of the problem is meant to apply to two kinds of practical situations. In the first we contemplate counts of nebulae in nonoverlapping regions photographed with the same instrument, so that $\theta_1(\xi) \equiv \theta_2(\xi)$. In this case $\omega_1\omega_2$ is empty, and the integrals over this region are zero. The second situation contemplated is that in which the photographs are taken with different instruments. The most important case of this category is when ω_1 and ω_2 coincide and thus coincide with their common part $\omega_1\omega_2$. In this case the integrals taken over $\omega_1 - \omega_1\omega_2$ and over $\omega_2 - \omega_1\omega_2$ are equal to zero, so that, in particular, $p_1(u, v, w) = 0$.

Using the probabilities (31), (32), and (33), the probability generating function of α_1 and β_1 is obtained easily. In so doing, for the sake of brevity, we shall omit the reference to (u, v, w) from the symbols of the three probabilities. We obtain

$$G_{\alpha_1, \beta_1}(t_1, t_2) = 1 - p_1(1 - t_1) - p_2(1 - t_2) - p_3(1 - t_1t_2) \tag{34}$$

and, therefore, using formula (30),

$$E(t_1^{N_{1j1}} t_2^{N_{2j1}} \mid u, v, w) = G_\nu[1 - p_1(1 - t_1) - p_2(1 - t_2) - p_3(1 - t_1t_2)]\,. \tag{35}$$

In order to obtain the probability generating function of N_{1j1} and N_{2j1}, we use formula (27) and the result quoted at the end of Section IV to the effect that, given that a cluster center is contained in the region R_j of volume $\Delta^3 > 0$, the probability density of the co-ordinates of the cluster center is constant over R_j and equal to $1/\Delta^3$. Thus we have

$$G_{N_{1j1}, N_{2j1}}(t_1, t_2) = \frac{1}{\Delta^3} \iiint_{R_j} G_\nu[1 - p_1(1 - t_1) - p_2(1 - t_2) - p_3(1 - t_1t_2)]\, du\,dv\,dw\,. \tag{36}$$

This formula may now be substituted in formula (26) to obtain the probability generating function of N_1 and N_2. However, before doing so, it is convenient to use the assumption that the function $f(\eta)$, representing the probability density of the co-ordinates of a galaxy, and also $\theta_1(\xi)$ and $\theta_2(\xi)$ are continuous and to apply the mean-value theorem to formula (36). Namely, the region R_j must contain at least one point, say (u_j, v_j, w_j) such that the value of formula (36) is equal to the integrand evaluated at this particular point. Denote

$$p_i(u_j, v_j, w_j) = p_{ij} \quad \text{for} \quad i = 1, 2, 3 . \tag{37}$$

Then

$$G_{N_{1j}, N_{2j}}(t_1, t_2) = G_r[1 - p_{1j}(1 - t_1) - p_{2j}(1 - t_2) - p_{3j}(1 - t_1 t_2)] . \tag{38}$$

Substituting this result in equation (25), we obtain

$$G_{N_1, N_2}(t_1, t_2)$$

$$= \exp\left\{\Delta^3 \sum_{j=1}^{\infty} h(G_r[1 - p_{1j}(1 - t_1) - p_{2j}(1 - t_2) - p_{3j}(1 - t_1 t_2)])\right\} . \tag{39}$$

This formula is valid, irrespective of the value of Δ. Using the assumption that the series on the right is convergent for all values of t_1 and t_2, it is easy to see that, as $\Delta \to 0$, the series in the right-hand side, multiplied by Δ^3, converges to a triple integral over the whole space, so that

$$G_{N_1, N_2}(t_1, t_2) = e^{\psi(t_1, t_2)} \tag{40}$$

with

$$\psi(t_1, t_2) = \int_{-\infty}^{+\infty}\int\int h\{G_r[1 - p_1(1 - t_1) - p_2(1 - t_2) - p_3(1 - t_1 t_2)]\}\, du\, dv\, dw , \tag{41}$$

where the symbols p_1, p_2, p_3 have the meaning defined in formulae (31), (32), and (33), respectively.

Formulae (40) and (41) determine the probability generating function of N_1 and N_2 in its final form. With the functions $h(t)$, $G_r(t)$, $f(\eta)$, and $\theta(\xi)$ not specialized, formulae (40) and (41) reflect only the general structure of the universe contemplated and not the details considered unimportant. For this reason, the properties of formula (40) which are independent of the unspecified functions are of particular interest.

VII. MOMENTS OF N_1 AND N_2

In the present section we use formula (41) to deduce general expressions for the moments and product moments of N_1 and N_2 in terms of the functions $h(t)$, $G_r(t)$, $f(\eta)$, and $\theta(\xi)$. The formulae so deduced reveal certain interesting properties of the variables N_1 and N_2 which are independent of the particular forms that the four functions may possess. Of course, in order to deal with these expressions, it is necessary to assume that the moments exist. This assumption appears very plausible and will be adopted from now on. More specifically, we shall limit our consideration to functions $h(t)$ and $G_r(t)$ which are indefinitely differentiable at $t = 1$.

In Section II we mentioned that the derivatives of the probability generating function evaluated at $t_1 = t_2 = \ldots = t_s = 1$ are connected with the moments of the variables concerned. A similar statement applies to the natural logarithm of the probability generating function. Since formula (41) involves two such logarithms, namely, $\psi(t_1, t_2)$ and $h(t)$, further work will be simplified if the connection between the moments and the derivatives of the logarithm of the probability generating function is given explicitly. The derivation of the formulae is elementary and therefore not given here. The formulae

reproduced refer to $\psi(t_1, t_2)$, but the reader will have no difficulty in applying them to $h(t)$ by analogy. Although not explicitly marked, all the derivatives appearing in the formulae are assumed to be evaluated at both arguments equal to unity. The symbol σ_{rs} will be used to denote the central product moment of order r with respect to N_1 and of order s with respect to N_2, so that

$$\sigma_{rs} = E\{[N_1 - E(N_1)]^r [N_2 - E(N_2)]^s\} \tag{42}$$

for $r, s = 0, 1, 2, \ldots$. With this notation, σ_{20} stands for the variance of N_1, etc. We have

$$\frac{\partial \psi}{\partial t_i} = E(N_i), \qquad i = 1 \quad 2, \tag{43}$$

$$\frac{\partial^2 \psi}{\partial t_1^2} = \sigma_{20} - E(N_1), \tag{44}$$

and a similar expression for $\partial^2\psi/\partial t_2^2$:

$$\frac{\partial^2 \psi}{\partial t_1 \partial t_2} = \sigma_{11}, \tag{45}$$

$$\frac{\partial^3 \psi}{\partial t_1^3} = \sigma_{30} - 3\sigma_{20} + 2E(N_1), \tag{46}$$

$$\frac{\partial^3 \psi}{\partial t_1^2 \partial t_2} = \sigma_{21} - \sigma_{11}, \text{ etc.} \tag{47}$$

The product moments σ_{rs} may be estimated from empirical data.

We now return to the expression for $\psi(t_1, t_2)$ given in formula (41) and compute the successive partial derivatives with respect to t_1 and t_2, substituting each time $t_1 = t_2 = 1$. In so doing, it will be convenient to write h_j and G_j for the jth derivatives of $h(t)$ and $G_\nu(t)$, respectively, evaluated at $t = 1$, and to write R_{kmn} for the triple integral

$$R_{kmn} = \int\int\int_{-\infty}^{+\infty} (p_1 + p_3)^k (p_2 + p_3)^m p_3^n \, du \, dv \, dw. \tag{48}$$

Notice that the substitution of $t_1 = t_2 = 1$ into formula (41) reduces the arguments of both G_ν and h to unity.

Taking derivatives of the first order, we obtain

$$E(N_1) = A_1 R_{100}, \qquad E(N_2) = A_1 R_{010}, \tag{49}$$

where

$$A_1 = h_1 G_1. \tag{50}$$

Derivatives of the second order yield the following three formulae:

$$\sigma_{20} - E(N_1) = A_2 R_{200}, \tag{51}$$

$$\sigma_{11} = A_2 R_{110} + A_1 R_{001} \tag{52}$$

$$\sigma_{02} - E(N_2) = A_2 R_{020}, \tag{53}$$

where, for the sake of brevity,

$$A_2 = h_2 G_1^2 + h_1 G_2. \tag{54}$$

Taking derivatives of the third order, we obtain

$$\sigma_{30} - 3\sigma_{20} + 2E(N_1) = A_3 R_{300}, \tag{55}$$

$$\sigma_{21} - \sigma_{11} = A_3 R_{210} + A_2 R_{101}, \tag{56}$$

$$\sigma_{12} - \sigma_{11} = A_3 R_{120} + A_2 R_{011} \tag{57}$$

$$\sigma_{03} - 3\sigma_{02} + 2E(N_2) = A_3 R_{030}, \tag{58}$$

where

$$A_3 = h_3 G_1^3 + 3 h_2 G_1 G_2 + h_1 G_3 . \tag{59}$$

The sequence of these equations can be continued indefinitely. However, the foregoing formulae are sufficient to give an idea of the nature of all the equations obtainable in this manner. The expressions on the left-hand sides are combinations of moments of N_1 and N_2 and, therefore, can be estimated from empirical data. The expressions on the right-hand side are products or sums of products of quantities of two different kinds. First, there are quantities A_j expressible in terms of h_i and G_i and thus, ultimately, in terms of moments of the variables γ and ν. It is important to notice that the A_j's are independent of the internal structure of the clusters, which is governed by the function $f(\eta)$, and of the distribution of apparent magnitude of galaxies, as reflected in the function $\theta(\xi)$. Also, the quantities A_j are independent of the regions ω_1 and ω_2.

The other kind of quantity appearing on the right-hand side of the equations are the triple integrals R_{kmn}. The simplest of these integrals, namely, R_{100}, R_{010}, and R_{001}, depend on the function $\theta(\xi)$ and on the regions ω_1 and ω_2 but not on anything else. In fact,

$$R_{100} = \iiint_{\omega_1} \theta_1(\xi)\, dx\, dy\, dz, \tag{60}$$

$$R_{010} = \iiint_{\omega_2} \theta_2(\xi)\, dx\, dy\, dz, \tag{61}$$

$$R_{001} = \iiint_{\omega_1 \omega_2} \theta_1(\xi)\, dx\, dy\, dz. \tag{62}$$

It will be sufficient to prove only one of these formulae, for example, the first. Referring to formulae (31) and (33), we have

$$p_1 + p_3 = \iiint_{\omega_1} f(\eta)\, \theta_1(\xi)\, dx\, dy\, dz, \tag{63}$$

and R_{100} is defined as the integral of this quantity with respect to u, v, w taken from $-\infty$ to $+\infty$ for each of the three variables. Now the variables u, v, w enter into formula (63) only through η. Therefore, changing the order of integration, we obtain

$$R_{100} = \iiint_{\omega_1} \left\{ \theta_1(\xi) \int_{-\infty}^{+\infty} \iiint f(\eta)\, du\, dv\, dw \right\} dx\, dy\, dz; \tag{64}$$

and it is easy to show that the internal triple integral is equal to unity regardless of the particular form of the function

$$f(\eta) = f\{[(x-u)^2 + (y-v)^2 + (z-w)^2]^{1/2}\}, \tag{65}$$

which, it will be remembered, represents the probability density of the co-ordinates of a galaxy belonging to a cluster centered at (u, v, w). This particular property of the function $f(\eta)$ implies that, whatever be u, v, w, the integral of $f(\eta)$ with respect to x, y, z, taken from $-\infty$ to $+\infty$ for each variable, must be equal to unity. Making the substitution

$$u = x + x' , \qquad y = y + y' , \qquad w = z + z' , \tag{66}$$

where x', y', and z' are new variables of integration, the internal integral in formula (64) is reduced to

$$\int_{-\infty}^{+\infty}\int\int f\{[x'^2 + y'^2 + z'^2]^{1/2}\}\, dx'\, dy'\, dz' = 1 , \tag{67}$$

which, combined with formula (64), proves formula (60). Formulae (61) and (62) are proved in exactly the same manner.

If it is assumed that the apparent luminosity of the galaxies varies inversely as the square of their distance (thus, if one ignores "red shift") and that the absolute magnitude of the galaxies is a random variable independent of the distance, then the functions $\theta_1(\xi)$ and $\theta_2(\xi)$ are relatively simple, and the integrals (59)–(61) can be evaluated as explicit functions of the limiting apparent magnitude. The resulting formula for $E(N_i)$ is well known.[12] Ordinarily, it is deduced on the assumption that the luminous objects (stars or galaxies) are distributed in space Poisson-wise. It is interesting that the same formula appears to hold on the more general assumption that the galaxies appear in clusters and that the cluster centers are quasi-uniformly distributed in space.

If the effect of red shift is taken into account, then the function $\theta(\xi)$ becomes complicated, and the values of R_{100}, R_{010}, and R_{001} must be obtained by numerical integration. The integrals R_{kmn} with $k + m + n > 1$ depend essentially not only on $\theta(\xi)$ but also on $f(\eta)$. In general, their evaluation appears to require numerical integration.

Perusing formulae (49)–(58), we see that they can be combined so as to eliminate the quantities A_j. The equations resulting from such eliminations connect the integrals R_{kmn} directly with the moments of N_1 and N_2. Thus, for example, combining formulae (49)–(53), we obtain, say,

$$\begin{aligned} Q(\omega_1, \omega_2) &\equiv \frac{R_{110}}{\{R_{200}R_{020}\}^{1/2}} \\ &= \frac{\sigma_{11}R_{100} - E(N_1)R_{001}}{R_{100}\{[\sigma_{20} - E(N_1)][\sigma_{02} - E(N_2)]\}^{1/2}} , \end{aligned} \tag{68}$$

which is an equation containing only integrals R_{kmn} and the moments of N_1 and N_2. Similar equations can be obtained by eliminating A_2 and A_3 from formulae (51) and (55)–(58).

The existence of relations between the integrals R_{kmn} and the moments of N_1 and N_2 is a very important fact because it creates the possibility of studying the internal structure of the clusters, more specifically, the functions $f(\eta)$ and $\theta(\xi)$, in a manner which is independent of how the cluster centers are distributed in space and independent of the variation of the number of galaxies from one cluster to another. While details of this study must be relegated to a later paper, some indications as to how this can be achieved are given in Section IX.

Returning to the quantities A_j, we see that they represent derivatives at $t = 1$ of the function $h[G_r(t)]$. This function can be interpreted as the logarithm of the probability generating function of the random variable ζ defined to be the total number of galaxies

[12] W. M. Smart, *Stellar Dynamics* (London: Cambridge University Press, 1938), p. 263.

belonging to all the clusters which have their centers in a specified region of unit volume. Once reasonable approximations to the functions $f(\eta)$ and $\theta(\xi)$ have been determined and given a substantial set of empirical material, any number of moments A_j can be obtained from equations such as (49)–(58). The estimates of these moments can then be used to approximate the distribution of ζ. Although of interest, ζ is not what one might consider a basic concept in the structure of the universe contemplated. Instead, our interest is directed toward the variables γ and ν.

Since the moments of A_j are simple combinations of quantities h_i and G_i, which, in turn, are simple functions of the moments of γ and ν, one might hope that knowledge of the moments A_j for $j = 1, 2, \ldots, s$ would make possible the evaluation of at least a few of the moments of γ and ν taken separately. Unfortunately, this is not the case because each A_j depends on both of the quantities h_j and G_j, which do not appear in $A_1, A_2, \ldots, A_{j-1}$. Thus, even with the knowledge of the functions $f(\eta)$ and $\theta(\xi)$, unless independent information regarding the distribution of γ and ν is obtained from other sources, no separate moments of γ and ν can be determined from any finite set of moments of N_1 and N_2. The next section gives an even stronger result to the same general effect.

VIII. NONIDENTIFIABILITY OF THE DISTRIBUTION OF CLUSTER CENTERS

In the present section we shall show that the same joint distribution of N_1 and N_2 can result from an infinity of different pairs of distributions of γ and ν and that, therefore, knowledge of the joint distribution of N_1 and N_2 is not sufficient to determine the distributions of γ and ν separately.

For this purpose we return to formula (41) and notice that the integrand depends not on the functions $h(t)$ and $G_\nu(t)$ taken individually but rather on the result of substituting $G_\nu(t)$ instead of the argument in $h(t)$. Thus the probability generating function $G_{N_1, N_2}(t_1, t_2)$ depends on the nature of the function, say,

$$H(t) = h[G_\nu(t)]. \tag{69}$$

Hence, if the two functions $h(t)$ and $G_\nu(t)$ are replaced by any other two functions, say, $h^*(t)$ and $G_\nu^*(t)$, such that, however,

$$h^*[G_\nu^*(t)] \equiv h[G_\nu(t)], \tag{70}$$

then this change will not produce any change in the joint distribution of N_1 and N_2. The existence of functions $h^*(t)$ and $G_\nu^*(t)$ having the above property is assured by the following theorem.

THEOREM.—*Whatever be the (infinitely divisible) distribution of γ with probability generating function*

$$G_\gamma(t \mid \mathfrak{V} = 1) = e^{h(t)}, \tag{71}$$

where

$$h(t) = -h_0 + \sum_{k=1}^{\infty} h_k t^k, \tag{72}$$

with $h_k \geqq 0$, $k = 0, 1, \ldots$ and $h(1) = 0$, and whatever be the distribution of ν, with probability generating function $G_\nu(t)$, there exists an infinity of Poisson laws with probability generating functions, say,

$$G_\gamma^*(t \mid \lambda) = e^{\lambda(t-1)}, \tag{73}$$

where λ is any positive number exceeding a certain limit λ_0, and a set of corresponding probability generating functions $G_\nu^*(t \mid \lambda)$ such that

$$G_\gamma[G_\nu(t) \mid \mathfrak{V} = 1] \equiv G_\gamma^*[G_\nu^*(t \mid \lambda) \mid \lambda]. \tag{74}$$

Proof.—In order to prove formula (74), we use equation (73) with the parameter λ unspecified, substitute it in (74), and take the logarithms of both sides. Using formulae (69) and (71), the identity to be proved is reduced to

$$H(t) = h[G_\nu(t)] = -h_0 + \sum_{k=1}^{\infty} h_k [G_\nu(t)]^k \equiv \lambda [G_\nu^*(t \mid \lambda) - 1] \tag{75}$$

or to

$$G_\nu^*(t \mid \lambda) \equiv 1 + \frac{1}{\lambda} H(t). \tag{76}$$

It is seen that every value of $\lambda > 0$ determines a corresponding function $G_\nu^*(t \mid \lambda)$. In order to complete the proof of the theorem, we have to show that formula (76) is a probability generating function. We shall show that this is true for an infinity of values of λ—in fact, for all values of λ which exceed a certain limit λ_0.

In order that formula (76) may be a probability generating function, it must have the following properties:

(i) $$G_\nu^*(1 \mid \lambda) = 1,$$

(ii) $$G_\nu^*(0 \mid \lambda) \geqq 0,$$

(iii) $$\frac{d^m G_\nu^*(t \mid \lambda)}{dt^m}\Big|_{t=0} \geqq 0 \qquad \text{for} \qquad m = 1, 2, \ldots.$$

In order to see that formula (i) is satisfied, we substitute $t = 1$ in formula (76) and then refer to formula (75). Since $G_\nu(1)$ is necessarily unity and since $h(1) = 0$, we obtain $H(1) = 0$ and formula (i) follows.

Proceeding to property (ii), we substitute $t = 0$ in formula (76) and again refer to (75). Since $G_\nu(0) = P\{\nu = 0\} = p_0$, say, we have

$$G_\nu^*(0 \mid \lambda) = 1 + \frac{1}{\lambda} H(0), \tag{77}$$

where

$$H(0) = -h_0 + \sum_{k=1}^{\infty} h_k p_0^k, \tag{78}$$

which is easily seen to be a finite negative number. Thus, condition (ii) will be satisfied if $\lambda \geqq -H(0) = \lambda_0$, say.

In order to prove condition (iii), we notice that

$$\frac{d^m G_\nu^*(t \mid \lambda)}{dt^m}\Big|_{t=0} = \frac{1}{\lambda} \frac{d^m H(t)}{dt^m}\Big|_{t=0} = \frac{1}{\lambda} \frac{d^m}{dt^m} \sum_{k=1}^{\infty} h_k [G_\nu(t)]^k \Big|_{t=0}. \tag{79}$$

Since the derivatives of $G_\nu(t)$, evaluated at $t = 0$, are all nonnegative and since the constants $h_k \geqq 0$ by hypothesis, property (iii) follows.

Obviously, formula (74) implies formula (70).

In order to illustrate the bearing of this theorem, assume for a moment that the true distribution of the number γ of cluster centers per unit volume is a particular negative binomial law with probability generating function

$$G_\gamma(t \mid \mathfrak{B} = 1) = [2 - t]^{-1} \tag{80}$$

and that this is combined with a specified binomial distribution of the number ν of galaxies per cluster, so that

$$G_\nu(t) = [\tfrac{1}{2}(1 + t)]^{1000}. \tag{81}$$

Then

$$H(t) = h[G_\nu(t)] = -\ln\{2 - [\tfrac{1}{2}(1 + t)]^{1000}\}, \tag{82}$$

and

$$G_\nu^*(t) = 1 - \frac{1}{\lambda}\ln\{2 - [\tfrac{1}{2}(1 + t)]^{1000}\}, \tag{83}$$

with

$$\lambda \geqq -H(0) = \ln\{2 - (\tfrac{1}{2})^{1000}\} = \lambda_0. \tag{84}$$

It follows that the joint distribution of N_1 and N_2 resulting from the true distributions (80) and (81) will be identical with that which would be observed if the number of cluster centers per unit volume followed a Poisson distribution with expectation λ satisfying (84) combined with the distribution of the number of galaxies per cluster as determined by formula (83). Naturally, therefore, observing the joint distribution of N_1 and N_2 and nothing else, it is impossible to decide whether the number of cluster centers per unit of volume follows a Poisson law or any other quasi-uniform distribution. This, of course, does not exclude the possibility that we can decide this question on other grounds.

IX. CONCLUDING REMARKS

All the preceding pages are given to deductions from the structural postulates regarding the spatial distribution of galaxies as enumerated in Section I and, in a more precise form, in Section III. The main result of this work is represented by formulae (40) and (41), which determine the joint distribution of the numbers N_1 and N_2 of galaxies visible on idealized photographs of two arbitrary regions ω_1 and ω_2. Confrontation of the theory thus developed with empirical facts requires specialization of at least some of the four functions involved in the model. The work done in this direction will be described in a subsequent publication.[13] However, before concluding the present paper, it seems advisable to include at least a few remarks indicating how formula (41) and its consequences (49)–(58) can be used for an empirical study of the actual distribution of galaxies.

Keeping in mind the general properties of the moments of N_1 and N_2 described in Section VII, it appears advisable to divide the empirical study into two parts: the internal structure of clusters and the distribution of cluster centers.

The theoretical results which are basic for the first part of the study are exemplified by equation (68). Because of the analogy between the definition of correlation coefficient and the expression $Q(\omega_1, \omega_2)$ on the left-hand side of equation (68), we propose to describe this quantity as the *quasi-correlation* between N_1 and N_2. At least in the early stages of the empirical study, the function $\theta_i(\xi)$ will be taken from the published work of Hubble[14] or Holmberg.[15] When this is done, the right-hand side of equation (68) contains only known quantities and the moments of N_1 and N_2, for which estimates from actual counts will be substituted. The selection of ω_1 and ω_2 and of m_1 and m_2 is at our disposal and may

[13] J. Neyman, E. L. Scott, and C. D. Shane, in preparation.

[14] *Mt. W. Contr.*, No. 548; *Ap. J.*, **84**, 158, 1936.

[15] *Medd. Lunds Obs.*, Ser. II, No. 128, 1950.

be adjusted to the material available. For example, ω_1 and ω_2 may mean two $1^\circ \times 1^\circ$ squares taken k degrees apart, with N_1 and N_2 representing the numbers of galaxies in these squares up to the limiting magnitude appropriate to the observations made at the Lick Observatory or any other. Then the regions ω_1 and ω_2 do not overlap, $\theta_1(\xi) = \theta_2(\xi)$, and formula (68) giving the quasi-correlation between N_1 and N_2 reduces to

$$Q(\omega_1, \omega_2) = \frac{R_{110}}{R_{200}} = \frac{\sigma_{11}}{\sigma_{20} - E(N_1)} = Q_k \quad \text{(say)}. \tag{85}$$

If the available set of data is substantial, then empirical values, say Q_k^*, of Q_k may be obtained for a number of values of k. If the present model approximates the actual distribution of galaxies, then, *solely by adjusting the function* $f(\eta)$, the sequence of quotients R_{110}/R_{200}, computed for $k = 1, 2, \ldots$, can be made to agree with the series of numbers Q_k^*. This is true of the quasi-correlation as defined in (68) and (85) but, perhaps a little unexpectedly, no such statement can be made with regard to the ordinary correlation coefficient between N_1 and N_2, say,

$$\rho = \frac{\sigma_{11}}{\sigma_{20}} = \frac{A_2 R_{110}}{A_2 R_{200} + E(N_1)}, \tag{86}$$

because the value of ρ depends on A_2 and hence on the distribution of cluster centers in space.

Having obtained empirical quasi-correlations Q_k^*, the search for an appropriate function $f(\eta)$ may be attempted by the trial-and-error method. We choose a plausible family of probability densities, say $f(\eta, \vartheta)$, perhaps depending on a single parameter ϑ. For selected values of ϑ a sequence of values of the quotient R_{110}/R_{200} is computed for $k = 1, 2, \ldots$. Each such sequence is compared with the empirical sequence of numbers Q_k^*. Finally, the value of the parameter, say ϑ^*, is determined which provides the best agreement between the quotients R_{110}/R_{200} and the numbers Q_k^*. The corresponding probability density $f(\eta, \vartheta^*)$ is then our first approximation to the unknown function $f(\eta)$ and is open to various tests of validity.

One such test may consist in using $f(\eta, \vartheta^*)$ to compute quasi-correlations between numbers N_1 and N_2 of galaxies in the same region $\omega_1 \equiv \omega_2$ but counted to two different limiting apparent magnitudes, $m_1 < m_2$. Empirical material with which results of this kind can be compared consists of two systems of counts covering the same region of the sky.

If the empirical numbers $Q_1^*, Q_2^*, \ldots$ cannot be approximated by any choice of the function $f(\eta)$, this would indicate that the probabilistic model of the structure of the universe is essentially wrong and that it should be modified, perhaps by including the effects of extinction by interstellar clouds, etc.

Once a plausible approximation $f(\eta, \vartheta^*)$ of $f(\eta)$ is obtained, a similar method may be used to find plausible approximations to the distributions of γ and ν. A certain number of moments A_j are estimated, as outlined in Section VII. Then approximations to $G_\gamma(t \mid \mathfrak{B} = 1)$ and $G_\nu(t)$ are sought among functions with few adjustable parameters.

At this point we should make a distinction between the following two situations. First, it is possible that some a priori considerations will suggest special forms of the distributions of γ and of ν which may be approximated by probability generating functions of known form involving several adjustable parameters. In this case the quantities h_k and G_k can be represented by known functions of the same parameters and, knowing the values of the moments A_j, the best-fitting values of the parameters can be found.

If no a priori knowledge of the distribution of γ and ν is available, then the best we can do is to refer to Section VIII above and to estimate that distribution of ν which, combined with a Poisson distribution of γ, could yield the joint distribution of N_1 and N_2 that is actually observed.

The treatment of this aspect of the problem requires setting

$$h(t) = \lambda(t-1), \qquad h_1 = \lambda, \qquad h_k = 0 \quad \text{for} \quad k > 1, \tag{87}$$

where $\lambda > 0$ is an adjustable parameter. Then, for $j = 1, 2, \ldots,$

$$A_j = G_i \lambda^j; \tag{88}$$

and, if the distribution of ν is approximated by a known distribution with several adjustable parameters, the best-fitting values of these parameters and of λ can be obtained from equations of the type of (88).

The present paper originated from conversations with Dr. C. D. Shane, director of the Lick Observatory, to whom the authors are deeply indebted. Although signed only by the present two authors, the paper should be considered as the first part of a broader study, involving not only theoretical considerations but also the analysis of empirical data, conducted jointly with Dr. Shane.

THE TIME OF RELAXATION FOR STARS IN A FLUCTUATING DENSITY FIELD

DONALD E. OSTERBROCK*
Yerkes Observatory
Received February 6, 1952

ABSTRACT

In this paper a statistical method similar to that used by Chandrasekhar and Münch in their most recent analysis of the brightness fluctuations in the Milky Way is used to find the time of relaxation for a star moving through a fluctuating density field. The time required for the star to change its direction of motion significantly because of gravitational interaction with the matter is calculated. The fluctuating density field represents a simplified model of the interstellar medium, and the computed time of relaxation for this case shows that the low-velocity stars can have had their velocities appreciably altered by gravitational interaction with the interstellar medium during 3×10^9 years, a result in agreement with that obtained by Spitzer and Schwarzschild.

1. INTRODUCTION

One of the fundamental results of observational astronomy is that the velocities of the stars in the neighborhood of the sun have a fairly smooth frequency-curve with a mean value and a dispersion about it; this frequency curve may be approximated in some sense or other by a Maxwellian distribution.[1] It is hard to believe that the stars originated with a velocity distribution of this type, and the fact that it approximates an equilibrium distribution strongly suggests that some agency has been at work reshuffling the velocities. It is well known that almost any kind of interaction process which changes star velocities will lead eventually to a Maxwellian distribution. More specifically, if the time of relaxation is defined as the time in which a star's velocity is appreciably altered by some interaction process, then after a period several times as long as the relaxation time there will be a reasonable approach to a Maxwellian distribution.

Now the first process one would think of as the mechanism for changing the velocities is the gravitational interaction between stars. However, it has long been known that the time of relaxation for this process is of the order of 10^{13} years for slow-moving stars in the vicinity of the sun,[2] and therefore it cannot have had any appreciable effect during 3×10^9 years.

The next process that comes to mind for changing stars' velocities is gravitational interaction between stars and interstellar matter,[3] for the latter is known to have a patchy, uneven distribution. According to all present estimates, the mass of an interstellar cloud is much greater than the mass of a star, so we would expect the clouds to have a much greater gravitational effect than the stars. The problem then is to find whether or not gravitational interaction between stars and interstellar matter can appreciably modify the velocities of the stars in times comparable with 3×10^9 years.

This problem has been studied by Spitzer and Schwarzschild,[4] who have applied the formulae derived for interactions between stars and stars, by substituting the approximate mass and velocity dispersion of the clouds for the corresponding parameters of the

* Atomic Energy Commission Pre-doctoral Fellow in Astrophysics.

[1] For a discussion of this point see S. Chandrasekhar, *Principles of Stellar Dynamics* (Chicago: University of Chicago Press, 1942), §1.2, and the references given there.

[2] See *ibid.*, chap. ii, and references given there.

[3] This was suggested by A. S. Eddington, *Nature*, **151**, 91, 1943, and presumably even before that.

[4] *Ap. J.*, **114**, 385, 1951.

perturbing stars. In their treatment, then, a unit of the interstellar matter is thought of as a large massive cloud, and its effect in changing stars' velocities is calculated as if all its mass were concentrated in a point.

Independently of these authors, work on the same problem had been started here from a somewhat different viewpoint. The interstellar matter is known to have a strongly fluctuating distribution, and the "edges" even of many of the dense clouds we see in Milky Way photographs are not sharply defined. With this point in mind, Chandrasekhar and Münch[5] suggested, in their analysis of the fluctuations in brightness of the Milky Way, an alternative method for describing the interstellar medium. According to their picture, the interstellar matter is distributed continuously, but with a strongly fluctuating density. Thus, instead of treating separate clouds as individual units, one uses on this picture statistical methods derived from the current theories of turbulence to treat the fluctuations in the density field. In particular, they assume that the density anywhere in the interstellar medium can be written in the form $\rho(\mathbf{r}) = \bar{\rho} + \delta\rho(\mathbf{r})$, where $\delta\rho(\mathbf{r})$, the density fluctuation, is a chance variable with a mean expectancy zero. However, the mean-square fluctuation in density, $\overline{\delta\rho^2}$, is not equal to zero, and the assumption is made that the correlation in the fluctuations in density at two points $\mathbf{r}_1$ and $\mathbf{r}_2$, $\overline{\delta\rho(\mathbf{r}_1)\delta\rho(\mathbf{r}_2)}$, is a function only of the distance $|\mathbf{r}_1 - \mathbf{r}_2|$ between the two points and hence of the form $F(|\mathbf{r}_1 - \mathbf{r}_2|)$. This correlation function defines a scale length, beyond which the correlation is sensibly zero; this scale length is considerably smaller than the dimension that would be assigned to a cloud on the picture of the interstellar matter as distributed in discrete clouds.[5]

Using the foregoing description of the interstellar medium proposed by Chandrasekhar and Münch, we shall evaluate the effect of a fluctuating density field on the velocities of stars moving through it.

II. THE METHOD OF CALCULATION

We shall now outline a method by which the time of relaxation for a star moving through a field of density fluctuations can be estimated. First, we calculate the correlation in the gravitational force at two points in the region. Denoting by $K_i(\mathbf{r})$ $(i = 1, 2, 3)$ the components of the force per unit mass at a point $\mathbf{r}$, we consider the correlation $\overline{K_i(\mathbf{r}_1)K_j(\mathbf{r}_2)}$ of the force components at two different points. On the assumptions of homogeneity and isotropy,[6] the tensor can be expressed in the form

$$\overline{K_i(\mathbf{r}_1)\,K_j(\mathbf{r}_2)} = A_1\xi_i\xi_j + A_2\delta_{ij}\,, \tag{1}$$

where $\xi = \mathbf{r}_1 - \mathbf{r}_2$ and A_1 and A_2 are two scalar functions depending only on the difference $|\mathbf{r}_1 - \mathbf{r}_2|$. We shall show how A_1 and A_2 can be expressed in terms of the function $F(r)$ describing the correlation of the density fluctuations.

Now we shall eventually be interested in finding the velocity changes of stars in this fluctuating field of densities. However, it is known that, in an infinite medium in which the forces are governed by an inverse-square law, the accelerations are infinite. This is, of course, not physically real but follows from the simplifying assumption that there is an infinite mass present; on account of the very long range of the inverse-square field, only the very distant regions contribute appreciably to this artificial divergence. In treatments of the two-body problem this divergence is avoided by imposing an upper limit to the volume over which contributions to the force on a star are integrated.[2,7]

In the present problem this effect of the infinite distribution of mass can be eliminated

[5] *Ap. J.*, **115**, 103, 1952.

[6] H. P. Robertson, *Proc. Cambridge Phil. Soc.*, **36**, 209, 1940.

[7] See R. S. Cohen, L. Spitzer, Jr., and P. McR. Routly, *Phys. Rev.*, **80**, 230, 1950, for a discussion of this point.

in a very natural way. For we wish to compute the effect of the density fluctuations about the mean density, which is independent of position and therefore has, on account of its symmetry of distribution, no gravitational effect on the star. Now we may assume that there is no net mass in the fluctuation field, that is, that

$$\int \delta\rho\,(\mathbf{r})\,dV = 0\,. \tag{2}$$

This is identically true for any distribution of mass of finite extent, and, by making this assumption, we remove the singularity connected with the infinite distribution of mass. An equivalent form of this assumption is

$$\int \overline{\delta\rho\,(0)\;\delta\rho\,(\mathbf{r})}\,dV = 0\,, \tag{3}$$

or, in terms of the correlation function $F(R)$,

$$\int_0^\infty F\,(R)\,R^2 dR = 0\,. \tag{4}$$

Now Chandrasekhar[8] has shown that it is a consequence of the equation of continuity that the value of the foregoing integral over $F(R)$ is constant in time, so that if it is once zero it will always be zero. Furthermore, this integral, which is, in fact, $2\pi^2 \mathrm{II}_0$ in his notation, is proportional to the coefficient of k^2 in the expansion of the spectrum of the density fluctuation in the wave-number space (k). Thus the vanishing of this integral simply means that there are no fluctuations as large as the size of the system, which just means that the infinite mass has been eliminated in this way.

Once we have found the force correlation tensor $\overline{K_i(\mathbf{r}_1)K_j(\mathbf{r}_2)}$, we can use it to calculate the changes in the velocity of a star passing through the medium. We do this by assuming the star to move, in a first approximation, with constant velocity in a straight line. The perturbations to this motion, caused by the fluctuating density field, are calculated.

This procedure then gives a relation between the changes in the squares of the velocity components and the time during which they change, which is valid for small changes. The time scale resulting from this equation is then the relaxation time desired.

It must be realized, however, that we have used a highly idealized picture of the interstellar medium. For we have, first of all, assumed the distribution of density fluctuations to be, in the mean, homogeneous and isotropic. We have thus specifically ignored the possibility of describing the distribution with height above the galactic plane of the interstellar matter, and its large-scale distribution with respect to the spiral arms. However, it is believed that these are secondary features which can reasonably be omitted in a preliminary investigation of the problem.

A more serious objection is that, in the method of calculation we have described, we are not allowing for the relative motions within the interstellar medium. In a theory in which the interstellar matter is not allowed to move, there can be no reaction on the interstellar matter of the star–interstellar-matter force and hence no possibility for the kinetic energy of a star to change. Furthermore, it is known from the work of Adams[9] that the large interstellar gas clouds have peculiar velocities of the order of 5–10 km/sec, and presumably the dust clouds, whether or not they are identical with the gas clouds, do also.

Nevertheless, we believe that this calculation may be applied to estimate the time of relaxation for stars in the actual interstellar medium, for the following reasons. If one examines the calculations of the time of relaxation for stars interacting with stars, he finds that the time required for the star to change its energy appreciably and the time required for it to change its direction of motion appreciably are both expressed by for-

[8] *Proc. R. Soc. London, A*, **210**, 18, 1951. [9] *Ap. J.*, **109**, 355, 1949.

mulae of the same form, but with numerical factors which are only slightly different. The dependence of both expressions on the dispersion of velocities of the perturbing stars is very weak, except that no energy is exchanged if they are fixed at rest and that a star suffers no change in energy or direction of motion if they are moving very fast. Hence, in the case of interaction of a star with other stars, the time required for the energy of the star to change appreciably can be found by calculating the time required for its direction of motion to be sensibly changed, assuming the perturbing stars all to be fixed. By analogy we may assume that the same is true for the effect on stars of interaction with the interstellar medium, although the time calculated in this way may be somewhat shorter than the time of relaxation for the energy to change, on account of the large masses of the clouds. This is admittedly a crude procedure; but a complete theory, which would involve a very complicated hydrodynamical problem of the reaction on interstellar matter caused by a passing star, seems at present both impossible on account of its complexity and unjustified on account of our limited knowledge of the interstellar medium.

This paper is intended primarily to initiate a new approach to the problem in terms of ideas now being increasingly used in current astronomical theory. We shall apply the result, according to the above arguments, to estimate the time of relaxation for a star moving through the interstellar medium in our galaxy.

III. THE FORCE CORRELATION

The force correlation functions can be found from the density correlation function by integrating over the gravitational attraction of each element of volume. The quantity desired is $\overline{K_i(0)K_j(z_0)}$, and, by the standard arguments of isotropic turbulence, all components with $i \neq j$ are zero, for they might just as well be positive as negative. Therefore, there are only two force correlation functions to be computed,

$$\overline{K_x(0)\,K_x(z_0)} = \overline{K_y(0)\,K_y(z_0)} \qquad \text{and} \qquad \overline{K_z(0)\,K_z(z_0)}.$$

These are related to the scalars A_1 and A_2 in equation (1) by

$$\overline{K_x(0)\,K_x(z_0)} = A_2\,, \qquad \text{and} \qquad \overline{K_z(0)\,K_z(z_0)} = z_0^2 A_1 + A_2\,. \tag{5}$$

We take $\boldsymbol{r}'$ and $\boldsymbol{r}''$ as two variables of integration and write down the product of the forces at the two points:

$$\boldsymbol{K}(0)\,\boldsymbol{K}(z_0) = G^2 \int\int \delta\rho\,(\boldsymbol{r}')\,\frac{\boldsymbol{r}'}{r'^3}\,\delta\rho\,(\boldsymbol{r}'')\,\frac{\boldsymbol{r}'' - z_0\boldsymbol{k}}{|\boldsymbol{r}'' - z_0\boldsymbol{k}|^3}\,d\tau'\,d\tau'', \tag{6}$$

where $d\tau'$ and $d\tau''$ stand for the elements of volume for $\boldsymbol{r}'$ and $\boldsymbol{r}''$, respectively, and $\boldsymbol{k}$ is a unit vector in the positive z direction. Now the average desired is

$$\begin{aligned}\overline{\boldsymbol{K}(0)\,\boldsymbol{K}(z_0)} &= G^2 \int\int \overline{\delta\rho\,(\boldsymbol{r}')\,\delta\rho\,(\boldsymbol{r}'')}\,\frac{\boldsymbol{r}'\,(\boldsymbol{r}'' - z_0\boldsymbol{k})}{r'^3\,|\boldsymbol{r}'' - z_0\boldsymbol{k}|^3}\,d\tau'\,d\tau'' \\ &= G^2\,\overline{\delta\rho^2} \int\int F\,(|\boldsymbol{r}' - \boldsymbol{r}''|)\,\frac{\boldsymbol{r}'\,(\boldsymbol{r}'' - z_0\boldsymbol{k})}{r'^3\,|\boldsymbol{r}'' - z_0\boldsymbol{k}|^3}\,d\tau'\,d\tau''.\end{aligned} \tag{7}$$

If we change the variables to $\boldsymbol{R} = \boldsymbol{r}'' - \boldsymbol{r}'$ and $\boldsymbol{r} = \boldsymbol{r}'$, with rectangular components X, Y, and Z and x, y, and z, respectively, we obtain

$$\overline{K_x(0)\,K_x(z_0)} = G^2\,\overline{\delta\rho^2} \int\int F(R)\,\frac{x\,(X + x)}{r^3\,|\boldsymbol{R} + \boldsymbol{r} - z_0\boldsymbol{k}|^3}\,d\tau_r\,d\tau_R$$

and

$$\overline{K_z(0)\,K_z(z_0)} = G^2\,\overline{\delta\rho^2} \int\int F(R)\,\frac{z\,(Z + z - z_0)}{r^3\,|\boldsymbol{R} + \boldsymbol{r} - z_0\boldsymbol{k}|^3}\,d\tau_r\,d\tau_R\,, \tag{8}$$

where $d\tau_r$ and $d\tau_R$ are the elements of volume for $\boldsymbol{r}$ and $\boldsymbol{R}$, respectively. Figure 1 shows the vectors and the relationships between them that are used in carrying out the integrations.

We shall now reduce the correlation $\overline{K_x(0)K_x(z_0)}/G^2\overline{\delta\rho^2}$ to a single integral over $\boldsymbol{R}$. First we take $\boldsymbol{r}$ constant and integrate over $\boldsymbol{R}$ by substituting $\boldsymbol{b} = z_0\boldsymbol{k} - \boldsymbol{r}$, which gives

$$\overline{K_x(0)\,K_x(z_0)} = G^2\overline{\delta\rho^2}\int d\tau_r\,\frac{x}{r^3}\int d\tau_R F(R)\,\frac{X - b_x}{|\boldsymbol{R}-\boldsymbol{b}|^3}. \tag{9}$$

We shall take, for evaluating the integral over $\boldsymbol{R}$, a spherical co-ordinate system with $\boldsymbol{b}$ as the axis from which the polar angle θ is measured, and the plane defined by the z axis and $\boldsymbol{b}$ as the plane from which the azimuthal angle ϕ is measured. Furthermore, the spherical co-ordinates of $\boldsymbol{b}$ as referred to the xyz axes are polar angle γ and azimuthal angle ψ. Therefore,

$$X = R\,[\sin\theta\,\cos\phi\,\cos\gamma\,\cos\psi - \sin\theta\,\sin\phi\,\sin\psi + \cos\theta\,\sin\gamma\,\cos\psi]\,; \tag{10}$$

and, integrating over ϕ, we have

$$\overline{K_x(0)\,K_x(z_0)} = 2\pi G^2\overline{\delta\rho^2}\int d\tau_r\,\frac{x}{r^3}\int dR\;F(R)\;R^2 \times\int_0^\pi \frac{d\theta\,\sin\theta}{|\boldsymbol{R}-\boldsymbol{b}|^3}\,[R\cos\theta\,\sin\gamma\,\cos\psi - b_x]\,. \tag{11}$$

The two drawings of Figure 2 show these angles and their relationships to $\boldsymbol{R}$, $\boldsymbol{b}$, and the xyz axes. Then, since $b_x = b\,\sin\gamma\,\cos\psi$, we have

$$\begin{aligned}\overline{K_x(0)\,K_x(z_0)} &= 2\pi G^2\overline{\delta\rho^2}\int d\tau_r\,\frac{x}{r^3}\,\sin\gamma\,\cos\psi \\ &\qquad\times\int_0^\infty dR\;F(R)\;R^2\int_0^\pi d\theta\,\sin\theta\,\frac{R\cos\theta - b}{|\boldsymbol{R}-\boldsymbol{b}|^3} \\ &= 2\pi G^2\overline{\delta\rho^2}\int d\tau_r\,\frac{x}{r^3}\,\sin\gamma\,\cos\psi \\ &\qquad\times\int_0^\infty dR\;F(R)\;R^2\int_0^\pi d\theta\,\frac{\sin\theta\,(R\cos\theta - b)}{(R^2+b^2-2Rb\cos\theta)^{3/2}}.\end{aligned} \tag{12}$$

To evaluate the double integral, we let $x = \cos\theta$, and $z = R/b$ in the range $0 < R < b$, and $z = b/R$ in the range $b < R < \infty$; we then have

$$\begin{aligned}&\int_0^\infty dR\;F(R)\,R^2\int_0^\pi d\theta\,\frac{\sin\theta\,(R\cos\theta - b)}{(R^2+b^2-2Rb\cos\theta)^{3/2}} \\ &\qquad= \frac{1}{b^2}\int_0^b dR\;F(R)\;R^2\int_{-1}^1 dx\,\frac{xz-1}{(1-2xz+z^2)^{3/2}} \\ &\qquad\quad+\int_b^\infty dR\;F(R)\int_{-1}^1 dx\,\frac{x-z}{(1-2xz+z^2)^{3/2}}.\end{aligned} \tag{13}$$

The two integrals over x are easily evaluated by expanding the integrands in a series of Legendre polynomials; in this manner we find that they have the values -2 and 0, respectively. Therefore,

$$\int_0^\infty dR\;F(R)\,R^2\int_0^\pi d\theta\,\frac{\sin\theta\,(R\cos\theta - b)}{(R^2+b^2-2Rb\cos\theta)^{3/2}} = -\frac{2}{b^2}\int_0^b dR\;F(R)\,R^2, \tag{14}$$

and so

$$\overline{K_x(0)\,K_x(z_0)} = -\frac{4\pi G^2\overline{\delta\rho^2}}{b^2}\int d\tau_r\,\frac{x}{r^3}\sin\gamma\cos\psi\int_0^b dR\;F(R)\,R^2. \tag{15}$$

It is simpler to integrate over $\boldsymbol{b}$ than over $\boldsymbol{r}$; thus, letting $\boldsymbol{r} = z_0\boldsymbol{k} - \boldsymbol{b}$ and $x = -b_x$, we have

$$\begin{aligned}\overline{K_x(0)\,K_x(z_0)} &= 4\pi G^2\overline{\delta\rho^2}\int_0^\infty db\;b^2\int_0^\pi d\gamma\,\sin\gamma\int_0^{2\pi}d\psi\,\frac{b_x\sin\gamma\cos\psi}{r^3b^2}\int_0^b dR\;F(R)\,R^2\\ &= 4\pi G^2\overline{\delta\rho^2}\int_0^\infty db\;b\int_0^\pi d\gamma\,\sin^3\gamma\int_0^{2\pi}d\psi\,\frac{\cos^2\psi}{|\boldsymbol{b}-z_0\boldsymbol{k}|^3}\int_0^b dR\;F(R)\,R^2 \qquad (16)\\ &= 4\pi^2G^2\overline{\delta\rho^2}\int_0^\infty db\;b\int_0^\pi\frac{d\gamma\,\sin^3\gamma}{(b^2+z_0^2-2bz_0\cos\gamma)^{3/2}}\int_0^b dR\;F(R)\,R^2.\end{aligned}$$

Again breaking the range of integration into two parts, $0 < b < z_0$ and $z_0 < b < \infty$, expanding in Legendre polynomials, and integrating, we obtain

$$\overline{K_x(0)\,K_x(z_0)} = \frac{16\pi^2}{3}G^2\overline{\delta\rho^2}\Big[\int_0^{z_0}\frac{b\,db}{z_0^3}+\int_{z_0}^\infty\frac{db}{b^2}\Big]\int_0^b dR\;F(R)\,R^2. \tag{17}$$

Since the correlation function appears in the integral over R but not in the integral over b, one further reduction may be made by exchanging the order of integration. This is an elementary integration, which gives

$$\overline{K_x(0)\,K_x(z_0)} = \frac{16\pi^2}{3}G^2\overline{\delta\rho^2}\Big[\int_0^{z_0}dR\;F(R)\,R^2\,\frac{3z_0^2-R^2}{2z_0^3}+\int_{z_0}^\infty dR\;F(R)\,R\Big]. \tag{18}$$

The parallel component force correlation may be evaluated in exactly the same way, and the result is

$$\overline{K_z(0)\,K_z(z_0)} = \frac{16\pi^2}{3}G^2\overline{\delta\rho^2}\Big[\frac{1}{z_0^3}\int_0^{z_0}dR\;F(R)\,R^4+\int_{z_0}^\infty dR\;F(R)\,R\Big]. \tag{19}$$

IV. THE VELOCITY VARIATION

On the assumption that the star moves, in a first approximation, in a straight line (along the z axis), we have the equation of motion,

$$\frac{d^2x_i}{dt^2} = K_i(z); \tag{20}$$

or, integrating, we have

$$\begin{aligned}\frac{dx_i}{dt} &= v_{0i}+\int_0^s K_i(z)\,dt\\ &= v_{0i}+\int_0^s K_i(z)\,\frac{dz}{v} \qquad (21)\\ &\simeq v_{0i}+\frac{1}{v}\int_0^s K_i(z)\,dz.\end{aligned}$$

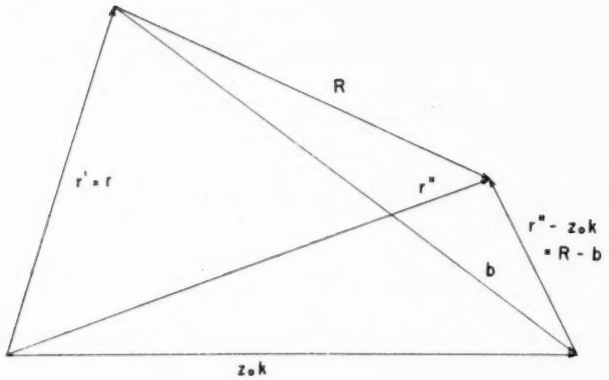

FIG. 1.—The vectors used in finding the force correlation from the density fluctuation correlation. Since the medium is assumed to be isotropic and homogeneous, the correlation depends only on the distance between the two points, which can therefore be chosen to lie on the z axis.

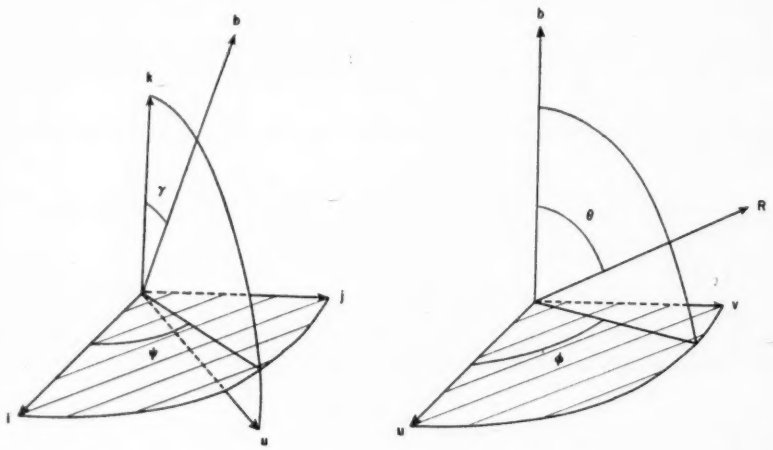

FIG. 2.—The angles used in carrying out the integrations over $\boldsymbol{R}$ and $\boldsymbol{r}$. The vectors $\boldsymbol{u}$ and $\boldsymbol{v}$ together with a unit vector in the direction of $\boldsymbol{b}$ form a right-handed orthogonal system of axes.

Here $v_{0i} = v$ for $i = z$, and zero otherwise is the initial velocity; x_i stands for one of the three rectangular components of the displacement of the star from its original position; s is the distance traveled along the z axis; and the formula applies for only small changes in velocity. Taking the average, we obtain

$$\overline{\frac{dx_i}{dt}} = v_{0i} + \frac{1}{v}\int_0^s \overline{K_i(z)}\, dz = v_{0i}, \tag{22}$$

since the force might just as well be positive as negative.

Squaring formula (21), we obtain

$$\overline{\left(\frac{dx_i}{dt}\right)^2} = v_{0i}^2 + \frac{1}{v^2}\int_0^s\int_0^s K_i(x)\, K_i(y)\, dx dy$$

or (23)

$$\overline{(\Delta v_i)^2} = \frac{\overline{K^2}}{v^2}\int_0^s\int_0^s R_i(|x-y|)\, dx dy,$$

where

$$\overline{K_i(x)\, K_i(y)} = \overline{K^2} R_i(|x-y|) = \overline{K_i(0)\, K_i(|x-y|)}$$

is the force correlation function derived in the previous section.

By transforming to the variables $x + y$ and $x - y$ and carrying out one integration, we easily obtain the formula

$$\overline{(\Delta v_i)^2} = \frac{2\overline{K^2}}{v^2}\int_0^s (s-t) R_i(t)\, dt. \tag{24}$$

Now for finding $\overline{(\Delta v_x)^2}$, we have

$$\frac{\overline{K^2}}{v^2} R_x(t) = \frac{16\pi^2}{3} G^2 \overline{\delta\rho^2}\left[\int_0^t \frac{3t^2 - R^2}{2t^3} F(R) R^2 dR + \int^\infty F(R) R dR\right]. \tag{25}$$

Writing

$$I_i(s) = \int_0^s (s-t) R_i(t)\, dt, \tag{26}$$

we have, on changing the order of integration,

$$\begin{aligned} I_x(s) &= \int_0^s F(R) R^2 dR \int_R^s \frac{3t^2 - R^2}{2t^3}(s-t)\, dt + \int_0^s F(R) R dR \int_0^R (s-t)\, dt \\ &\quad + \int_s^\infty F(R) R dR \int_0^s (s-t)\, dt \\ &= \frac{s^2}{2}\int_s^\infty F(R) R dR + \frac{3s}{2}\left[\int_0^s F(R) R^2 \ln\frac{s}{R}\, dR - \frac{1}{2}\int_0^s F(R) R^2 dR\right] \\ &\quad + \frac{3}{2}\int_0^s F(R) R^3 dR - \frac{1}{4s}\int_0^s F(R) R^4 dR. \end{aligned} \tag{27}$$

It is interesting to notice the behavior of this expression for small s. Since $F(R) \to 1$ as $R \to 0$, the limiting form as $s \to 0$ is

$$I_x(s) \to \frac{s^2}{2}\int_0^\infty F(R) R dR. \tag{28}$$

Since $s = vt$, this expresses the usual result that, in any statistically fluctuating motion, $\overline{(\Delta v_i)^2} \propto t^2$ for times short in comparison with the time required to pass through an elementary fluctuation.[10]

However, to find the change in the star's velocity, we want the limiting form for large values of s corresponding to the times required to pass through several elementary fluctuations. Since the correlation function drops to zero for distances greater than the scale length of the fluctuations, we have

$$I_x(s) \to \frac{3s}{2}\left[\int_0^s F(R) R^2 \ln \frac{s}{R}\, dR - \frac{1}{2}\int_0^s F(R) R^2 dR\right] = \frac{3s}{2}\int_0^\infty F(R) R^2 \left(\ln \frac{s}{R} - \frac{1}{2}\right) dR . \tag{29}$$

Now, according to our assumption that the net mass in the fluctuation field is zero (cf. eq. [2]), we have

$$\int_0^\infty F(R) R^2 dR = 0 ; \tag{30}$$

and so the limiting form for $I_x(s)$ is

$$I_x(s) \to \frac{3s}{2}\int_0^\infty F(R) R^2 \ln \frac{s}{R}\, dR . \tag{31}$$

Now the correlation function can involve R only in the dimensionless ratio R/r_0, where r_0 is the scale length of the density fluctuations, and so may be written as

$$F(R) = f\left(\frac{R}{r_0}\right). \tag{32}$$

Then, on account of equation (30), we may write

$$I_x(s) \to -\frac{3s r_0^3}{2}\int_0^\infty x^2 \ln x f(x)\, dx . \tag{33}$$

Thus, finally, we have, from equations (24), (25), (26), and 33),

$$\overline{(\Delta v_x)^2} = \frac{16\pi^2 G^2 \overline{\delta\rho^2} r_0^3}{v^2}\left[-\int_0^\infty x^2 \ln x f(x)\, dx\right] s , \tag{34}$$

or, since $s = vt$,

$$\overline{(\Delta v_x)^2} = \frac{16\pi^2 G^2 \overline{\delta\rho^2} r_0^3}{v}\left[-\int_0^\infty x^2 \ln x f(x)\, dx\right] t . \tag{35}$$

Once again this is the expected result that, for long times, $\overline{(\Delta v_x)^2} \propto t$, a typical statistical effect.

A similar treatment gives, for the parallel velocity change,

$$I_z(s) = \tfrac{1}{2} s^2 \int_s^\infty F(R) R dR + \tfrac{3}{2} s \int_0^s F(R) R^2 dR - \frac{3}{2}\int_0^s F(R) R^3 dR + \frac{1}{2s}\int_0^s F(R) R^4 dR ; \tag{36}$$

[10] See, e.g., G. I. Taylor, *Proc. London Math. Soc.*, **20**, 196, 1922.

and the limit for large s is

$$I_z(s) \to \tfrac{3}{2} s \int_0^\infty F(R) R^2 dR = 0. \tag{37}$$

According to these results, a star moving through such a fluctuating density field has its velocity at right angles to its original direction of motion increased, while its velocity in the original direction does not change. However, it is obvious that a star moving in a field of fixed density fluctuations, as we are considering here, cannot possibly change its kinetic energy. What happens is that $\overline{\Delta v_z}$ decreases proportionally to t, just enough to keep the kinetic energy constant in the mean. This does not appear from the analysis (see eq. [22]), because we have made the approximation that the star moves in a straight line and it is just the deviations from the straight line that decrease v_z.

V. THE TIME OF RELAXATION

The time scale in which the star's direction of motion is appreciably changed may be found by substituting v^2 for $\overline{(\Delta v_z)^2}$ in equation (35); this gives the time of relaxation,

$$T_D = \frac{v^3}{16\pi^2 G^2 \overline{\delta\rho^2} r_0^3 \left[-\int_0^\infty x^2 \ln x f(x)\, dx \right]}. \tag{38}$$

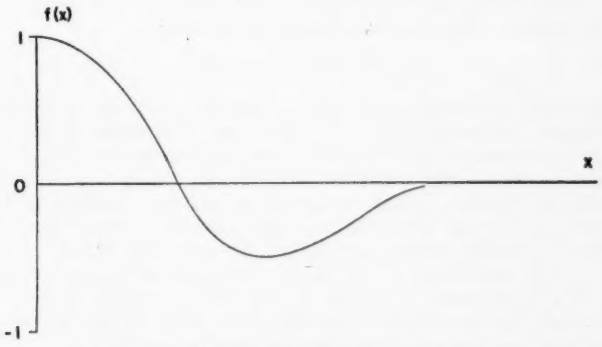

FIG. 3.—The general form of the density fluctuation correlation function $f(x)$

It may be noted that, by the definition of the correlation function, $f(0) = 1$, while $f(x) \to 0$ as $x \to \infty$. Furthermore, by equation (30), there must be a range of x in which $f(x) < 0$, and so the function has a form similar to that sketched in Figure 3. A density correlation function with a second positive wave beyond the negative wave would be very hard to conceive of physically. For correlation functions like that shown in Figure 3, the integral $\int_0^\infty x^2 \ln x\, f(x) dx$ is always negative.

A simple formula for the density correlation function which satisfies the conditions of the problem is

$$F(R) = \left(1 - \frac{R}{3r_0}\right) e^{-R/r_0} \tag{39}$$

or

$$f(x) = \left(1 - \frac{x}{3}\right) e^{-x}. \tag{40}$$

For this function,

$$\int_0^\infty x^2 \ln x f(x)\, dx = -2\,; \tag{41}$$

and, in general, we may expect that in order of magnitude the integral will always be around -1. It should be noted, however, that, if the density fluctuation correlation function has appreciable values for R much larger than r_0, then the absolute value of the integral is considerably greater than 1 and the time of relaxation is correspondingly reduced. This form of the density correlation function will arise if there is an appreciable number of large clouds that were not taken into account in the analysis from which the values of r_0 and $\overline{\delta\rho^2}$ are taken. Conversely, if the correct correlation function describing such a density distribution with a long tail toward large R were used, the integral of equation (41) would have an absolute value of the order of 1, but the value of r_0 would be larger.

VI. CONCLUSION

By the methods outlined above, the time of relaxation for a star moving in a fluctuating density field may be calculated. According to the arguments of the introduction, this result may be applied to estimate the time of relaxation for a star moving through the interstellar matter in the galaxy. From the data in the paper of Chandrasekhar and Münch we take $\overline{\delta\rho^2} = 15\overline{\rho^2} \simeq 2 \times 10^{-47}$ gm^2 cm^{-6} and $r_0 \simeq 7$ psc. With these numbers substituted in equation (38), the relaxation time becomes

$$T_D = 2.6 \times 10^6\, v^3 \text{ years}, \tag{42}$$

where v is expressed in kilometers per second. The velocity v must be interpreted as the velocity with respect to the mean velocity of the interstellar matter in the sun's neighborhood, and hence presumably with respect to the local standard of rest. Thus, according to this calculation, stars with velocities of 10 km/sec would have interacted for just about one time of relaxation during the age of the galaxy, estimated as 3×10^9 years. The actual value of the time of relaxation is quite sensitive to the adopted scale length of the density fluctuations, but it appears that, for any value of this length reasonably compatible with the observations, this time of relaxation will be much smaller than the time of relaxation for star-star interactions and not too much greater than the age of the galaxy. This result then implies that the stars have begun to be affected by the interstellar matter but have not yet come into equipartition with it.

The reason that the interaction with the interstellar matter gives so short a relaxation time in comparison with that given by interaction with stars may be seen by comparing our equation (38) with the expression for the time of relaxation derived from the two-body problem,[2]

$$T_D = \frac{v^3}{8\pi N G^2 m_1^2 H(x_0) \ln [D_0 v_2^2 / G(m_1 + m_2)]}.$$

Here N stands for the number of field stars per unit volume; m_1 for the mass of a typical field star; $H(x_0)$ is a function of order of magnitude unity depending on the velocity dispersion of the field stars; and D_0 is the mean distance between field stars. In this case Nm_1 is the mean density of matter in the form of stars, while in our expression $\sqrt{\overline{\delta\rho^2}}$ is, in order of magnitude, the same as the mean density of interstellar matter. We know

from observational data[11] that in the neighborhood of the sun these two densities are of the same order of magnitude. The essential difference between the two expressions for relaxation times is thus the factor $1/m_1$ (mass of a star) in the case of interaction with stars and $1/r_0^3\sqrt{\delta\rho^2}$ ("mass of a fluctuation") in the case of interaction with interstellar matter. It is the very large mass of an individual density fluctuation which makes the interstellar matter so efficient in changing a star's velocity.

The logarithmic cutoff occurring in the two-body analysis, $\ln[D_0 v_2^2/G(m_1 + m_2)]$, does not appear in our expression but is similar to the integral

$$-\int_0^\infty x^2 \ln x f(x)\, dx ,$$

which has the order of magnitude 1. For star-star interactions, the cutoff factor is of the order of $\ln 10^{10} \simeq 25$.

I wish to thank Professor S. Chandrasekhar both for his initial suggestion of this problem to me and for his constant encouragement and advice to me. Also I wish to thank the Atomic Energy Commission for support under a Pre-doctoral Fellowship.

[11] G. P. Kuiper, *A. J.*, **53**, 194, 1948.

MODEL SOLAR ATMOSPHERES*

LAWRENCE H. ALLER AND A. KEITH PIERCE
McMath-Hulbert Observatory, University of Michigan, Pontiac, Michigan
Received February 13, 1952

ABSTRACT

An iteration method is described for obtaining model stellar atmospheres when the temperature as a function of optical depth is known. This process is applied to the solar atmosphere, using an empirical temperature distribution based on observations of limb darkening. The total pressure, the electron pressure, and the absorption coefficient are tabulated as functions of the optical depth for different hydrogen-to-metal ratios. In addition, two solar models with He/H ratios of $\frac{1}{5}$ and $\frac{1}{10}$ are tabulated and compared with other models.

INTRODUCTION

For the interpretation of the profiles of the dark lines in the solar spectrum and their center-limb variations, it is necessary to know how the gas pressure P_g, the electron pressure P_e, the local temperature T, and the coefficient of continuous absorption κ_λ change with the optical depth τ_λ at the wave length in question. A self-consistent set of these quantities defines a model atmosphere. We may suppose the atmosphere of a star such as the sun to be in hydrostatic equilibrium, in which event the increase in pressure with τ is given by

$$\frac{dP}{d\tau} = -\frac{g}{\bar{\kappa}}. \tag{1}$$

Here $d\tau$ is the element of optical depth in radiation integrated over all frequencies. It is related to the mean mass-absorption coefficient $\bar{\kappa}$ by $d\tau = \bar{\kappa}\rho dx$. Further, g is the average acceleration of gravity in the atmosphere, and P may be identified with the total pressure P_g.

The value of $\bar{\kappa}$ depends on the temperature and electron pressure, which, in turn, depend on τ. The dependence of the temperature on τ must be known or assumed. One may use a theoretical gray-body approximation or, as in the present calculations, a $T(\tau)$ relationship derived from limb-darkening observations. The relation between the gas pressure, electron pressure, and temperature involves the assumed abundances of hydrogen, helium, and the metals.

Model solar atmospheres have been calculated by a number of workers.[1] Among the more recent computations we may mention those by Strömgren,[2] Münch,[3] and de Jager.[4] The various models differ from one another because of the different assumptions about the continuous absorption coefficient, the ratio of metals to hydrogen, and the dependence of the temperature on τ. In our computations we shall use various hydrogen/metal ratios and an "empirical" dependence of temperature on τ. We shall also examine the influence of admixtures of helium upon the model.

* Supported in part by Contract N6-onr-232-V with the Office of Naval Research.

[1] A. Unsöld, *Physik der Sternatmosphären* (Berlin: J. Springer, 1938); S. Chandrasekhar, *Radiative Transfer* (Oxford: Clarendon Press, 1950).

[2] *Festschrift für Elis Strömgren* (Copenhagen: E. Munksgaard, 1940). "Tables of Model Stellar Atmospheres," *Pub. mind. Medd. Københavns Obs.*, No. 138, 1944.

[3] *Ap. J.*, **106**, 217, 1947; **107**, 265, 1948.

[4] *Proc. Acad. Amsterdam*, **51**, 731, 1948.

THE VARIATION OF TEMPERATURE WITH OPTICAL DEPTH

In a previous paper[5] we utilized data on the energy distribution at the center of the solar disk, together with limb-darkening measures, to obtain the temperature T as a function of the optical depth τ_λ at certain observed wave lengths λ. In order to obtain T as a function of τ, the optical depth in the integrated radiation, it is necessary to know the ratio $\bar{\kappa}/\kappa_\lambda$ as a function of temperature.

We assume that the negative hydrogen ion is the principal source of opacity in the solar atmosphere. Accordingly, we may take κ_λ from the calculations by Chandrasekhar and Breen,[6] and compute

$$\bar{\kappa} = \int \kappa_\lambda \frac{F_\lambda}{F}\, d\lambda\,, \tag{2}$$

where the dependence of the flux ratio F_λ/F on optical depth has been given by Chandrasekhar[7] for a gray body. At large optical depths the contribution of atomic hydrogen to the absorption coefficient must be added.

Following the notation of Chandrasekhar and Münch, we may write

$$\bar{\kappa}\,(\tau) = \frac{1 - x_H}{m_H}\,[P_e a_\tau(H^-) + a_\tau(H)\,] \tag{3}$$

for a pure hydrogen atmosphere. Münch[8] has calculated the absorption coefficients $a_\tau(H^-)$ and $a_\tau(H)$ to an optical depth of 1.4. To a sufficient degree of accuracy we may use his results in our present computations, taking the values from his table with $\theta = 5040/T$ rather than τ as argument. We have extended these computations to $\tau = 2.0$.

TABLE 1

TEMPERATURE AS A FUNCTION OF OPTICAL DEPTH

τ	Tentative T(° K)	Final Adopted T(° K)	τ	Tentative T(° K)	Final Adopted T(° K)
0.00	4500° K	4500° K	0.60	6040° K	5860° K
0.01	4640	4600	0.70	6150	5950
0.02	4720	4670	0.80	6250	6030
0.04	4850	4780	0.90	6350	6110
0.06	4950	4860	1.00	6430	6180
0.08	5040	4940	1.20	6590	6320
0.10	5120	5010	1.40	6730	6450
0.15	5270	5150	1.60	6870	6570
0.20	5410	5270	1.80	6990	6680
0.30	5620	5460	2.00	7100	6780
0.40	5790	5620	2.50	7380	7020
0.50	5920	5750			

With both $\bar{\kappa}$ and κ_λ known as functions of T for the solar atmosphere, we now compute τ as a function of τ_λ for the wave lengths of observation: $\lambda\lambda$ 5485, 6980, 9920, and 11973. Since T is known as a function of τ_λ for each of these wave lengths, we obtain four different temperature distributions which must be averaged in some manner. The $T(\tau_\lambda)$-curves are closely similar and can be brought into coincidence by slight changes in the adopted value of κ_λ. The temperature distribution tentatively adopted is given in column 2 of Table 1. A necessary condition that must be fulfilled is that this temperature dis-

[5] K. Pierce and L. Aller, *Ap. J.*, **114**, 145, 1951.
[6] *Ap. J.*, **104**, 430, 1946.
[7] *Ap. J.*, **101**, 328, 1945.
[8] *Ap. J.*, **106**, 217, 1947.

tribution reproduce the observed energy flux from the sun. If T_e is the effective temperature of the sun, then

$$T_e^4 = 2\int_0^\infty T^4(\tau) E_2(\tau)\, d\tau\,, \tag{4}$$

where E_2 is the exponential integral. The temperature distribution of Table 1 leads to a computed effective temperature which is much too high. The mean absorption coefficient, $\bar{\kappa}$, appears to be too small. The simplest remedy is to multiply $\bar{\kappa}$ by a constant C. Then

$$\tau' = C\int \frac{\bar{\kappa}}{\kappa_\lambda}\, d\tau_\lambda = C\tau\,, \tag{5}$$

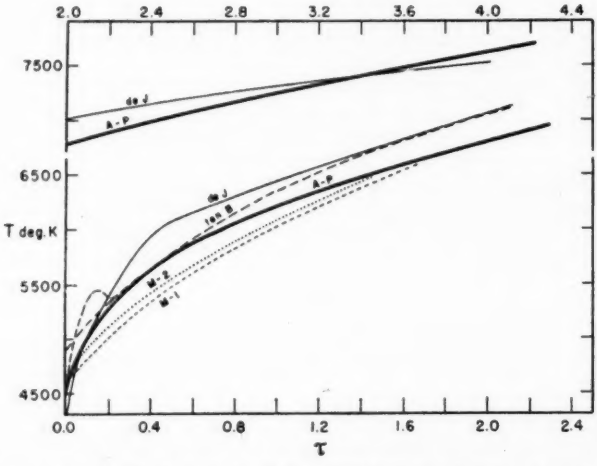

FIG. 1.—Temperature distribution in the solar atmosphere as a function of optical depth. *de J:* Neven and de Jager; *ten B:* ten Bruggencate, Gollnow, and Jäger. Between $\tau = 0.0$ and 0.2 the result is based on eclipse observations of limb darkening; this is then fitted to an earlier temperature distribution of de Jager. *M*-1: Münch, second approximation for a nongray atmosphere, T_2. *M*-2: Münch, for gray atmosphere. *A-P:* Aller and Pierce, empirical temperature distribution, $C = 1.35$. (Note extension of scale of optical depth at top of diagram.) For the Neven and de Jager data τ refers to the monochromatic optical depth at λ 5000 in Figs. 1, 2, and 4; for the results by ten Bruggencate *et al.*, τ refers to the monochromatic optical depth at λ 6400, while Münch and the present writers employ τ as the optical depth in the integrated radiation.

and C can be adjusted so that the right-hand member of equation (4) reduces to T_e^4 when τ' is substituted throughout. Following the discussion by C. W. Allen,[9] we have taken the effective temperature of the sun as 5784° K. Then C is found to be 1.35, as compared with 1.42 derived by Chandrasekhar and Münch. For $T_e = 5713°$ K a value of $C = 1.47$ would have given the correct flux.

The necessity for introducing such a large correction factor is unfortunate. Part of this factor certainly arises from the neglect of line absorption, but it is not proved that all of it originates in this way. The existence of other agents of continuous absorption cannot be excluded. At the present time we have no means of identifying such agents.

In Figure 1 we compare our adopted empirical temperature distribution ($C = 1.35$) with those suggested by Münch,[10] ten Bruggencate, Gollnow and Jäger,[11] and Neven

[9] *Observatory*, **70**, 154, 1950. [10] *Ap. J.*, **107**, 265, 1948. [11] *Zs. f. Ap.*, **27**, 223, 1950.

and de Jager. In our diagrams the abscissa, τ, should be understood as τ_0, the monochromatic optical depth at λ 5000, wherever the Neven-de Jager data are plotted. Approximately, $\tau_0 = 0.72\tau$. There are advantages in calculating a model atmosphere with τ_λ as argument but our results would not have been significantly different if we had used $\tau(\lambda\ 5485)$, for example, rather than τ. Except at the surface and at extreme depths, the temperature of our model is higher than in Münch's model. The finally adopted temperature distribution is given in the last column of Table 1.

THE CHOICE OF A CHEMICAL COMPOSITION

Before models of the solar atmosphere can be calculated, a chemical composition must be adopted. The important factor is the ratio, A, of hydrogen to the metals, since the latter supply virtually all the electrons throughout the layers relevant to the production of the dark-line and the continuous solar spectrum. Strömgren and, later, Münch carried

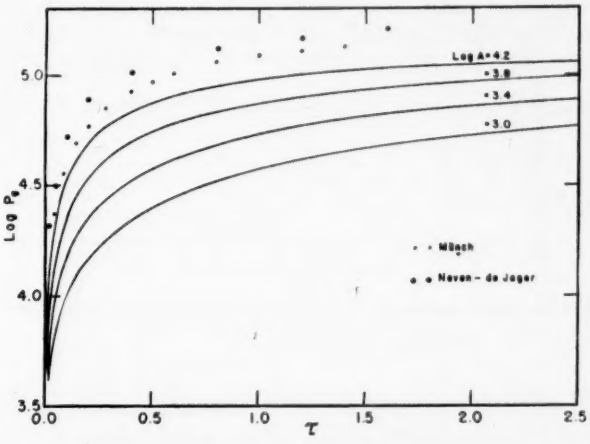

FIG. 2.—Log of total pressure versus the optical depth for various hydrogen-to-metal ratios. The points for Münch and Neven-de Jager are for log $A = 4.2$.

out calculations of models for different assumed values of the ratio of hydrogen to the metals, namely, log $A = 3.0$, 3.4, 3.8, and 4.2, and the former has given tables of P_e and P_g as a function of temperature for different values of the parameter A. For comparison with the results of Münch[3] and Strömgren,[2] we have carried out calculations for the same values of log A. The results are shown in Figures 2–4 and are discussed in the concluding section of the paper.

The study of the model in which log $A = 3.4$ has been extended through a consideration of the abundance of helium. Models for two different values of the ratio of hydrogen to helium have been investigated. In the first of these, we have assumed a medium consisting of 200 helium atoms, 0.432 (iron + silicon + magnesium + nickel) atoms, and 0.011 (sodium + calcium + aluminum) atoms per thousand hydrogen atoms. This composition was used some years ago by one of the authors in discussing the atmospheres of Sirius and γ Geminorum.[12] The metal atoms were thus separated into two groups with average ionization potentials of 7.9 and 5.8 e.v., respectively. We refer to models based on this mixture as $He(\frac{1}{5})$ models.

[12] L. H. Aller, *Ap. J.*, **96**, 321, 1942.

More recently Miss Underhill,[13] from a study of the *He* II lines in 10 Lacertae, has concluded that the *He*/*H* ratio should be more nearly in the neighborhood of $\frac{1}{20}$ or $\frac{1}{25}$. This result is in harmony with the *He*/*H* ratio found by one of the authors in a study of *He* I lines in γ Pegasi. Accordingly, we have computed a second model in which the ratio of *He* to *H* is taken as $\frac{1}{20}$.

The addition of helium has no effect on $\bar{\kappa}/\kappa_\lambda$. Although helium contributes nothing to

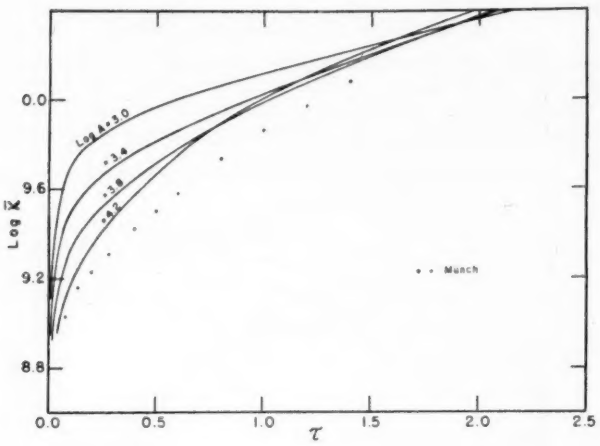

FIG. 3.—Log of the opacity versus optical depth for various hydrogen-to-metal ratios. Münch's values are for log $A = 4.2$.

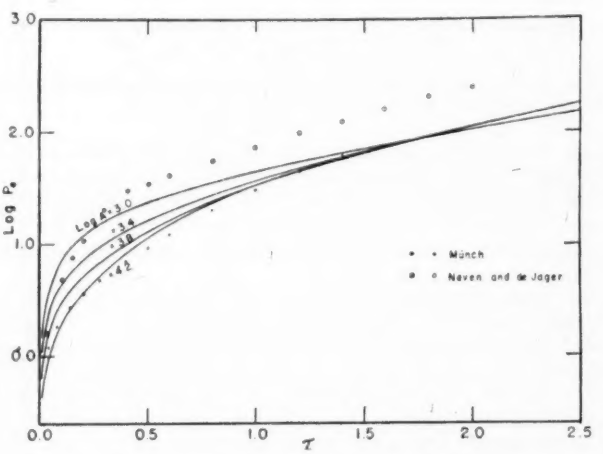

FIG. 4.—Log of the electron pressure versus optical depth for various hydrogen-to-metal ratios. The points of Münch and Neven and de Jager are for log $A = 4.2$.

[13] *Canadian J. Phys.*, **29**, 447, 1951.

the continuous absorption, it does decrease the absorption coefficient per gram of stellar material by dilution. For layers of the same optical depth, the gas pressure, therefore, will be greater than in a star deficient in helium. We have restricted our models involving helium to $\log A = 3.4$. It is easy to see how other models are affected by the addition of helium. The value of $\bar{\kappa}$ will be depressed, P_g for a given τ will be increased, and P_e will be but little affected.

THE CALCULATION OF THE MODEL ATMOSPHERES

The computation of the different models has been carried out as follows: For each composition we have a definite relation between P_g and P_e governed by Saha's equation. The continuous absorption coefficient may be written as

$$\bar{\kappa} = \beta C \frac{1 - x_H}{m_H} [P_e a(H^-) + a(H)]. \tag{6}$$

In this equation β is the fraction of the total weight contributed by H, and it is set equal to 1 for the atmospheres consisting only of H and the metals. The factor $(1 - x_H)$ gives the fraction of H atoms that are neutral; throughout the relevant layers hydrogen is nearly all neutral.

Since $\bar{\kappa} = f(P_e, \theta)$ and $P_g = P_g(P_e, \theta)$, we can plot $\bar{\kappa} = \bar{\kappa}(P_g, \theta)$. Thus, from equation (1), we write

$$dP_g = \frac{g}{\bar{\kappa}(P_g, \theta)} d\tau. \tag{7}$$

Multiplying by P_g and integrating, we get

$$\begin{aligned} P_g^2 &= 2g \int \frac{P_g}{\bar{\kappa}(P_g, \theta)} d\tau, \\ &= 2g \int \frac{P_g}{\bar{\kappa}(P_g, \theta)} \frac{d\tau}{d\theta} d\theta. \end{aligned} \tag{8}$$

The differential quotient $d\tau/d\theta$ is computed once and for all, and the integrations are carried out with respect to θ rather than with respect to τ. The iterations then converge quickly, chiefly as a consequence of the fact that the dependence of $P_g/\bar{\kappa}(P_g, \theta)$ on P_g is not sharp, especially at large values of θ. For example, when $\theta = 1.0$, $\log P_g/\bar{\kappa}$ changes by only 0.3 when $\log P_g$ varies by 1.5.

To get an initial approximation, let us suppose that all the metals are singly ionized, then

$$P_e \sim \frac{P_g}{A(1 + D)}, \tag{9}$$

where D is the ratio of the number of helium to the number of hydrogen atoms. Here $D = 0.20$ for the He $(\frac{1}{5})$ model, 0.05 for the He $(\frac{1}{20})$ model, and 0 for all other cases. Continuing the first approximation, we let

$$\bar{\kappa} = \beta C \frac{P_e}{m_H} a(H^-) \tag{10}$$

and

$$dP_g = \frac{g m_H A(1 + D)}{\beta C P_g} \frac{1}{a(H^-)} d\tau. \tag{11}$$

Substituting dP_g in equation (7), and integrating we obtain

$$P_g^{(0)} = \left[\frac{2 g m_H A(1 + D)}{\beta C P_g} \int \frac{d\tau}{a(H^-)} \right]^{1/2}. \tag{12}$$

TABLE 2

MODEL ATMOSPHERES

τ	LOG $A=3.0$			LOG $A=3.4$			LOG $A=3.8$			LOG $A=4.2$		
	log P_g	log P_e	log $\bar{\kappa}$	log P_g	log P_e	log $\bar{\kappa}$	log P_g	log P_e	log κ	log P_g	log P_e	log $\bar{\kappa}$
0.01	3.37	0.18	9.17	3.47	9.95	8.95	3.72	9.81	8.81	3.90	9.60	8.60
0.02	3.62	0.32	9.30	3.77	0.11	9.16	3.97	9.96	8.95	4.15	9.76	8.75
0.04	3.77	0.53	9.48	3.93	0.35	9.22	4.12	0.17	9.11	4.29	9.99	8.93
0.06	3.87	0.68	9.59	4.04	0.50	9.41	4.22	0.31	9.21	4.40	0.13	9.04
0.08	3.96	0.78	9.65	4.13	0.60	9.47	4.31	0.41	9.29	4.49	0.24	9.13
0.10	4.02	0.86	9.70	4.19	0.67	9.51	4.36	0.48	9.34	4.54	0.32	9.17
0.15	4.10	0.99	9.77	4.28	0.79	9.58	4.46	0.62	9.41	4.64	0.47	9.26
0.20	4.17	1.07	9.81	4.35	0.88	9.63	4.53	0.72	9.47	4.70	0.58	9.33
0.30	4.26	1.20	9.88	4.45	1.02	9.71	4.63	0.84	9.57	4.77	0.77	9.46
0.40	4.34	1.30	9.93	4.52	1.12	9.77	4.69	1.01	9.65	4.83	0.94	9.58
0.50	4.41	1.37	9.98	4.57	1.22	9.82	4.74	1.11	9.72	4.88	1.06	9.68
0.60	4.45	1.43	0.01	4.62	1.30	9.87	4.78	1.21	9.78	4.91	1.18	9.76
0.70	4.49	1.50	0.04	4.65	1.36	9.91	4.81	1.29	9.84	4.93	1.28	9.83
0.80	4.52	1.55	0.07	4.68	1.43	9.95	4.83	1.37	9.89	4.95	1.36	9.89
0.90	4.55	1.60	0.10	4.71	1.49	9.99	4.85	1.44	9.94	4.97	1.44	9.95
1.00	4.57	1.64	0.12	4.73	1.55	0.03	4.87	1.51	9.99	4.98	1.52	0.00
1.20	4.61	1.72	0.17	4.77	1.65	0.10	4.90	1.64	0.08	5.00	1.65	0.11
1.40	4.65	1.80	0.22	4.80	1.77	0.18	4.92	1.75	0.21	5.02	1.77	0.19
1.60	4.68	1.88	0.27	4.82	1.86	0.24	4.94	1.86	0.25	5.03	1.88	0.27
1.80	4.70	1.96	0.33	4.84	1.95	0.31	4.96	1.96	0.32	5.05	1.98	0.34
2.00	4.72	2.04	0.38	4.86	2.03	0.37	4.97	2.04	0.38	5.06	2.07	0.40
2.50	4.77	2.22	0.52	4.89	2.20	0.50	4.99	2.22	0.52	5.07	2.26	0.54

TABLE 3

MODEL ATMOSPHERES WITH HELIUM

τ	LOG $A=3.4$, AND $\frac{1}{8}$ *He*			LOG $A=3.4$, AND $\frac{1}{20}$ *He*		
	log P_g	log P_e	log $\bar{\kappa}$	log P_g	log P_e	log $\bar{\kappa}$
0.01	3.74	0.02	8.74	3.66	9.98	8.87
0.02	4.02	0.17	8.85	3.92	0.15	9.02
0.04	4.17	0.38	9.02	4.07	0.37	9.21
0.06	4.28	0.53	9.15	4.17	0.52	9.31
0.08	4.36	0.65	9.24	4.25	0.62	9.39
0.10	4.41	0.74	9.31	4.30	0.70	9.45
0.15	4.51	0.89	9.41	4.39	0.83	9.53
0.20	4.58	0.99	9.47	4.45	0.93	9.58
0.30	4.67	1.13	9.55	4.54	1.07	9.66
0.40	4.73	1.23	9.61	4.61	1.18	9.72
0.50	4.78	1.32	9.65	4.65	1.28	9.77
0.60	4.82	1.38	9.69	4.69	1.36	9.82
0.70	4.85	1.46	9.73	4.72	1.42	9.87
0.80	4.88	1.52	9.77	4.75	1.49	9.91
0.90	4.90	1.58	9.81	4.78	1.55	9.95
1.00	4.92	1.64	9.84	4.80	1.60	9.98
1.20	4.96	1.75	9.92	4.83	1.70	0.05
1.40	4.99	1.85	9.99	4.86	1.80	0.12
1.60	5.01	1.94	0.05	4.88	1.90	0.18
1.80	5.03	2.02	0.11	4.90	1.98	0.24
2.00	5.05	2.10	0.16	4.92	2.06	0.30
2.50	5.08	2.27	0.29	4.95	2.23—	0.42

This gives us our starting value of P_g. With an initial estimate of $P_g^{(0)}$ available for each θ, we may compute the corresponding P_e. Then, with P_e and θ given, $\kappa(P_e, \theta)$ can be found, and the product

$$\frac{2gP_g}{\bar{\kappa}(P_e, \theta)} \frac{d\tau}{d\theta}$$

computed. The integration of this quantity (see eq. [8]) gives $P_g^{(1)}$, and the process is repeated until two successive operations give the same dependence of P_g on τ. Convergence is usually very rapid.

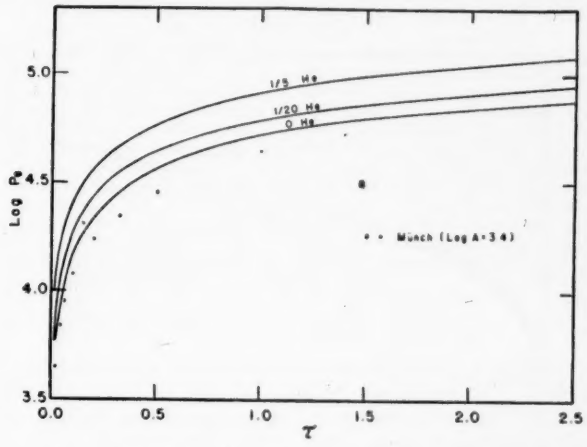

FIG. 5.—Log P_g versus τ for various *He* content. Log $A = 3.4$

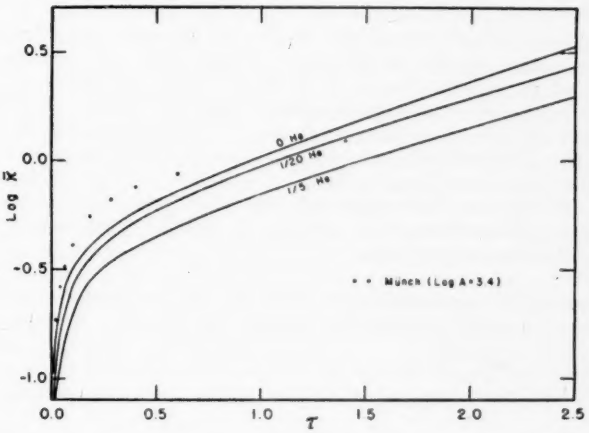

FIG. 6.—Log $\bar{\kappa}$ versus τ for various *He* content. Log $A = 3.4$

COMPARISON OF THE MODEL ATMOSPHERES

The results of the integrations are given in Tables 2 and 3 and are compared with the results of others in Figures 2–7. Table 2 gives, for optical depths τ in the interval 0.01–2.50, the values of log P_g, log P_e, and log $\bar{\kappa}$ for four different ratios, A, of hydrogen to metals. The four models of Table 2 are defined by the values of log A = 3.0, 3.4, 3.8, and 4.2. In Table 3 we have tabulated the results for two helium models in which log A = 3.4 and the ratio of He/H is $\frac{1}{5}$ and $\frac{1}{20}$ by number of atoms.

Figure 2 shows the relation between log P_g and τ for log A = 3.0, 3.4, 3.8, and 4.2. It should be pointed out that, for a given optical depth and composition, Münch's pressures are systematically greater than ours, as are also those of Neven and de Jager.[14]

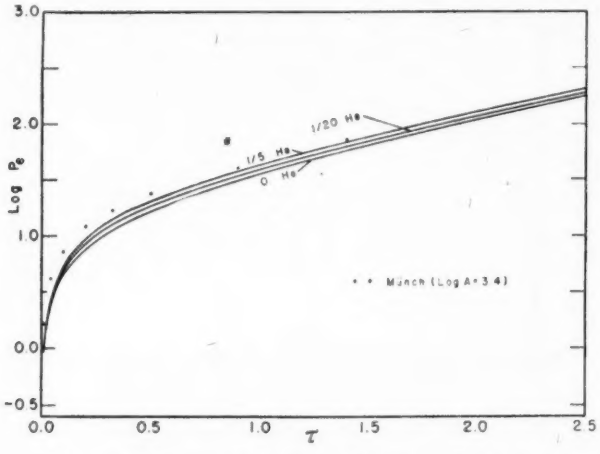

FIG. 7.—Log P_e versus τ for various He content. Log A = 3.4

Similarly, Münch's values of log $\bar{\kappa}$ are smaller than our own (Fig. 3), but the electron pressures are closely comparable (Fig. 4). In Figures 5–7 we have illustrated the dependence of log P_g, log $\bar{\kappa}$, and log P_e upon τ for models with helium-to-hydrogen ratios of 0, $\frac{1}{20}$, and $\frac{1}{5}$. The helium models are all computed with log A = 3.4. The influence of helium is strongly felt by an increase in log P_g and a decrease in opacity as greater amounts of He are added to the atmosphere. The effect is small on log P_e.

The detailed variation of log P_g, log P_e, and log $\bar{\kappa}$ with τ depends markedly not only on the assumed chemical composition but also on the temperature variation. Hence, on the observational side, efforts should be made to obtain an improved temperature distribution for the solar atmosphere.

The authors wish to express their thanks to Mr. William Potter and Mr. Edwin Dennison, who assisted with the numerical calculations.

[14] *B.A.N.*, 11, 291, 1951.

THE EQUATION OF TRANSFER AND THE RESIDUAL INTENSITIES IN SPECTRUM LINES

G. R. BURBIDGE* AND E. MARGARET BURBIDGE
Harvard College Observatory and Yerkes Observatory
Received February 25, 1952

ABSTRACT

The equation of transfer for a spectrum line has been obtained, following earlier work by Strömgren, for lines arising from the level $n = 2$. Certain cyclic processes have been taken into account. The solutions of the equation of transfer for a point in the line and a point in the neighboring continuum are written down following the work of Chandrasekhar. Criteria for the appearance of emission at any point in the line are obtained and discussed. The results are compared with those obtained by Miss Underhill. The theory is applied numerically to calculate the condition for emission to appear at the centers of the Balmer lines $H\alpha$, $H\beta$, and $H\gamma$ under a chosen range of stellar temperatures and electron pressures. The simplifying assumptions have been made that the line center is produced in the surface layer of the atmosphere and that Stark effect is not important here. The results show that at high temperatures the condition for emission in terms of the departure of the atmosphere from thermodynamic equilibrium will not be difficult to fulfil. It is also found that the condition for emission is relatively insensitive to the values of the coefficients of line absorption, continuous absorption, and electron scattering, corresponding to a wide range of stellar conditions.

I. INTRODUCTION

The well-known problem of the condition for the formation of emission lines in stellar spectra was first formulated by Schuster[1] in 1905. He showed that lines formed by absorption as distinct from scattering, in an atmosphere in which continuous scattering as well as continuous absorption was present, could appear in emission if the temperature gradient were small.

In 1928 Milne[2] returned to this problem, using his approximation to the solution of the equation of transfer. He distinguished between, and treated separately, the formation of a line by pure scattering and that by pure absorption. In the former case he showed that emission-line formation was not possible; here he pointed out that cyclic quantum transitions were not formally equivalent to monochromatic scattering and hence did not enter into his problem. In the latter case he reached the same conclusions as Schuster, but from numerical results he showed that the condition for the occurrence of emission demanded a value of the continuous scattering coefficient much larger than any to be expected under the physical conditions prevailing in a stellar atmosphere.

In a recent paper Miss Underhill,[3] in a discussion of transfer problems in an atmosphere with continuous scattering and continuous absorption, reconsidered the two cases of Milne. She confirmed Milne's conclusion concerning lines formed by pure scattering but pointed out that his conclusion regarding lines formed by pure absorption depended on the approximations made in his solution. She showed that strong lines formed by "pure absorption" in a hot stellar atmosphere, taking into account electron scattering, could be in emission if the temperature gradient in the atmosphere were small enough.

In this paper an attempt has been made to obtain conditions for the occurrence of lines in emission which will apply over a wide range of stellar temperatures where lines are formed under conditions intermediate between "pure absorption" and "pure scattering,"

* Agassiz Fellow.

[1] *Ap. J.*, **21**, 1, 1905.

[2] *M.N.*, **89**, 3, 1928.

[3] *Ap. J.*, **110**, 340, 1949.

i.e., lines which are formed by a combination of coherent scattering and cyclic transitions. With appropriate modifications the condition obtained is applicable generally, but here only residual intensities at the centers of the first three Balmer lines of hydrogen have been considered.

II. DERIVATION OF THE EQUATION OF TRANSFER FOR LINES WHOSE LOWER LEVEL IS GIVEN BY $n = 2$

The analysis here is derived by modifying the discussion by Strömgren[4] of the formation of resonance lines in the solar spectrum, and it is given briefly, since it follows Strömgren's work closely.

We consider the number of ways of populating and depopulating a level k (> 2) as follows:

1. Transitions to and from the ground state,
2. Transitions to and from level $n = 2$,
3. Collisional excitation from, and de-excitation to, the ground state,
4. Collisional excitation from, and de-excitation to, the level $n = 2$,
5. The capture of free electrons into level k by the ionized atom, and the radiative ionization of the neutral atom in the kth excited state.

Other ways of populating and depopulating have not been considered. Now let

N_p = Actual number of atoms in the pth state.

$N_p^{(0)}$ = Number of atoms in the pth state under conditions of thermodynamic equilibrium.

a_{k1}, a_{k2} = Probability coefficients per unit time that an atom pass from state k to states 1 and 2, respectively, with the spontaneous emission of radiation.

b_{k1}, b_{k2} = Probability coefficients per unit time that an atom pass from state k to states 1 and 2, respectively, with the emission of radiation, induced by the radiation field.

b_{1k}, b_{2k} = Probability coefficients per unit time that an atom pass from states 1 and 2, respectively, to state k, with the absorption of radiation.

$c_{1k}, c_{2k}, c_{k1}, c_{k2}$ = Probability coefficients per unit time that an atom pass from states 1 to k, 2 to k, k to 1, and k to 2, respectively, as a result of collisions.

C_{fk}, C_{kf} = Probability coefficients for capture and radiative ionization, respectively, into and out of level k.

$C_{fk}^{(0)}, C_{kf}^{(0)}$ = Corresponding capture and ionization coefficients into and out of level k for a state of thermodynamic equilibrium.

$h\nu, h\nu'$ = Energies released in the transitions k to 2 and k to 1, respectively.

$B_\nu(T), B_{\nu'}(T)$ = Planck intensities at frequencies ν and ν'.

$J_\nu, J_{\nu'}$ = Mean intensities at frequencies ν and ν'.

We define the quantity ξ such that:

$$N_p = \xi_p N_p^{(0)} . \tag{1}$$

[4] *Zs. f. Ap.*, **10**, 237, 1935.

Then, by equating the number of populations to the number of depopulations, we obtain the equation of statistical equilibrium:

$$N_1 b_{1k} J_{\nu'} + N_2 b_{2k} J_\nu + N_1 c_{1k} + N_2 c_{2k} + C_{fk} = \xi_k N_k^{(0)} (a_{k1} + b_{k1} J_{\nu'} + a_{k2} + b_{k2} J_\nu + c_{k1} + c_{k2} + C_{kf}) . \tag{2}$$

It should be remembered that the terms $N_k b_{k1} J_{\nu'}$ and $N_k b_{k2} J_\nu$ (the stimulated emissions) act like "negative absorptions," since they are directional. However, it is convenient to keep these terms on the right-hand side of the equation.

Now we have (cf. Strömgren, *op. cit.*, eqs. [24] and [27])

$$\begin{aligned} N_1 b_{1k} B_{\nu'}(T) &= \xi_1 N_k^{(0)} \{ a_{k1} + b_{k1} B_{\nu'}(T) \}, \\ N_2 b_{2k} B_\nu(T) &= \xi_2 N_k^{(0)} \{ a_{k2} + b_{k2} B_\nu(T) \}, \end{aligned} \tag{3}$$

and

$$C_{fk} = \xi_i \xi_e \frac{C_{kf}^{(0)}}{C_{kf}} N_k^{(0)} C_{kf} = \xi_1 Q N_k^{(0)} C_{kf} , \tag{4}$$

where

$$Q = \frac{\xi_i \xi_e}{\xi_1} \frac{C_{kf}^{(0)}}{C_{kf}} \tag{5}$$

(the suffixes occurring in ξ_i and ξ_e refer to ions and electrons). If we neglect the terms involving collisional excitation and de-excitation, we then have

$$\xi_2 \left\{ \frac{\xi_1}{\xi_2} \frac{J_{\nu'}}{B_{\nu'}} (a_{k1} + b_{k1} B_{\nu'}) + \frac{J_\nu}{B_\nu} (a_{k2} + b_{k2} B_\nu) + \frac{\xi_1}{\xi_2} Q C_{kf} \right\} = \xi_k \{ (a_{k1} + b_{k1} J_{\nu'}) + (a_{k2} + b_{k2} J_\nu) + C_{kf} \}$$

or

$$\frac{\xi_k}{\xi_2} = \frac{(\xi_1/\xi_2)(J_{\nu'}/B_{\nu'})(a_{k1} + b_{k1} B_{\nu'}) + (J_\nu/B_\nu)(a_{k2} + b_{k2} B_\nu) + (\xi_1/\xi_2) Q C_{kf}}{(a_{k1} + b_{k1} J_{\nu'}) + (a_{k2} + b_{k2} J_\nu) + C_{kf}} . \tag{6}$$

Now the equation of transfer in the line having frequency ν, including continuous scattering in addition to continuous absorption, will be:

$$-\mu \frac{dI_\nu}{\rho dz} = (\kappa_\nu + \sigma_\nu + \sigma) I_\nu - \sigma J_\nu - \kappa_\nu B_\nu - j_\nu , \tag{7}$$

where κ_ν, σ_ν, and σ represent the continuous absorption coefficient, line-absorption coefficient, and continuous scattering coefficient, respectively, and j_ν is the contribution to the emission provided by scattering from the line transition k-2. We can write $j_\nu^{(0)} = \sigma_\nu^{(0)} B_\nu(T)$, the corresponding value in thermodynamic equilibrium, and then:

$$j_\nu = \xi_k j_\nu^{(0)} .$$

Since σ_ν can be written

$$\sigma_\nu = \xi_2 \sigma_\nu^{(0)} ,$$

in the same notation, then

$$j_\nu = \frac{\xi_k}{\xi_2} \sigma_\nu B_\nu(T) . \tag{8}$$

If we substitute equation (8) in equation (7), we get

$$-\mu \frac{dI_\nu}{\rho dz} = (\kappa_\nu + \sigma_\nu + \sigma) I_\nu - \sigma J_\nu - \kappa_\nu B_\nu - \frac{\xi_k}{\xi_2} \sigma_\nu B_\nu .$$

We shall now substitute the value of ξ_k/ξ_2 given by equation (6) in the equation of transfer. The resulting equation will not, however, reduce to the simple form derived by Strömgren because of the additional terms in $J_{\nu,\nu'}$ and $B_{\nu,\nu'}$ due to the stimulated emissions. In order to obtain a form of the equation of transfer which can be solved, approximations must be made. We shall treat the stimulated emissions as numerical corrections to the spontaneous emissions.

We could now let B_ν and $B_{\nu'}$ be the Planck intensities corresponding to a temperature T_0 and J_ν and $J_{\nu'}$ be the intensities corresponding to black-body radiation of temperature T_e diluted by the factor W. This gives

$$a_{k1}+b_{k1}B_{\nu'}=a_{k1}\{1+(e^{h\nu'/kT_0}-1)^{-1}\},$$

$$a_{k1}+b_{k1}J_{\nu'}=a_{k1}\{1+W(e^{h\nu'/kT_e}-1)^{-1}\},$$

and similar expressions for the transition k–2. We should then need to assign values to T_0, T_e, and W, and the most reasonable would be that T_0 is the boundary temperature of the star, T_e the effective temperature, and W the dilution factor depending on the angle subtended by the star at the point in the atmosphere under consideration. However, it is not possible to assign unique values, independent of frequency, and therefore, since further approximations will be involved in any case, we shall put

$$W(e^{h\nu'/kT_e}-1)^{-1}=(e^{h\nu'/kT_0}-1)^{-1}$$

and a similar equation for the frequency ν. Then

$$\frac{\xi_k}{\xi_2}=\frac{\left\{\frac{\xi_1}{\xi_2}\frac{J_{\nu'}}{B_{\nu'}}a_{k1}[1+(e^{h\nu'/kT_0}-1)^{-1}]+\frac{J_\nu}{B_\nu}a_{k2}[1+(e^{h\nu/kT_0}-1)^{-1}]+\frac{\xi_1}{\xi_2}QC_{kf}\right\}}{a_{k1}[1+(e^{h\nu'/kT_0}-1)^{-1}]+a_{k2}[1+(e^{h\nu/kT_0}-1)^{-1}]+C_{kf}}. \tag{6a}$$

We will now put

$$\frac{C_{kf}}{a_{k1}[1+(e^{h\nu'/kT_0}-1)^{-1}]+a_{k2}[1+(e^{h\nu/kT_0}-1)^{-1}]+C_{kf}}=\epsilon. \tag{9}$$

The substitution of equations (6*a*) and (9) in the equation of transfer gives

$$\begin{aligned}-\mu\frac{dI_\nu}{\rho dz}=(\kappa_\nu+\sigma_\nu+\sigma)I_\nu-\{\sigma+(1-\epsilon)\sigma_\nu\}J_\nu-\left(\kappa_\nu+\frac{\xi_1}{\xi_2}Q\epsilon\sigma_\nu\right)B_\nu\\-\left(\frac{B_\nu}{B_{\nu'}}\frac{J_{\nu'}}{J_\nu}\frac{\xi_1}{\xi_2}-1\right)\frac{a_{k1}[1+(e^{h\nu'/kT_0}-1)^{-1}]}{C_{kf}}\epsilon\sigma_\nu J_\nu.\end{aligned} \tag{10}$$

It is possible to arrive at a similar equation by making different approximations if we return to the equation of statistical equilibrium (2) and treat the stimulated emissions as negative absorptions. Then we have, neglecting collision terms,

$$N_1b_{1k}\left(1-\frac{N_k}{N_1}\frac{\varpi_1}{\varpi_k}\right)J_{\nu'}+N_2b_{2k}\left(1-\frac{N_k}{N_2}\frac{\varpi_2}{\varpi_k}\right)J_\nu+C_{fk}=\xi_kN_k^{(0)}(a_{k1}+a_{k2}+C_{kf}),$$

where ϖ_1, ϖ_2, and ϖ_k are the statistical weights of the states 1, 2, and k, respectively. By the same reasoning as before this leads to

$$\frac{\xi_k}{\xi_2}=\frac{\frac{\xi_1}{\xi_2}\frac{J_{\nu'}}{B_{\nu'}}a_{k1}\frac{\left(1-\frac{\xi_k}{\xi_1}e^{-h\nu'/kT_0}\right)}{(1-e^{-h\nu'/kT_0})}+\frac{J_\nu}{B_\nu}a_{k2}\frac{\left(1-\frac{\xi_k}{\xi_2}e^{-h\nu/kT_0}\right)}{(1-e^{-h\nu/kT_0})}+\frac{\xi_1}{\xi_2}QC_{kf}}{a_{k1}+a_{k2}+C_{kf}}. \tag{6b}$$

In order to reduce this to the same form as previously, it is necessary to put $(\xi_k/\xi_1) = (\xi_k/\xi_2) = 1$ in the small terms on the right-hand side of equation (6*b*). We then derive the equation of transfer as given by equation (10) if we put

$$\epsilon = \frac{C_{kf}}{a_{k1} + a_{k2} + C_{kf}}. \tag{9a}$$

This is the same result we should get by neglecting stimulated emissions altogether, and it seems to us that the former approximation is to be preferred.

By following the work of Pannekoek[5] on ion and electron concentrations in an atmosphere which departs from conditions of thermodynamic equilibrium, in which it is assumed that ions and free electrons come predominantly from ionization from the ground state, it is found that

$$\frac{\xi_i \xi_e}{\xi_1} = \frac{C_{1f}}{C_{1f}^{(0)}}, \tag{11}$$

so that, from equation (5),

$$Q = \frac{C_{1f}}{C_{1f}^{(0)}} \frac{C_{kf}^{(0)}}{C_{kf}}. \tag{12}$$

If we return to equation (10) and write

$$\frac{\xi_1}{\xi_2} Q = Q', \tag{13}$$

and also make the approximation

$$\frac{B_\nu}{B_\nu'} \frac{J_\nu'}{J_\nu} \frac{\xi_1}{\xi_2} = 1, \tag{14}$$

the equation of transfer becomes

$$-\mu \frac{dI_\nu}{\rho dz} = (\kappa_\nu + \sigma_\nu + \sigma) I_\nu - \{\sigma + (1-\epsilon)\sigma_\nu\} J_\nu - (\kappa_\nu + Q'\epsilon\sigma_\nu) B_\nu \tag{15}$$

(cf. Strömgren, *op. cit.*, eq. [37]).

If ξ_1/ξ_2 becomes small for considerable departure from thermodynamic equilibrium, it is probable that equation (14) is no longer valid and that

$$\frac{B_\nu}{B_{\nu'}} \frac{J_{\nu'}}{J_\nu} \frac{\xi_1}{\xi_2} < 1.$$

In this case, if we combine the coefficients of $\sigma_\nu J_\nu$ in the second and fourth terms on the right-hand side of equation (10), the equation of transfer can be rewritten:

$$-\mu \frac{dI_\nu}{\rho dz} = (\kappa_\nu + \sigma_\nu + \sigma) I_\nu - \{\sigma + (1-\epsilon')\sigma_\nu\} J_\nu - (\kappa_\nu + Q''\epsilon'\sigma_\nu) B_\nu, \tag{15a}$$

where

$$\epsilon < \epsilon' \quad \text{and} \quad Q''\epsilon' = Q'\epsilon. \tag{16}$$

Cillié[6] has shown that the probability for ionization of an atom from state n is given by the formula

$$C_{nf} = \frac{512\pi^5}{3\sqrt{3}} \frac{m e^{10}}{c^3 h^6} \frac{Z^4}{n^5} Ei\left(\frac{\chi_n}{kT}\right), \tag{17}$$

where $Ei(x)$ is the well-known exponential integral, and χ_n is the ionization potential from level n. Strömgren[4] has shown that

$$\frac{C_{1f}}{C_{1f}^{(0)}} = \frac{Ei(\chi_1/kT)}{Ei(\chi_1/kT_0)} W, \tag{18}$$

[5] *B.A.N.*, **3**, 207, 1925.

[6] *M.N.*, **92**, 820, 1932.

where T is the actual temperature corresponding to the radiation field, T_0 is the local equilibrium temperature, and W is a dilution factor by which the right-hand side of equation (17) must be multiplied to give the ionization probability in a stellar atmosphere.

The analysis here will be confined to the conditions at the center of a spectrum line, which we will assume is formed in the surface region of the atmosphere. In this case T_0 is equal to the assumed boundary temperature, and $T = T_e$, $W = \frac{1}{2}$. For $W < \frac{1}{2}$ and a fixed value of T_0, T_e will increase. Hence $Ei(\chi_n/kT_e)$ will increase as W decreases. The effect of this on the value of C_{1f} computed for a stellar atmosphere is shown in Table 1, in which $Ei(\chi_1/kT_e)W$ is evaluated for a series of boundary temperatures under

TABLE 1

VALUES OF $Ei(\chi_1/kT_e)$

T_0	$Ei(\chi_1/kT_e)W \times 10^5$ (a)	$Ei(\chi_1/kT_e)W \times 10^5$ (b)
10,080° K	0.013	0.296
16,800	2.98	10.50
25,200	53.57	70.03
28,000	97.34	104.5
30,000	139.9	133.2
34,000	256.5	143.9
42,000	624.1	365.9

two approximations:

(a) $\qquad W = \frac{1}{2}, \qquad T_0 = (\sqrt{3}/4)^{1/4} T_e;$

(b) $\qquad W = \frac{1}{16}, \qquad T_0 = (\frac{1}{2}) T_e.$

Using equation (18), equation (12) becomes

$$Q = \frac{Ei(\chi_1/kT_e)}{Ei(\chi_1/kT_0)} \frac{Ei(\chi_k/kT_0)}{Ei(\chi_k/kT_e)}. \tag{19}$$

Now in equation (15), Q' involves the unknown term ξ_1/ξ_2, and hence it cannot be accurately determined. However, if conditions do not depart far from thermodynamic

TABLE 2

VALUES OF Q' FOR $H\alpha$, $H\beta$, AND $H\gamma$

T_0	$Q'(H\alpha)$	$Q'(H\beta)$	$Q'(H\gamma)$
25,200° K	3.01	3.26	3.34
28,000	2.68	2.94	2.99
30,000	2.55	2.74	2.81
34,000	2.34	2.44	2.52
42,000	2.01	2.08	2.13

equilibrium, so that we can make the approximation that $\xi_1/\xi_2 = 1$, Q' can be calculated. In Table 2, values of Q' are given, calculated under this approximation from equation (19), for the lines $H\alpha$, $H\beta$, and $H\gamma$ for several boundary temperatures.

For large departures from thermodynamic equilibrium an additional factor will enter. The level k will be populated by electrons cascading into it subsequent to capture into

levels $n\,(>k)$. To take account of this, it will be necessary to include an additional term in the left-hand side of equation (1) of the form

$$\sum_{i=k+1}^{\infty} g_i C_{fi}\,, \qquad \text{where} \qquad g_i \leqslant 1\,.$$

Equation (6) then becomes

$$\xi_2 \left\{ \frac{J_{\nu'}}{B_{\nu'}} \frac{\xi_1}{\xi_2}\, a_{k1} + \frac{J_\nu}{B_\nu}\, a_{k2} + \frac{\xi_1}{\xi_2} Q C_{kf} + \frac{\sum_{i=k+1}^{\infty} g_i C_{fi}}{\xi_2 N_k^{(0)}} \right\} = \xi_k\,(a_{k1} + a_{k2} + C_{kf})\,. \tag{6a}$$

Under these conditions Q' in equation (15) is replaced by

$$\left\{ Q' + \frac{\sum_{i=k+1}^{\infty} g_i C_{fi}}{\xi_2 N_k^{(0)} C_{kf}} \right\},$$

and equation (16) becomes

$$Q''\epsilon' = \left\{ Q' + \frac{\sum_{i=k+1}^{\infty} g_i C_{fi}}{\xi_2 N_k^{(0)} C_{kf}} \right\} \epsilon\,. \tag{16a}$$

Thus it is seen that strong departure from thermodynamic equilibrium results in an effective increase in the value of ϵ over the value given by equation (9). A second consequence is that Q' is increased by the term

$$\frac{\sum_{i=k+1}^{\infty} g_i C_{fi}}{\xi_2 N_k^{(0)} C_{kf}}\,.$$

III. THE EVALUATION OF THE RESIDUAL INTENSITY AT A POINT IN THE LINE

If we write

$$t_\nu = \int_z^\infty (\kappa_\nu + \sigma_\nu + \sigma)\, \rho\, dz \tag{20}$$

and put

$$\lambda_\nu = \frac{\kappa_\nu + \epsilon_\nu \sigma_\nu}{\kappa_\nu + \sigma_\nu + \sigma}\,, \tag{21}$$

equation (15) becomes

$$\mu \frac{dI_\nu}{dt_\nu} = I_\nu - \tfrac{1}{2}(1-\lambda_\nu) \int_{-1}^{+1} I_\nu(\mu')\, d\mu' - B_\nu \left\{ \lambda_\nu \left(\frac{\kappa_\nu + Q'_\nu \epsilon_\nu \sigma_\nu}{\kappa_\nu + \epsilon_\nu \sigma_\nu} \right) \right\}. \tag{22}$$

This equation can now be written in the form used by Chandrasekhar.[7] Assuming that B_ν is a linear function of τ_ν, we make the following substitutions:

$$B_\nu = B_\nu^{(0)} + B_\nu^{(1)} \tau_\nu\,, \tag{23}$$

$$B'_\nu = D_\nu B_\nu\,, \tag{24}$$

[7] *Radiative Transfer* (Oxford: Clarendon Press, 1950), chap. xii.

where

$$D_\nu = \frac{\kappa_\nu + Q'_\nu \epsilon_\nu \sigma_\nu}{\kappa_\nu + \epsilon_\nu \sigma_\nu}. \tag{25}$$

Here $B_\nu^{(0)}$ and $B_\nu^{(1)}$ are constants introduced by Chandrasekhar (*op. cit.*, p. 322, eq. [22]).

It follows that

$$B'_\nu = B_\nu^{(0)'} + \frac{\lambda_\nu}{(1+\epsilon_\nu \eta'_\nu)} B_\nu^{(1)'} l_\nu, \tag{26}$$

where

$$\eta'_\nu = \frac{\epsilon_\nu \sigma_\nu - \sigma}{\epsilon_\nu (\kappa_\nu + \sigma)}. \tag{27}$$

It will be assumed in the following analysis that D_ν, λ_ν, ϵ_ν, and η'_ν are independent of depth in the atmosphere.

Using equations (24) and (26), equation (22) becomes

$$\mu \frac{dI_\nu}{dl_\nu} = I_\nu - \tfrac{1}{2}(1-\lambda_\nu) \int_{-1}^{+1} I_\nu(\mu')\, d\mu' - \left\{ B_\nu^{(0)'} + B_\nu^{(1)'} \frac{\lambda_\nu}{(1+\epsilon_\nu \eta'_\nu)} \right\} \lambda_\nu l_\nu. \tag{28}$$

Equation (28) is exactly similar to that of Chandrasekhar (*ibid.*, p. 322, eq. [24]), except for the substitution here of B'_ν for B_ν and η'_ν for η_ν. Hence the solutions of this equation given by Chandrasekhar can be taken over directly.

The emergent flux at frequency ν is given by (*ibid.*, p. 327, eq. [70])

$$F = \frac{2\lambda^{3/2}}{1+\epsilon\eta'} B^{(1)'} \left\{ a_2 + \frac{(1+\epsilon\eta')}{\lambda} \frac{B^{(0)'}}{B^{(1)'}} a_1 + \frac{(1-\lambda)}{2\lambda^{1/2}} a_1^2 \right\} \tag{29}$$

(here the suffix η has been dropped), a_1 and a_2 are the first and second moments of the H function defined by Chandrasekhar and have been tabulated for the argument λ (*ibid.*, p. 328, Table 23).

By putting $\sigma_\nu = 0$ in equation (21), we obtain

$$\lambda_{\text{cont}} = \frac{\kappa_\nu}{\kappa_\nu + \sigma}. \tag{30}$$

Using equation (30), it is found that the emergent flux in the continuous spectrum at frequency ν is given by

$$F_{\text{cont}} = 2(\lambda_{\text{cont}})^{1/2} B^{(1)} \left\{ (a_2)_{\text{cont}} + \frac{B^{(0)}}{B^{(1)}} (a_1)_{\text{cont}} + \frac{(1-\lambda_{\text{cont}})(a_1)^2_{\text{cont}}}{2(\lambda_{\text{cont}})^{1/2}} \right\}. \tag{31}$$

Hence the residual intensity at frequency ν in the absorption line is given by:

$$\frac{F}{F_{\text{cont}}} = \frac{\dfrac{2\lambda^{3/2} B^{(1)'}}{1+\epsilon\eta'} \left\{ a_2 + \dfrac{(1+\epsilon\eta')}{\lambda} \dfrac{B^{(0)'}}{B^{(1)'}} a_1 + \dfrac{(1-\lambda)}{2\lambda^{1/2}} a_1^2 \right\}}{2(\lambda_{\text{cont}})^{1/2} B^{(1)} \left\{ (a_2)_{\text{cont}} + \dfrac{B^{(0)}}{B^{(1)}} (a_1)_{\text{cont}} + \dfrac{(1-\lambda_{\text{cont}})}{2(\lambda_{\text{cont}})^{1/2}} (a_1)^2_{\text{cont}} \right\}}, \tag{32}$$

and the condition for emission is

$$\frac{F}{F_{\text{cont}}} > 1 . \tag{33}$$

In order to put equation (32) in a form convenient for computation, we make the substitutions:

$$\eta = \frac{\sigma_\nu}{\kappa_\nu} \tag{34}$$

and

$$\frac{1}{\rho} = \frac{\sigma}{\kappa_\nu} . \tag{35}$$

Then, using equations (25), (21), (30), and (27), we have

$$D = \frac{1+Q'\epsilon\eta}{1+\epsilon\eta} , \tag{36}$$

$$\lambda = \frac{1+\epsilon\eta}{1+\eta+1/\rho} , \tag{37}$$

$$\lambda_{\text{cont}} = \frac{\rho}{\rho+1} , \tag{38}$$

$$1+\epsilon\eta' = \left(\frac{\rho}{\rho+1}\right)(1+\epsilon\eta) . \tag{39}$$

By substitution of equations (32), (36), (37), (38), and (39) in equation (33), the condition for emission becomes

$$\left(\frac{1+Q'\epsilon\eta}{1+\epsilon\eta}\right)\left\{\left(\frac{1+\epsilon\eta}{1+1/\rho+\eta}\right)^{3/2} a_2 + \left(\frac{1+\epsilon\eta}{1+1/\rho+\eta}\right)^{1/2}\left(\frac{\rho}{\rho+1}\right)(1+\epsilon\eta)\frac{B^{(0)}}{B^{(1)}}\, a_1 \right.$$
$$\left. + \left[\frac{1/\rho+\eta\,(1-\epsilon)}{1+1/\rho+\eta}\right]\left(\frac{1+\epsilon\eta}{1+1/\rho+\eta}\right)\frac{a_1^2}{2}\right\} > \left(\frac{\rho}{\rho+1}\right)^{3/2}(1+\epsilon\eta) \tag{40}$$
$$\times\left\{(a_2)_{\text{cont}} + \frac{B^{(0)}}{B^{(1)}}(a_1)_{\text{cont}} + \left(\frac{\rho+1}{\rho}\right)^{1/2}\left(\frac{1}{\rho+1}\right)\frac{(a_1)_{\text{cont}}^2}{2}\right\} .$$

The approximation $\eta \gg 1$ is valid over the range of values that we shall investigate numerically. In this case condition (40) becomes

$$(1+Q'\epsilon\eta)\left\{\frac{a_2}{\eta^{3/2}(1+\epsilon\eta)^{1/2}} + \frac{a_1}{\eta^{1/2}(1+\epsilon\eta)^{1/2}}\left(\frac{\rho}{\rho+1}\right)\frac{B^{(0)}}{B^{(1)}} + \frac{(1-\epsilon)}{\eta\,(1+\epsilon\eta)}\,\frac{a_1^2}{2}\right\}$$
$$> \left(\frac{\rho}{\rho+1}\right)^{3/2}(a_2)_{\text{cont}} + \left(\frac{\rho}{\rho+1}\right)^{3/2}(a_1)_{\text{cont}}\frac{B^{(0)}}{B^{(1)}} + \frac{\rho}{(\rho+1)^2}\,\frac{(a_1)_{\text{cont}}^2}{2}$$

or

$$\frac{B^{(0)}}{B^{(1)}}(Q'x-y) > (z-Q'w) , \tag{41}$$

where

$$x = \frac{\epsilon \eta^{1/2} a_1}{(1+\epsilon\eta)^{1/2}}, \tag{42}$$

$$v = \left(\frac{\rho}{\rho+1}\right)^{1/2} (a_1)_{\text{cont}} - \frac{a_1}{\eta^{1/2}(1+\epsilon\eta)^{1/2}}, \tag{43}$$

$$z = \left(\frac{\rho}{\rho+1}\right)^{1/2} (a_2)_{\text{cont}} + \frac{(a_1)^2_{\text{cont}}}{2(\rho+1)} - \frac{1}{\eta(1+\epsilon\eta)}\left(\frac{\rho+1}{\rho}\right)\left\{\frac{(1+\epsilon\eta)^{1/2}}{\eta^{1/2}} a_2 + \frac{(1-\epsilon)}{2} a_1^2\right\}, \tag{44}$$

$$w = \left(\frac{\epsilon}{1+\epsilon\eta}\right)\left(\frac{\rho+1}{\rho}\right)\left\{\frac{(1+\epsilon\eta)^{1/2}}{\eta^{1/2}} a_2 + \frac{(1-\epsilon)}{2} a_1^2\right\}. \tag{45}$$

Criterion (41) can be further simplified under the conditions $\epsilon\eta \gg 1$, $\rho \gg 1$, and under other intermediate conditions (e.g., $\epsilon\eta$ not $\gg| 1$, $\rho \gg 1$).

We have the following relationship (cf. Underhill[3]):

$$\frac{B^{(0)}}{B^{(1)}} = (1 - e^{-h\nu/kT_0}) \frac{kT_0^2}{h\nu} \left(\frac{dT}{d\tau}\right)^{-1}_{\tau=0} \frac{\kappa_\nu + \sigma}{\kappa + \sigma}, \tag{46}$$

where

$$\kappa_\nu = \bar{\kappa}(1 + \delta_\nu) \tag{47}$$

and δ_ν measures the departure from grayness of the atmosphere. If we write, as a first approximation for the temperature distribution of the atmosphere,

$$T^4 = T_0^4 (1 + \tfrac{3}{2}\tau) \tag{48}$$

then, by differentiation,

$$\left(\frac{dT}{d\tau}\right)_{\tau=0} = \frac{3T_0}{8}. \tag{49}$$

Substituting equations (35), (47), and (49) in equation (46), we get

$$\frac{B^{(0)}}{B^{(1)}} = (1 - e^{-h\nu/kT_0}) \frac{kT_0}{h\nu} \frac{8}{3}\left(1 + \frac{\rho\delta_\nu}{\rho + 1 + \delta_\nu}\right). \tag{50}$$

If we let

$$(1 - e^{-h\nu/kT_0}) \frac{kT_0}{h\nu} = K, \tag{51}$$

the condition for emission (41) becomes

$$\left(Q' - \frac{y}{x}\right) > (z' - Q'w')\left(1 + \frac{\rho\delta_\nu}{\rho + 1 + \delta_\nu}\right)^{-1}, \tag{52}$$

where

$$z' = \frac{z}{xK}\frac{3}{8}, \qquad w' = \frac{w}{xK}\frac{3}{8}.$$

A better approximation to the temperature-distribution function through the atmosphere is that given by Chandrasekhar (*op. cit.*, p. 296) in the form

$$T^4 = T_e^4 \{\tfrac{3}{4}[\tau + q(\tau)] + c\}, \tag{53}$$

where

$$T_0^4 = T_e^4 \frac{\sqrt{3}}{4}$$

and c is a constant defined using the weight functions introduced by Chandrasekhar.

Differentiating equation (53), we obtain

$$\left(\frac{dT}{d\tau}\right)_{\tau=0} = \frac{T_0}{\sqrt{3}} \left\{\frac{3}{4}\left[1 + \left(\frac{dq}{d\tau}\right)_{\tau=0}\right]\right\}, \tag{54}$$

and substitution of equation (54) in equation (46) gives

$$\frac{B^{(0)}}{B^{(1)}} = (1 - e^{-h\nu/kT_0}) \frac{kT_0}{h\nu} \frac{4}{\sqrt{3}} \left\{1 + \left(\frac{dq}{d\tau}\right)_{\tau=0}\right\}^{-1} \left(1 + \frac{\rho\,\delta_\nu}{\rho + 1 + \delta_\nu}\right). \tag{55}$$

If we use equation (55) in equation (41), the more general condition for emission is obtained, namely,

$$\left(Q' - \frac{y}{x}\right) > (z'' - Q'w'') \left\{1 + \left(\frac{dq}{d\tau}\right)_{\tau=0}\right\} \left(1 + \frac{\rho\,\delta_\nu}{\rho + 1 + \delta_\nu}\right)^{-1}, \tag{56}$$

where

$$z'' = \frac{z}{xK} \frac{\sqrt{3}}{4}$$

and

$$w'' = \frac{w}{xK} \frac{\sqrt{3}}{4}.$$

In Section V we shall obtain conditions (52) and (56) in numerical form for the centers of the lines $H\alpha$, $H\beta$, and $H\gamma$ formed in atmospheres having various temperatures and pressures.

IV. THE EFFECT OF ϵ AND Q' ON THE RESIDUAL INTENSITY IN THE LINE

Referring back to the equation of transfer (15) and the expression for the residual intensity in the line (32), we see that there are six cases which can be treated formally by allowing $1/\rho$, ϵ, and Q' to take the following values:

(*a*) $\frac{1}{\rho} = 0, \quad \epsilon = 0;$

(*b*) $\frac{1}{\rho} = 0, \quad 0 < \epsilon < 1, \quad Q' = 1;$

(*c*) $\frac{1}{\rho} = 0, \quad 0 < \epsilon < 1, \quad Q' > 1;$

(*d*) $\frac{1}{\rho} > 0, \quad \epsilon = 0;$

(*e*) $\frac{1}{\rho} > 0, \quad 0 < \epsilon < 1, \quad Q' = 1;$

(*f*) $\frac{1}{\rho} > 0, \quad 0 < \epsilon < 1, \quad Q' > 1.$

The quantity Q' enters into the equation of transfer only in the term $\epsilon\sigma_\nu B_\nu Q'$. Consequently, when $\epsilon = 0$, Q' vanishes from the equation of transfer.

a) From equation (38), $\lambda_{\text{cont}} = 1$, and from equation (27), $\eta = \eta'$. Hence, using equation (32), we obtain

$$\frac{F}{F_{\text{cont}}} = \frac{\{\lambda^{3/2}a_2 + [\lambda(1-\lambda)/2]a_1^2\} + \lambda^{1/2}a_1[B^{(0)}/B^{(1)}]}{\frac{1}{3} + \frac{1}{2}[B^{(0)}/B^{(1)}]}, \tag{57}$$

since

$$a_1(1) = \tfrac{1}{2} \tag{58}$$

and

$$a_2(1) = \tfrac{1}{3} \tag{59}$$

from the table given by Chandrasekhar. Further, using this table of moments, it can easily be shown that, if we write

$$f_1(\lambda) = \left\{\lambda^{3/2}a_2 + \frac{\lambda(1-\lambda)}{2}a_1^2\right\} \tag{60}$$

and

$$f_2(\lambda) = \lambda^{1/2}a_1, \tag{61}$$

then $f_1(\lambda)$ and $f_2(\lambda)$ are both functions which decrease with decreasing values of λ. Now $B^{(0)}/B^{(1)} > 0$, and the maximum values of a_1 and a_2 are given by equations (58) and (59). Consequently, since in equation (57) $\lambda < 1$, it follows that

$$\frac{F}{F_{\text{cont}}} < 1,$$

i.e., no emission is possible.

This case is exactly that treated by Miss Underhill[3] of a line formed by pure scattering with $\sigma = 0$.

b) Here as in case (*a*), $\lambda_{\text{cont}} = 1$, $\eta = \eta'$, and, from equations (32), (58), (59), (60), and (61), we obtain

$$\frac{F}{F_{\text{cont}}} = \frac{[f_1(\lambda)/(1+\epsilon\eta)] + f_2(\lambda)[B^{(0)}/B^{(1)}]}{\frac{1}{3} + \frac{1}{2}[B^{(0)}/B^{(1)}]}. \tag{62}$$

It follows, therefore, in the same way as for case (*a*), that

$$\frac{F}{F_{\text{cont}}} < 1,$$

i.e., no emission is possible.

By putting $\epsilon = 1$, we obtain the case of a line formed by pure absorption, treated by Miss Underhill. Now for pure absorption involving the atomic transition, for example, between levels 1 and 2, none of the absorbed radiation is re-emitted in the transition 2–1. That is to say, the second level is depopulated only by upward transitions to higher discrete states or by collisions (not considered here). However, it is not satisfactory to allow ϵ to depart considerably from zero in this way and not to consider the effect due to Q''s being greater than unity, for the conditions will obviously depart strongly from normal atmospheric conditions and the number of free electrons and ions must be large.

c) Here again $\lambda_{cont} = 1$, $\eta = \eta'$, and

$$\frac{F}{F_{cont}} = \frac{D\{[f_1(\lambda)/(1+\epsilon\eta)] + f_2(\lambda)[B^{(0)}/B^{(1)}]\}}{\frac{1}{3} + \frac{1}{2}[B^{(0)}/B^{(1)}]}, \tag{63}$$

and the condition for emission is given by equation (41), where

$$\left(\frac{\rho}{\rho+1}\right) = 1, \qquad (a_1)_{cont} = \tfrac{1}{2}, \qquad (a_2)_{cont} = \tfrac{1}{3}$$

are substituted in equations (42), (43), (44), and (45). This is a limiting case for the low end of the stellar temperature scale treated numerically for $H\alpha$, $H\beta$, and $H\gamma$ in the following section.

d) Here continuous electron scattering is taken into account, and

$$\lambda = \frac{\rho}{\rho+1+\rho\eta},$$

$$\lambda_{cont} = \frac{\rho}{\rho+1},$$

i.e., $\lambda < \lambda_{cont}$ and

$$\frac{F}{F_{cont}} = \frac{([\rho+1]/\rho) f_1(\lambda) + f_2(\lambda)[B^{(0)}/B^{(1)}]}{([\rho+1]/\rho) f_1(\lambda_{cont}) + f_2(\lambda_{cont})[B^{(0)}/B^{(1)}]}. \tag{64}$$

Now $f_1(\lambda) < f_1(\lambda_{cont})$ and $f_2(\lambda) < f_2(\lambda_{cont})$. Therefore, it follows that

$$\frac{F}{F_{cont}} < 1,$$

i.e., no emission is possible.

Case (*d*) is the case treated by Miss Underhill for a line formed by pure scattering with electron scattering present.

e) Here

$$\lambda = \frac{\rho+\rho\epsilon\eta}{\rho+1+\rho\eta},$$

$$\lambda_{cont} = \frac{\rho}{\rho+1}.$$

It follows that

$$\frac{F}{F_{cont}} = \frac{([\rho+1]/\rho)(1+\epsilon\eta)^{-1} f_1(\lambda) + f_2(\lambda)[B^{(0)}/B^{(1)}]}{([\rho+1]/\rho) f_1(\lambda_{cont}) + f_2(\lambda_{cont})[B^{(0)}/B^{(1)}]} \tag{65}$$

and, for emission,

$$\frac{B^{(0)}}{B^{(1)}}\{f_2(\lambda) - f_2(\lambda_{cont})\} > \left(\frac{\rho+1}{\rho}\right)\left\{f_1(\lambda_{cont}) - \frac{f_1(\lambda)}{(1+\epsilon\eta)}\right\}.$$

Since $B^{(0)}/B^{(1)} > 0$, the left-hand side of this inequality will be negative unless $\lambda > \lambda_{cont}$, or, using equations (21) and (30), unless

$$\epsilon > \frac{\rho}{\rho+1}. \tag{66}$$

Miss Underhill's case of lines formed by pure absorption, with electron scattering present, fulfilled condition (66), since her case corresponded to the value $\epsilon = 1$.

It is thus possible for the emission condition to be satisfied in this case, the most favorable circumstances being when $B^{(0)}/B^{(1)}$ and $1/\rho$ are large.

f) This is the most general case and the condition for emission is given by equation (41). It will be applied numerically in the following section.

V. THE RESIDUAL INTENSITIES IN THE BALMER LINES $H\alpha$, $H\beta$, AND $H\gamma$

If the boundary temperature, electron pressure, and the constituents of a stellar atmosphere are specified, the atomic coefficients σ_ν, κ_ν, and σ can be calculated at any wave length.

The value of ϵ under given conditions can be calculated from equation (9), since C_{kf}, a_{k1}, and a_{k2} can be evaluated or are tabulated for $k = 3$, 4, and 5; the error introduced by using equation (9) for large departures from thermodynamic equilibrium has been discussed qualitatively in Section II.

The quantity Q', as given by equations (13), (16), and (16*a*), is more difficult to determine and will be considered an unknown quantity in equations (52) and (56). From equation (52) a numerical relationship is then obtained in which the unknown factors are δ_ν and Q'. From the more general case represented by equation (56) a numerical relationship is obtained between δ_ν, $(dq/d\tau)_{\tau=0}$ (which effectively measures the temperature gradient at the surface), and Q'.

The temperature range 10,080°–42,000° has been taken to cover stars of spectral types in the range A0–O. Two electron pressures, $P_e = 4 \times 10^2$ dynes and $P_e = 4 \times 10^3$ dynes, which were used by Miss Underhill[8] to represent giant and dwarf characteristics, have been used. The constituents of the atmosphere were taken to be hydrogen and helium in the proportions 85:15 by number. The small amounts of other elements do not contribute appreciably to the atomic coefficients and consequently have been ignored. These proportions were used in the construction of a model atmosphere by Miss Underhill[9] for a hot star, so that some parts of her calculation of the atomic coefficients could be taken over directly.

The proportions of hydrogen and helium are such that 1 gm of star material contains 0.585 gm of hydrogen and 0.415 gm of helium. It then follows for the mixture that the continuous absorption coefficient per gram of star material is given by

$$\kappa_\nu = 0.585\,(1 - x_H)\,k_\nu(H) + 0.415\,(1 - x_{He\,I} - x_{He\,II})\,k_\nu(He\,I) + 0.415\,(x_{He\,I})\,k_\nu(He\,II) \tag{67}$$

in the usual notation. Here x_H, $x_{He\,I}$, $x_{He\,II}$ may be calculated for the various values of temperature and electron pressure from the ionization equation.

The absorption coefficients for hydrogen and ionized helium are given by [9, 10].

$$k_\nu(H) = \frac{F(H)\,D(H)}{u^3}\,(1 - e^{-u}), \tag{68}$$

$$k_\nu(He\,II) = \frac{F(He\,II)\,D(He\,II)}{u^3}\,(1 - e^{-u}), \tag{69}$$

[8] *Pub. Dom. Ap. Obs. Victoria*, **8**, 385, 1951.

[9] *Pub. Copenhagen Obs.*, No. 151, 1950.

[10] A. Unsöld, *Physik der Sternatmosphären* (Berlin: J. Springer, 1938), p. 117.

where

$$u = \frac{h\nu}{kT}, \tag{70}$$

$$F(H) = \frac{64\pi^4}{3\sqrt{3}} \frac{m e^{10}}{c h^3 m_H} \frac{e^{-u_1(H)}}{(kT)^3}, \tag{71}$$

$$D(H) = \sum_{n=3}^{9} \frac{e^{u_n(H)}}{n^3} + \frac{e^{u_{10}(H)}}{2u_1(H)}, \tag{72}$$

$$F(He\ \text{II}) = \frac{64\pi^4}{3\sqrt{3}} \frac{m e^{10}}{c h^3 m_{He}} (2^4) \frac{e^{-u_1(He\ \text{II})}}{(kT)^3}, \tag{73}$$

$$D(He\ \text{II}) = \sum_{n=5,\ 6}^{9} \frac{e^{u_n(He\ \text{II})}}{n^3} + \frac{e^{u_{10}(He\ \text{II})}}{2u_1(He\ \text{II})}, \tag{74}$$

$$u_n(H) = \frac{1}{n^2} \frac{R_H h c}{kT}, \tag{75}$$

$$u_n(He\ \text{II}) = \frac{4}{n^2} \frac{R_{He} h c}{kT}. \tag{76}$$

The terms taken in the summation $n = 3$ to $n = 9$ in equation (72) are sufficient to enable $k_\nu(H)$ to be calculated for the range $3646 < \lambda < 8204$ A, within which lie the lines $H\alpha$, $H\beta$, and $H\gamma$. In equation (74) the summation is taken from $n = 5$, for $H\beta$ and $H\gamma$, and from $n = 6$ for $H\alpha$. Values of $F(H)D(H)$ and $F(He\ \text{II})D(He\ \text{II})$ were taken from Tables 1 and 2 of the paper by Miss Underhill[9] for boundary temperatures greater than 25,200°.

Atomic-absorption coefficients are available only for neutral helium for continua from levels 1^1S, 2^1S, 2^3S, 2^1P, and 2^3P; but, since the wave length for 2^1P, the highest level, is 3682 A and we are concerned with wave lengths greater than this, we have used the hydrogen-like approximation,[9] in which

$$k_\nu(He\ \text{I}) = \frac{1}{m_{He}} (1 - e^{-u}) \frac{64\pi^4}{3\sqrt{3}} \frac{e^{10} m}{c h^6} \frac{e^{-u_i}}{\nu^3} \left\{ Z_{\text{eff}}^4 \left[\sum_{n=3}^{5} \frac{e^{u_n}}{n^3} + \frac{e^{u_5} - 1}{2u_1} \right] + \frac{2}{u_1} \right\}. \tag{77}$$

The mean value of Z_{eff} for $n = 3$, 4, and 5 has been used.

The coefficient of electron scattering, σ, is given by

$$\sigma = \sigma_e \left\{ \frac{0.585}{m_H} x_H + \frac{0.415}{m_{He}} (x_{He\ \text{I}} + 2x_{He\ \text{II}}) \right\}, \tag{78}$$

where σ_e is the Thompson scattering coefficient per electron.

The line-absorption coefficient, σ_ν, per gram of star material, corrected for stimulated emission, is given by

$$\sigma_\nu = \frac{\sqrt{\pi} e^2}{m c} \frac{f N}{\Delta\nu_D} H(a, v)(1 - e^{-u}). \tag{79}$$

It will be seen that we have not taken into account the Stark effect in the computation of σ_ν. However, for high temperatures the line-absorption coefficient is given predominantly by Doppler broadening and damping of the dispersion type.[8] In the computation below we shall be concerned with residual intensities at the centers of the Balmer lines $H\alpha$, $H\beta$, and $H\gamma$ arising in the surface layer of the stellar atmosphere. It is difficult to

estimate the error in σ_ν due to neglect of Stark effect at the line center for the lower temperatures without a detailed calculation, but we assume that it will be small. Here N is the number of atoms in the lower level of the transition, $\Delta\nu_D$ is the Doppler width of the line, and $H(a, v)$ is the broadening function of the line defined by

$$H(a, v) = \frac{a}{\pi}\int_0^\infty \frac{e^{-y^2}}{(v-y)^2+a^2}\,dy. \tag{80}$$

For the center of the line $v = 0$, also $a = \gamma/(4\pi\Delta\nu_D)$. Values of $H(a, 0)$ have been taken from the table computed by Harris.[11] The absorption-line f-values have been taken from the tables of Menzel and Pekeris,[12] and values of γ from Condon and Shortley.[13]

In order to obtain intermediate values of λ from the table of Chandrasekhar, (a) for values near to unity, a_1 and a_2 were plotted against λ, and values were read off the result-

TABLE 3

VALUES OF ϵ

T	ϵ			T	ϵ		
	$H\alpha$	$H\beta$	$H\gamma$		$H\alpha$	$H\beta$	$H\gamma$
10,080° K	0.008	0.015	0.018	30,000° K	0.038	0.045	0.042
16,800	.020	.028	.029	34,000	.042	.048	.045
25,200	.032	.039	.038	42,000	0.048	0.054	0.050
28,000	0.035	0.043	0.041				

TABLE 4

INEQUALITIES FOR $H\alpha$

T	$(Q'-y/x)$	$(z'-w'Q')$		$(z''-w''Q')$		$(1+\rho\delta_\nu/[\rho+1+\delta_\nu])$
	y/x	z'	w'	z''	w''	$\rho\delta_\nu/[\rho+1+\delta_\nu]$
$P_e=4\times10^2$						
10,080° K	5.4	3.3	0.0002	3.8	0.0002	$150\delta_\nu/151+\delta_\nu$
16,800	3.6	1.6	.0004	1.9	.0005	$20\ \delta_\nu/21+\delta_\nu$
25,200	2.9	1.2	.0007	1.3	.0008	$5.4\ \delta_\nu/6.4+\delta_\nu$
28,000	2.7	1.1	.0009	1.2	.0010	$3.8\ \delta_\nu/4.8+\delta_\nu$
30,000	2.6	1.0	.0010	1.2	.0012	$3.2\ \delta_\nu/4.2+\delta_\nu$
34,000	2.5	1.0	.0017	1.1	.0020	$2.7\ \delta_\nu/3.7+\delta_\nu$
42,000	2.3	0.9	.0055	1.1	.0064	$1.6\ \delta_\nu/2.6+\delta_\nu$
$P_e=4\times10^3$						
10,080	5.4	3.3	.0002	3.8	.0002	$1478\ \delta_\nu/1479+\delta_\nu$
16,800	3.6	1.6	.0004	1.9	.0005	$217\ \delta_\nu/218+\delta_\nu$
25,200	3.0	1.1	.0006	1.3	.0007	$54\ \delta_\nu/55+\delta_\nu$
28,000	2.9	1.0	.0007	1.2	.0008	$38\ \delta_\nu/39+\delta_\nu$
30,000	2.8	1.0	.0008	1.1	.0009	$31\ \delta_\nu/32+\delta_\nu$
34,000	2.6	0.9	.0010	1.1	.0012	$23\ \delta_\nu/24+\delta_\nu$
42,000	2.5	0.8	0.0036	1.0	0.0042	$16\ \delta_\nu/17+\delta_\nu$

[11] *Ap. J.*, **108**, 112, 1948.

[12] *M.N.*, **96**, 82, 1936.

[13] *Theory of Atomic Spectra* (Cambridge: At the University Press, 1935).

ing curves; (*b*) for values near 0, a_1 and a_2 were plotted against $\lambda^{1/2}$, and these curves were used.

Numerical values of ϵ were determined by using equation (9). The coefficients a_{k1} and a_{k2} were obtained from the tables of Menzel and Pekeris,[12] and the photoionization probabilities from equation (17), using a dilution factor $W = \frac{1}{2}$. These values are given in Table 3.

In Tables 4, 5, and 6 both sides of the inequalities (52) and (56) are given for $H\alpha$, $H\beta$, and $H\gamma$.

TABLE 5

INEQUALITIES FOR $H\beta$

T	$(Q'-y/x)$	$(z'-w'Q')$		$(z''-w''Q')$		$(1+\rho\delta_\nu/[\rho+1+\delta_\nu])$
	y/x	z'	w'	z''	w''	$\rho\delta_\nu/[\rho+1+\delta_\nu]$
$P_e=4\times10^2$						
10,080	4.1	3.2	0.0005	3.7	0.0006	$65\ \delta_\nu/66+\delta_\nu$
16,800	3.1	1.7	.0012	2.0	.0014	$9.3\ \delta_\nu/10.3+\delta_\nu$
25,200	2.6	1.3	.0026	1.5	.0030	$2.6\ \delta_\nu/3.6+\delta_\nu$
28,000	2.5	1.2	.0030	1.4	.0035	$1.9\ \delta_\nu/2.9+\delta_\nu$
30,000	2.4	1.2	.0038	1.3	.0044	$1.6\ \delta_\nu/2.6+\delta_\nu$
34,000	2.3	1.1	.0065	1.3	.0075	$1.5\ \delta_\nu/2.5+\delta_\nu$
42,000	2.1	1.0	.0125	1.2	.0144	$0.9\ \delta_\nu/1.9+\delta_\nu$
$P_e=4\times10^3$						
10,080	4.1	3.2	.0005	3.7	.0006	$642\ \delta_\nu/643+\delta_\nu$
16,800	3.2	1.7	.0011	1.9	.0013	$100\ \delta_\nu/101+\delta_\nu$
25,200	2.8	1.2	.0019	1.4	.0022	$26\ \delta_\nu/27+\delta_\nu$
28,000	2.7	1.1	.0021	1.3	.0024	$18\ \delta_\nu/19+\delta_\nu$
30,000	2.6	1.1	.0024	1.2	.0028	$15\ \delta_\nu/16+\delta_\nu$
34,000	2.6	1.0	.0032	1.2	.0037	$12\ \delta_\nu/13+\delta_\nu$
42,000	2.5	0.9	0.0065	1.1	0.0075	$9\ \delta_\nu/10+\delta_\nu$

TABLE 6

INEQUALITIES FOR $H\gamma$

T	$(Q'-y/x)$	$(z'-w'Q')$		$(z''-w''Q')$		$(1+\rho\delta_\nu/[\rho+1+\delta_\nu])$
	y/x	z'	w'	z''	w''	$\rho\delta_\nu/[\rho+1+\delta_\nu]$
$P_e=4\times10^2$						
10,080	3.8	3.2	0.0011	3.7	0.0013	$47\ \delta_\nu/48+\delta_\nu$
16,800	3.1	1.9	.0027	2.2	.0031	$6.9\ \delta_\nu/7.9+\delta_\nu$
25,200	2.6	1.4	.0062	1.6	.0072	$2.0\ \delta_\nu/3.0+\delta_\nu$
28,000	2.5	1.4	.0079	1.6	.0091	$1.4\ \delta_\nu/2.4+\delta_\nu$
30,000	2.4	1.3	.0095	1.5	.0110	$1.2\ \delta_\nu/2.2+\delta_\nu$
34,000	2.3	1.2	.0158	1.4	.0182	$1.1\ \delta_\nu/2.1+\delta_\nu$
42,000	2.1	1.2	.0303	1.4	.0350	$0.7\ \delta_\nu/1.7+\delta_\nu$
$P_e=4\times10^3$						
10,080	3.8	3.2	.0011	3.7	.0013	$465\ \delta_\nu/466+\delta_\nu$
16,800	3.2	1.8	.0024	2.1	.0028	$74\ \delta_\nu/75+\delta_\nu$
25,200	2.9	1.3	.0043	1.5	.0050	$20\ \delta_\nu/21+\delta_\nu$
28,000	2.8	1.2	.0049	1.4	.0057	$14\ \delta_\nu/15+\delta_\nu$
30,000	2.8	1.2	.0055	1.4	.0064	$12\ \delta_\nu/13+\delta_\nu$
34,000	2.7	1.1	.0074	1.3	.0085	$9\ \delta_\nu/10+\delta_\nu$
42,000	2.5	1.0	0.0140	1.2	0.0162	$7\ \delta_\nu/8+\delta_\nu$

VI. DISCUSSION

From Tables 4, 5, and 6 it is seen that both w and w' are always very small, and consequently, except for very large values of Q', the terms $w'Q'$ and $w''Q'$ will be unimportant.

In the approximation described by equation (52), we see by comparison with Table 2 that, for the higher temperatures, small increases in the value of Q' over those computed under the assumptions of Strömgren could satisfy the condition for emission. By comparison with Table 3 we see that the values of Q' necessary for emission decrease for increasing temperature, while the corresponding values of ϵ increase. The general feature of these results—that values of Q' for emission decrease with increasing boundary temperature—is in agreement with the general conclusions of Miss Underhill.[3]

The necessity for introducing another term which is to be added to Q' for strong departure from thermodynamic equilibrium (cf. eq. [16*a*]) means that in these cases the effective value of Q' will be increased, and it is under these conditions that emission may be able to occur.

An interesting feature of the results obtained here is that, over a wide range of temperatures and over a factor of 10 in electron pressures, the values of Q' necessary for emission to take place vary but little. It must be remembered that these tables have been calculated with values of ϵ which, as was pointed out in Section II, are at best only approximate. It is felt, however, that Tables 4, 5, and 6 are of interest in showing the general trend of results.

It is clear that the unknown factors which appear either explicitly or implicitly in the mathematical criteria which describe the condition for emission cannot be accurately determined until a method dealing with the physical properties of atmospheres which depart strongly from thermodynamic equilibrium has been applied.

We are deeply indebted to Professor S. Chandrasekhar, F.R.S., and to Professor B. Strömgren for advice and encouragement during the course of this work and for reading the manuscript in draft. Our grateful thanks are also due to Professor D. H. Menzel for reading the draft and for giving helpful criticism and advice. One of us (E. M. B.) is grateful to the International Astronomical Union for a grant which has enabled her to work at the Yerkes Observatory.

THE PHYSICAL THEORY OF METEORS. III. CONDITIONS AT THE METEOR SURFACE*

RICHARD N. THOMAS
University of Utah and U.S. Naval Ordnance Test Station
Received February 21, 1952

ABSTRACT

The conditions at the meteor surface are investigated. It is concluded that the conventional linearized heat-transfer equation cannot be applied to determine the surface temperature of meteors. On the basis of the reaction-rate approach, it is concluded either that the meteor surface vaporizes in all cases or that, if melting occurs, the droplets are so small as to require energies equal to some 50 per cent of the vaporization energy to separate them from the meteor surface.

In the preceding paper of this series,[1] a summary was presented of various attempts to evaluate the heat-transfer efficiency coefficient, Λ, defined by the equation (ρ and v are air density and meteor velocity):

$$\text{Heat transfer} = \Lambda \rho \frac{v^3}{2} \text{ per unit projected area}. \tag{1}$$

Results from free-flight studies on low-melting-point solids at relatively low velocity, wind-tunnel experiments on carbon dioxide pellets, and an analysis of the meteor results to date were included. A later compilation[2] of all these results added one more set of data —some information on very high-velocity pellets. In the terrestrial laboratory experimental work the mass loss was measured directly, and the heat-transfer efficiency coefficient was computed from the measures. In the meteor work, on the other hand, only the parameter (where Γ is the retardation coefficient and ζ the energy to ablate unit mass of meteor material),

$$\sigma = \frac{\Lambda}{2\Gamma\zeta}, \tag{2}$$

could be determined from the observations. While the terrestrial laboratory results on Λ were rather rough, owing to the experimental limitations, the scatter was still only a factor of 2 or so. On the other hand, the values of σ ranged over a factor of 10.

It was decided that the retardation coefficient Γ could not stand a variation of a factor of 10, and so it was deleted as the major cause in the variation of σ. On the other hand, it was possible that Λ would vary by this large amount—but such a variation would necessarily be systematic. It was observed that the variation in σ did not depend systematically upon the air density or meteor speed. Consequently, attention fell on ζ. One had then two possibilities. On the one hand, some meteors may melt and some vaporize —in which case σ varies. The observed rather continuous distribution of σ values over the factor of 10 spread would be in harmony with the suggestion, since one would a priori expect a rather continuous gradation between melting and vaporizing, in the sense that those meteors which melt actually lose the material from the surface in the form of droplets. Consequently, ζ would increase with decreasing droplet size. Alternatively, the meteors might fragment, and the effective ζ decrease. The problem is to decide between the two cases. In Paper II a preference was expressed for the fragmenting as the explanation for the variation in σ, on more or less intuitive grounds. In the present

* Work supported in part by ONR.

[1] F. L. Whipple and R. N. Thomas, *Ap. J.*, **114**, 448, 1951. Hereafter called "Paper II."

[2] F. L. Whipple and R. N. Thomas, *J. Aer. Sci.*, **18**, 636, 1951.

discussion we propose to make use of the general kind of technique developed in the first paper[3] of this series to establish the conjecture on somewhat firmer ground by investigating in detail the conditions on the surface of the meteor at the time that the meteor is observed. We note that observation of the meteor implies sufficient mass loss from the surface to build up a cloud of meteor gas which radiates by collisional excitation from the air molecules.

In brief, the paper compares fusion and vaporization as the ablation source. The discussion falls into two parts. First, we consider the physical conditions which must hold in the "hot" surface layer of the meteor. The essential point here is whether we can describe the surface layer in terms of the macroscopic, conventional, linearized heat-transfer equation or whether we must adopt some other viewpoint, such as that of Paper I. In the second part of the paper, we consider the conditions of energy balance in the hot surface layer to determine the manner of ablation, assuming the ablation rate to be thermally controlled.

I. HEAT TRANSFER WITHIN THE METEOR SURFACE

The early discussion on the problem of melting versus vaporization for a meteoroid was carried through by Öpik,[4] who suggested that the stony meteors have sufficiently low heat conduction that only the surface layer would be effectively heated and the meteor would consequently vaporize. On the other hand, the heat-conduction coefficient would be sufficiently large for the metals that, coupled with a rather rapid rotation of the meteor, sufficient heat would migrate inward to permit only melting. To investigate these conclusions, we consider the conventional linearized thermodynamic heat-transfer equation.

Our problem is the classical one of a solid having a constant rate of supply of energy at one end. We may extend the model somewhat, to include the case in which the atoms themselves actually penetrate the surface, by allowing for the possibility of a distribution of energy sources over some small thickness, l, at one end of the solid. This region in which energy sources are distributed is quite small, since its depth corresponds to the penetration by an atom having several hundred volts translational energy. We assume, then, a distribution of energy sources over this small zone—which we shall call the "reaction zone"—within which the incident atoms are stopped. We assume that within this zone the generation of energy is constant per unit time and per unit volume. Let us introduce the quantity

$$S = \frac{Q}{c\rho_s}, \tag{3}$$

where Q is the energy supply per unit projected area on the meteor. Then the classical formula for the temperature rise (that is, the amount that the temperature rises above the original temperature at a given point) is:[5]

$$\Delta T = \frac{S}{2\sqrt{\pi a}\,l}\int_0^l \int_0^t (t-\tau)^{-1/2} \exp\left[-\frac{(\lambda - x)^2}{4a(t-\tau)}\right] d\tau\, d\lambda, \tag{4}$$

where $a = k/c\rho_s$, the thermal diffusivity; x and t are distance from the end of the solid and the time since the heat commenced to flow; and k, c, and ρ_s are the thermal conductivity, specific heat, and density of the solid. Thus in this formulation we neglect initially any loss of material from the surface of the solid and simply inquire into the temperature

[3] M. A. Cook, H. Eyring, and R. N. Thomas, *Ap. J.*, **113**, 475, 1951. Hereafter called "Paper I."

[4] *Tartu Obs. Pub.*, Vol. **29**, No. 5, 1937.

[5] L. Rand, A. C. Ingersoll, and O. J. Zobel, *Heat Conduction* (New York: McGraw-Hill Book Co., Inc., 1948), chap. viii.

rise at given points in the solid for given times. We may simplify the above equation to write

$$\Delta T = \frac{Q}{2lk\sqrt{\pi}} \int_0^l \int_Y^\infty y^{-2} \exp[-y^2(\lambda - x)^2]\, dy\, d\lambda, \tag{5}$$

where

$$y = [4a(l-\tau)]^{-1/2}, \quad \text{and} \quad Y = (4al)^{-1/2}.$$

We note now that solutions for equation (5) are tabulated for the case $l = 0$. For other cases we must, in general, carry out numerical solutions. We note, however, that we are not interested in solutions of equation (5) for very large values of t. At the time the meteor first becomes visible, conditions at its surface must be such that there is a significant rate of mass loss. Thus, if this picture represented by equation (5) is valid, ΔT must be sufficiently large to bring the meteor surface to at least its melting point. On the other hand, the temperature could not have been much in excess of the boiling point for a significantly long time prior to the onset of luminosity. We note now from equation (1) that the heat transfer is proportional to the air density, ρ, which decreases by about a factor of 6 for every 10-km increase in altitude. Thus, over 1 second, a typical meteor with velocity 30 km/sec goes through an atmospheric region over which ρ varies by about 10^2. Thus, if we consider times of 1 second and in equation (1) use the value of ρ at the height of appearance of the meteor, we will have made a liberal estimate of the energy effective in raising the meteor temperature.[6] Furthermore, we are primarily interested in the temperature at distances from the surface comparable to the value of l—i.e., essentially at the surface itself. Introducing $z = \lambda - x$ and $w = yz$, equation (5) may be simplified to

$$\Delta T = \frac{Q}{2lk}\left[\frac{1}{\sqrt{\pi}\,Y}\int_{x-l}^{x} e^{-Y^2z^2}\,dz - \int_{x-l}^{x} z\left(1 - \frac{2}{\sqrt{\pi}}\int_0^{Yz} e^{-w^2}\,dw\right)dz\right]. \tag{6}$$

Expanding, for small yz, we have

$$\Delta T \cong \frac{Q}{2k}\left\{\frac{1}{Y\sqrt{\pi}} - \frac{(2x-l)}{\sqrt{\pi}} + \frac{Y}{3\sqrt{\pi}}\,\frac{x^3-(x-l)^3}{l} \cdots\right\}. \tag{7}$$

CASE I

For $l = 0$—i.e., the energy is transferred directly to the surface, with the incident atoms either absorbed in the first few atomic layers of the solid or else transferring their energy in some other manner directly to the surface of the solid—we have, for the temperature of the surface ($x = 0$),

$$\Delta T = \frac{Q}{2k}\,\frac{1}{\sqrt{\pi}\,Y}. \tag{8}$$

Thus we see that the temperature rises as the square root of the time.

CASE II

For nonzero l, we have, for the surface temperature, just equation (7). Actually, however, we are interested in the temperature at the end of the zone which is heated by direct impact of the atmospheric atoms; hence we obtain ($x = l$)

$$\Delta T = \frac{Q}{2k}\left[\frac{1}{\sqrt{\pi}\,Y} - \frac{l}{\sqrt{\pi}} + \frac{Yl^3}{3\sqrt{\pi}} + \cdots\right]. \tag{9}$$

We must, of course, apply the equation only for small Yl. For any nonzero value of Y, the results show that the first term is essentially the important one; for the value of l is quite small. Thus, for any l appreciably less than Y^{-1}, it does not make much differ-

[6] More exactly, this value should be divided by $(\beta v \cos Z)$ if Z is the inclination of the meteor path to the vertical and β is the logarithmic density gradient.

ence for the temperature at the end of the reaction zone what width we assume for l (or the temperature within the reaction zone, also, of course). Thus, after a time

$$t >> \frac{l^2}{4a},$$

the reaction zone is essentially isothermal. Since the reaction zone is probably (?) a maximum of 10^3 lattice spacings thick, we see that the difference between these various thicknesses of the reaction zone for a solution of the heat-transfer equation is completely trivial.

We may now form an estimate of the temperature in the above regions by using for Q the rate at which energy arrives from the atmosphere, calculated by equation (1) and the method described in the preceding two papers. The value of Λ is somewhat uncertain, ranging between 1×10^{-2} and 5×10^{-2}, according to the best estimates we have at present, as discussed in Paper II of this series. Thus we have, for the higher value of Λ,

$$Q = 3 \cdot 10^{13} s^3 \rho \text{ ergs cm}^{-2} \text{ sec}^{-1}, \tag{10}$$

where s is velocity in units of 10 km/sec and ρ is the air-density ratio to the sea-level value $1.2 \cdot 10^{-3}$ gm/cm^{-3}.

For an iron meteor, then ($a = 0.181$, $k = 0.62 \cdot 10^7$ cgs units),

$$\Delta T = 1.2 \cdot 10^6 s^3 \rho l^{1/2}. \tag{11}$$

As discussed above, we choose the value of $s^3\rho$ at the initial observation of the meteor. From the available data,[7,8,9] we have a range in the value of log $s^3\rho$ at the point of initial observation from -3.49 to -4.75 (see Table 1). Thus we see that we would expect a

TABLE 1

METEOR SURFACE-TEMPERATURE RISE FROM EQUATION (11)

log $s^3\rho$	ΔT $x=0$
-3.53	$3.5 \cdot 10^2$
-4.48	$4.0 \cdot 10$

maximum temperature rise of some 400° for the maximum value of $s^3\rho$ and some 40° for the minimum value of $s^3\rho$ at the initial point of the meteor trajectory. While we may expect some kind of volatilization from the meteor surface, even though the temperature is not quite to the boiling point of the material, it is difficult to see how we could expect an appreciable loss of material from the meteor at such low temperatures as computed above. It would seem, then, that we should reject the possibility that the conventional heat-transfer equation suffices to describe the temperature of the meteor surface.

We have, in the foregoing, treated only iron meteors and the one-dimensional heat transfer. Because we have chosen the whole range of observed values (presently available from Whipple and Jacchia's data[7,8,9]), we note that, so long as *one* meteor is of the iron-nickel type, our conclusion is valid. (We note further that recent work[10] on terrestrially launched metallic particles would appear to lead to the same conclusion regarding the method of computing surface temperature.) We might, however, expect the solution for a small, rapidly rotating body to behave somewhat differently from the above. Without discussing the more involved solution for this problem, we note that the essential physical aspect is a raising of the temperature in the central regions, which then reduces the

[7] L. G. Jacchia, *Harvard Obs. Meteor Tech. Rept.*, No. 3 (1949).
[8] L. G. Jacchia, *Harvard Obs. Meteor Tech. Rept.*, No. 4 (1949).
[9] F. L. Whipple, *Rev. Mod. Phys.*, **15**, 246, 1943.
[10] J. S. Rinehart, W. A. Allen, and W. C. White, *J. Appl. Phys.*, **23**, 297, 1952.

heat flow from, and raises the temperature of, the surface. Then we note that (*a*) from equation (5), with $l = 0$, the temperature does not drop to half its surface value until a distance about 0.35 cm from the surface; and (*b*) using the maximum value of s^3r in Table 1 and in Whipple's work,[9] a 1-gm *Fe* meteor (radius 0.31 cm) will have "trapped" enough energy to raise about $\frac{1}{20}$ gm to the melting temperature. Thus, from (*a*) we would expect the small, rapidly rotating meteor to be essentially isothermal at the point of appearance, while from (*b*) such a result insures the temperature to be considerably below the melting temperature. (Calculations made for $1 \cdot 10^{10}$ ergs/gm to heat to melting), $s = 3$, $\cos Z = 1$.)

In essence, we require a model in which the heat builds up on the surface to a much greater degree, less being conducted inward. In terms of the heat-transfer equation, such a result could be obtained by decreasing the heat conductivity, k. Physically, however, the situation corresponds to the energy apparently being used up in ablation before a significant amount is conducted inward. If, then, some kind of thermodynamic—i.e., macroscopic—treatment is still to be used, some model such as that of the reaction zone postulated in Paper I of this series might seem preferable. In Paper I only the case of ablation by vaporization was considered. We still have, then, to resolve the problem posed in Paper II by the scatter of the observed σ values. We note specifically that, by adopting the model of Paper I, we assume the ablation rate to be thermally controlled.

II. THE CONDITIONS OF ENERGY BALANCE IN THE REACTION ZONE

Having decided in Section I that some such model as that of the reaction zone discussed in Paper I must hold for this case of very rapid heat transfer, we attempt to resolve the dilemma posed by the scatter of the σ values. That is, we attempt to decide whether the scatter in σ values may arise from a variation between vaporization and melting in the ablation process or whether the more likely alternative is fragmenting of the meteoroid. We note now that the essential characteristic of the reaction-zone model is that of being an isothermal zone, with the temperature fixed by the balance between the heat input and the heat output from radiation and ablation losses. From Paper I we have an expression for the rate of energy loss by vaporization, namely,

$$\frac{f^*}{f}\frac{kT}{h}\, e^{-\epsilon/kT}\left(\frac{\rho_s}{\mu_s m_H}\right)^{2/3}\Delta H\,, \tag{12}$$

where f^* and f are partition functions for the activated and solid state; ϵ is the activation energy; and ΔH is the energy to ablate one atom. From radiation we have the energy loss,

$$\sigma_1 T^4\,, \tag{13}$$

which leaves the energy loss from melting to be considered. The energy loss from this last term is somewhat difficult to estimate, since, as already mentioned, it depends on the size of the droplets which leave the body. Furthermore, the process occurs in two stages—the melting and the ablation. In the ablation-by-vaporization model, the isothermal reaction zone corresponds to the activated state, and there is assumed to be no further energy barrier to the atoms leaving the surface. In an ablation-by-fusion model, energy is required to separate the fluid from the surface—or into droplets. Thus there exists a problem in the fusion model as to which is the rate-determining process—melting or loss of molten material. If we now adopt this reaction-rate model for the hot zone of the meteor surface, we can readily show that a solution to this question of the rate-determining process in the fusion model indicates the most probable situation to be one of vaporization. Consider the argument.

We note that the reaction-rate approach implies that the slowest of the two above processes determines the rate of the reaction and may be written in the same form as equation (12), in which ϵ represents the activation energy of the process and ΔH the

energy expended in carrying one atom through the ablation process. We now determine the temperature of the reaction zone by equating the sum of equations (12)—written for vaporization or for fusion—and (13) to equation (1). As remarked in Paper I, there is considerable uncertainty in f^*/f. For the fusion model there is added an uncertainty in ΔH, resulting from the uncertainty in droplet size. The range of ΔH is covered by the one extreme, where the droplets are single atoms and

$$\Delta H = \epsilon_v + \tfrac{5}{2} kT , \tag{14}$$

to the case of pure melting and no droplets:

$$\Delta H = \epsilon_l + 3kT \tag{14a}$$

where ϵ_v and ϵ_l are, respectively, the energies to vaporize and to melt at 0° K. As in Paper I, we take f^*/f to be $3\theta_s/4T$ with an uncertainty of a factor $(\theta_s/\theta^*)^2$, where θ is the Debye characteristic frequency. We now note that the resulting value of the temperature is essentially fixed by the value of ϵ in the exponent of equation (12)—i.e., by the adopted activation energy—with only relatively small influence by the remaining terms. The assertion may be demonstrated numerically by computing the surface temperature of the meteor by the two models—vaporization and fusion. Such a computation requires a value of Λ. We have earlier remarked (and discussed in Paper II) on the uncertainty in Λ resulting from the uncertainty in ζ, the energy of ablation per unit mass. Since we have

$$\zeta \cong \frac{\Delta H}{\mu_s m_H} , \tag{15}$$

we may rewrite the energy-balance equation in terms of σ as follows:

$$\frac{\sigma_1 T^4}{\Delta H} + \frac{f^*}{f}\frac{kT}{h} e^{-\epsilon/kT}\left(\frac{\rho_s}{\mu_s m_H}\right)^{2/} \cong \frac{\sigma \Gamma \rho v^3}{\mu_s m_H} . \tag{16}$$

(The approximation indicated results from the use of ζ in the meteor analysis as a constant, while ΔH depends on T. The values of T to be obtained, however, show this uncertainty to be less than some 20 per cent of ζ—and hence negligible.) Now, considering an iron meteor and introducing

$$\tau = \frac{\epsilon_v}{kT} = \frac{4.925 \cdot 10^4}{T} , \tag{17}$$

we may rewrite equation (16) as follows:

$$M + 10^{-2.84}\tau^{-3}(1 + 0.4\tau)^{-1} = 10^{8.69}\sigma r s^3 ; \tag{16.1}$$

for

$$M = e^{-\tau} \text{ for vaporization} \tag{16.1a}$$

and

$$M = e^{-\epsilon\tau/\epsilon_v} \text{ for fusion and equation (14)} , \tag{16.1b}$$

while for fusion and equation (14a), equation (16) becomes

$$e^{-\epsilon\tau/\epsilon_v} + 10^{-2.84}\tau^{-3}\left(1 + \frac{\tau}{3}\frac{\epsilon_l}{\epsilon_v}\right)^{-1}\frac{5}{6} = 10^{8.69}\sigma r s^3 , \tag{16.2}$$

and the ϵ for the fusion-ablation process is as yet undecided. In Section I we had a range of observed $\log rs^3$ at the initial point of the meteor trail from -3.53 to -4.48. The $\log \sigma rs^3$ values for these two meteors again represent the extreme range, from -15.03 to -16.21. (The associated values of σ do *not* represent the extreme range discussed in Paper II; the present data are those for which values of r, s, and σ have been published[7] for the initial point and the point of maximum light.) If we now assume that the rate-determining process is the melting and hence take $\epsilon = \epsilon_l$ in equations (16.1a) and

TABLE 2

SURFACE TEMPERATURE OF METEOR FROM EQUATIONS (16)

log $\sigma r s^3$	Eq. (16.1a) $\epsilon = \epsilon_v$	Eqs. (16.1b)–(16.2) $\epsilon = \epsilon_l$
−15.03	3340	125
−16.21	2740	105

TABLE 3*

METEOR SURFACE TEMPERATURE, ASSUMING ABLATION BY VAPORIZATION

Meteor No.†	log σ‡	log r§	s‖	T
642 i	−11.47	−5.43	3.19	3150
m		−4.20	3.02	3850
660 i	−11.50	−3.94	1.37	3340
m		−3.28	1.31	3720
689 i	−11.84	−6.04	6.47	3120
m		−5.14	6.12	3600
697 i	−11.87	−5.63	3.44	2890
m		−4.16	3.16	3650
705 i	−11.73	−5.95	3.10	2740
m		−4.57	3.06	3460
710 i	−11.74	−5.67	3.15	2880
m		−3.96	2.92	3800
712 i	−11.71	−5.44	2.99	2980
m		−4.01	2.90	3780
736 i	−11.41	−5.33	3.66	3340
m		−4.44	3.60	3880
778 i	−11.89	−5.72	3.51	2860
m		−3.96	3.29	3800

* It is of some interest to note that the computed temperature at the time of first appearance of the meteor falls very close to the 2900° K value at which the radiation term in equations (16) equals the ablation term. It is tempting to assume that vaporization is indeed the ablation mechanism and that the meteor surface begins to ablate only when radiation cannot dissipate the heat transferred to the surface sufficiently rapidly to hold the temperature below the 2900° value. Clearly, the scatter of the values in Table 3 and the difference in resolution of different meteor cameras will not appreciably affect such a conclusion if the above type of analysis is valid. (We note again that we have assumed all meteors to be iron in the foregoing discussion.)

† "i" refers to the initial point; "m" refers to the point of maximum light on the meteor path.

‡ See n. 6.

§ L. G. Jacchia, *Harvard Repr. Ser.* II-31 (Tech. Rept. No. 3 [1949]).

‖ L. G. Jacchia, *Harvard Repr. Ser.* II-32 (Tech. Rept. No. 4 [1949]).

(16.2), we may tabulate the resulting values of T computed from equation (16) as shown in Table 2. Thus, from Table 2 we see that it does not matter which of the expressions (14) for ΔH is used. Once $\epsilon = \epsilon_l$ is chosen, the surface temperatures computed are far below the 1800° K melting point of iron. (The dynamic pressure ρv^2 is less than 1 atm., so that there are no pressure effects.) Thus such a choice of ϵ—i.e., of the rate-determining process—leads to an inconsistency. In order, then, to apply the reaction-zone model to the fusion process, we must assume the slow process to be the shedding of the molten material. Then the value of ϵ used depends on the droplet size. We note, however, from the foregoing results that the ϵ value must be essentially the ratio (melting temperature to the temperatures in the second column of Table 2) times ϵ_v, or (0.5–0.6) ϵ_v. For such a situation the alternative equations (14) and (14*a*) for ΔH effectively converge as $\epsilon \rightarrow \epsilon_v$ (since ϵ_l in eq. [14*a*] is to be replaced by ϵ and $\frac{1}{2}kT$ is small).

We then have two results. First, from the last paragraph and equation (15) we see that the ζ value cannot vary by more than a factor of 2, owing to this change from fusion to vaporization. Thus we must conclude that, if this reaction-zone model is adopted, the scatter in the observed σ values (covering a range of a factor of 10) cannot come solely from a variation in ζ. Consequently, we favor the interpretation of the scatter in σ as coming from a fragmenting of the meteor. Thus the smallest observed σ values should be those used in obtaining the heat-transfer efficiency coefficient, Λ. Second, it seems doubtful whether ϵ can be so close to ϵ_v without the ablation process being, indeed, vaporization. (The droplet size corresponding to $\epsilon \sim \frac{1}{2}\epsilon_v$ is $\sim 10^{-6}$ cm.)

III. COMMENTARY

In the preceding two sections we have investigated the conditions at the meteor surface from the self-consistency requirement that the theory adopted shall, given the heat transfer at the point of appearance of the meteor, predict significant ablation. The conventional heat-transfer equation is rejected on the basis of this requirement, because physically the heat flows inward too rapidly to allow the temperature to build up to a sufficiently high value for ablation to occur. If we adopt a reaction-rate approach, we also reject ablation-by-fusion with melting the rate-determining step, because physically the predicted ablation rate is too high to permit a significant temperature rise. Thus these two rejected approaches are complementary, in the sense of defining the physical picture of the two extremes wherein the surface temperature can build up. On the one hand, the heat flows out of the material; on the other, the material "leaves" before sufficient heat "arrives." We see, then, that the discussion of the ϵ value necessary to permit fusion is actually a discussion of the physical conditions necessary to build up the minimum temperature from which significant ablation can occur. The reaction-rate approach is then simply a structure to formulate the process *under the assumption* that it proceeds at a *thermally controlled* rate. If, now, fragmenting and sputtering occur significantly, the phenomenon is not thermal, and our theory is invalid. Until experiments are performed under similar conditions, one cannot choose absolutely between the thermal and the nonthermal processes. It does, however, seem to me somewhat significant that the temperatures computed at the point of meteor appearance, from the reaction-rate approach, lie very close to the boiling point—i.e., just where they must lie if the meteor is to appear at the observed height. The complete set of calculations for the available data, on the assumption of vaporization, appears in Table 3. For fusion, we have no a priori knowledge of ϵ. The best we could do is to invert the process, demanding that T exceed the melting point, and hence determine ϵ and infer a maximum-size droplet.

I am indebted to W. A. Allen and J. S. Rinehart for discussion on the present problem and terrestrial experimental work concerned with it, to F. L. Whipple for the same relative to the meteors, and to H. Eyring and M. A. Cook for discussion of the general problems.

THE DETERMINATION OF A LIGHT-TIME ORBIT*

JOHN B. IRWIN
Goethe Link Observatory, Indiana University
Received April 2, 1952

ABSTRACT

The apparent variation of period arising from the variation of distance of an eclipsing binary from the observer as a result of the gravitational attraction of a distant third component is considered. Woltjer's analytical method is extended and modified. Tables are presented which form the basis of a new graphical method which is both accurate and short.

The following problem was first considered by Woltjer:[1] to determine the elliptic orbit of a star if the distance of the star from an arbitrary fundamental plane (a plane perpendicular to the line of sight) is given by observation as a function of time. This problem arises in the interpretation of the apparent variation of period of an eclipsing binary caused by the changing light-time resulting from the orbital motion of the eclipsing system with reference to a third star; examples are Algol,[2] SV Centauri,[3] and RT Persei.[4] The interpretation of such an observed variation of period may be complicated by the presence of a fourth component, by the rotation of the line of apsides of the small elliptical orbit of the eclipsing pair, or by little-understood changes of period, arising perhaps from changes in the internal structure of one or both of the eclipsing components. The problem of the determination of the light-time orbit will occur with increasing frequency as the observational data become more accurate and extend over greater stretches of time.

If z is the distance of the center of mass of the eclipsing pair from the tangent plane which is perpendicular to the line of sight and which passes through the center of mass of all three stars, then, as is well known,

$$z = r \sin i \sin(v+\omega). \tag{1}$$

It is more convenient for our purposes to consider z', the distance referred to another (and parallel) plane perpendicular to the line of sight which passes through the *center* of the elliptical orbit of the eclipsing pair about the common center of mass of all three stars. These two reference planes will coincide if ω is 0° or 180° or if the orbit is circular. If τ is the light-time and c the velocity of light, then

$$\tau = \frac{z'}{c} = \frac{r \sin i \sin(v+\omega) + a e \sin\omega \sin i}{c}, \tag{2}$$

or

$$\tau = K \frac{1}{\sqrt{(1-e^2\cos^2\omega)}} \left[\frac{1-e^2}{1+e\cos v} \sin(v+\omega) + e \sin\omega\right], \tag{3}$$

where

$$K = \tfrac{1}{2}(\tau_{\max} - \tau_{\min}) = \frac{a \sin i \sqrt{(1-e^2\cos^2\omega)}}{2.590 \times 10^{10}}, \tag{4}$$

* Publications of the Goethe Link Observatory, Indiana University, No. 8.

[1] *B.A.N.*, **1**, 93, 1922.

[2] O. J. Eggen, *Ap. J.*, **108**, 1, 1948.

[3] D. O'Connell, *Riverview College Pub.*, No. 9, 1949; S. Gaposchkin, *Pub. A.S.P.*, **63**, 148, 1951.

[4] R. S. Dugan, *Contr. Princeton U. Obs.*, No. 17, 1938.

τ and K are in days, and a, the semi-major axis, is in kilometers. It can be shown that the expression

$$\frac{1}{\sqrt{(1-e^2\cos^2\omega)}}\left[\frac{1-e^2}{1+e\cos v}\sin(v+\omega)+e\sin\omega\right]$$

varies between ± 1. The quantity τ is to be taken in the sense of observed time *minus* computed time, where the computed time is $t = t_o + EP'$. If the observational errors are zero and the interpretation correct, then $\tau = \Delta t_{(o-c)}$. The unknowns of the problem, seven in number, are $a \sin i$, e, ω, T, P, t_o, and P'. The last two elements refer to the

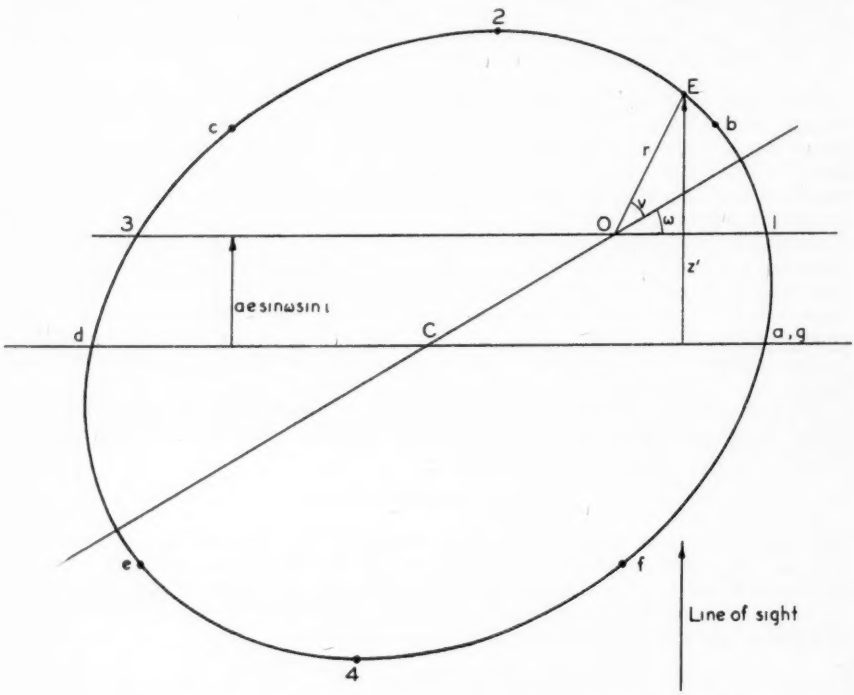

FIG. 1.—E is the eclipsing binary whose light-time curve is shown in Figure 2. The line dCa is the intersection of the orbit plane and the tangent plane through the center of the ellipse. For convenience i is here taken to be 90°.

eclipsing light-curve and are difficult to determine accurately unless τ has gone through at least two maxima or two minima.

The *shape* of the light-time-curve as represented by equation (3) is somewhat similar to the shape of a *velocity-curve* having half the eccentricity and with ω decreased by 90°. For example, the *velocity-curve* for $e = 0.30$ and $\omega = 30°$ closely approximates the shape of a light-time-curve with $e = 0.60$ and $\omega = 120°$. The approximation is even better for smaller eccentricities. If a set of standard velocity-curves[6] is available, a very good preliminary value of e and ω of a light-time-curve can be obtained by fitting the best *velocity-*

[6] E. S. King, *Harvard Ann.*, **81**, 231, 1920.

curve to the observations, then doubling the resulting spectroscopic eccentricity, and increasing the spectroscopic ω by 90°.

If we define $h = (t_d - t_a)/P$, it is easy to show (referring to Fig. 1 and remembering that the areal velocity of the radius vector is constant) that

$$h = \frac{t_d - t_a}{P} = \frac{1}{2} - \frac{e \sin \omega}{\pi \sqrt{(1 - e^2 \cos^2 \omega)}}. \tag{5}$$

Furthermore, if we define $A_1 = (KP)^{-1} \int_{t_a}^{t_d} \tau dt$ and $A_2 = (KP)^{-1} \int_{t_d}^{t_g} \tau dt$, it can be shown,[6] after some considerable algebra, that

$$A_1 - A_2 = \frac{2}{\pi}, \tag{6}$$

and

$$A_1 + A_2 = \frac{-\frac{1}{2} e \sin \omega}{\sqrt{(1 - e^2 \cos^2 \omega)}}, \tag{7}$$

from which

$$h = \frac{1}{2} + \frac{2(A_1 + A_2)}{\pi}, \tag{8}$$

where A_1 is positive and A_2 negative; they are dimensionless and are shown in Figure 2.

The points of inflection of the light-time-curve occur at points *1* and *3*, where $\tau = Ke \sin \omega / \sqrt{(1 - e^2 \cos^2 \omega)}$ and where the *velocity-curve* shows a maximum or minimum. Following Woltjer,[1] if α_1 is the maximum positive slope angle of the light-time-curve and α_2 is *minus* the maximum negative slope angle, α_1 and α_2 both being positive quantities, it follows that

$$e \cos \omega = \frac{\tan \alpha_1 - \tan \alpha_2}{\tan \alpha_1 + \tan \alpha_2}. \tag{9}$$

If τ_p is the value of τ at periastron and T is the time of periastron passage, then

$$\tau_p = \frac{K \sin \omega}{\sqrt{(1 - e^2 \cos^2 \omega)}}, \tag{10}$$

and T is the time at that particular value of τ—of the two possibilities—where the curve is steeper. If the orbit is nearly circular, T becomes indeterminate; in such a case, either t_a, which is directly obtainable from the light-time-curve, or t_1, the time corresponding to the more conventional ascending node, would be preferred; t_1 is on the ascending branch of the curve at that point where $\tau = Ke \sin \omega / \sqrt{(1 - e^2 \cos^2 \omega)}$.

The quantities α_1, α_2, K, and h can be quickly derived from the light-time-curve, so that a solution for the orbital elements is easily made with the aid of equations (9), (5), (4), and (10) in that order. This method may be considered to be a modification of Woltjer's analytical method. Although very quick, it suffers from two disadvantages: (1) it is difficult to determine *accurately* the values of the *maximum* and *minimum* slopes, which means that the value of $e \cos \omega$ as derived from equation (9) may be very uncertain; and (2) there is no way of estimating the errors or uncertainties of the derived orbital elements. For these reasons a numerical-graphical method is given below that overcomes these disadvantages.

We will focus attention at those points on the light-time curve where $\tau = 0.7\,K$, 0, and $-0.7\,K$. These are the points *b* and *c*, *a*, *d*, and *g*, and *e* and *f*, respectively. They are shown in Figures 1 and 2. Values of $(t - T)/P$ can be calculated for these points for any predetermined values of e and ω by solving equation (3) for v, the true anomaly, and

[6] I am indebted to Mr. Robert W. Donselman for pointing out the relationship expressed in eq. (6), which led, in turn, to eq. (7).

then calculating M, the mean anomaly, by means of the Allegheny tables,[7] or by means of the well-known relations:

$$\tan \tfrac{1}{2}E = \left(\frac{1-e}{1+e}\right)^{1/2} \tan \tfrac{1}{2}\tau, \tag{11}$$

$$\frac{t-T}{P} = \frac{M}{2\pi} = \frac{E - e\sin E}{2\pi}. \tag{12}$$

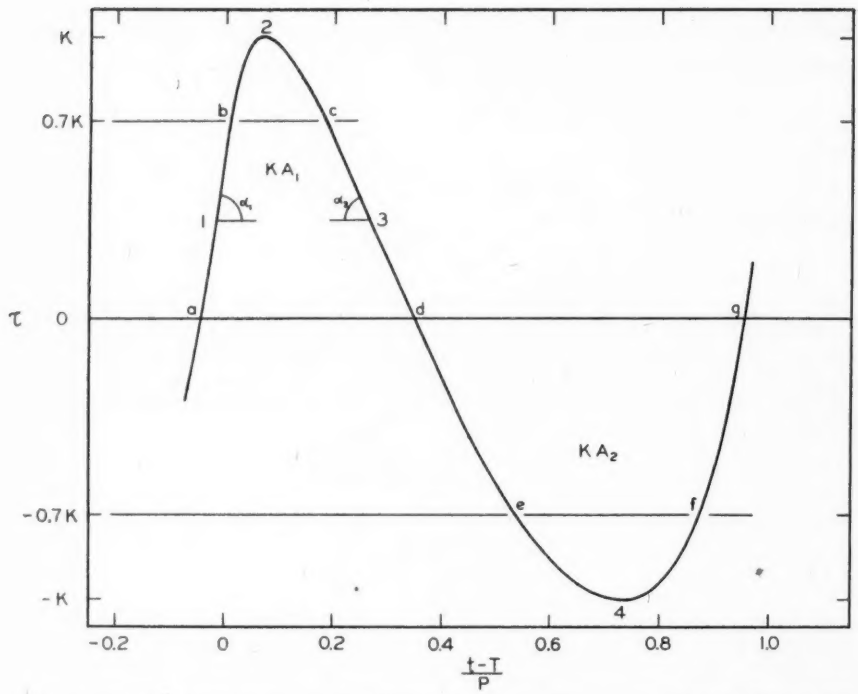

FIG. 2.—The light-time curve for $e = 0.60$ and $\omega = 30°$, corresponding to the orbit shown in Figure 1.

T can be eliminated by taking differences between appropriate pairs of times. The following dimensionless parameters that have been chosen are functions of e and ω only:

$$h = \frac{t_d - t_a}{P}, \qquad s_1 = \frac{t_b - t_a}{P}, \qquad p_1 = \frac{t_e - t_b}{P},$$

$$s_2 = \frac{t_d - t_c}{P}, \qquad p_2 = \frac{t_f - t_e}{P},$$

$$s_3 = \frac{t_e - t_d}{P}, \tag{13}$$

$$s_4 = \frac{t_g - t_f}{P}.$$

[7] *Pub. Allegheny Obs.*, Vol. 2, No. 17, 1912.

TABLE 1

$$h = \frac{t_d - t_a}{P}$$

ω	270	255	240	225	210	195	180	165	150	135	120	105	90
ω	270	285	300	315	330	345	0	15	30	45	60	75	90
e													
0.00	0.500	0.500	0.500	0.500	0.500	0.500	0.500	0.500	0.500	0.500	0.500	0.500	0.500
0.10	.532	.531	.528	.523	.516	.508	.500	.492	.484	.477	.472	.469	.468
0.20	.564	.562	.555	.545	.532	.517	.500	.483	.468	.455	.445	.438	.436
0.30	.595	.593	.584	.569	.549	.526	.500	.474	.451	.431	.416	.407	.405
0.40	.627	.624	.613	.594	.568	.536	.500	.464	.432	.406	.387	.376	.373
0.50	.659	.655	.642	.620	.588	.547	.500	.453	.412	.380	.358	.345	.341
0.60	.691	.687	.673	.649	.612	.561	.500	.439	.388	.351	.327	.313	.309
0.70	.723	.719	.706	.681	.640	.578	.500	.422	.360	.319	.294	.281	.277
0.80	.755	.751	.741	.718	.677	.604	.500	.396	.323	.282	.259	.249	.245
0.90	0.786	0.785	0.778	0.763	0.729	0.650	0.500	0.350	0.271	0.237	0.222	0.215	0.214

TABLE 2

$$s_1 = \frac{t_b - t_a}{P}; \qquad s_2 = \frac{t_d - t_c}{P}; \qquad s_3 = \frac{t_e - t_d}{P}; \qquad s_4 = \frac{t_g - t_f}{P}$$

ω for s_1	0	15	30	45	60	75	90	105	120	135	150	165	180
ω for s_2	180	165	150	135	120	105	90	75	60	45	30	15	0
ω for s_3	180	195	210	225	240	255	270	285	300	315	330	345	360
ω for s_4	360	345	330	315	300	285	270	255	240	225	210	195	180
e													
0.00	0.123	0.123	0.123	0.123	0.123	0.123	0.123	0.123	0.123	0.123	0.123	0.123	0.123
.10	.112	.111	.111	.112	.114	.116	.119	.122	.125	.128	.131	.133	.135
.20	.101	100	100	101	105	.109	.114	.120	.126	.133	.138	.142	.146
.30	.090	.088	.088	.090	.095	.102	.110	.118	.128	.137	.145	.152	.157
.40	.079	.076	.076	.080	.086	.095	.105	.116	.128	.140	.151	.161	.168
.50	.068	.063	.064	.070	.078	.089	.101	.114	.128	.143	.157	.170	.179
.60	.057	.051	.053	.060	.071	.083	.096	.111	.127	.144	.162	.178	.190
.70	.045	.039	.043	.052	.064	.077	.092	.107	.124	.143	.164	.185	.201
.80	.034	.027	.034	.046	.060	.073	.087	.102	.118	.138	.162	.190	.213
0.90	0.023	0.017	0.030	0.046	0.059	0.071	0.082	0.094	0.108	0.126	0.151	0.187	0.224

ω for s_1	180	195	210	225	240	255	270	285	300	315	330	345	360
ω for s_2	360	345	330	315	300	285	270	255	240	225	210	195	180
ω for s_3	0	15	30	45	60	75	90	105	120	135	150	165	180
ω for s_4	180	165	150	135	120	105	90	75	60	45	30	15	0
e													
0.00	0.123	0.123	0.123	0.123	0.123	0.123	0.123	0.123	0.123	0.123	0.123	0.123	0.123
.10	.135	.135	.135	.134	.133	.131	.128	.125	.122	.119	.116	.114	.112
.20	.146	.147	.147	.146	.142	.138	.133	.127	.120	.114	.109	.104	.101
.30	.157	.159	.159	.156	.151	.145	.137	.128	.119	.110	.102	.095	.090
.40	.168	.171	.171	.167	.160	.152	.142	.130	.119	.107	.095	.086	.079
.50	.179	.183	.182	.177	.169	.158	.146	.133	.119	.104	.090	.077	.068
.60	.190	.195	.194	.186	.176	.164	.151	.136	.120	.103	.085	.069	.057
.70	.201	.208	.204	.195	.183	.169	.155	.140	.123	.104	.083	.062	.045
.80	.213	.220	.213	.200	.187	.173	.160	.145	.129	.109	.084	.057	.034
0.90	0.224	0.230	0.217	0.201	0.188	0.176	0.164	0.152	0.139	0.121	0.096	0.059	0.023

These seven parameters are tabulated in Tables 1, 2, and 3 as functions of e and ω. The accuracy of the tables is better than 0.0006.

INSTRUCTIONS TO THE COMPUTER

Given the observations, draw the τ ($= \Delta t_{[o-c]}$)—or light-time-curve—with assumed values of t_o and P' (the period of eclipses). Both the position and (essentially) the slope of the $\tau = 0$ axis are dependent upon the assumed values of t_o and P', and the correct choice of these elements may be quite difficult to make, unless there are at least two well-defined maxima or minima. Equations (6) and (8) may be useful at this point in fixing these elements. t_o is so chosen that the $\tau = 0$ axis is the mean axis, halfway between τ_{max} and τ_{min}. The light-time orbit period, P, can now be read from the curve; the times corresponding to the points a, b, c, d, e, f, and g can also be read from the curve and the seven parameters calculated as defined by equations (13).

The value of each parameter, in turn, may now be expressed as a curve on the ω-e plane by interpolating in the appropriate table. One (or more) of these parameters may be omitted if the observational data necessary to its determination are weak or missing. If the fundamental assumptions are correct and the observations without error, the curves so plotted should meet at a point, thereby fixing the values of e and ω. In any practical case the curves will not meet at a point, and some kind of mean intersection must be adopted. An example is the solution for the 188.4-year light-time curve of Algol as shown in Figure 3. New values of the seven parameters should be interpolated from the tables by making use of the adopted values of e and ω; and, by adopting the time at some well-determined point on the curve, it will be found possible to represent the seven points and compare them with the observations. A horizontal shift (or correction) in the time scale may be conveniently made here. A correction to either or both the maximum and the minimum values of τ, and hence K and t_o, may also be made. If the agreement with the observations is not entirely satisfactory, the tables will indicate what changes in e and ω are necessary and possible. The value of T, the time of periastron passage, may be obtained by making use of equation (10); the computer should be familiar with the remarks immediately following this equation. If T occurs very close to the time of τ_{max} or τ_{min} (points *2* or *4*), a more satisfactory determination of T is possible by computing v_2 or v_4, the true anomalies at these points, from[8]

$$\sin(v_2 + \omega) = \sqrt{(1 - e^2 \cos^2 \omega)}\,; \tag{14}$$

$$\sin(v_4 + \omega) = -\sqrt{(1 - e^2 \cos^2 \omega)}\,. \tag{15}$$

The mean anomaly and $t_2 - T$ (or $t_4 - T$) follow immediately from equations (11) and (12) or by making use of the Allegheny tables.[7] The value of $a \sin i$ is calculated from equation (4).

A representation of the final adopted orbital elements may now be made by making use of equation (3). The writer has found it convenient and practical to calculate τ for values of v every 15° from 0° to 345° inclusive. The times for these true anomalies can be quickly obtained with the aid of the Allegheny tables. If the computer at this point feels that he must indulge in a least-squares correction, analytical expressions for the differential coefficients have been published by Scott.[9] In view of the difficulty in accurately fixing t_o and P' and because of complications that may arise from other phenomena that would cause a variation of period, such a least-squares solution would not, in general, be required.

[8] As is well known from spectroscopic binary theory, $\cos(v + \omega) = -e \cos \omega$ at these points, which correspond to the times when the velocity-curve crosses the γ axis.

[9] *Harvard Bull.*, No. 912, 1940. I am informed by Dr. O. J. Eggen that a correction to one of Scott's formulae has been published by Vasilieva, *Astr. Circ. Acad. Sci. USSR*, No. 75, 1948. This reference is not immediately available to me.

The writer's original interest in this problem was stimulated by Dugan and Wright's paper[10] concerning the remarkable variation of period of the 1.66-day eclipsing binary SV Centauri. Their published times of minima can be satisfied with tolerable accuracy by a light-time orbit with $e = 0.50$ and $\omega = 90°$. Unfortunately, the resulting mass function is 6800; it would be unrealistic to attach any reality to the assumptions leading to such a result. O'Connell[3] has suggested a mass function of the order of at least 10,000

TABLE 3

$$p_1 = \frac{l_c - l_b}{P}; \qquad p_2 = \frac{l_f - l_e}{P}$$

ω for p_1	270	255	240	225	210	195	180	165	150	135	120	105	90
ω for p_1	270	285	300	315	330	345	0	15	30	45	60	75	90
ω for p_2	90	75	60	45	30	15	0	345	330	315	300	285	270
ω for p_2	90	105	120	135	150	165	180	195	210	225	240	255	270
e													
0.00	0.253	0.253	0.253	0.253	0.253	0.253	0.253	0.253	0.253	0.253	0.253	0.253	0.253
.10	.276	.275	.273	.269	.265	.259	.253	.247	.242	.237	.233	.231	.230
.20	.299	.297	.293	.286	.276	.265	.253	.241	.230	.221	.214	.209	.208
.30	.321	.319	.313	.303	.288	.272	.253	.235	.218	.204	.193	.187	.185
.40	.344	.341	.334	.320	.302	.279	.253	.228	.205	.186	.173	.165	.162
.50	.367	.364	.355	.339	.316	.287	.253	.220	.190	.167	.152	.142	.140
.60	.390	.387	.377	.360	.333	.296	.253	.210	.173	.147	.129	.120	.117
.70	.412	.409	.400	.383	.353	.309	.253	.197	.153	.124	.106	.097	.094
.80	.435	.433	.425	.409	.379	.327	.253	.179	.127	.097	.081	.074	.071
0.90	0.458	0.456	0.452	0.441	0.416	0.360	0.253	0.146	0.090	0.066	0.055	0.050	0.049

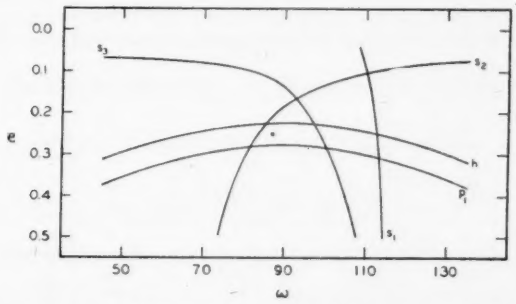

FIG. 3.—The solution for the 188.4-year variation of period of Algol. Eggen's solution is the filled circle. The uncertainties in e and ω are greater than indicated because of the uncertainties of both P and P'.

and has deduced a mass function of 49 for still another hypothetical component by considering the systematic run of the residuals from an empirical parabolic formula. This latter result would also seem to be an unsatisfactory answer. The cause of the variation of period of this system, which has, by far, the greatest known amplitude of variation, must still be considered to be unknown. Until the correct explanation is forthcoming a certain amount of doubt must be attached to every other light-time orbit solution.

[10] *Contr. Princeton U. Obs.*, No. 19, 1939.

THE DETERMINATION OF A SPECTROSCOPIC BINARY ORBIT*

JOHN B. IRWIN
Goethe Link Observatory, Indiana University
Received March 27, 1952

ABSTRACT

Tables are presented that enable the computer to obtain quickly from the velocity-curve an accurate solution for the orbital elements of a spectroscopic binary. Applications to the velocity-curves of Boss 4496 and ε Arietis are given.

The most frequently used method of orbit computation for a spectroscopic binary is probably that of Lehmann-Filhés.[1] Although this method is fairly rapid and is of considerable analytical elegance, the accuracy of the solution depends not only on observations over the *entire* radial-velocity-curve but also on the accurate determination of the *times* of maximum and minimum velocity. The solution is weak, therefore, if these times are poorly fixed by the observations or if sections of the velocity-curve are poorly observed or not observed at all. This latter situation occurs quite frequently, for example, in the case of double-lined binaries at those times when the spectral lines of the two components cannot be separately measured. Furthermore, once the orbital elements have been determined by this method and a theoretical curve drawn, it is not immediately obvious to an inexperienced computer—if the fit with the observations is not completely satisfactory—as to just what adjustments to the elements should be made. In addition, it is not possible to estimate accurately the uncertainties or probable errors of the derived elements.

The method to be presented here is based on techniques somewhat similar to those to be found in the well-known Russell method for the solution of eclipsing binary light-curves. Attention will be focused on certain points or "levels" of the velocity-curve, and tables have been computed and are here presented which enable the computer to obtain very quickly a solution which need be based upon only the best-observed portions of the velocity-curve.

The observed velocity, V_o, is given by the well-known equation:[2,3]

$$V_o = \gamma + \frac{dz}{dt} = \gamma + K\,[\cos(v+\omega) + e\cos\omega]\,, \tag{1}$$

where

$$K = \frac{a\sin i}{13{,}750\,P\,(1-e^2)^{1/2}}; \tag{2}$$

γ is the velocity of the system, K is in km/sec, $a \sin i$ is in kilometers, and P is in mean solar days.

The mean velocity, V_m, is defined by

$$V_m = \tfrac{1}{2}\,(V_{\max} + V_{\min}) = \gamma + K\,e\cos\omega\,. \tag{3}$$

Eliminating γ between equations (1) and (3), we have:

$$\cos(v+\omega) = \frac{V_o - V_m}{K}. \tag{4}$$

* *Publications of the Goethe Link Observatory, Indiana University*, No. 7.

[1] *A.N.*, **136**, 17, 1894.

[2] J. A. Hynek, *Astrophysics* (New York: McGraw-Hill Book Co., 1951), chap. x.

[3] R. G. Aitken, *The Binary Stars* (New York: McGraw-Hill Book Co., 1935), chap. vi.

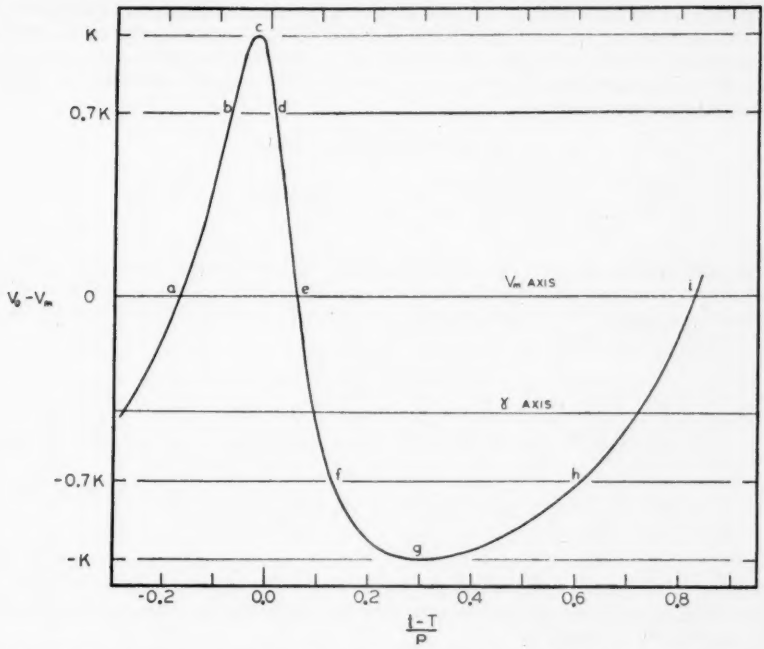

FIG. 1.—The times corresponding to the points *a* to *i* are used to calculate the nine parameters

TABLE 1

$$h = \frac{t_e - t_a}{P}$$

ω.....	0	15	30	45	60	75	90	105	120	135	150	165	180
ω.....	360	345	330	315	300	285	270	255	240	225	210	195	180
e													
0.00..	0.500	0.500	0.500	0.500	0.500	0.500	0.500	0.500	0.500	0.500	0.500	0.500	0.500
.10..	.436	.439	.445	.455	.468	.483	.500	.517	.532	.545	.555	.561	.564
.20..	.374	.378	.390	.409	.435	.466	.500	.534	.565	.591	.610	.622	.626
.30..	.312	.318	.335	.363	.402	.448	.500	.552	.598	.637	.665	.682	.688
.40..	.252	.259	.280	.315	.365	.429	.500	.571	.635	.685	.720	.741	.748
.50..	.196	.203	.225	.265	.326	.406	.500	.594	.674	.735	.775	.797	.804
.60..	.142	.149	.171	.213	.281	.379	.500	.621	.719	.787	.829	.851	.858
.65..	.118	.124	.145	.186	.256	.363	.500	.637	.744	.814	.855	.876	.882
.70..	.094	.100	.119	.158	.229	.345	.500	.655	.771	.842	.881	.900	.906
.75..	.072	.077	.094	.130	.199	323	500	677	801	.870	.906	.923	.928
.80..	.052	.056	.070	.100	.166	.296	.500	.704	.834	.900	.930	.944	.948
.85..	.034	.037	.047	.071	.128	.261	.500	.739	.872	.929	.953	.963	.966
.90..	.0187	.0204	.027	.043	.086	.211	.500	.789	.914	.957	.973	.980	.981
0.95..	0.0067	0.0073	0.0099	0.0168	0.039	0.133	0.500	0.867	0.961	0.983	0.990	0.993	0.993

Cos $(v + \omega)$ varies between ± 1, and the times corresponding to any predetermined value of the quantity $(V_o - V_m)/K$ can be read off the *observed* velocity-curve. For such predetermined values the angle $v + \omega$ can be *calculated* from equation (4), and, furthermore, for any assumed e and ω the values of $(t - T)/P$ can be calculated by means of the well-known relations[4]

$$\tan \tfrac{1}{2}E = \left(\frac{1-e}{1+e}\right)^{1/2} \tan \tfrac{1}{2}v \tag{5}$$

and

$$\frac{t-T}{P} = \frac{M}{2\pi} = \frac{E - e \sin E}{2\pi}. \tag{6}$$

The predetermined values of $(V_o - V_m)/K$ are here chosen to be 0.0, ± 0.7, and ± 1.0. These points on the velocity-curve are approximately equally spaced in time if the eccentricity is small. The following dimensionless parameters that have been chosen are functions of e and ω only:

$$h = \frac{t_e - t_a}{P}; \tag{7}$$

$$s_1 = \frac{t_b - t_a}{P}, \quad s_2 = \frac{t_e - t_d}{P}, \quad s_3 = \frac{t_f - t_e}{P}, \quad s_4 = \frac{t_i - t_h}{P}; \tag{8}$$

$$p_1 = \frac{t_c - t_b}{P}, \quad p_2 = \frac{t_d - t_b}{P}, \quad p_3 = \frac{t_g - t_f}{P}, \quad p_4 = \frac{t_h - t_f}{P}. \tag{9}$$

Here t_a, t_e, and t_i refer to points on the V_m axis; t_b and t_d refer to points where $(V_o - V_m)/K = 0.7$; t_f and t_h refer to points where $(V_o - V_m)/K = -0.7$; and t_c and t_g refer to the times of maximum and minimum velocities, respectively. These points are graphically illustrated in Figure 1.

The nine parameters defined in equations (7), (8), and (9) are tabulated in Tables 1–4 as functions of e and ω. The tables were derived from equation (4) by first calculating v, the true anomaly, for the predetermined values of $(V_o - V_m)/K$ and for values of ω every 15° from 0° to 90°, inclusive. The mean anomalies were next calculated (in degrees), and the final tables formed by subtracting appropriate mean anomalies and dividing by 360. The calculations were not particularly laborious. The accuracy of these tables is better than 0.0006 when three decimal places are given and 0.00006 when four places are given. It has been found possible, because of symmetry, to condense the tabulation of these nine parameters into only four tables. Table 3 may not be useful at all times because of the occasional difficulty in accurately locating the points c and g. This table may be of great usefulness in special cases, such as σ Piscium,[5] where only a small fraction of the velocity-curve is observable. A combination of any two of the nine parameters should usually suffice to determine e and ω.

INSTRUCTIONS TO THE COMPUTER

Given the observations and the velocity-curve drawn with the value of P assumed as known, the first steps are to fix the V_m axis as defined by equation (3) and to determine K from:

$$K = \tfrac{1}{2}(V_{\max} - V_{\min}). \tag{10}$$

The points a, b, c, d, e, f, g, h, and i are located as indicated in Figure 1, the times for these points read off the velocity-curve where possible, and the nine parameters calcu-

[4] For $e \leqq 0.77$ the Allegheny tables (*Pub. Allegheny Obs.*, Vol. 2, No. 17, 1912) will be found very convenient to use, rather than making use of eqs. (5) and (6).

[5] E. P. Belserene, *Ap. J.*, **105**, 229, 1947; *Lick Obs. Contr.*, Ser. II, No. 16.

lated as defined by equations (7), (8), and (9). As previously indicated, it may not be possible in the case of a double-lined binary to fix any or all of h, s_1, s_2, s_3, or s_4; or it may not be possible to fix points c and g—and hence p_1 and p_2—with any degree of accuracy from the observations.[6] For each known parameter a curve is plotted as shown in Figure 2, where e is the ordinate and ω the abscissa. The curve for each parameter is most easily

TABLE 2

$$s_1 = \frac{t_b - t_a}{P}; \qquad s_2 = \frac{t_e - t_d}{P}; \qquad s_3 = \frac{t_f - t_e}{P}; \qquad s_4 = \frac{t_i - t_h}{P}$$

ω for s_1	0	15	30	45	60	75	90	105	120	135	150	165	180
ω for s_2	360	345	330	315	300	285	270	255	240	225	210	195	180
ω for s_3	180	195	210	225	240	255	270	285	300	315	330	345	360
ω for s_4	180	165	150	135	120	105	90	75	60	45	30	15	0
e													
0.00	0.123	0.123	0.123	0.123	0.123	0.123	0.123	0.123	0.123	0.123	0.123	0.123	0.123
.10	.113	.119	.125	.131	.138	.143	.147	.149	.149	.147	.143	.137	.131
.20	.101	.111	.123	.137	.150	.163	.173	.178	.178	.173	.163	.150	.136
.30	.088	.101	.118	.138	.161	.184	.202	.213	.213	.202	.183	.160	.137
.40	.073	.088	.109	.136	.168	.204	.235	.253	.253	.234	.202	.167	.134
.50	.058	.074	.096	.128	.171	.222	.271	.302	.301	.269	.220	.169	.126
.60	.044	.057	.079	.114	.166	.237	.312	.362	.360	.309	.234	.164	.112
.65	.037	.049	.070	.105	.161	.242	.334	.397	.396	.330	.238	.158	.103
.70	.030	.041	.060	.093	.152	.244	.357	.438	.436	.353	.240	.149	.092
.75	.023	.032	.049	.080	.139	.243	.381	.486	.484	.376	.238	.136	.078
.80	.0167	.024	.038	.065	.122	.236	.407	.543	.540	.400	.230	.119	.063
.85	.0110	.0162	.026	.048	.099	.220	.433	.613	.609	.424	.213	.096	.047
.90	.0061	.0092	.0154	.030	.070	.188	.459	.703	.698	.447	.181	.067	.029
0.95	0.0022	0.0034	0.0059	0.0123	0.033	0.124	0.484	0.827	0.822	0.465	0.117	0.032	0.0119

ω for s_1	180	195	210	225	240	255	270	285	300	315	330	345	360
ω for s_2	180	165	150	135	120	105	90	75	60	45	30	15	0
ω for s_3	0	15	30	45	60	75	90	105	120	135	150	165	180
ω for s_4	360	345	330	315	300	285	270	255	240	225	210	195	180
e													
0.00	0.123	0.123	0.123	0.123	0.123	0.123	0.123	0.123	0.123	0.123	0.123	0.123	0.123
.10	.131	.125	.119	.113	.108	.105	.102	.101	.101	.102	.105	.108	.113
.20	.136	.123	.111	.101	.093	.087	.083	.082	.082	.083	.087	.093	.101
.30	.137	.117	.100	.087	.078	.071	.066	.064	.064	.067	.071	.078	.088
.40	.134	.108	.088	.073	.062	.056	.051	.049	.049	.052	.056	.063	.073
.50	.126	.095	.073	.058	.048	.042	.038	.036	.036	.038	.042	.048	.058
.60	.112	.078	.057	.043	.035	.030	.027	.025	.025	.027	.030	.035	.044
.65	.103	.069	.048	.036	.029	.024	.022	.0204	.0204	.022	.024	.029	.037
.70	.092	.059	.040	.029	.023	.0191	.0170	.0160	.0160	.0170	.0192	.023	.030
.75	.078	.048	.032	.023	.0175	.0144	.0128	.0120	.0120	.0128	.0145	.0176	.023
.80	.063	.037	.024	.0165	.0126	.0103	.0090	.0085	.0085	.0091	.0103	.0127	.0167
.85	.047	.026	.0159	.0109	.0082	.0066	.0058	.0054	.0054	.0058	.0067	.0083	.0110
.90	.029	.0151	.0090	.0060	.0045	.0036	.0031	.0029	.0029	.0031	.0036	.0045	.0061
0.95	0.0119	0.0058	0.0033	0.0022	0.0016	0.0013	0.0011	0.0010	0.0010	0.0011	0.0013	0.0016	0.0022

[6] The determination of t_c and t_g may also be time-consuming and, for that reason, may often be omitted with little loss of accuracy. The technique of determination would be similar to the fixing of the date of maximum or minimum light of a variable star. See, for example, Campbell and Jacchia, *The Story of Variable Stars* (Philadelphia: Blakiston Co., 1941), Fig. 22.

calculated by entering the appropriate table and either interpolating for e at the various tabular values of ω or vice versa. The curves so plotted, because of observational errors, will not all meet at a point. The computer must here use his own judgment—with due regard to the nature of his observational material—as to what final values of e and ω to adopt. It may be convenient to take the curves in groups of two or three or possibly use the mean of only those intersections that are strongly determinate.

TABLE 3

$$p_1 = \frac{l_c - l_b}{P}; \qquad p_3 = \frac{l_g - l_f}{P}$$

ω for p_1	0	15	30	45	60	75	90	105	120	135	150	165	180
ω for p_3	180	195	210	225	240	255	270	285	300	315	330	345	360
e													
0.00	0.127	0.127	0.127	0.127	0.127	0.127	0.127	0.127	0.127	0.127	0.127	0.127	0.127
.10	.105	.108	.111	.116	.122	.128	.135	.141	.147	.151	.153	.153	.151
.20	.086	.090	.096	.104	.114	.126	.140	.154	.167	.177	.183	.183	.177
.30	.068	.073	.080	.090	.104	.121	.142	.165	.188	.207	.218	.218	.207
.40	.053	.057	.065	.075	.091	.112	.139	.173	.209	.241	.259	.259	.239
.50	.039	.043	.050	.060	.076	.098	.131	.175	.228	.278	.309	.308	.276
.60	.027	.031	.036	.045	.059	.082	.117	.171	.243	.319	.370	.369	.316
.65	.022	.025	.030	.038	.050	.072	.108	.165	.248	.342	.406	.405	.338
.70	.0175	.0197	.024	.030	.042	.061	.096	.156	.251	.366	.448	.446	.361
.75	.0132	.0149	.0181	.024	.033	.050	.083	.144	.250	.391	.496	.493	.385
.80	.0093	.0106	.0130	.0172	.025	.039	.067	.126	.244	.417	.553	.550	.410
.85	.0060	.0069	.0085	.0114	.0167	.027	.050	.103	.228	.445	.623	.620	.436
.90	.0032	.0037	.0046	.0063	.0095	.0160	.031	.073	.196	.474	.713	.708	.461
0.95	0.0011	0.0013	0.0016	0.0023	0.0035	0.0061	0.0128	0.035	0.132	0.504	0.836	0.831	0.485

ω for p_1	180	195	210	225	240	255	270	285	300	315	330	345	360
ω for p_3	0	15	30	45	60	75	90	105	120	135	150	165	180
e													
0.00	0.127	0.127	0.127	0.127	0.127	0.127	0.127	0.127	0.127	0.127	0.127	0.127	0.127
.10	.151	.146	.141	.135	.128	.122	.116	.111	.107	.105	.104	.104	.105
.20	.177	.167	.154	.140	.126	.114	.103	.095	.089	.086	.084	.084	.086
.30	.207	.187	.164	.141	.120	.103	.090	.080	.073	.068	.066	.066	.068
.40	.239	.207	.171	.138	.111	.090	.075	.064	.057	.053	.051	.051	.053
.50	.276	.226	.173	.130	.097	.075	.060	.049	.043	.039	.037	.037	.039
.60	.316	.240	.169	.116	.081	.058	.045	.036	.030	.027	.026	.026	.027
.65	.338	.245	.163	.106	.071	.050	.037	.029	.025	.022	.021	.021	.022
.70	.361	.247	.154	.094	.060	.041	.030	.024	.0196	.0174	.0164	.0164	.0175
.75	.385	.245	.141	.081	.049	033	023	0180	.0148	.0131	.0123	.0123	.0132
.80	.410	.238	.123	.066	.038	.024	.0170	.0129	.0106	.0093	.0087	.0087	.0093
.85	.436	.221	.100	.049	.027	.0164	.0112	.0084	.0068	.0060	.0056	.0056	.0060
.90	.461	.189	.070	.030	.0156	.0093	.0062	.0046	.0037	.0032	.0030	.0030	.0032
0.95	0.485	0.125	0.033	0.0124	0.0060	0.0034	0.0022	0.0016	0.0013	0.0011	0.0010	0.0010	0.0011

Using the adopted values of e and ω, the computer may now find it advantageous to extract from the tables new values of all nine parameters. Using these values and any one of the more strongly determined points on the velocity-curve, computed values of the nine points a to i can be plotted and compared with the observations. If the agreement is not entirely satisfactory, the tables will indicate what changes in e and ω are necessary

and possible. A horizontal shift (or correction) in the time scale may conveniently be made here. A correction to either or both of the maximum or minimum velocities, and hence K and V_m, can also be quickly made.

The velocity of the system, γ, is now obtained from

$$\gamma = V_m - K e \cos \omega , \tag{11}$$

and the time of periastron passage, T, can be obtained from

$$V_p = V_m + K \cos \omega , \tag{12}$$

where V_p is the radial velocity at that time, that is, when $v = 0°$. Two points of the velocity-curve will have this ordinate; but, because $v + \omega = 0°$ at point c and $v + \omega =$

TABLE 4

$$p_2 = \frac{t_d - t_b}{P}; \qquad p_4 = \frac{t_h - t_f}{P}$$

ω for p_2	0	15	30	45	60	75	90	105	120	135	150	165	180
ω for p_4	180	165	150	135	120	105	90	75	60	45	30	15	0
e													
0.00	0.253	0.253	0.253	0.253	0.253	0.253	0.253	0.253	0.253	0.253	0.253	0.253	0.253
.10	.210	.211	.215	.221	.229	.239	.251	.263	.275	.285	.294	.299	.301
.20	.171	.173	.179	.189	.204	.222	.244	.268	.293	.317	.337	.350	.354
.30	.137	.139	.146	.158	.176	.200	.231	.268	.308	.348	.382	.405	.413
.40	.106	.108	.115	.128	.148	.176	.214	.263	.319	.378	.431	.466	.479
.50	.079	.081	.087	.099	.119	.148	.191	.250	.325	.407	.482	.534	.552
.60	.055	.057	.062	.072	.090	.117	.162	.229	.324	.435	.538	.609	.633
.65	.044	.046	.051	.060	.075	.101	.145	.215	.319	.448	.569	.649	.677
.70	.035	.036	.040	.048	.061	.085	.126	.198	.312	.460	.601	.693	.723
.75	.026	.027	.030	.037	.048	.068	.106	.176	.300	.472	.637	.739	.771
.80	.0186	.0194	.022	.026	.035	.052	.084	.151	.282	.483	.676	.788	.821
.85	.0120	.0125	.0141	.0173	.024	.036	.061	.120	.255	.494	.724	.841	.872
.90	.0065	.0067	.0076	.0095	.0132	.0206	.037	.082	.212	.504	.783	.897	.923
0.95	0.0023	0.0024	0.0027	0.0034	0.0048	0.0077	0.0151	0.038	0.138	0.516	0.869	0.955	0.969

ω for p_2	180	195	210	225	240	255	270	285	300	315	330	345	360
ω for p_4	360	345	330	315	300	285	270	255	240	225	210	195	180
e													
0.00	0.253	0.253	0.253	0.253	0.253	0.253	0.253	0.253	0.253	0.253	0.253	0.253	0.253
.10	.301	.299	.294	.285	.275	.263	.251	.239	.229	.221	.215	.211	.210
.20	.354	.350	.337	.317	.293	.268	.244	.222	.204	.189	.179	.173	.171
.30	.413	.405	.382	.348	.308	.268	.231	.200	.176	.158	.146	.139	.137
.40	.479	.466	.431	.378	.319	.263	.214	.176	.148	.128	.115	.108	.106
.50	.552	.534	.482	.407	.325	.250	.191	.148	.119	.099	.087	.081	.079
.60	.633	.609	.538	.435	.324	.229	.162	.117	.090	.072	.062	.057	.055
.65	.677	.649	.569	.448	.319	.215	.145	.101	.075	.060	.051	.046	.044
.70	.723	.693	.601	.460	.312	.198	.126	.085	.061	.048	.040	.036	.035
.75	.771	.739	.637	.472	.300	.176	.106	.068	.048	.037	.030	.027	.026
.80	.821	.788	.676	.483	.282	.151	.084	.052	.035	.026	.022	.0194	.0186
.85	.872	.841	.724	.494	.255	.120	.061	.036	.024	.0173	.0141	.0125	.0120
.90	.923	.897	.783	.504	.212	.082	.037	.0206	.0132	.0095	.0076	.0067	.0065
0.95	0.969	0.955	0.869	0.516	0.138	0.038	0.0151	0.0077	0.0048	0.0034	0.0027	0.0024	0.0023

180° at point g, there should be no ambiguity unless T occurs at, or very close to, the time of V_{max} or V_{min}. For such cases it may be advisable to determine the value of v at the point a, where $v + \omega = 270°$, or at the point e,[7] where $v + \omega = 90°$, and find T by determining M for this v, either using equations (5) and (6) or the Allegheny tables.[4] A final representation may now be made with the aid of equation (1). If the computer at this point feels that the observational material is sufficiently good, he should proceed to a least-squares differential correction.

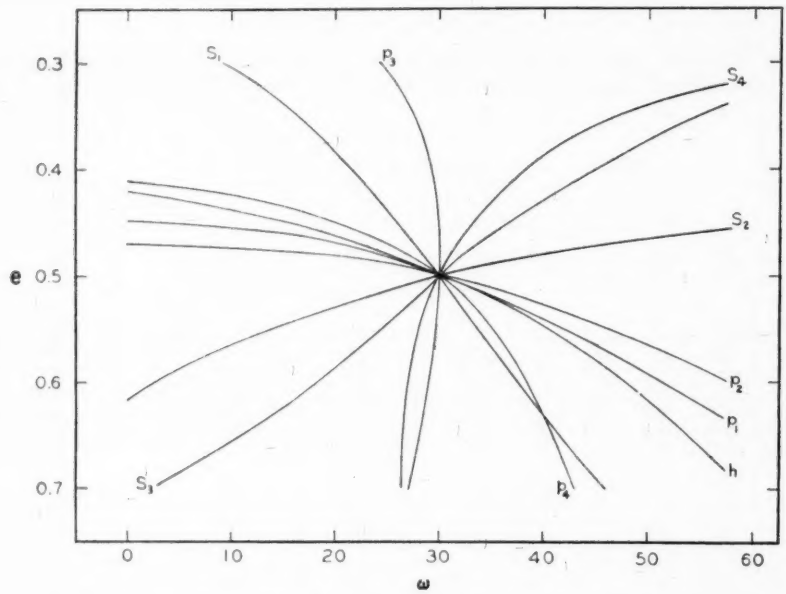

FIG. 2.—The "theoretical" solution of the velocity-curve shown in Figure 1

The above procedure may be modified slightly in the case of a double-lined spectroscopic binary. A graphical or least-squares solution for γ and the mass ratio might first be made by the ingenious method proposed by O. C. Wilson.[8] Knowing γ, a determination of $e \cos \omega$ could be made from

$$e \cos \omega = \frac{V_m - \gamma}{K}. \tag{13}$$

[7] Or at any other of those points where $\cos (v + \omega)$ is accurately known.

[8] *Ap. J.*, **93**, 29, 1941. In Wilson's notation the mass ratio is $r = m_u/m_v = -dv/du$ and r is determined from the negative slope of the straight line defined by the observations plotted on the u–v plane, where u and v are the observed velocities of the respective components. Strictly speaking, the form of Wilson's least-squares equation of condition: $\gamma(1 + r) - ur = v$, is not entirely correct, inasmuch as there are observational errors in *both* co-ordinates. The analysis may be further complicated by the fact that the u velocities may have different weights than the v velocities. Perhaps a better result might be obtained if two solutions were to be made, the second one using the equation of condition: $\gamma(1 + r)/r - v/r = u$. An appropriately weighted mean of the results of the two solutions could then be taken. A more refined—but lengthier—technique, if the u and v velocities are of equal weight, would be to minimize the sum of the squares of the residuals perpendicular to the line. I am indebted to Mr. Arthur N. Cox for bringing these points to my attention.

This value of $e \cos \omega$ could be expressed as a curve on the ω–e plot and would assist in the solution for these two quantities. The rest of the solution would proceed as before, either after appropriately "reflecting" one set of velocities about the γ axis or by making separate solutions for the two velocity-curves and combining the results with appropriate weights, remembering that ω for one star is 180° different from the ω for the other star.

An illustration of the above method is shown in Figure 3, where a solution is made for e and ω for the double-lined spectroscopic binary Boss 4496.[9] A preliminary determination of γ and r was made by the method of O. C. Wilson[8] and $e \cos \omega$ determined from equation (13) and plotted on the figure. Average values of the various parameters were

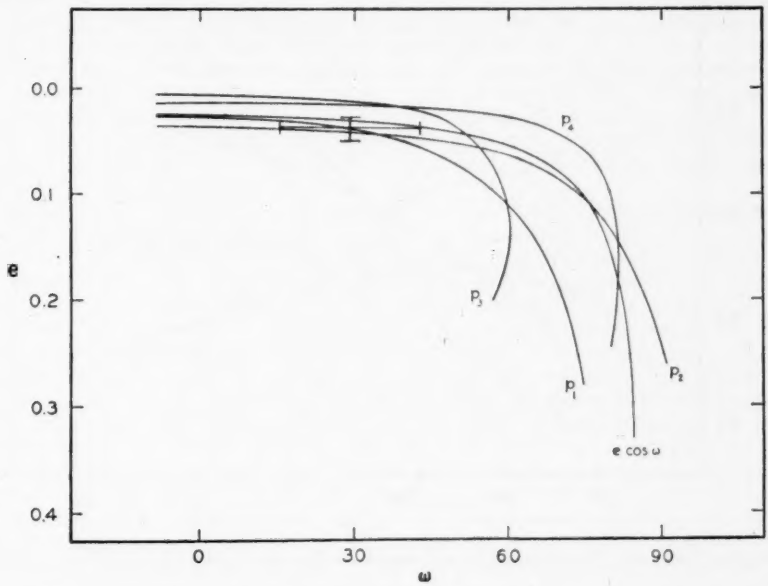

FIG. 3.—The solution for Boss 4496. The least-squares solution gives $e = 0.04 \pm 0.011$, $\omega = 29° \pm 13°.7$. The indeterminacy of ω is clearly shown. The positions of the curves vary markedly with small changes in the values of the parameters.

used as derived from the *two* velocity-curves. The least-squares values of e and ω are shown with their respective probable errors. The indeterminacy of ω is not primarily due to the method or to the observations but, as is well known,[10] is a fundamental feature of nearly circular orbits. In general, the *amount* of distortion (from a sine curve) is primarily dependent on the value of e, whereas how, or at what point, that distortion appears in the velocity-curve depends on ω. If the distortion is at or below the limit of detection, then ω—and also T—must necessarily be quite indeterminate. The technique of analysis in such cases would seem to be to assume $e = 0$ and to proceed with a least-squares solution by the method of Sterne,[11] where e, ω, and T are essentially replaced by $e \sin \omega$,

[9] J. Sahade and J. L. Dessy, *Ap. J.*, **115**, 53, 1952.

[10] W. J. Luyten, *Pub. Obs. U. Minnesota*, **2**, 53, 1936; *Ap. J.*, **84**, 85, 1936.

[11] *Harvard Repr.*, No. 222; *Proc. Nat. Acad. Sci.*, **27**, 175, 1941.

$e \cos \omega$, and T_0, where T_0 represents the time at which the mean longitude $M + \omega$ is equal to zero. Figure 4 illustrates the solution of the velocity-curve of ι Arietis,[12] a single-lined spectroscopic binary of moderate eccentricity. The least-squares values of e and ω, together with their probable errors, are shown in the figure.

The advantages of the precomputed method presented in this paper would seem to be (1) its accuracy, (2) its rapidity, (3) the possibility of making adjustments in the elements *before* the final representation, (4) the fact that the uncertainties in the adopted values of e and ω are indicated on the ω–e plot, and (5) the method's ability to make use

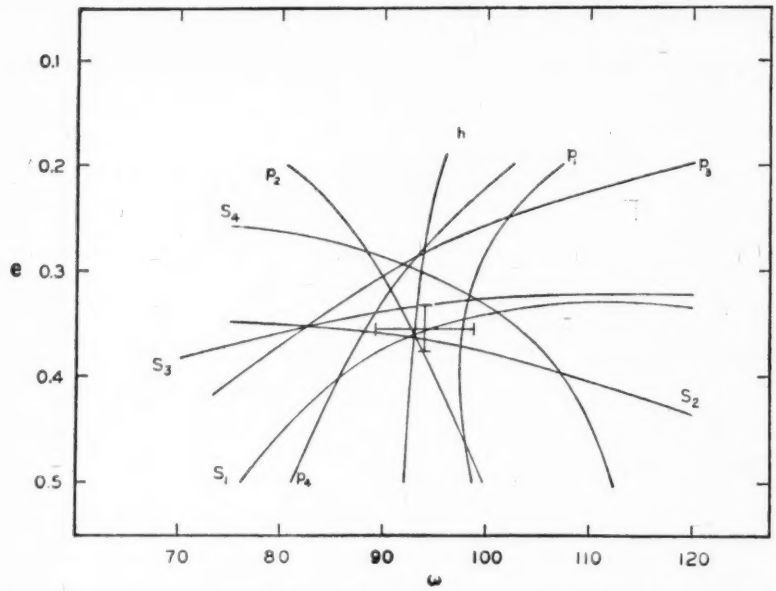

FIG. 4.—The solution for ι Arietis. The least-squares solution gives: $e = 0.356 \pm 0.022$, $\omega = 94°.04 \pm 4°.72$.

of only the well-observed portions of the velocity-curve. For these reasons this method would seem to have very definite advantages in comparison to the method of Lehmann-Filhés. At those observatories, however, where a standard set of velocity-curves[13] is available and is used in routine fashion for the determination of preliminary elements preparatory to a least-squares correction, the method presented here would seem to be somewhat slower and more complex.

I would like to express my thanks to Drs. W. J. Luyten, R. M. Petrie, and O. Struve for a number of valuable comments and suggestions.

[12] K. C. Gordon, *Ap. J.*, **103**, 16, 1946; *Lick Obs. Contr.*, Ser. II, No. 12.

[13] E. S. King, *Harvard Ann.*, **81**, 231, 1920.

NOTES

HD 160641, A HYDROGEN-DEFICIENT O-TYPE STAR*

During a systematic low-dispersion study of the spectra of early-type stars being carried on at the Yerkes Observatory, Dr. W. W. Morgan obtained several spectrograms of the faint star HD 160641.[1] Upon examination of these spectrograms he noted that, although the spectrum resembled to a certain extent that of a late O-type supergiant star, the hydrogen lines in the spectrum appeared abnormally weak, while the *C* III blend near λ 4650 was excessively strong, and several other lines appeared which are not usually seen on comparable spectrograms of normal stars. Two well-exposed spectrograms have been subsequently obtained at the McDonald Observatory and studied by the writer, at Dr. Morgan's suggestion. One of these covers the photographic region of the spectrum with a dispersion of 76 A/mm at $H\gamma$, the other the ultraviolet region with a dispersion of 88 A/mm at λ 3600.

Measurement of the McDonald spectrograms shows that the faint lines near the positions of the hydrogen lines are largely due to *He* II, with slight blending due, in some cases, to *N* III, rather than to hydrogen. There is no real evidence of the presence of hydrogen at all in the region of the spectrum studied. Strong lines arise from *He* I, *Ne* II, *C* III, *N* III, and *Si* IV, while weaker lines are due to *He* II, *O* II, and *O* III. The *He* II line λ 4686 and the *N* III lines at λλ 4634–4642 are quite weak in absorption; these lines occur in emission in the Of stars. Interstellar *Ca* II is present in considerable strength. Figure 1 shows the photographic region of the spectra of HD 160641 and α Cam, an O9.5 I*a* star. Aside from the hydrogen lines, the most striking difference between the two spectra is the extraordinary strength of the two features due to *C* III which arise from 39.8 e.v. These are the blend near λ 4069 and the line at λ 4187. The *C* III blend near λ 4650 arising from 29.4 e.v. appears strongly even in the spectrum of normal supergiant stars of early type but is still further enhanced in the spectrum of HD 160641 and is, in fact, the strongest line in the spectrum. A notable feature shown by the helium spectrum is the considerably greater enhancement in the peculiar star of the diffuse singlets, indicated above the spectra, than of the diffuse triplets, indicated below. The spectrum of HD 160641 in the ultraviolet region is shown in Figure 2, along with spectra of the B1 I*a* star κ Cas and the B-type hydrogen-poor star discovered some years ago by Dr. D. M. Popper,[2] HD 124448. The higher members of the Balmer series, well seen in κ Cas, are not visible in the two lower spectra, while the higher members of the diffuse triplet series of helium continue far into the ultraviolet in the two hydrogen-poor stars. It will be recalled that Popper measured the discontinuity at the limit of this helium series in HD 124448. This discontinuity is undoubtedly smaller in the case of HD 160641, in line with the lower intensity of the helium lines. The helium lines below the Balmer limit are undoubtedly stronger in HD 160641 than in any normal star, as is also true of a number of ultraviolet lines of *Ne* II.

The McDonald spectrograms covering the photographic and ultraviolet regions of the

* *Contributions from the McDonald Observatory, University of Texas*, No. 212.

[1] $\alpha = 17^h36^m0$, $\delta = -17°51'$ (1900); $m_v = 9.8$, according to Stebbins, Huffer, and Whitford. The *Henry Draper Catalogue* classification is "B," with the added remark, "Perhaps of Class Oe5." The galactic co-ordinates are: $l = 337°$, $b = +5°$.

[2] *Pub. A.S.P.*, **54**, 160, 1942; **58**, 370, 1946; and **59**, 320, 1947. The writer is indebted to Dr. Popper for permission to reproduce a spectrogram taken by him of this object.

spectrum were taken on September 15 and 20, 1951, respectively. The radial velocity determined on the first spectrogram from six presumably reliable unblended lines (λ 4089 and λ 4116 of *Si* IV, λ 4097 and λ 4103 of *N* III, and λ 4156 and λ 4187 of *C* III) was +100 km/sec, but the helium lines gave velocities differing from this. The velocity given by the diffuse singlets (λλ 4009, 4144, and 4388) was +82 km/sec, and that given by the diffuse triplets (λ 4026 and λ 4471) was only + 74 km/sec. A possible explanation of these velocity differences might be that they are due to the presence in unusual strength of the forbidden absorption components of these helium lines, which lie to the violet of the normal lines. On the second spectrogram only the ultraviolet diffuse triplet helium lines were measured. The mean velocity given by seven lines was +113 km/sec, with considerable scatter. In view of the discrepancy found in the photographic region between the velocity given by the helium lines and that given by other elements this velocity can be considered only as a confirmation of the high radial velocity of the star. It may be significant that the helium line λ 3554 gave a large positive residual (+60 km/sec) with respect to the mean of the other helium lines measured. In this case the strong forbidden component lies to the red of the normal line.[3]

A further study of the spectrum of HD 160641 with higher dispersion will be necessary to confirm the velocity differences among the various lines, as well as to investigate the constancy of radial velocity of the star. Since the object is situated at a low galactic latitude, one may use the strength of the interstellar K line to determine a rough value of its luminosity. From a comparison of the strength of the K line of HD 160641 with that of several B-type stars in the same direction for which spectroscopic true distance moduli have been determined by Dr. Morgan, the distance of this star has been estimated to be about 2000 parsecs. Use of the color index determined by Stebbins, Huffer, and Whitford,[4] together with a necessarily rather uncertainly estimated intrinsic color, leads to a visual absolute magnitude of the order of −3.

It may be mentioned in conclusion that the star HD 160641 is the hottest known member of a group of objects whose atmospheres appear to be deficient in hydrogen. This group also includes HD 124448,[2] the well-known peculiar A-type star *υ* Sgr,[5] and the star HD 30353,[6] as well as the variable stars of the R CrB type and a number of cooler nonvariable carbon stars of which HD 182040[7] is typical.

WILLIAM P. BIDELMAN

YERKES AND MCDONALD OBSERVATORIES
March 28, 1952

[3] Y. Ishida and T. Tamura, *Sci. Pap. Jap. Inst. Phys. and Chem. Res.*, **13**, 115, 1930.

[4] *Ap. J.*, **91**, 20, 1940.

[5] J. L. Greenstein and W. S. Adams, *Mt. W. Contr.*, No. 738; *Ap. J.*, **106**, 339, 1947.

[6] William P. Bidelman, *Ap. J.*, **111**, 333, 1950.

[7] R. H. Curtiss, *Pub. Mich. Obs.*, **2**, 184, 1916.

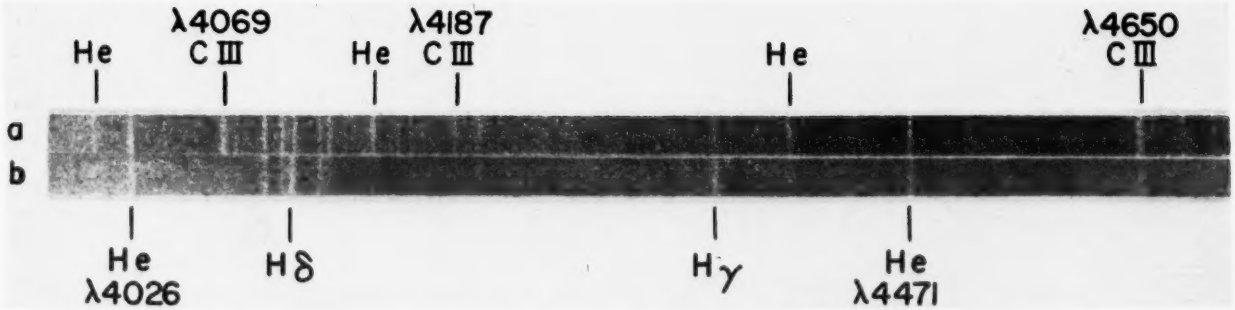

FIG. 1.—The photographic region of the spectra of (*a*) HD 160641 and (*b*) the O9.5 I*a* star α Cam. In the peculiar star the weak line near the wave length of *Hγ* is predominantly due to *He* II, and that near the wave length of *Hδ* is the *N* III line at λ 4103, normally blended with *Hδ*. Members of the diffuse singlet series of helium are indicated above the spectra, those of the diffuse triplet series below. The strength of the lines of C III is an outstanding feature of the spectrum of HD 160641.

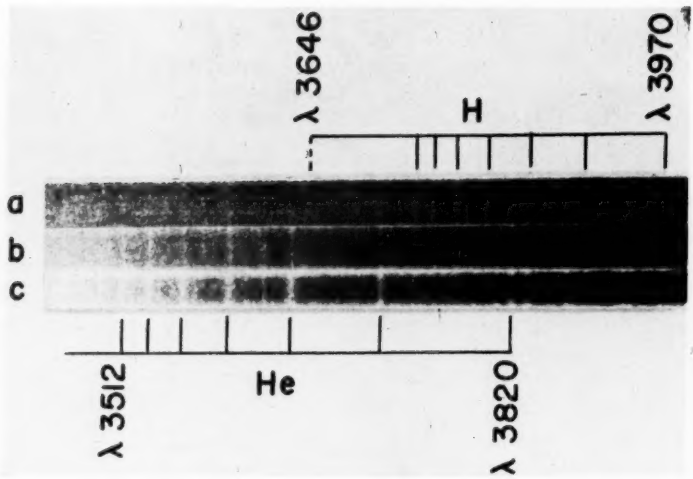

FIG. 2.—A portion of the ultraviolet region of the spectra of (*a*) the B1 I*a* star κ Cas, (*b*) HD 160641, and (*c*) HD 124448. The lines marked are higher members of the Balmer series and the diffuse triplet series of helium. The great strength of these helium lines and the absence of the hydrogen lines in the spectra of the two hydrogen-deficient objects are evident.

THE SPECTRUM OF NOVA DQ HERCULIS (1934) IN 1950*

P. SWINGS AND P. D. JOSE†
McDonald Observatory
Received January 24, 1952

ABSTRACT

Seven spectrograms of Nova DQ Herculis obtained in May and October, 1950, reveal that the striking changes in the spectrum of the nebulosity observed between 1942 and 1949 continue, while the mean velocity of expansion remains practically the same as in previous years.

The spectrograms of Novo DQ Herculis obtained in 1947 and 1949 revealed striking changes in the nebular spectrum of this nova since 1940.[1] The [*O* III] lines, which were of very high intensity in 1940 and 1942, had become weak; [*Ne* III], [*Ne* V], and [*Fe* VII] had almost disappeared. On the other hand, λ 4686 *He* II had increased in intensity relative to the Balmer lines. The nebular spectrum was progressing toward a stage characterized by strong [*O* II], *He* II, *N* III, and *Hα*, the other usual emissions, especially [*O* III] and [*Ne* III], having practically disappeared. Such an evolution is of interest in relation to the physical problems presented by the planetary nebulae as well as by the nova shells.

For this reason it appeared of interest to secure additional spectroscopic material on this nova. Seven spectrograms were obtained with the Cassegrain spectrograph of the McDonald Observatory, on May 20 (two plates), 21, 22, 23, 30, and October 17, 1950, using the quartz and glass prisms and the *f*/1 and *f*/2 cameras. Three of these spectrograms are excellent, especially that of May 22, which was measured twice. The slit passed through the nucleus in an east-west direction, hence at an angle of approximately 45° with the axis of the shell. The magnitude of the nucleus was estimated as between 14 and 15, that is, very nearly the same as before the outburst ($m_p = 14.6$).

The nucleus has a very intense continuous spectrum in the ultraviolet; actually this continuum is still intense at λ 3400. There seem to be very broad intensity fluctuations in the continuum, somewhat like the wide emission lines of a Wolf-Rayet spectrum. However, these suspected features are too faint and too wide for measurement. At any rate, the nucleus must be a very hot object.

The *Hβ*, *Hγ*, and *Hδ* lines still reveal the double structure which was studied in previous years. Of all the hydrogen lines, *Hγ* provides the most accurate value for the separation between the components. *Hα* is perturbed by [*N* II]. The dispersion at *Hβ* is lower than at *Hγ*, and *Hδ* is asymmetrical on account of the blending by *N* III lines. The two maxima in *Hγ* are measured at λ 4338.0 and λ 4346.7, giving a separation of 8.7 A or 601 km/sec. The mean velocity of expansion in 1950 is thus 300 km/sec, that is, the same as in 1949, 1947, and 1942. The resolution of our 1950 spectrograms is too low to permit us to determine accurately the range in velocities by the measurement of the outer and inner edges of the components. From a comparison with spectrograms of the same resolution obtained in 1949, 1947, and 1942, it is evident that the range in velocities has not changed much.

Table 1 describes the 1950 emission spectrum. The first column lists the wave lengths of the intensity maxima in the lines, except for *Hβ*, *Hγ*, and *Hδ*, where the centers of the doublets are given. The approximate extensions of the lines are tabulated in the second

* *Contributions from the McDonald Observatory, University of Texas*, No. 211.

† Now at Aberdeen Proving Grounds, Md.

[1] P. Swings and P. D. Jose, *Ap. J.*, **110**, 475, 1949.

column. The wave lengths have been corrected for the radial velocity of the nova, assuming $v = -33$ km/sec, as found by Humason.[2] The intensities in successive years are given in the third to seventh columns.[3]

Examination of Table 1 reveals the following variations in the spectrum: (*a*) [*Ne* V], which was fairly strong in 1940, is now absent or too weak to appear on the continuous background (which is still fairly strong at γ 3426); (*b*) [*Ne* III] is no longer observed in

TABLE 1

THE EMISSION SPECTRUM OF NOVA DQ HERCULIS

MEAN λ	APPROXIMATE EXTENSION	INTENSITIES					IDENTIFICATION
		1950	1949	1947	1942	1940	
3425.8	.....	Absent	*	0?	0–1	3	[*Ne* V]
3587	.....	Absent	*	0	0	1	[*Fe* VII]
3727.2	3719–3734	20	15	8	5	6	[*O* II]
3756.8	3751–3763	2	5	3	3	6	*H*12, *O* III
3774.3	.....	0	2	.....	.....	2	*H*11
3797.9	.....	0	3	2	1	2	*H*10
3839.3	.....	1	5	2	1–2	3	*H*9
3869	.....	Absent	0–1	1	1–2	6	[*Ne* III]
3889.3	3880–3899	4	7	3	3	6	*H*8, *He* I
3916.4	.....	0	.....	.....	.....	.....	*C* II
3970.4	3962–3978	2	8	4	4	7	*H*ε
4032.6	.....	0	3	1	1–0	1	(*He* I)
4069.9	4062–4080	4	8	3	2	4	[*S* II]
4100.2†	4092–4110	25	20n	10n	10	7	*H*δ, *N* III
4268.0	4260–4275	2	5	4	2–3	3	*C* II
4341.6‡	4330–4350	10	10	8	8	6	*H*λ
4363.8	.....	1	6	4	4	4	[*O* III]
4381.3	4372–4388	2	7	5	4	3	*N* III
4641.6	4628–4655	8	11	10	10	6	*N* III
4686.3	4675–4697	12	12	8	7	5	*He* II
4862.3§	4847–4875	10	10	12	12	8	*H*β
4918.1	.....	1	.....	.....	.....	1	(*He* I)
4964.8	.....	0	2	10	20	15	[*O* III]
5006.7	4999–5016	2	6	15	30	25	[*O* III]
5276	.....	Absent	Absent	1–0	*	1	[*Fe* VII]
(5755)	.....	Absent	0–1	1–2	*	6	[*N* II]
5876	.....	1	2	3	*	4	*He* I
6086	.....	Absent	Absent	*	*	1	[*Fe* VII]
6301.0	6286–6316	6	2	*	*	5	[*O* I]
6362.6	.....	1	1	*	*	3	[*O* I]
6566.9	6533–6604	100	50	*	*	15	*H*α, [*N* II]

* Region not covered.

† Components of the doublet at 4098.0, 4106.1.

‡ Components of the doublet at 4338.0, 4346.7.

§ Components of the doublet at 4857.3, 4865.7.

1950; (*c*) [*O* II] has become very strong; (*d*) the auroral transition as well as the nebular transitions of [*O* III] has become very weak; (*e*) the nebular transitions of [*N* II] are blended in *H*α, but the auroral transition λ 5755 is not observed; (*f*) *He* I has become weaker relative to *H* and *He* II.

[2] *Pub. A.S.P.*, **55**, 74, 1943.

[3] P. Swings and O. Struve, *Ap. J.*, **92**, 295, 1940; **94**, 296, 1941; and **96**, 468, 1942; P. Swings and P. D. Jose, *op. cit.*

Our spectrograms integrate over regions of the nebulosity where different physical conditions prevail. In some cases the central part of the nova was trailed; on other spectrograms it was kept as stationary as average seeing conditions permitted on a weak and diffuse object like N Her. Our material corresponds to the central part of the nebulosity. Accurate guiding on the nucleus was never possible. On two plates the tips of the lines (outer ends of the ellipses) are fully separated from the "continuous" spectrum of the nucleus. From the Mount Wilson spectrograms[2] taken around 1942 and from direct photographs[4] it was apparent that the emitting atoms giving rise to the luminosity of the various parts of the nebulosity were not the same. Nevertheless the observed variations of the global nebular spectrum are puzzling. The disappearance of [*Ne* III], [*Ne* V], and [*Fe* VII], the fading of [*O* III], and the enhancement of [*O* II] point to a general decrease in ionization and density. However, the strengthening of *He* II relative to *H* and especially to *He* I would indicate that, at least in parts of the nebulosity, the ionization of *He* has increased. The great intensity of *N* III parallels the relative strengthening of *He* II. It appears likely that the strong variations of the integrated spectrum of the nebulosity are, at least partly, related to the inhomogeneity of the shell. Already in 1942 Baade[4] had clearly shown that [*N* II] regions were imbedded within the [*O* III] nebulosity. The evolution of regions where different physical conditions prevail must also be different. However, this does not exclude departures of the ultraviolet radiation of the nucleus from that of a black body,[1] resulting in an irregular distribution among the stages of ionization[5] or in peculiar fluorescence phenomena.

Our thanks are due Dr. J. W. Swensson for his help with the measurements and reductions.

[4] W. Baade, *Pub. A.S.P.*, **54**, 244, 1942.

[5] I. S. Bowen and P. Swings, *Ap. J.*, **92**, 105, 1947.

The
FACE
of the
MOON

BY RALPH B. BALDWIN

An answer, in terms of the meteorite theory, to the question of how the moon came to exist in its present form.

The study of the moon—a mirror for the study of the earth.

256 pages. 6¼"×9¼". Illustrated. $5.00.

THE UNIVERSITY OF CHICAGO PRESS

New 1952 Models

35-mm. EXAKTA "VX"

Single Lens Reflex Camera

One lens both for viewing and picture taking assures perfect sharpness, accurate exposure, maximum depth of field, and correct composition for color. You always see the exact image before you take the picture —whether the subject is an inch or a mile away, whether it is microscopic or gigantic, whether it is moving or stationary. Instantly interchangeable lenses permit telephoto, wide angle, close-up, copy and microscope photography. With f2.8 Zeiss Tessar "T" Coated Lens with Pre-Set Diaphragm Control.....$269.50 tax included

Write Dept. 1100 For Free Booklet "X"

NATURE PHOTOGRAPHY WITH MINIATURE CAMERAS by Alfred M. Bailey (Denver Museum of Natural History). This eminent explorer and scientist displays his finest Exakta photographs and others along with explanatory material. 35 full page photographs. 64 pages.....50c

EXAKTA CAMERA COMPANY

46 W. 57th St. New York 1, N.Y.

THE OBSERVATORY

FOUNDED 1877

* * *

A Magazine presenting current developments in Astronomy by means of Articles, Correspondence, Notes on discoveries and Reviews of important astronomical books. The papers read at the Meetings (Astronomical & Geophysical) of the Royal Astronomical Society and the discussions which follow are also fully reported.

* * *

Annual subscription for 6 issues, post free, £1
should be sent to

The Editors, ROYAL GREENWICH OBSERVATORY
Herstmonceux Castle, Hailsham, Sussex, England

IMPORTANT BOOKS IN THE HISTORY OF ASTRONOMY

THE ARYABHATIYA OF ARYABHATA
An Ancient Indian Work on Mathematics and Astronomy

Translated with Notes by WALTER EUGENE CLARK

Aryabhata's work, which was composed in A.D. 499, is probably the earliest preserved Indian mathematical and astronomical text bearing the name of an individual author; the earliest Indian text to deal specifically with mathematics; and the earliest preserved astronomical text from the third or scientific period of Indian astronomy. This is the first complete translation from the Sanskrit of this historical document.

120 pages 7½ × 5¼ $2.50

LATIN TREATISES ON COMETS BETWEEN 1238 and 1368 A.D.

By LYNN THORNDIKE

This volume publishes for the first time the Latin texts of important tracts on comets observed between 1238 and 1368 A.D. Among the treatises are works by Aegidius of Lessines, Gerardus de Silteo, Peter of Limoges, Geoffrey of Meaux, and John of Legnano. As a summary of the Aristotelian doctrine of comets, the commentaries of Thomas Aquinas and of Albertus Magnus on Aristotle's *Meteorology* are included in English translation.

286 pages 6 × 9 *Index* $5.00

THE SPHERE OF SACROBOSCO AND ITS COMMENTATORS

By LYNN THORNDIKE

A critical edition of the Latin text, together with an English translation, of the SPHERE of John of Sacrobosco—for centuries the best and best known manual of astronomy by a Western author. Also included is the hitherto unpublished commentary by Robert of England, with an English translation. In addition, the commentary of Cecco d'Ascoli and the commentary ascribed to Michael Scot are made available for the first time outside of rare books printed in abbreviated Latin.

506 pages 6 × 9 *Index* $10.00

THE UNIVERSITY OF CHICAGO PRESS